

See discussions, stats, and author profiles for this publication at: <https://www.researchgate.net/publication/303896894>

Development of a multi-modal tactile force sensing system for deep-sea applications

Thesis · February 2016

CITATIONS

11

READS

4,780

1 author:



Peter Kamppmann

Rosenxt Group, Bremen

33 PUBLICATIONS 502 CITATIONS

SEE PROFILE

Development of a multi-modal tactile force sensing system for deep-sea applications

von Peter Kampmann

Dissertation

zur Erlangung des Grades eines Doktors der
Ingenieurwissenschaften
- Dr.-Ing. -

Vorgelegt im Fachbereich 3 (Mathematik & Informatik)
der Universität Bremen
im Februar 2016

Datum des Promotionskolloquiums: 20. Mai 2016

Gutachter: Prof. Dr. Frank Kirchner (Universität Bremen)
Prof. Dr. Oliver Zielinski (Universität Oldenburg)

Abstract

With the increasing demand for autonomy in robotic systems, there is a rising need for sensory data sensed via different modalities. In this way system states and the aspects of unstructured environments can be assessed in the most detailed fashion possible, thus providing a basis for making decisions regarding the robot's task. Compared to other sensing modalities, the sense of touch is underrepresented in today's robots. That is where this thesis comes in. A tactile sensing system is developed that combines several modalities of contact sensing. Using such a system enables comprehensive tactile acquisition of the objects in the contact area of a robotic end-effector. Furthermore, the multi-modal approach of the system increases confidence in the tactile signal as events perceived by the different tactile sensory channels can be compared. The resulting number of sensor elements also poses challenges to integration into robotic end-effectors because the available space is limited. Sensing modalities that are sensitive to contact forces often require an integration space directly at the contact location, thus leading to competing requirements.

The use of the tactile sense in robotic grippers is of great relevance especially for robotic systems in the deep sea. Up to now manipulation systems in master-slave control mode have been used in this area of application. An operator performing the manipulation task has to rely on visual feedback coming from cameras. Working on the ocean's seafloor means having to cope with conditions of limited visibility caused by swirled-up sediment. Tactile sensing systems can help to speed up manipulation tasks under these conditions or even make them possible. Application in the deep sea poses additional challenges for the development of a tactile sensing system as the employed measurement principles have to cope with the environmental conditions, such as ambient pressure and water. Besides the measurement principles, the acquisition electronics as well as the actuation methods have to withstand the high pressures (in the framework of this thesis the developed system and its components are evaluated at pressures of up to 600 bar, corresponding to a depth of 6,000 m). These topics are explored within this work. The feasibility of the developed concepts is evaluated in combination with an industrial manipulator arm for deep-sea applications and within a pressure chamber.

The great amount of data - originating from the acquisition of various sensors of different modality - requires local and decentralized pre-processing. The processing electronics integrated into the gripper system can be used to prepare the sensor information so as to enable derivation of manipulation task directly from them. Through this approach it is possible to implement behavior right the earliest state in the processing chain of robotic systems that form the foundation for autonomous exploration of objects. The measurement principles and processing algorithms evaluated and developed in this thesis are not limited to the application under water. Especially the approach involving decentralized sensor data processing makes it possible to handle the increasing complexity in robotic systems of the next generation.

Zusammenfassung

Mit dem Wunsch nach steigender Autonomie künftiger Robotersysteme steigt der Bedarf an sensorischen Zuströmen unterschiedlichster Modalität. So können Systemzustände und unstrukturierte Umgebungen so gut wie möglich registriert - und auf Basis der erfassten Messwerte Entscheidungen abgeleitet werden. Der Tastsinn ist bei heutigen Robotersystemen allerdings noch unterrepräsentiert. Hier setzt diese Arbeit an: Es wird ein taktiles Sensorsystem entwickelt, welches mehrere Modalitäten zur Messung von Kontaktkräften vereint. Auf diese Weise wird ein möglichst umfassende taktile Erfassung der Objekte an der Kontaktfläche eines robotischen Endeffektors angestrebt, aber auch die Robustheit des taktilen Signals durch Abgleich der einzelnen Modalitäten erreicht. Die daraus resultierende Vielzahl von Sensoren bedeutet aber auch gleichzeitig eine Herausforderung bei der Integration in robotische Endeffektoren, welche typischerweise über einen begrenzten Bauraum verfügen. Zudem benötigen Sensoren zur Erfassung von Kontaktkräften einen Integrationsplatz direkt an der Kontaktfläche, was bei mehreren Modalitäten mit ähnlichen Anforderungen zu konkurrierenden Integrationsanforderungen führt.

Insbesondere bei Systemen für den Einsatz in der Tiefsee ist die Nutzung von taktilen Sensoren in Greifersystemen von hoher Relevanz, da hier bisher lediglich Greifersysteme im Master-Slave-Betrieb eingesetzt werden, deren Rückkopplung an einen Operator über Kamerasysteme realisiert wird. Taktile Systeme können dabei helfen, Manipulationsvorgänge zu beschleunigen oder gar erst zu ermöglichen, da gerade bei Arbeiten am Meeresgrund die Sichtbedingungen durch aufgewirbeltes Sediment stark beeinträchtigt werden können. Für die Entwicklung eines taktilen Sensorsystems bedeutet der Einsatz in der Tiefsee eine zusätzliche Herausforderung, da die verwendeten Messverfahren idealerweise unabhängig von der Wassersäule funktionieren. Neben den Messprinzipien müssen auch die Ausleseelektroniken und die Aktuationsverfahren des Manipulators den hohen Drücken (in dieser Arbeit bis 600 bar, dies entspricht etwa einer Meerestiefe von 6.000 m) standhalten. Diese Themen werden in der Arbeit behandelt und die Umsetzung anhand von Experimenten an einem Industriemanipulator und in einer Druckkammer verifiziert.

Die hohe Datenmenge - entstanden durch die Erfassung einer Vielzahl an Sensoren unterschiedlicher Modalität - erfordert zudem die lokale und dezentrale Vorverarbeitung der Sensorinformationen. Die integrierten Recheneinheiten im Greifersystem können zur Aufbereitung der Sensorinformationen zum direkten Ableiten von Manipulationsaufgaben genutzt werden. Hierdurch lassen sich bereits auf den ersten Verarbeitungsebenen in Robotersystemen Verhalten implementieren, die den Grundstein für die autonome Exploration von Objekten legen. Die auf diese Weise erforschten Messverfahren und Auswertealgorithmen sind nicht nur auf den Einsatz von Unterwassersystemen beschränkt. Insbesondere die dezentrale Sensordatenvorverarbeitung stellt einen Ansatz zur Bewältigung der zunehmenden Komplexität von Robotersystemen der nächsten Generation dar.

Danksagung

Ohne die Unterstützung einer Vielzahl von Menschen wäre die Fertigstellung dieser Arbeit nicht möglich gewesen. An dieser Stelle möchte ich daher einigen Menschen Danken, deren Anteil am Erfolg dieser Arbeit besonders hoch ist.

Mein besonderer Dank gilt meinem Doktorvater Professor Dr. Frank Kirchner für die Unterstützung in der Durchführung der Doktorarbeit in den vergangenen Jahren. Durch die Möglichkeit, am Robotics Innovation Center des Deutschen Forschungszentrums für künstliche Intelligenz forschen zu dürfen, habe ich in den vergangenen sieben Jahren unter idealen Bedingungen in vielen Disziplinen der Robotik mein Wissen vertiefen können. Insbesondere für sein Vertrauen, mir bereits in frühen Jahren des Beruflebens die Leitung von Projekten und Teams zu übertragen, möchte ich mich bedanken.

Mein weiterer Dank gilt allen Kollegen am DFKI, sei es auf wissenschaftlicher, technischer und administrativer Ebene. Die angenehme und freundliche Zusammenarbeit in den letzten Jahren ist mit vielen tollen Erinnerungen verbunden und eine Zeit, die ich nicht missen möchte.

Ein Großteil der Arbeit ist während der Durchführung des Projektes SeeGrip entstanden. Insbesondere meinem ehemaligen Kollegen Dr. Johannes Lemburg möchte ich für die tolle gemeinsame Arbeit in dieser Zeit danken. Das Ausreizen des technisch derzeit Machbaren, die unermüdliche Arbeit bis tief in die Nacht hinein und die vielen anregenden Diskussionen haben diese Arbeit sehr geprägt. Mein Dank gilt zudem der Mitarbeit der weiteren Kollegen Achint Aggarwal, Matthias Goldhoorn, Hendrik Hanff, Florian Hühn, Tim Tiedemann, Lan Yue Ji und Martin Zenzes. Ohne sie wäre der wissenschaftliche Erfolg des Projektes nicht möglich gewesen.

Die abschließenden Experimente für diese Arbeit konnte ich während meiner Mitarbeit am Projekt LIMES durchführen. Hierfür danke ich meinem Kollegen Dr. Sebastian Bartsch für die Möglichkeit der Durchführung dieser Arbeiten.

Weiterhin Danke ich den den studentischen Mitarbeitern, die mich während meiner Doktorarbeit mit ihren Abschlussarbeiten und ihrer Assistenz bei Experimenten unterstützt haben: Finn Hoffmann, Antony Pfoetzscher, Henry Süssen und Timo Stoffregen.

Für Anregungen, Kritik und Verbesserungsvorschläge beim Verfassen dieser Arbeit möchte ich mich bei Daniel Kühn, Dr. Johannes Lemburg, Bertold Bongardt und Professor Dr. Oliver Zielinski bedanken.

Weiterer Dank gilt meinen Freunden, meinen Eltern, meinem Bruder und meiner Freundin Nina für Ihren Rückhalt in den vergangenen Jahren. Sie haben mich jederzeit unterstützt und für angenehme Abwechslung außerhalb der Arbeit gesorgt. Insbesondere in der Schreibphase der Arbeit haben sie mich selten gesehen, aber dennoch nicht vergessen, vielen Dank dafür!

Contents

1	Introduction	1
1.1	Motivation	1
1.2	Objectives	3
1.3	Frame of the thesis	5
1.4	Structure of the thesis	5
2	Definitions	9
2.1	Deep-sea	9
2.2	Tactile sensing	9
2.3	Intrinsic tactile sensing	10
2.4	Extrinsic tactile sensing	11
2.5	Passive sensing	11
2.6	Active sensing	11
2.7	Runtime and memory complexity	11
3	State of the Art	13
3.1	Biological concepts of tactile sensing	13
3.1.1	Modalities for tactile sensing in the human hand	13
3.1.2	Exploration procedures for identifying objects by touch	15
3.2	Multi-modal tactile sensing in robotics	16
3.3	Tactile sensors for underwater applications	19
3.4	Tactile sensing processing systems	20
3.5	Manipulators with tactile feedback	22
3.5.1	Land-based robotic end-effectors	23
3.5.2	Robotic grippers for underwater applications	25
3.6	Discussion	29
4	System Design	33
4.1	Mechanical concept	33
4.1.1	Morphology	34
4.1.2	Actuation	38
4.2	Required sensing capabilities	40
4.3	Sensing absolute overall force and torque	41
4.4	Sensing dynamic contact properties	44
4.5	Sensing geometry information	46
4.6	Proprioceptive Sensing	50
4.7	Decentralized hardware architecture for tactile sensing	50

4.7.1	Processing force-torque data	51
4.7.2	Processing piezoelectric sensor data	52
4.7.3	Processing fiber-optic sensor data	54
4.7.4	Embedded sensing module for static and dynamic contact measurement	58
4.7.5	Processing gripper pose information	59
4.7.6	Further processing electronics in the gripper	59
4.7.7	Topology of the designed hardware architecture	61
4.8	Integrated gripper system	62
4.9	Discussion	63
5	Handling complexity by local pre-processing	67
5.1	Reduction of data transmission	70
5.1.1	Sensor-value-dependent data transmission	70
5.1.2	Handling the fiber-optic sensor array data	72
5.1.3	Camera data acquisition	73
5.1.4	Optical fiber extraction	74
5.1.5	Calibration	84
5.1.6	Spatial relationship	88
5.2	Local control for load balancing in robotic systems	93
5.2.1	Tactile controlled grasping	94
5.2.2	Contour following	99
5.3	Discussion	102
6	Experiments	107
6.1	Experiment environments	108
6.1.1	Deep-sea manipulator: Schilling Robotics Orion 7P	108
6.1.2	Pressure chamber	109
6.1.3	Manipulator for applications on land: Mitsubishi PA-10	110
6.1.4	Experiment guide	111
6.2	Preparations for application in deep-sea conditions	111
6.2.1	Electronics	112
6.2.2	Sensors	115
6.2.3	Sealing connectors	120
6.3	Experiments in combination with an underwater manipulator	122
6.3.1	Distinguishing objects of similar shape	122
6.3.2	Evaluation of piezoelectric sensor signal feedback	125
6.4	Experiments under high pressure	126
6.4.1	Experimental setup using a single finger	127
6.4.2	Sensor signal variations between air and water	128
6.4.3	Pressure dependency of sensor feedback	129
6.4.4	Long-term sensor response under deep-sea conditions	130
6.4.5	Ability to perceive geometries under deep-sea conditions	132
6.4.6	Center of pressure detection in deep-sea conditions	133
6.4.7	Performance comparison of fiber-optic sensing interfaces	136
6.5	Local behavior evaluation: contour following	138
6.6	Discussion	141

7 Conclusion and Outlook	145
7.1 Conclusions related to the thesis objectives	145
7.2 Further results	151
7.3 Lessons learned	152
7.4 Outlook	154
List of Figures	159
List of Tables	167
Acronyms	169
References	171

Chapter 1

Introduction

1.1 Motivation

Execution of repetitive tasks and working in environments too dangerous for humans are driving factors for the development of robots in an industrial context. Today's robotic systems are able to accomplish this in factory environments by executing simple tasks with high precision and velocity. The envisioned cooperation between humans and robots and the adoption of more complex tasks like operation in disaster zones require robotic systems to act in dynamic, unstructured environments.

To achieve this goal, the development focus of robotic systems is shifting towards increasing autonomy to implement complex mission scenarios. A prerequisite for highly autonomous systems is extensive acquisition of their own state and the environmental conditions through a variety of sensors of different modality since reacting to system states or external events is only possible if they can be perceived.

The thesis addresses this situation with the aim of improving the capabilities of touch sensation during intervention tasks of robotics systems in deep-sea environments.

Current state of underwater manipulation

The relevance of touch sensing in underwater manipulation can be explained using the following scenario, which is a typical example of a manipulation task in deep-sea environments. A remotely operated vehicle (ROV) equipped with a manipulator arm is maneuvered to the operational area from a supply vessel located several thousand meters above it at sea level. The underwater manipulator is controlled using a joystick that resembles the kinematics of the gripper. Visual feedback from cameras supports the operator during manipulation. Currents acting on the ROV or the object to be handled cause continuous unpredictable displacements between the end-effector and the object in all degrees of freedom. The distance between the operational

area and the manipulator can only be estimated and variations from the original object's dimensions occur based on effects such as corrosion or marine growth. Turbid water conditions that limit the operator's view of the operational area cumulate to form the unstructured mission conditions and may cause delays or even abortion of the planned task.

The foreseen development in underwater manipulation indicates an increasing demand for dexterous manipulation. Offshore construction sites are moving to the deeper areas of the oceans. The drilling platform *Perdido Spar* is already moored in depths of 2,500 m [Technip USA, Inc., 2011]. Tasks during inspection and assembly that are carried out by divers in shallow water have to be performed by ROVs at these depths. There is growing interest in increasing autonomy in this domain as well and the use of autonomous underwater vehicles autonomous underwater vehicles (AUVs) for autonomous manipulation is the subject of investigation in research projects. As a result, the diversity and the demands on manipulation tasks are rising.

Use of contact sensing towards autonomous underwater manipulation

To reduce the dependency on visual feedback during underwater robotic manipulation, the development of contact sensing for the application under water is seen as a necessary step to increase robustness and enable autonomy in underwater manipulation. Additionally, sensing the different modalities of touch is beneficial for the whole range of intervention tasks, starting from support in hazy water conditions in which vision is limited, and extending to monitoring the grasp state and quality as well as autonomous object exploration and identification.

The required sensing techniques for acquiring touch information, such as contact location, geometry, texture, overall force and temperature, are referred to as tactile measurement principles. Within the scope of the thesis, the discussion on tactile sensing is narrowed down to the modalities influenced by contact forces as these are the most relevant in manipulation tasks [Tegin and Wikander, 2005]. Hence, the modality temperature is not investigated further.

Known approaches for tactile sensing underwater

Compared to developments of end-effectors with tactile sensors for applications on land, little development is documented in relevant literature concerning the underwater and deep-sea domain. The works in [Lane et al., 1997], [Meng et al., 2006] and [Fresnada, 2012] define the three major contributions to this field in the last twenty years. Most developments were evaluated regarding applicability at depths below 100 m, the spatial sensor resolution is sparse and the selected measurement principles often are not designed to be independent of the water column.

Possible explanations for the small number of developed systems include the demanding environmental conditions a sensing system has to face in the deep sea. The inherent surrounding water requires concepts for the protection of electronic parts from direct contact with water. Furthermore, it is necessary to deal with the pressure acting on electronics and sensing elements, which rises with increasing depth.

Current research topics related to tactile sensing

Taking the human skin as a model, several findings on the specialization of mechanoreceptors and the encoding of tactile information have influenced the development of touch sensation for robots.

[Wettels et al., 2014] and [Mittendorfer and Cheng, 2011] based their development on the observation that the human skin comprises mechanoreceptors that are sensitive to specific modalities [George A. Gescheider, 2009]. They incorporated specialized measurement principles for acquisition of the different characteristics of contact information. While this approach improves the robustness of the acquired sensor information, it also leads to integration conflicts as many sensing mechanisms for touch measurement require integration in the contact area of the end-effector. Finding solutions for such of competing requirements is generally symptomatic for integration of complex robotic systems.

[Cutkosky et al., 2008] proposed a tactile information flow that not only contains information perceived by exteroceptive force sensors. Data stemming from proprioceptive measurements like the gripper pose or torque applied by the actuation modules is necessary to determine object properties in combination with acquisition of contact information.

Implementation of a multi-modal tactile sensing system raises questions regarding the processing architecture of the sensory data. Extracting information from the amount of data generated by such a system creates considerable processing load in a mobile autonomous robotic system. Since most of the information sampled at the end-effector positions leads to a reaction at the same place, local processing and control are logical steps to reduce the communication intensity and workload of central processors of the robot. The current developments of embedded systems allow the integration of powerful processors into the structure of the end-effector enabling the implementation of behavior locally.

1.2 Objectives

The objective of this thesis is to contribute to the scientific advancement of tactile sensing in the domain of underwater robotics by

developing a multi-modal tactile force sensing system for deep-sea applications

The term *deep-sea* refers to depths of up to 6,000 m. This main objective can be divided into three sub-goals:

- **Identification of suitable measurement principles for multi-modal tactile force sensing in the deep-sea**

A variety of measurement principles for perceiving touch information exist for applications on land and new sensor systems are continuously undergoing development. The high ambient pressure and the surrounding water necessitate careful selection of suitable measurement principles. Some sensing solutions require placement of electronic parts directly in the contact area. Precautions have to be taken to prevent short circuits and damage by the ambient pressure. Other working principles compare the forces acting on a cavity that contains a gas under normal pressure. Measurement methods using this approach have to acquire the increasing pressure induced by the water column in addition to acting contact forces in effect. The thesis presents a combination of sensors that enables multi-modal tactile sensing regardless of the ambient pressure created by the water column.

- **Local pre-processing as a solution for handling complex robotic systems**

The sensory information generated by the sensor elements of each sensing modality imposes decisions on the processing architecture of a robotic system. The recent advances in miniaturizing embedded systems with high processing power enable pre-processing of sensory data and local behavior implementation in order to distribute the load within a robotic system. This thesis demonstrates how local pre-processing, starting from data acquisition and extending to local behavior implementation and local control, can support the handling of increasingly complex robotic systems.

- **Validation of the approaches under relevant conditions**

The third objective of this thesis is validation of the theoretical and algorithmic concepts for a multi-modal tactile force sensing system for deep-sea applications. The tactile sensing system developed, comprising sensors and the processing system, is evaluated in a pressure chamber at 600 bar ambient pressure, corresponding to a depth of 6,000 m. This involves integration into a multi-limb end-effector and the preparatory steps for safely operating the system while in contact with water. Further validation of the developments is conducted in combination with a deep-sea manipulator arm.

1.3 Frame of the thesis

Most of the research activities that led to this thesis were carried out during the SeeGrip project (grant no. 03SX291) and the LIMES project (grant no. 50RA1218) at the Robotics Innovation Center of the German Research Center for Artificial Intelligence in Bremen. The goal of the SeeGrip project was to develop an autonomous underwater gripper with tactile feedback for form-closed and force-closed object manipulation. The tactile sensing system design, the work on pressure-tolerant electronics and the experimental validation under water and in the pressure chamber were performed during this project.

The goal of the LIMES project was to learn intelligent motions for kinematically complex robots designed for exploration in space. Behavior implementation and validation on a robotic manipulator on land were realized during this project

1.4 Structure of the thesis

The structure of the thesis is depicted in Figure 1.1. Definitions of several terms are indicated in chapter 2 for better understanding of the terms used in the chapters that follow. To classify the objectives, an overview of the state of the art is provided for the fields this thesis addresses. It starts with a presentation of the findings regarding tactile sensory information and its encoding in the human skin. The available approaches of multi-modal tactile force sensing systems for robotics are presented discussing the modalities of touch that can be sensed using these sensors. This section is followed by an overview of the tactile processing systems known today and their integration into structures of robotic systems. The state of the art is completed by an overview of the manipulation systems for application on land and underwater described in relevant literature. The insights from the study of the state of the art are summarized in a discussion used as the basis for determining requirements of the system design and pre-processing.

The layout of the morphology of the gripper that was developed alongside the sensing system and the selection of suitable measurement principles for application in deep-sea environments are discussed in the further course of the thesis. Chapter 4 addresses the research questions that are summarized under the first sub-goal of this thesis. Sensor techniques for sensing different modalities of touch are presented and a detailed explanation is given for why the selected measurement principles are suitable for operation under varying ambient pressure. The designed acquisition electronics for each sensing modality completes the chapter on the design of the tactile sensing system. The research on this domain led to a publication which served as a basis for this chapter:

[Kampmann and Kirchner, 2012]:

A Tactile Sensing System for Underwater Manipulation

Peter Kampmann, Frank Kirchner

Proceedings of the workshop on: Advances in Tactile Sensing and Touch Based Human-Robot Interaction to be held in conjunction with the 7th ACM/IEEE International Conference on Human-Robot Interaction (HRI 2012), 3/2012

The selected sensors together with their acquisition electronics give an indication of the volume of data acquired every second. Handling the obtained data is the topic of chapter 5. It deals with the research questions of the second subgoal. Pre-processing algorithms are presented that range from sensor value extraction to local behavior of varying complexity. The motivation for each algorithmic solution is explained with respect to the target application and processing platform. The foundations of this chapter were laid in the journal publication:

[Kampmann and Kirchner, 2014]:

Integration of Fiber-Optic Sensor Arrays into a Multi-Modal Tactile Sensor Processing System for Robotic End-Effectors

Peter Kampmann, Frank Kirchner

Sensors - Open Access Journal , MDPI - Open Access Publishing, Special Issue Tactile Sensors and Sensing Systems, number 14(4), pp. 6854-6876, Apr/2014.

The practical validation of the selected measurement principles for the deep sea together with the designed processing electronics and application of the developed pre-processing algorithms are part of the experiment chapter. It thus addresses the third subgoal of the thesis. Using a system for underwater and deep-sea applications requires several precautions to cope with the environmental conditions. Electronic components have to be shielded from contact with water and the effects of high ambient pressure have to be investigated. The approaches to tackle the demanding environmental conditions are validated in the initial sections of the experiment chapter. The feasibility of the design decisions is demonstrated using two mission scenarios. To depict the ability to distinguish objects by touch, the developed gripper is evaluated in combination with an industrial underwater manipulator. Further experiments evaluate the independence from varying ambient pressure conditions in a pressure chamber. The insights gained in these experiments were published in the following articles and journals:

[Kampmann and Kirchner, 2015]:

Towards a fine-manipulation system with tactile feedback for deep-sea environments

Peter Kampmann, Frank Kirchner

Robotics and Autonomous Systems, 67:115 – 121, Special Issue Advances in Autonomous Underwater Robotics

[Kampmann et al., 2012]:

Hybrid pressure-tolerant electronics

Peter Kampmann, Johannes Lemburg, Hendrik Hanff, Frank Kirchner

Proceedings of the Oceans 2012 MTS/IEEE Hampton Roads Conference & Exhibition. OCEANS MTS/IEEE Conference (OCEANS-2012), October 14-19, Hampton Roads, Virginia, USA

The thesis concludes with a final chapter on the achievements and a discussion of the lessons learned. As all scientific research raises new questions, an outlook is given presenting thoughts on the continuation of research on tactile sensing for underwater manipulation.

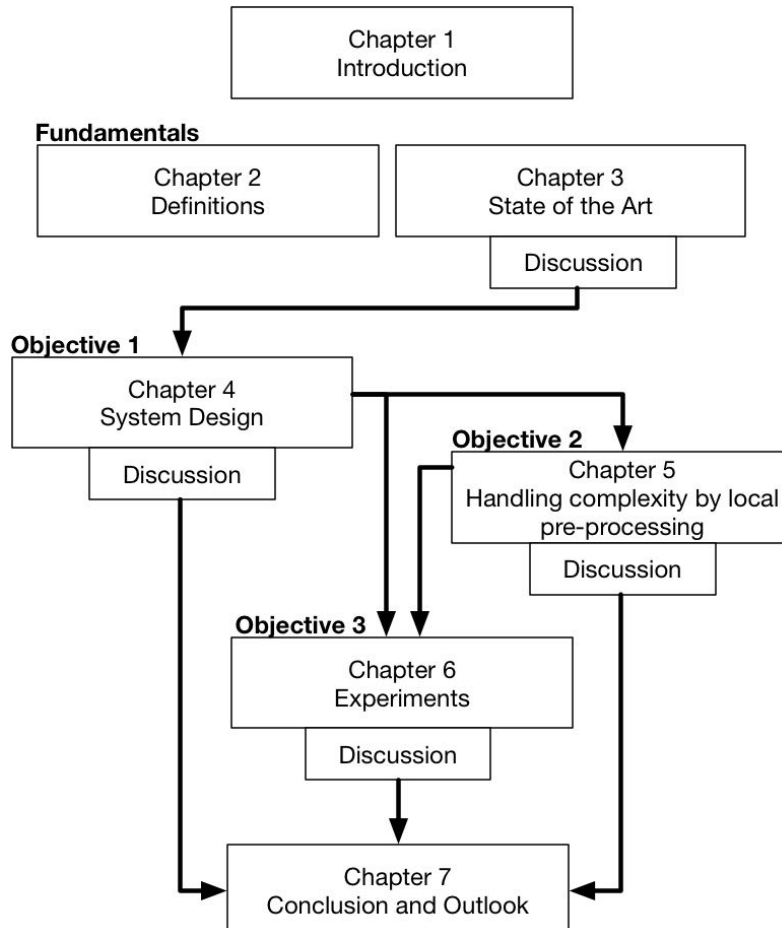


Figure 1.1: Structure of the thesis

Chapter 2

Definitions

Definitions for terms that are used throughout the thesis are introduced within this chapter.

2.1 Deep-sea

The maximum depth of the oceans is greater than the height of the highest mountains above sea level. The deepest area of the oceans is the *Challenger Deep* which is at a depth of 10,924 m [Barry and Hashimoto, 2009]. It is surprising that most classifications start referring to deep-sea already at a depth of 200 m [Tyler, 2003] and [Smith et al., 2008]. A comparative study computes the mean depth of the oceans to 3,682 m [Charette and Walter, 2010].

A system that is capable of working at depths of 6,000 m is able to reach up to 97 % of the earth's seafloor [Michel et al., 2003]. The development of the multi-modal tactile force sensing system in this thesis strives to achieve this depth rating.

2.2 Tactile sensing

There are various definitions of the term tactile sensing. [Jayawant, 1989] define tactile sensing as the capability to continuously detect forces in an array. The authors of [Dahiya et al., 2010] define tactile sensing as the detection and measurement of contact parameters in a predetermined contact area together with subsequent pre-processing of the signals. Thus, a tactile sensor is not only defined by its capability to sense a certain stimulus, but also by its pre-processing. This definition requires the inclusion of electronic acquisition components as a part of a tactile sensor. Technological progress regarding electronic components like analog to digital converters (ADCs) advances in a matter of years, whereas measurement principles do not change their

theory of operation. The proposed definition necessitates a frequent review on current electronic components when comparing tactile sensors with one another, thus complicating the review.

The definition chosen for this thesis comes from [Nicholls and Lee, 1989]: Here, a tactile sensor is defined as a device that measures parameters of a contact interaction between the device and a physical stimulus. This approach also encompasses single point measurements of forces and torques.

2.3 Intrinsic tactile sensing

The term *intrinsic tactile sensing* was introduced by [Bicchi, 1990]. It refers to the computation of incoming forces by a sensor placed inside the structure of an end-effector rather than by sensor arrays at the contact location. A typical setup for intrinsic tactile sensing is the use of a force-torque sensor that is integrated below a spherical shaped fingertip (compare Figure 4.29). Based on the known geometry of the finger surface, it is possible to calculate contact location as well as the contact forces acting on the end-effector. Distinguishing multi-contact points is not possible with this approach. This sensing method is mostly used in precision grasps [Tegin and Wikander, 2005].

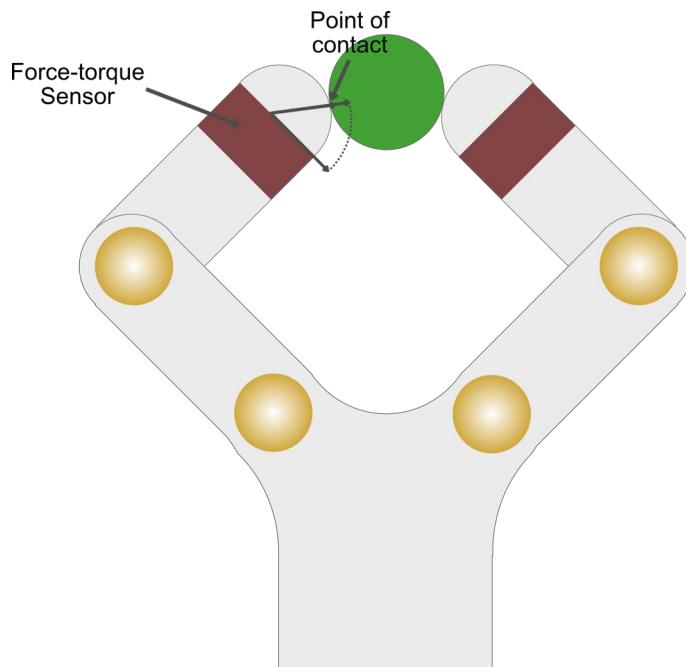


Figure 2.1: Schematic drawing of a gripper with force-torque sensors for *intrinsic tactile sensing*

2.4 Extrinsic tactile sensing

Following the definition of the term *intrinsic tactile sensing*, extrinsic tactile sensors are all sensors that are placed along the contact area and measure incoming stimuli across an area or at a single contact point.

2.5 Passive sensing

The expression *passive sensing* is used when tactile feedback is analyzed without repositioning the sensor by moving the manipulator to which the sensor is attached.

2.6 Active sensing

In the case where the object that is to be explored exceeds the dimensions of the tactile sensor, moving the sensor across the tactile feature is called *active sensing*.

2.7 Runtime and memory complexity

A metric to evaluate the performance of an algorithm compares its runtime with regard to the input parameters. Often this metric is also referred to as big O-Notation as the result of the metric is mostly given in form similar to

$$O(N) = x \quad (2.1)$$

In this equation the runtime complexity O is expressed in dependency of the number of input parameters N resulting in a runtime of x . In the case of a linear relationship the following equation would hold:

$$O(N) = N \quad (2.2)$$

Consequently, in a situation where the runtime of an algorithm grows exponentially with the size of the input parameters, one would express this as:

$$O(N) = e^N \quad (2.3)$$

Using this approach, the absolute runtime in time scale is not relevant because this information only holds for a specific hardware configuration. Especially in the case of using embedded systems where hardware resources are limited, this metrics enables identification of algorithms that have low requirements regarding processing power. In general, the lower the dependency between the input parameters and the

runtime of an algorithm is, the lower are the requirements regarding computing time. As embedded devices generally have a limited instruction set and function at low operating frequencies compared to standard central processing units (CPUs), a low computing time is beneficial for implementation with such devices.

The same notation can be used to express the memory consumption depending on the size of the input parameters. Further information on describing runtime complexity using the O-Notation can be found, for instance, in [Kleinberg and Tardos, 2006].

Chapter 3

State of the Art

This section provides an overview of the state of the art of the topics that this thesis addresses. The conclusion at the end of this chapter discusses the findings based on the state of the art presented.

3.1 Biological concepts of tactile sensing

Emulating the capabilities of biological systems drives the development of technical systems. The human hand is an impressive example of implementation of the sense of touch in nature. Its sensing capabilities and the findings on tactile data encoding and exploration strategies are presented here.

3.1.1 Modalities for tactile sensing in the human hand

Aside from its protecting function, the human skin comprises a variety of receptors that are sensitive to different modalities of the ambient conditions in the contact region. Nociceptors respond to painful conditions based on mechanical or thermal events. Other receptors react to varying temperature conditions. The receptors that are sensitive to touch are found in different layers and areas of the skin. These mechanoreceptors vary in their distribution, morphology and dimension.

The focus here is on the mechanoreceptors mainly found in the glabrous skin as these are mainly affected during object manipulation. Four different types of mechanoreceptors for perceiving touch stimuli were identified. These receptors can be grouped by the way they react to a constant stimulus and by the size of their receptive fields [Lederman and Browne, 1988]. Fast adapting tactile units (FA) only respond in the transient phases of stimulation, whereas slowly adapting (SA) units show a sustained discharge [Lederman, 1991]. A further distinction between these two types is based on the size of the receptive fields.

Table 3.1: Mechanoreceptors in the glabrous skin (with data from: [Dahiya et al., 2010], [Johansson and Flanagan, 2009] and [Lederman, 1991])

Type	FA2	SA2	SA1	FA1
Stimulus frequency (Hz)	40-500+	10-500+	0.4-3	3-40
Spatial density (cm^{-2}) at fingertip	21	49	70	140
Receptive field (mm^2)	12.6	101.0	11.0	12.6
Indentation threshold (mean μm)	0.08	300	30	6
Sensitivity to static force	No	Yes	Yes	No

Although the different mechanoreceptors are designated in the relevant literature as Pacinian corpuscles, Ruffini endings, Merkel cells and Meissner corpuscles, the role of the tactile receptors is the subject of ongoing research. [George A. Gescheider, 2009] addressed the question of whether Ruffini endings are found in the glabrous area of the skin. [Lumpkin et al., 2010] discuss the role of Merkel cells in touch reception. Many researchers refer to tactile units by their adaption type. This approach will be used here as well. Table 3.1 summarizes some important properties of the mechanoreceptors.

Researchers have investigated the sensitivity of mechanoreceptors to certain aspects of contact during manipulation and exploration. According to reports of several groups, each of the mechanoreceptors reacts with high sensitivity to a certain type of stimulation. Based on the size of their receptive fields, [Vallbo and Johansson, 1984] state that FA1 and SA1 receptors are responsible for localizing contact stimuli on the skin surface and acquire details of the surface structure at the contact location. FA2 receptors respond to rapid onset and offset of deformations of the skin [George A. Gescheider, 2009] and high frequency vibrations [Dahiya et al., 2010], while SA1 units are ideally sensitive to steady deformation and low-frequency vibration [George A. Gescheider, 2009]. Ruffini corpuscles are reported to be sensitive to indentation and stretching of the skin; moreover, directional sensitivity can be observed [Vallbo and Johansson, 1984]. Like FA2 receptors, FA1 units are known to respond to rapidly occurring small changes in indentation but with a lower sensitivity in frequency [Grünwald, 2008].

In addition to the contact information coming from the receptors in the contact area, the posture of the fingers is needed to put the position of the perceived tactile stimuli into a global context. Proprioceptive information is therefore needed to determine the movements of the fingers. According to [Johansson and Flanagan, 2009], this information is received through signals from the muscle spindles of the joints and the signals from cutaneous afferents in the skin.

[Vallbo and Johansson, 1984] have investigated the encoding of tactile afferent signals coming from the mechanoreceptors. The spike trains triggered by a contact stimulus are depicted in Figure 3.1.

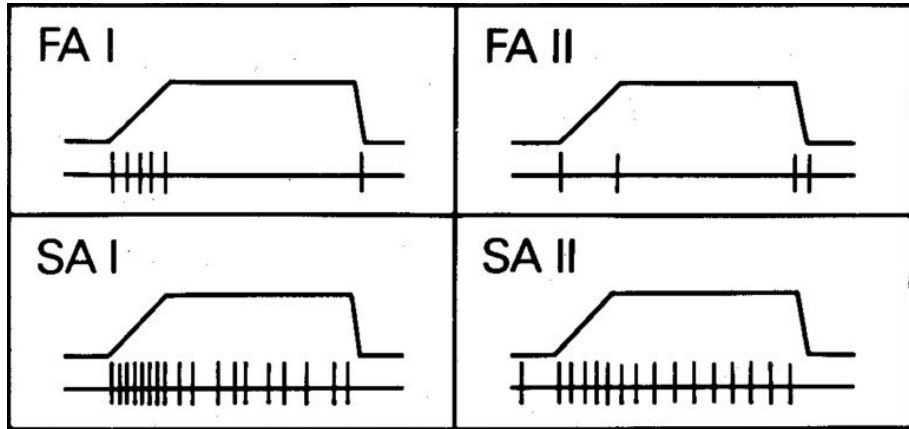


Figure 3.1: Spike trains in response to a tactile stimulus from the different types of mechanoreceptors (from [Vallbo and Johansson, 1984])

The signal sequence of the stimulus is sketched above the spike train response in each subfigure for the various mechanoreceptors. As expected, the fast adapting types are only responding to changes in the signal while the slowly adapting mechanoreceptors respond during the whole contact sequence. Differences can be found in the frequency over the duration of contact. While the fast adapting afferents of type one respond with high frequency during changes, their spike trains exhibit only single spikes in the case of a new stable contact state. Corresponding observations can be made for the slowly adapting types. The mechanoreceptors of type one respond with high frequency during the beginning of contact with decreasing feedback over time while those of type two are responding with constant frequency during the contact phase.

3.1.2 Exploration procedures for identifying objects by touch

Recognizing objects by touch alone is one of the capabilities humans achieve with their hands. The authors of [Lederman, 1991] found out that humans use systematic and purposive movements to determine object properties. These exploration steps can be categorized and are summarized to exploratory procedures that are performed to acquire knowledge about an object (compare Figure 3.2). The different procedures provide indications of the necessary sensing modalities and dexterous capabilities of the hand to perform tactile exploration and are thus briefly considered here.

The *texture* of objects can be acquired using the vibration feedback perceived during lateral motion. During object recognition this feature is helpful to distinguish

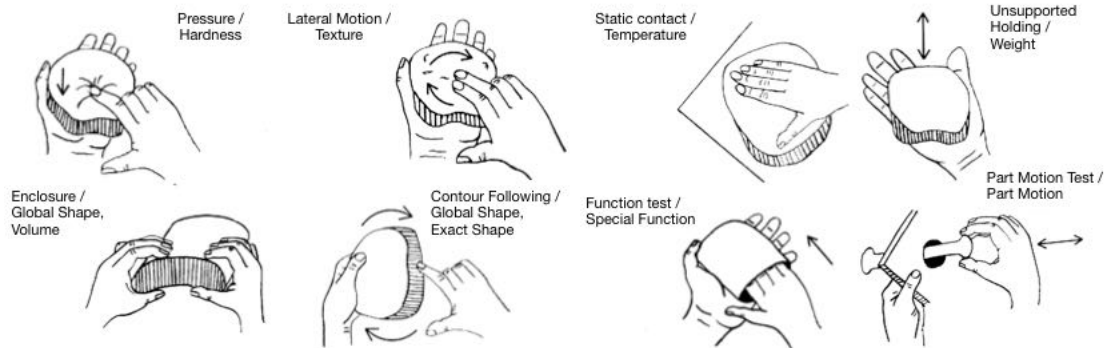


Figure 3.2: Procedures performed by humans to explore unknown objects by touch, from: [Lederman, 1991]

objects of similar geometries. Another way of identifying objects with similar geometry is via information about the object's *hardness*. It is acquired by applying pressure to the object's surface. The *weight* of an object is another important feature which is sensed by lifting an object. *Thermal properties* of objects give further indication of the material used. This property is acquired by applying a constant contact between the hand and the object's surface. A rough estimation of the object's *global shape* is achieved by adjusting the fingers and the palm to the contours of an object, whereas the *exact shape* of an object is sensed by following the contour. Further exploration procedures mentioned include the evaluation of specific functions and movable parts of objects.

3.2 Multi-modal tactile sensing in robotics

Early technical implementations of tactile sensing systems were based on single measurement principles that allowed the acquisition of contact and its location [Fearing, 1987]. Further aspects of contact, such as overall weight or slippage, were derived by computing this information from the measured signal. The limitations of the measurement quality of information that is derived from a single modality were recognized in [Allen and Michelman, 1990]. As a result of this observation, a tactile sensing system was designed that incorporates several sensing modalities to increase robustness and quality of the sensor feedback. As the integration efforts for a single tactile sensor are considerable in terms of mechanical integration and signal conversion [Tegin and Wikander, 2005], combining several sensor modalities adds to the complexity. The recent developments in multi-modal tactile sensors that were successfully integrated into manipulation systems are discussed in this section. Apart from the sensors used, the electric interfaces for data acquisition are also presented.

The development of a combination of tactile sensors for detecting force at the con-

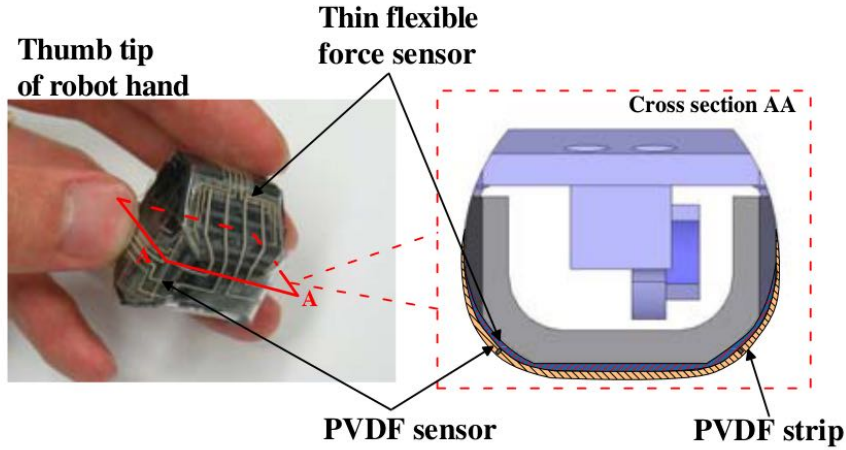


Figure 3.3: Multi-modal tactile sensor module for integration into the fingertips of the SKKU Hand (from [Choi et al., 2005])

tact location and possible slippage is presented in [Choi et al., 2005]. The sensor was designed for integration into the fingertips of the SKKU hand [Choi et al., 2006]. To build the sensor, sheets of polyester film were used as a base. Lanes of resistive ink and strips made of polyvinylidene fluoride (PVDF), a material that exhibits piezoelectric properties, form the sensitive part of this multi-modal sensor solution. 24 force sensing elements and one dynamic sensing module were realized. Due to the flexibility of the materials chosen, the sensor can be bent. Figure 3.3 shows the final setup of the sensor. Amplification circuits for both sensor types and signal conversion electronics were created to be integrated into robotic structures near the sensor.

The authors of [Mittendorfer and Cheng, 2011] describe their development of a multi-modal tactile sensing unit that is designed to cover large areas of robotic structures. Therefore, a hexagonal shape of the sensor modules was chosen that allows coverage of three-dimensional structures with reduced gaps. The so-called Hex-o-Skin system comprises sensing modalities for acquiring information about pre-touch, light touch and ambient temperature. The information is sampled by four phototransistors, a three-axis accelerometer and seven temperature sensors. The data acquisition is performed directly on the sensing modules while the transfer to processing units is realized using communication channels to the adjacent sensing modules. The system developed is shown in Figure 3.4.

A multi-modal tactile sensing module called BioTac is discussed in [Wettels et al., 2014]. Unlike the previously presented sensors, this module is not intended to be integrated into structures of an end-effector, but serves as a structural element of a robotic finger. Its sensing capabilities comprise perceiving contact forces, micro-vibrations and thermal flux. Sensing these modalities is achieved by

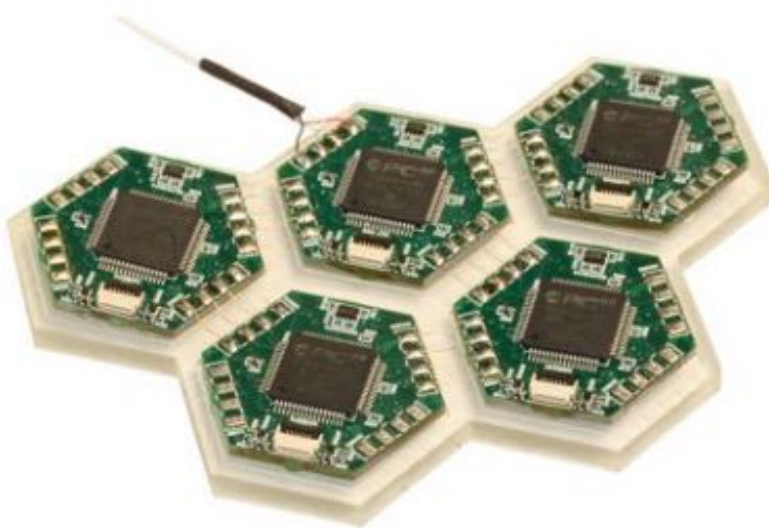


Figure 3.4: Sensor skin consisting of hexagonal shaped contact sensing modules [Mittendorfer and Cheng, 2011]

a variety of sensors depicted in Figure 3.5. Central elements of the structure are cavities filled with an electrically conductive fluid. In the event of contact, vibrations occurring at the surface are transmitted through the fluid to a pressure sensor. The vibrational feedback is enhanced by artificial fingerprints applied on the sensor cover.

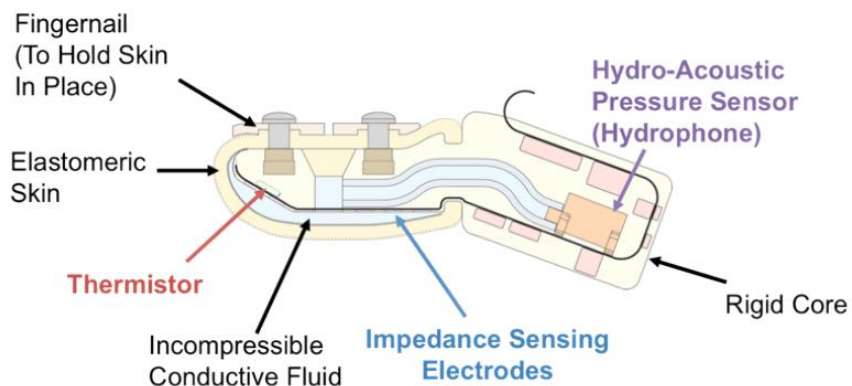


Figure 3.5: Multi-modal force sensing module for robot fingertips ([Wettels et al., 2014])

The signal acquired by the pressure sensor is decomposed into its alternating current (AC) and direct current (DC) component. While the AC signal represents the vibration feedback, the DC part furnishes information on the overall pressure applied to the contact surface. Contact geometries are sensed by 19 electrodes in the contact

area by measuring an increase of conductivity in the fluid. The thermal properties of objects are obtained by a combination of heating elements and a thermistor. A change in the temperature results in changes in the conductivity of the fluid. It also affects the electrodes responsible for contact sensing, which is why the thermistor serves as a temperature compensator as well. The electronics required for signal acquisition are integrated into the structure. It consists of an analogue to digital converter and a micro-controller unit.

3.3 Tactile sensors for underwater applications

To support operators of deep-sea manipulators with force feedback, [Dennerlein et al., 2000] developed a vibrotactile sensing system for existing two-jaw grippers. Their approach incorporates sensors in the contact region of the gripper. A vibration display is attached to the controller device used by the operator of the manipulator. Forces acting on the gripper normal and tangential to the surface are perceived by four strips of piezoelectric material integrated into silicone rubber that is placed between the original gripper surface and a metal plate. The electronic circuits for signal amplification and acquisition are mounted near the sensor itself using the oil pressure compensation of the manipulator. The working principle was verified in a pressure chamber simulating the ambient conditions at a depth of up to 4,000 m.

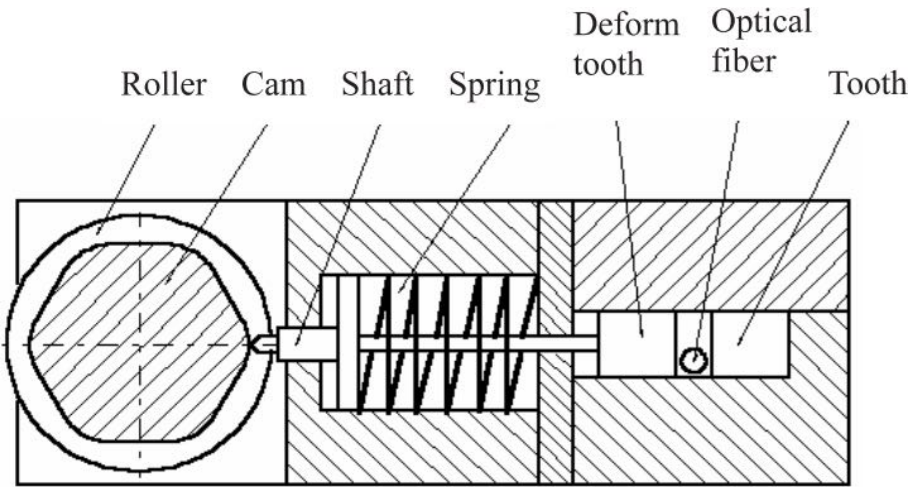


Figure 3.6: Proposed tactile sensor for sensing sliding objects based on microbending fiber-optic sensing [Tan et al., 2008]

A sensing device for perceiving sliding objects during manipulation was proposed by [Tan et al., 2008]. The designed sensor follows the concepts of microbending fiber-optic sensors [Lagakos et al., 1987]. The working principle of these sensors is based

on the modulation of a static light signal runs through an optical fiber. Sensors for perceiving temperature, acceleration as well as pressure and magnetic fields were implemented using this concept. The measurement method is applied to an underwater sensor by using a roller at the contact region (compare Figure 3.6). Movements of objects across the contact surface cause a displacement of the roller resulting in a deformation of an optical fiber leading to a measurable in the signal intensity. The authors state that when using this approach, the sensor is suitable for measuring speed and distance of objects sliding on the contact surface.

3.4 Tactile sensing processing systems

Early hardware architectures in autonomous mobile robotics systems were designed in a centralist manner. A set of processing units located in the central body handles the communication, motor control and signal processing [Nilsson, 1984]. As a result of the technological advancement of robotic components, the introduction of cascaded controllers and striving for increasing sensor data quality in terms of noise, resolution and sampling frequency, the requirements for communication bandwidth and processing load are rising. Changes in the architectural concepts became necessary. Starting with local analogue to digital conversion for sensors [Cordes et al., 1997], intelligent actuation modules [Kuwada et al., 2006] as well as local preparation of sensor data for interpretation and control, the hardware architectures of robots are shifting to decentralized topologies [Ly et al., 2004].

First attempts to implement local pre-processing for tactile sensors are reported in [Raibert and Tanner, 1982]. The authors state that the driving aspect of their approach is to reduce the impact of the wiring efforts required for addressing the sensor elements. Furthermore, local pre-processing provides an opportunity to filter, reduce and interpret the tactile information prior to sending the data to control processors. The system developed is shown in Figure 3.7.

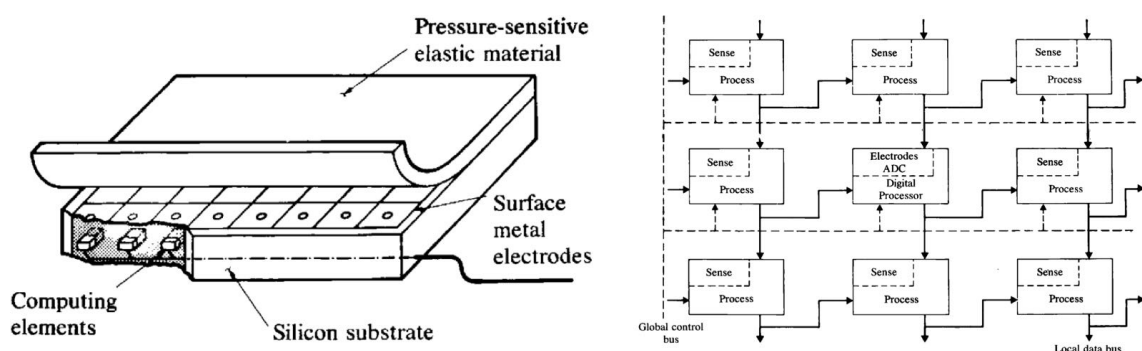


Figure 3.7: Tactile sensor in combination with a tactile sensing computer (from: [Raibert and Tanner, 1982])

Conductive plastic is used as a contact sensing material. Electrodes on the top of the designed circuit measure changes in resistance due to deformation by pressure. The sensor data is acquired in parallel for each tactile element. Besides analog to digital conversion, each cell of the designed electronics consists of additional computing elements that each allow simple calculations on the data. Bus systems enable the exchange of sensor values between neighboring processor cells. The capabilities of the system were demonstrated by implementing a 2D convolution algorithm for feature recognition running in parallel on the processor developed. The system was realized for a tactile sensor comprising an array of 6 x 3 elements with dimensions of 6.1 x 4.8 mm.

The authors of [Odeberg, 1995] use embedded systems in the processing chain between the sensors and a central processing unit to pre-process the data and transmit high-level information to the host on request. The system setup consists of a micro-controller acquiring the sensor data from a tactile sensor array. Overall contact force and the center of pressure as well as the circumference of the contact area are pre-calculated for transmission to upstream devices. Algorithms having runtime complexities suitable for efficient computation on processors with limited operating speed and memory were therefore developed.

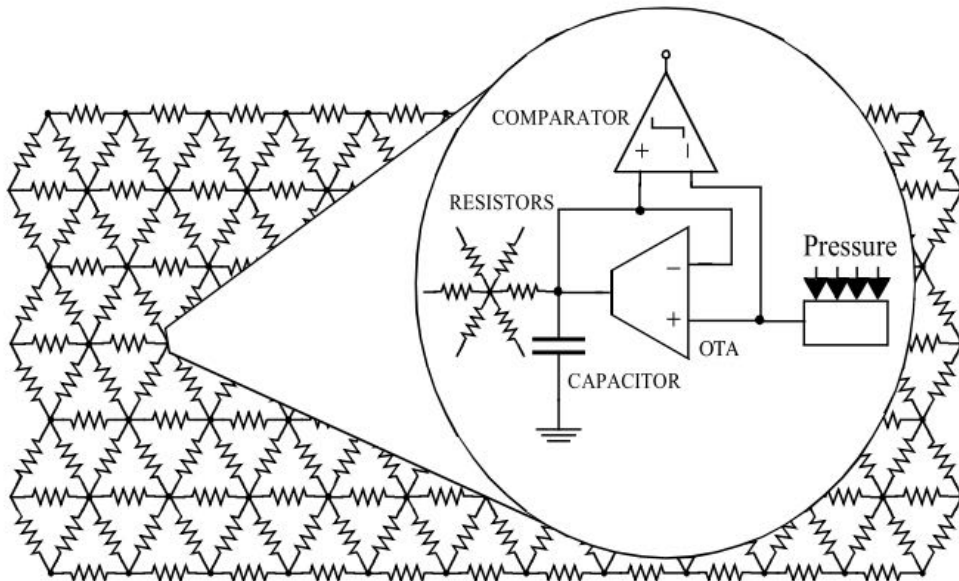


Figure 3.8: Architectural concept for a tactile retina for the detection of slipping objects (from: [Maldonado-López et al., 2006])

The challenges faced due to increasing array sizes of tactile sensors and computation complexity are also the motivation behind the work discussed in [Maldonado-López et al., 2006]. The inspiration of the approach chosen for local pre-

processing comes from research on the encoding of signals from the human retina. As the data coming from a tactile array can be interpreted as an image, approaches from image processing can be applied. Thus, a system for detecting slippage on the tactile sensors based on a motion detection algorithm is proposed. The implementation concept is depicted in Figure 3.8. The details of the processing circuit for a single tactile element are highlighted in the circular window. The network of resistors makes it possible to take into account the voltage levels of neighboring tactile elements resulting in the computation of a spatio-temporal average. Combined with the pressure-dependent voltage coming from the sensor array, this circuit enables operation under varying levels of ambient pressure. The detection of slippage itself is achieved by integrating the capacitor which introduces a time delay. The circuit of the resistor network in combination with the capacitor thus implements a spatio-temporal high-pass filter. Adaptation of the sensitivity of the circuit to certain frequency ranges is achieved by dimensioning the capacitor and the operational transconductance amplifier (OTA). The whole approach was realized in an application specific integrated circuit (ASIC) having 16 units for processing the data of tactile elements. Through the use of analog electric parts the system runs with optimal reaction times regardless of any sampling frequency or system speed.

[Cannata and Maggiali, 2006] have developed a system that pre-processes the sensor information acquired from a force-torque sensor and a tactile sensor array. Both sensors were developed for integration into the MAC hand. In order to keep the load of the CAN bus system low, the center of pressure and ellipsoid approximating the contact region are pre-computed based on the tactile array sensor information.

The work in [Ciobanu et al., 2013] presents a tactile pre-processing pipeline that prepares sensor data coming from a BioTac tactile sensor system presented in section 3.2. Parasitic influences resulting from ambient conditions generated by the robotic system itself or caused by the combination of chosen measurement principles require processing of the sensor data prior to interpretation. The authors therefore developed modules for noise filtering and algorithms compensating the effects of drift, gravity and motor vibration. Based on the processed information, tactile maps are generated that are additionally used to estimate incoming forces and the contact location. The proposed system was implemented on a standard PC using the Robot Operating System (ROS).

3.5 Manipulators with tactile feedback

A variety of modules for tactile sensing and approaches for processing the tactile data can be found in relevant literature. Developments of end-effectors that have tactile sensors incorporated are rather rare. This section presents highlights from

the state of the art grippers for applications on land. The presentation focuses on the way sensors for perceiving the sense of touch have been integrated. Gripper systems applicable for usage under water are shown in the section that follows.

3.5.1 Land-based robotic end-effectors

Gifu Hand III [Mouri et al., 2002] is a five-fingered anthropomorphic hand with 16 degrees of freedom. The inner structure of the finger elements contains the actuation modules, which is why the tactile sensors were placed on top of the structure of the manipulator (compare Figure 3.9 on the left).

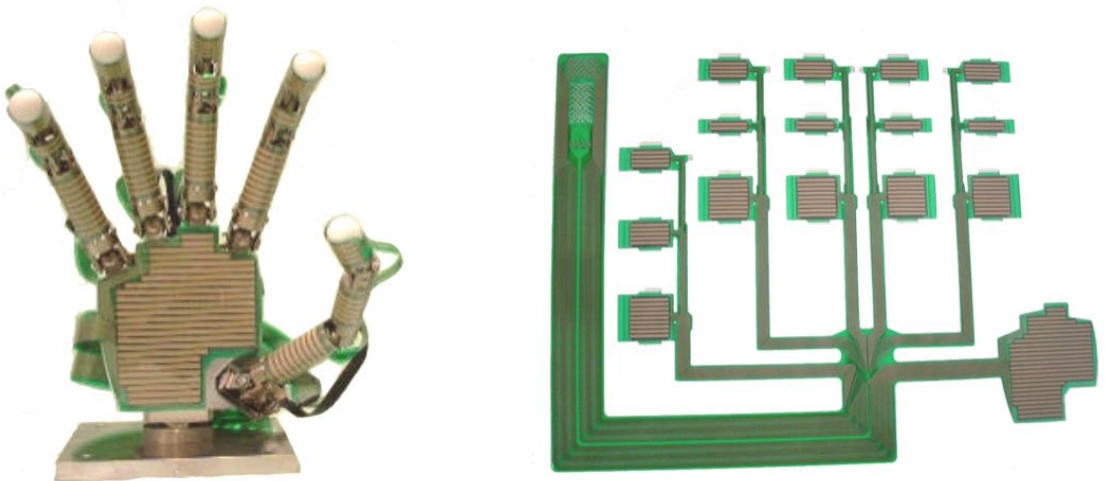


Figure 3.9: Assembled Gifu Hand 3 (left), structure of the tactile sensor module (right) (from: [Mouri et al., 2002])

The tactile sensor system is built on a single structure made of thin plastic film. The flexible base material allows bending of the sensor to follow the shape of the finger modules of the gripper. The measurement principle is based on force sensing resistor technology. Sensor data acquisition and processing are handled on a PC outside the gripper system. The total number of sensor elements of the tactile sensing system is 859. While the demonstrated approach is easy to maintain in terms of replacing the sensor, its interconnections and the sensor itself are prone to damage during manipulation.

One of the most highly integrated robotic hands even today is the DLR/HIT Hand 2 System [Liu et al., 2008]. This five-fingered system comprises 15 degrees of freedom, the hardware architecture consists of one digital signal processor (DSP) and one field programmable gate array (FPGA) in each finger. Another FPGA is integrated into the palm of the hand. A cross-sectional view of the finger structure of DLR/HIT Hand 2 is depicted in Figure 3.10.

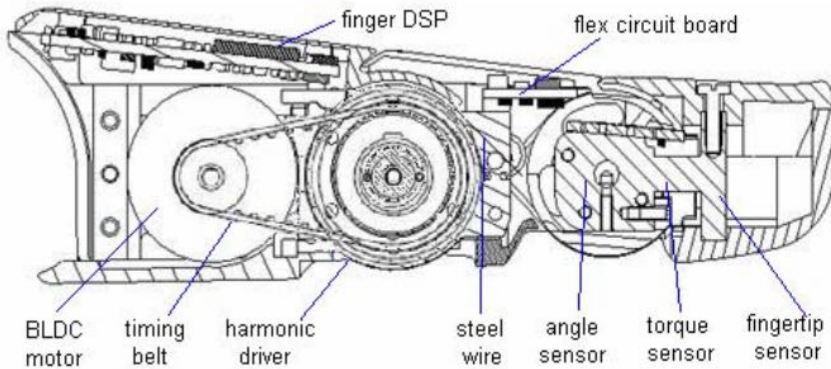


Figure 3.10: Cross-sectional view of the finger structure of the DLR/HIT Hand 2 (from: [Liu et al., 2008])

As can be seen, the space within the open skeleton structure of the gripper is mainly occupied by the actuation modules and electronics. A tactile sensor array was not integrated within the finger structure, a force-torque sensor placed in the fingertip (referred to as fingertip sensor in the figure) enables the application of intrinsic tactile sensing [Bicchi, 1990]. Multi-contact points cannot be differentiated using this approach.

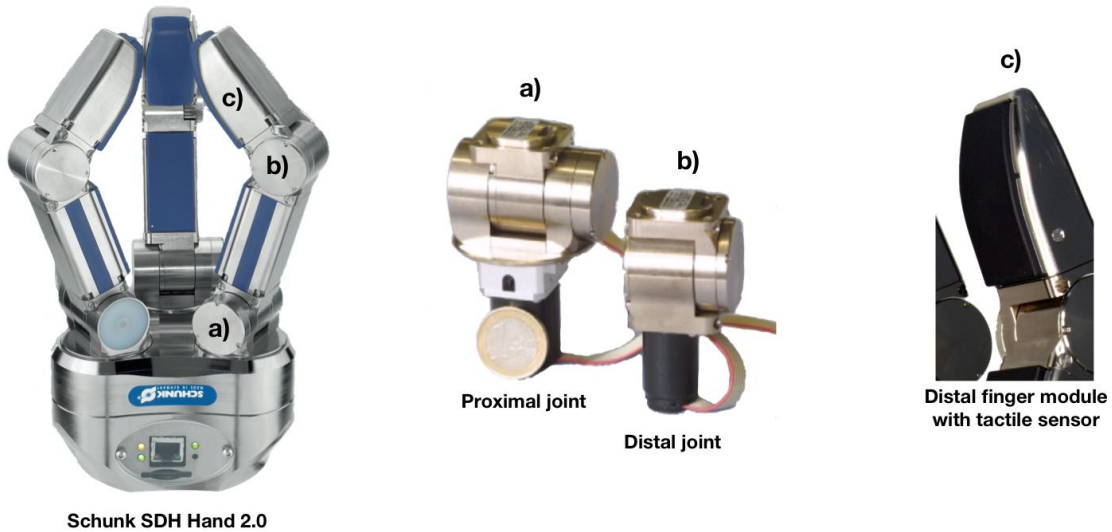


Figure 3.11: Schunk Dexterous Hand 2.0 (left), details of the actuation modules in the joints (center), tactile sensing module in the distal finger elements (with material from: [Schunk GmbH & Co. KG, 2008] and [Weiss Robotics GmbH & Co. KG, 2009])

A three-fingered gripper system with tactile feedback for industrial applications was developed by the company Schunk. The gripper has seven degrees of freedom,

each finger element can be equipped with a tactile sensor element. The tactile sensing modules consist of the force sensing unit based on a resistive measurement principle using a polymer with immersed conductive particles [Weiss and Wörn, 2005] and the acquisition electronics. A skin made of silicone protects the sensor material. The gripper is shown in Figure 3.11. The integrated sensing modules are curved in one dimension, the overall height of the sensing module of about 5 mm [Weiss Robotics GmbH & Co. KG, 2009] allows integration in the limited area between the joints which is partly occupied by the actuation modules (compare Figure 3.11 b) and c)).

3.5.2 Robotic grippers for underwater applications

A commonly used manipulation system for industrial and research applications under water is the Orion 7 deep-sea manipulator manufactured by Schilling Robotics.



Figure 3.12: Example of a standard manipulation arm used in the deep-sea

The manipulator is depicted in Figure 3.12. It is rated for depths of up to 6,000 m and is actuated in seven degrees of freedom using hydraulics. Potentiometers in the joints acquire the position of the joints. It can be either configured for position or rate control. The gripping force in the claw reaches forces of up to 4,448 N, weights of 68 kg can be lifted at full extension of the arm.

The following robotic grippers represent the state of the art in underwater manipulation systems with tactile feedback. All systems presented are prototype implementations of dexterous end-effectors.

The motivation for development of the AMADEUS dexterous sub-sea hand presented in [Lane et al., 1997] is to prevent damage to grasped objects occurring through excessive contact forces in traditional jaw gripper systems. The gripper is actuated by three cylindrical metal bellows in each finger structure elongating in the longitudinal direction with increasing supply pressure. This configuration makes it possible to tune the grasping pose during manipulation tasks. The maximum force exerted on the fingertips of the gripper is reported to be 15.45 N. The gripper design is shown in Figure 3.13.

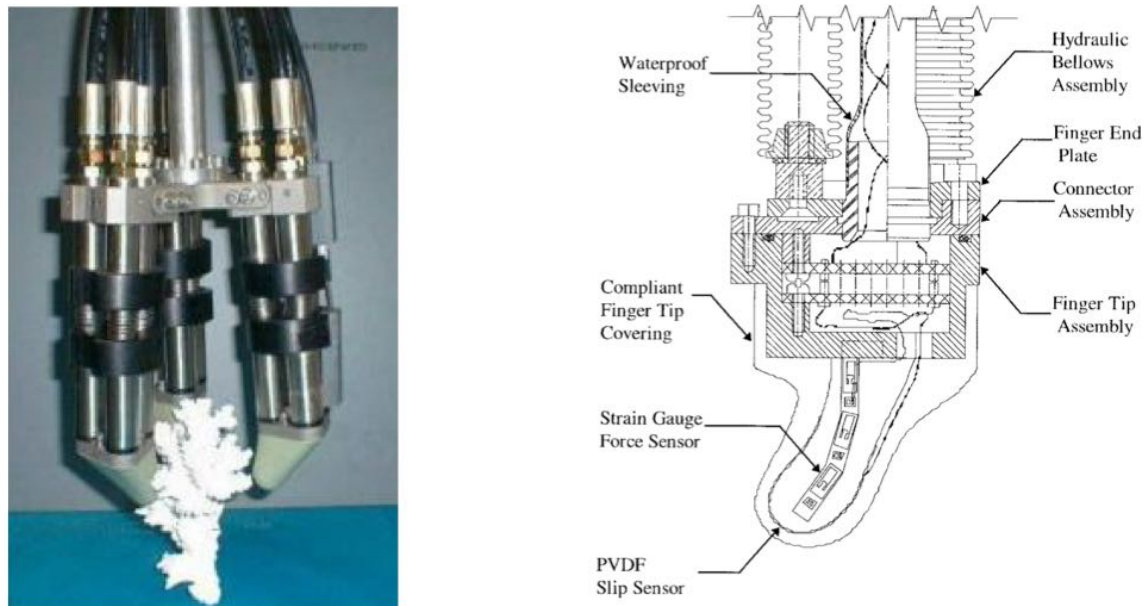


Figure 3.13: Morphology of the AMADEUS dexterous gripper (left) and finger structure (right) (from: [Lane et al., 1997])

The gripper's fingertips are equipped with sensors to detect force and slippage. Twelve strain gauges are placed in the contact region of the fingertip (compare Figure 3.13 on the right). Assuming point contact, the incoming force can be calculated and its components in the x,y and z dimension can be derived. In order to detect slipping objects, a layer of PVDF material is applied to the inner structure of the fingertip. As this material exhibits piezoelectric properties, algorithms for monitoring the excitation of the sensor were implemented to register occurring slip. The wiring for the sensors is put in pressurized housings, keeping water contact and the ambient pressure away from the components. The sensors themselves are covered with silicone rubber to increase their robustness during manipulation. The position of the finger base is measured by using potentiometers assembled in oil filled casings. Sensors for perceiving the position of the fingertip were not integrated. The authors state that the designed tactile system is suitable for perceiving point contacts as they oc-

cur during precision grasps. A sensor array solution for sensing force and slip during surface contact that is acting independent of the ambient pressure was not identified. All electronics for signal conversion and the sensor processing are integrated into standard PCs placed outside of the gripper under normal pressure.

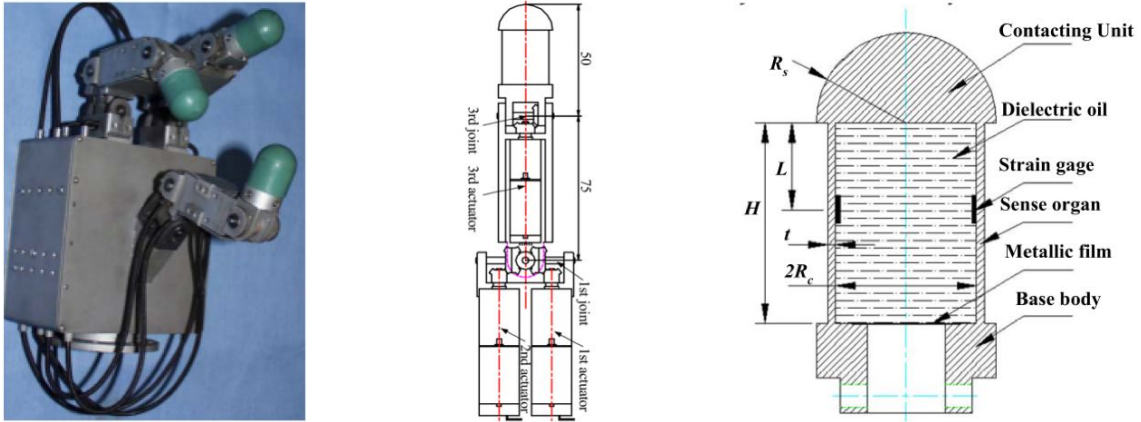


Figure 3.14: Structure of the Heu Hand II gripper (left), cross-sectional view of a finger (center) and fingertip structure (right) (from: [Meng et al., 2006])

A gripper system that can be used as a tool grasped by the jaw gripper of standard manipulators for deep-sea applications is described in [Meng et al., 2006]. The system comprises three fingers, each having three joints. The setup is shown in Figure 3.14. Brushed DC motors are used for actuation. The motors are placed within the limb structure of the gripper. Twelve strain-gauge sensors integrated in the distal limb of each finger make it possible to calculate forces and moments exerted on the fingertip module. The electronics for analog to digital conversion as well as for the motor actuation are integrated into a pressurized housing at the finger base that protects the electronic parts from the ambient pressure.

An end-effector with touch sensing capabilities for use on an autonomous underwater vehicle (AUV) is discussed in [Bemfica et al., 2014]. The gripper is designed as a three-fingered system with each finger having two degrees of freedom. The two outer fingers are rotatable around the gripper base. The assembled system is shown in Figure 3.15 on the left. Each finger is actuated by a tendon mechanism driven by a brushed DC motor that is integrated in the gripper base. This setup enables each finger to exert a force of up to 150 N during continuous operation.

A force-torque sensing system based on an optical measurement principle [Palli et al., 2014] is installed in the fingertips. The working principle of the sensor is depicted in Figure 3.16. It consists of a light-emitting diode (LED), a skin, a mirror and photodetectors. The LED emits light onto the mirror that is connected with the inside of the skin. The light is reflected by the mirror. Eight photodetectors

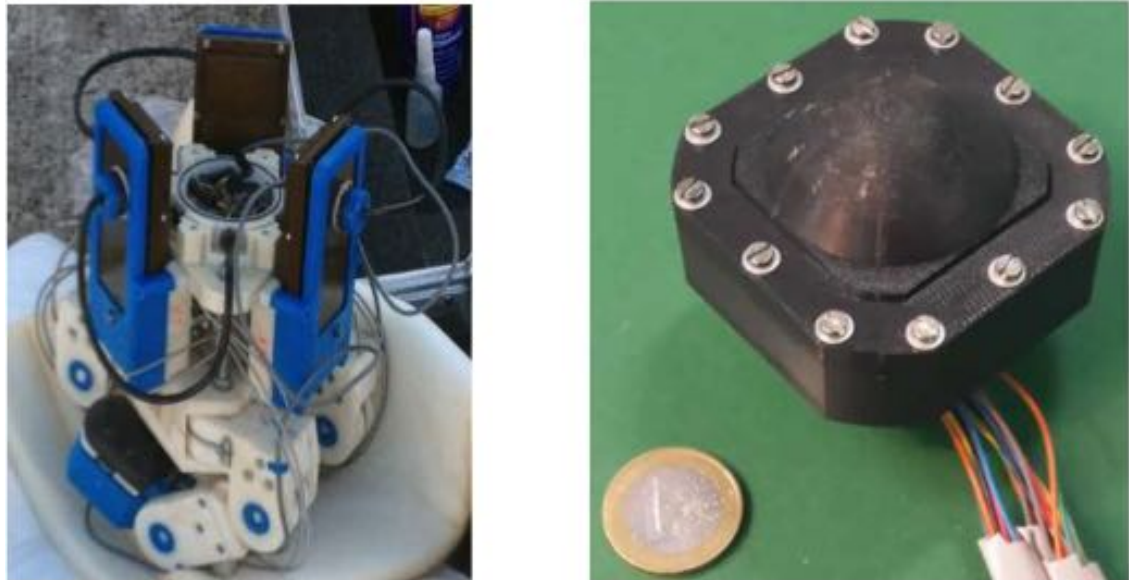


Figure 3.15: Structure of the gripper (left), details of the tactile sensor (right), from: [Palli et al., 2014]

(PD) are aligned around the LED, capturing the light that is reflected by the mirror. Depending on the deflection of the skin and the corresponding movement of the mirror, changes in light intensity are recognized by the photodetectors. These changes can be used to calculate the forces and torques acting on the sensor.

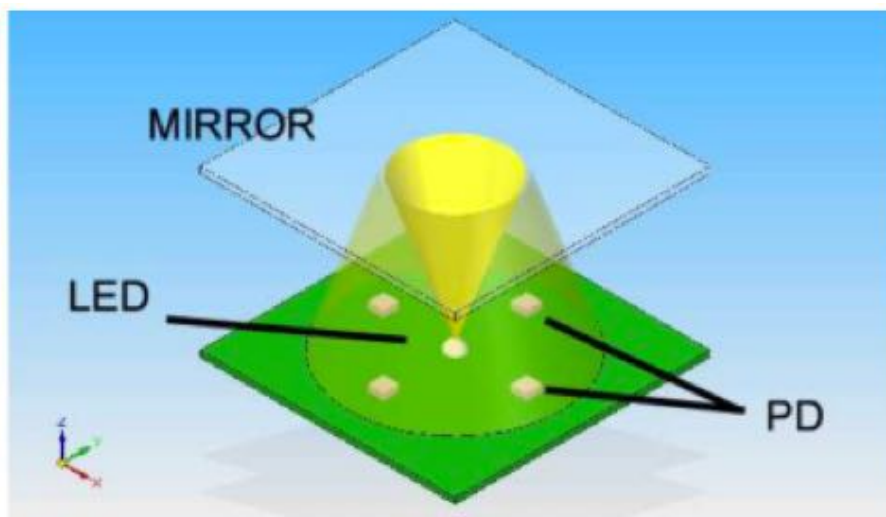


Figure 3.16: Measurement principle of the optical force-torque sensor (from: [Palli et al., 2014])

This measurement principle is based on the reflection of light within a cavity filled with air under normal pressure. With increasing ambient pressure the cavity

is compressed. This effect requires a recalibration of the sensor at different depths. The sensing principle only works until compression by the surrounding water column leads to a collapse of the cavity. The system was tested at depths of 25 m.

3.6 Discussion

The human hand as an archetype for tactile sensing in robotics

The human hand is equipped with an overwhelming number of mechanoreceptors that support the sense of touch. The number of mechanoreceptors in the glabrous skin alone is estimated to be around 17,000 units [Lederman, 1991]. The findings that have been obtained by the trials to replicate the full dexterous capabilities of the human hand are also valid for the sense of touch: the gap between biomechanical systems and the implementation of technical systems is currently too large to be able to plainly copy the human hand [Grebenstein et al., 2012]. The question whether the mechanical capabilities as well as the sensing density of the human hand should be taken as a model for achieving dexterous manipulation in robotics is a subject of discussion. Considering the application scenario that is addressed in this thesis, humans are able to interact with objects under limited visibility solely by using modalities of touch in the hand. These modalities are therefore considered to be a valid functional model for the integration of the sense of touch in robotic systems.

Using this insight as a starting point, sensing requirements have to be defined to replicate the multi-modal nature of touch-sensing in humans. The exploration of unknown objects places high demands on the sensing capabilities since every property that can be perceived by touch supports the generation of knowledge. The exploration steps found in humans during object exploration can therefore be used to define sensing requirements. Selected measurement principles that meet the requirements have to be evaluated with regard to application in deep-sea environments.

Advantages of multi-modal sensing

Further aspects support a design of the sensing system that combines several modalities of touch. One reason is the assumption that the derivation of tactile properties from a single sensor results in less confidence and quality of the sensor data compared to a system where ideal measurement principles for each modality are used. This observation is also supported by findings of other researchers, e.g. [Tegin and Wikander, 2005], [Arg, 2010], [Mittendorfer and Cheng, 2011].

The approach of including different sensors in the contact region of robotic systems poses challenges in terms of integration as several sensors have to be placed and electrically interfaced in the same area without interfering each other. On the

processing side, the approach of using ideally suited measurement principles for perceiving the modalities of touch leads to a simplification of the sensor processing as the mathematical operations to derive them can be omitted. The approach has some similarities to the architectural concepts of polling versus interrupts used in communication with sensors and its processing. Deriving the information from a sensor that is not primarily sensitive to the required property is like polling a sensor by continuously computing the desired property and analyzing it. A sensor that is sensitive to the desired property is triggered only in cases where relevant information of this property of contact is perceived. Further computation is therefore only needed in cases where there is actually relevant sensor feedback.

Benefits of local pre-processing

Another aspect that was presented is the way tactile data should be processed. Starting with small sensor patches [Raibert and Tanner, 1982], increasing the spatial dimensions, densities, resolution and dynamic response is one of the driving aspects in the development of tactile sensors. All these technical improvements produce the volume of data that needs to be processed. Following the approach of hardware architectures for robots that use a single central processing unit, there are increasing requirements on the communication side as well as in terms of computing power. Distributing the processing load within the robotic system via local pre-processing reduces the effects of increasing data volumes. By transmitting processed high-level information to upstream processing units, communication bandwidth as well as processing power for high-level computing can be saved for other tasks. Approaches to implementing such a decentralized processing architecture for tactile sensors are discussed in section 3.4.

The required information for locally controlling behavior during manipulation or exploration becomes available by extending the proposed approaches from local signal pre-processing to signal analysis. Following the definition of [Alexiou et al., 2010] where distributed decision-making is regarded as one of the key features for implementing complex systems, the ability to react to tactile events without the requirement to include upstream processing units supports this approach.

State of underwater grippers with tactile sensing

Concerning the application of tactile sensing in the underwater domain, the integration density with respect to sensors and electronic processing is low compared to their counterparts for land-based applications. Developments like multi-modal sensing and local pre-processing have not been introduced yet. Only little information on depth rating can be found in relevant literature for state-of-the-art underwater manipulators with tactile sensing. It can be concluded that research activities have

focused on the application of tactile sensors under conditions involving direct contact with water. Deep-sea regions have thus not been reached so far. Reasons for this can be found in the demanding ambient conditions and the related efforts to integrate sensors as well as electrical components into robotic end-effectors.

Chapter 4

System Design

The required sensing capabilities are summarized and suitable measurement principles are presented for each of them based on the conclusions derived from the observations made by studying the state of the art. The selection of each sensing modality is geared to its applicability in deep-sea conditions.

In addition to the identified measurement principles, it is important to develop suitable electronics to acquire and process the sensor data. The designed electronics to implement decentralized hardware architecture for local pre-processing is therefore presented.

Further driving aspects regarding the design of a sensor system and its processing hardware include the way the sensors and their processing electronics are integrated into a gripper structure. A look at the gripper systems presented in the section on the state of the art reveals that many robotic end-effectors have limited space available in the limb structures for placing sensors that measure contact properties. As the tactile system discussed here is developed along with a fine manipulation system for deep-sea application, the integration of contact sensing technology was emphasized during the development process. The first sections in this chapter present the mechanical design considerations for realization of the gripper. Further details on the gripper development can be found in [Lemburg et al., 2011] and [Kampmann and Kirchner, 2015].

The findings made during the system design are summarized in the discussion in this chapter.

4.1 Mechanical concept

The mechanical concept of a robotic system is influenced by requirements regarding the application and integration of components. Finding a solution for the mechanical structure can be regarded as an iterative process where the competing integration requirements are balanced. The following sections describe the decisions made in

terms of the morphology of the gripper and the actuation concept.

4.1.1 Morphology

While designing the morphology for a robot end-effector, the limb dimensions as well as the number and types of degrees of freedom are oriented to the task for which the manipulator is developed.

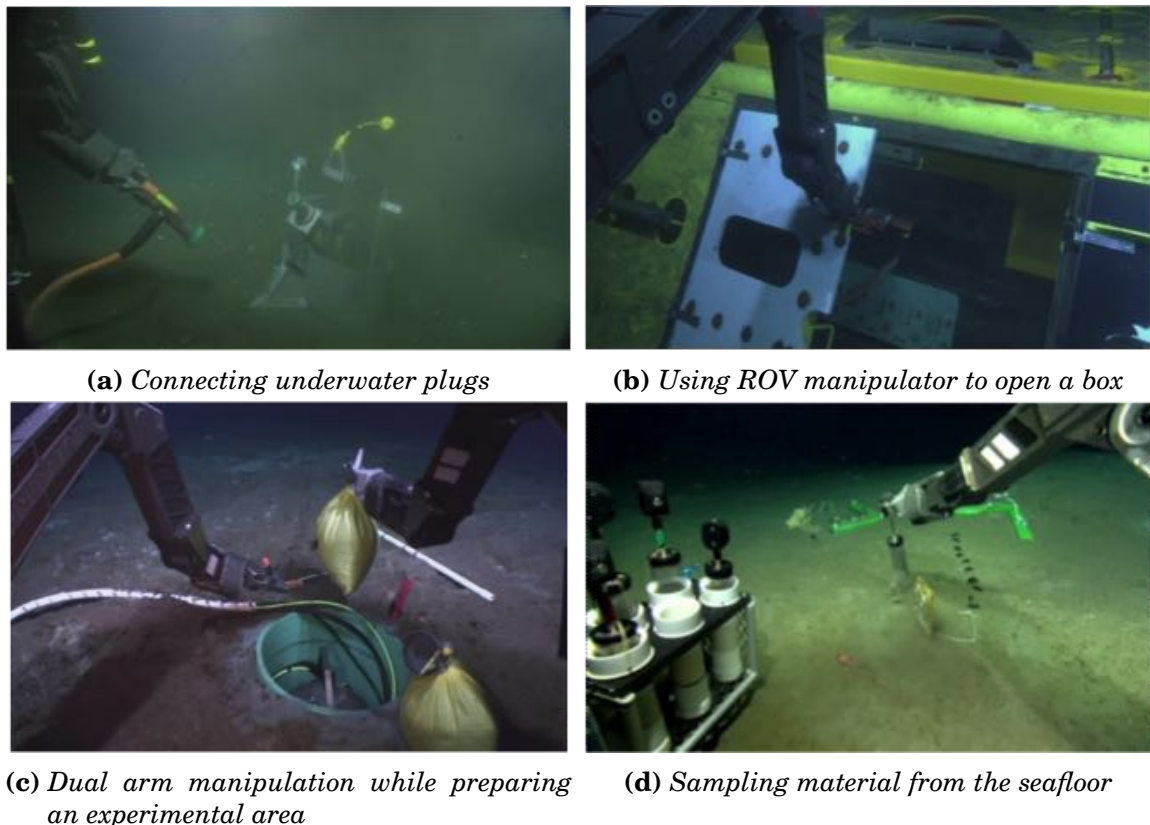


Figure 4.1: Summary of underwater manipulation tasks performed in the scientific domain using a jaw gripper (images courtesy of: [Ocean Networks Canada, 2014])

Examples of underwater manipulation tasks performed in research missions are shown in Figure 4.1. [Jun et al., 2008] and [Bahleda, 2002] describe the tasks performed by manipulators in industrial applications as drilling and cutting and removal of aquatic growth. In [Bai and Bai, 2012] manipulators are reported to be used for handling plugs and assembling deep-sea construction sites in the oil and gas industry. Although these operations are probably feasible with less dexterous end-effectors than the ones mentioned with regard to scientific missions, in unstructured situations like the disaster recovery of Deepwater Horizon oil spill in 2010 the manipulation tasks become increasingly complex. An example of the tasks during

the trials to close the blowout prevention system (BOP) is shown in Figure 4.2. Here, a deep-sea manipulator arm attached to an ROV is used to turn a socket wrench so as to initiate the closure of the BOP manually. This operation, which can be compared to a peg-in-a-hole task, is complex, especially without force feedback and depth information.



Figure 4.2: Peg-in-a-hole task ROV intervention during the Deepwater Horizon incident (image Source: U.S. Coastguard)

It can be observed that the described operations are versatile in terms of manipulation as well as with regard to size and geometry of the handled objects. Many of the tasks were originally performed by divers. As construction sites shift to greater depths, this is not feasible anymore. Thus, it can be expected that the variety and complexity of tasks in robotic manipulation will increase in the future.

Consequently, the end-effectors of ROVs can be seen as a replacement of the manipulation capabilities of divers in the deep sea. The diagram depicted in Figure 4.3 shows the types of grasp that can be realized by the human hand depending on the number of fingers used for the grasp.

The capabilities using a tetradigital or pentadigital grasp mostly differ in the size of the objects compared to the human hand. More than three fingers are mostly used in grasps where additional stabilization is advantageous or where the grasped object is too big to be grasped with three fingers. In technical systems the size limitation can be coped with by adapting the dimensions of the fingers. As the number of grasp types realizable with a robotic gripper rises, its mechanical and control complexity

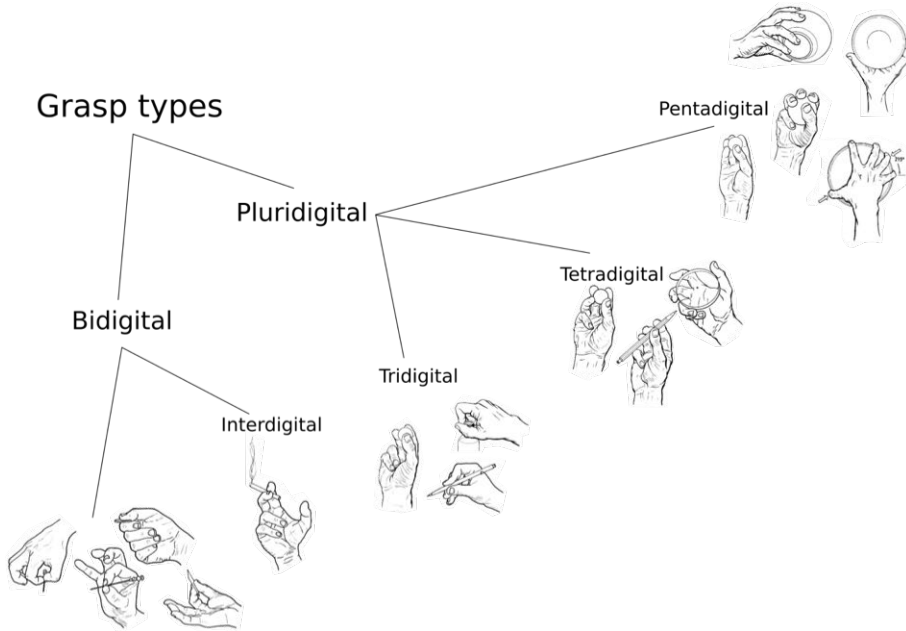


Figure 4.3: Taxonomy of grasp types of the human hand (from [Kapandji, 2007])

increases as well [Feix et al., 2009].

By adapting the finger dimensions of the gripper design to the robot's operational area and making a compromise between the number of feasible grasps and the robustness and ease of control, implementation of the gripper as a three-fingered symmetric system results in a multifunctional robot end-effector suitable for a variety of manipulation tasks. The symmetry of the gripper results in a design with two opposable thumbs which compensate for the additional degrees of freedom in the basal joints of the human hand. According to [Kapandji, 2007], the types of grasp that can be obtained through this design are: tweezer grasp between the two thumbs and between one thumb and the middle finger, a tridigital grasp as well as a palmar grasp.

Notably, industrial divers in the usually cold working environment offshore are also limited to using three fingers based on the gloves they are using (compare Figure 4.4). These gloves are designed for maintaining the body temperature longer by reducing the contact area.

To ensure optimal form closure when in touch with objects, as many limbs as possible are desirable to ideally adapt to the object's geometry. A biological archetype for this approach is the tentacles of an octopus arm, which is capable of adapting its shape to various kinds of structures. Gripper systems in which the finger elements are designed based on the fin-ray effect [Wegener, 2007] are technical implementations with ideal form closure. A drawback of this design is the complex acquisition of contact forces on the gripper surface since the bending of the fin-ray structure has therefore to be measured. An alternative approach to form closure is to integrate as



Figure 4.4: A three-fingered glove for industrial divers working offshore

many limbs into each finger module as possible. As the complexity to control the system and the weight of the gripper increases with every joint and the force exertable with every limb decreases, this approach is not favorable.

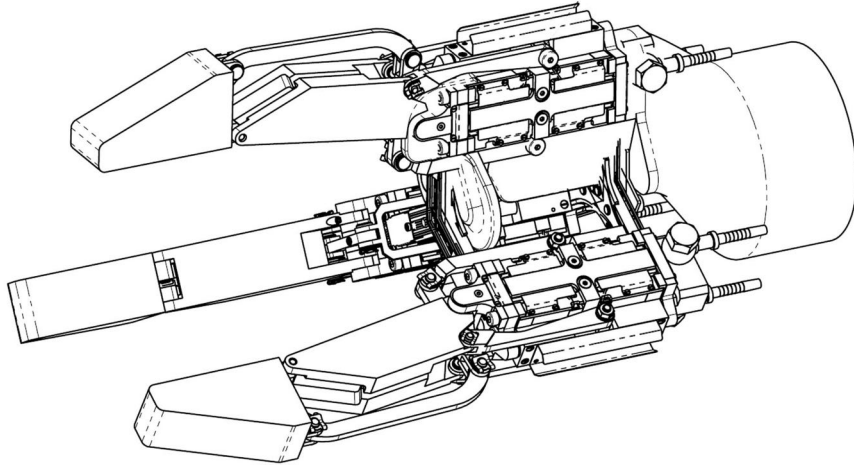


Figure 4.5: Morphology of the designed gripper

As a compromise between force closure and form closure, the developed gripper is designed using two limbs for every finger module. In summary, the system comprises 7 degrees of freedom (DoF): each of the three fingers has two independently controllable limbs, the opposable thumbs are coupled in their motion. The resulting morphology of the gripper is depicted in Figure 4.5. Possible grasp configurations that can be achieved with the design are parallel grasp, tweezer grasp and an ar-

rangement of the fingers at equal distances of 120° .

4.1.2 Actuation

Careful placement of the actuators and selection of the method of force transmission to the joints are necessary as this affects the remaining space for integration of sensors and processing electronics. Integrating the actuators directly at the joints results in a compact actuation design [Liu et al., 2008], but leaves little integration space for tactile array sensors. By pursuing an open-skeleton approach and placing the actuation at the base of the hand [Cannata and Maggiali, 2006], the contact area of the end-effectors remains free for integration of tactile sensors. A solution based on cantilevers is selected for force transmission from the base of the hand. This way of transmitting the forces to the joints does not require further integration space in the limb structure. Compared to other options like tendon driven force transmission, this approach is also more resistant to dirt and abrasion. A solution where the tendons run within the structure of the gripper is not feasible as it influences the integration space in the limb structure, which is reserved for tactile sensing and processing.

Selecting the actuation principle itself is another design criterion. The underwater grippers presented in section 3 use either DC motors or hydraulics. To be compatible to commercial deep-sea manipulator arms powered by hydraulics, this was chosen as the main actuation principle. By using hydraulics, the gripper can be directly attached to the hydraulic circuit of a manipulator arm by replacing the standard jaw gripper end-effector.

Servo valves are commonly used actuation modules in hydraulic deep-sea manipulators like the Orion 7P from Schilling Robotics. Integrating such modules for every controllable degree of freedom in the gripper results in a bulky setup, which is why this approach was not chosen. Instead, micro solenoid valves were selected. These devices, originating from biotechnology were integrated into the base of each finger using a cantilever as the force transmission to the joints. A comparison of the dimensions of these valves is given in Figure 4.6.

A section view of the micro solenoid valves is depicted in Figure 4.7. By applying voltage to the valve coils, a magnetic field is generated. The generated field causes the mobile anchor to be drawn towards the stationary anchor, inducing the valve to open. By removing the applied voltage, the closing spring pushes the mobile anchor back into the closing position.

At a maximum operating pressure of 50 bar these valves function at pressure levels four times smaller than the usual supply pressure of industrial deep-sea manipulators, which operate at around 200 bar. At these pressure levels the piston of the chosen valves do not allow any fluid transfer as the magnetic field of the coils is



Figure 4.6: Comparison of standard hydraulic valves for deep-sea manipulators (front) and the selected micro solenoid valves (back)

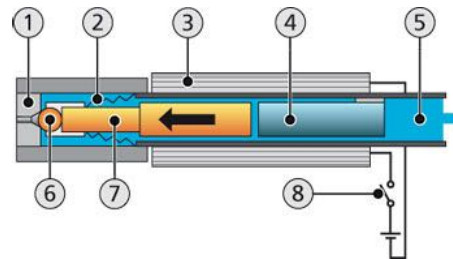


Figure 4.7: Section view of micro solenoid valves. 1: Valve seat, valve nozzle; 2: Closing spring; 3: Valve coil; 4: Stationary anchor; 5: Medium; 6: Valve ball; 7: Mobile anchor; 8: Switch (Source: [Fritz Gyger AG, J])

not strong enough to open the valves. To lower the supply pressure for the gripper, a pressure reducer was incorporated into the hydraulic circuit of the gripper.

To actuate one degree of freedom in the end-effector, four micro solenoid valves are combined into a hydraulic circuit as depicted in Figure 4.8. To move the piston forward and backward, two valves work together pushing and pulling the hydraulic fluid to and from the piston, resulting in a corresponding movement.

The described hydraulic circuit is implemented for the movements of the finger limbs. In total, 24 valves are integrated. Hydraulic pistons for rotary movements are more difficult to design and require considerable integration space. To overcome this and to evaluate the usability of DC motors in deep-sea, a brushless DC motor was selected for performing the rotary movements needed to rotate the opposable

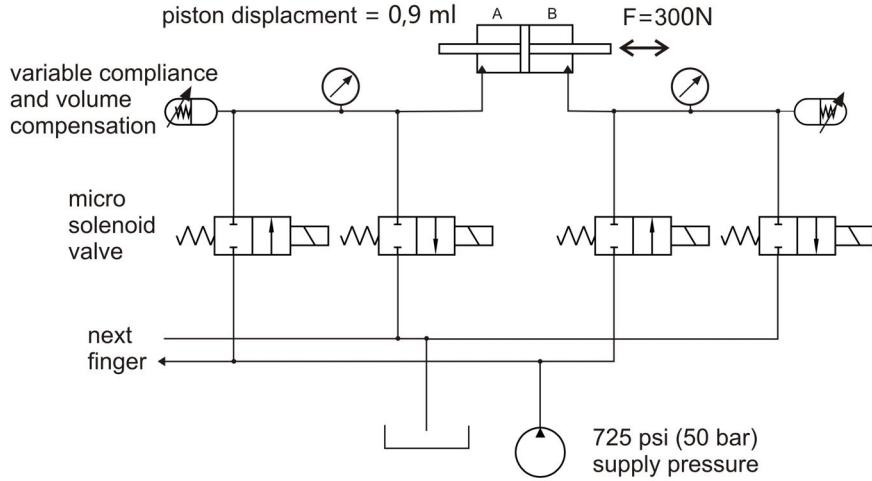


Figure 4.8: Hydraulic circuit in the finger modules of the gripper for one DoF [Lemburg et al., 2011]

thumbs.

Further details regarding the development of the hydraulic actuation as well as experimental results on the performance can be found in [Lemburg et al., 2011].

4.2 Required sensing capabilities

As for the mechanical design, the required sensing capabilities of a robotic system depend on the task to be performed. Within the scope of the developed system, a general purpose manipulation tool is envisioned that is able to support manipulation tasks in the deep sea in cases of limited visibility. The touch sensing capabilities of the manipulator are required to sense as many aspects of contact as possible. The task can be compared to the tactile exploration procedures used by humans to gain knowledge about unknown objects by touch as presented in section 3.1.2.

The properties of contact that are derived to implement the presented exploration procedures by means of robots are shown in Figure 4.9. During manipulation tasks the mechanical properties of contact are the most interesting [Tegin and Wikander, 2005]. The thermal aspects of touch sensing will not be covered here. An analysis of the required sensing capabilities points out the influence of the manipulator pose in every exploration step. Tactile perception is not limited to exteroceptive information, but also requires proprioceptive data from the joints of the end-effector and its manipulator. Furthermore, the dexterity of the manipulation system also influences the performance of tactile exploration.

The design decision to rely on sensor feedback from several measurement principles for the acquisition of contact information can be refined at this point. Measuring

				
	Array static sensing	Dynamic sensing	Absolute force	Manipulator pose
Material hardness			X	X
Texture		X		X
Global shape				X
Exact shape	X		X	X
Weight			X	X
Part motion test	X	X	X	X
Function test	X	X	X	X

Figure 4.9: Derived sensing capabilities for implementing exploration tasks

the overall force-torque that acts on the contact surface by means of a dedicated force-torque sensor is of advantage in comparison to a summation of the feedback from array sensor elements. It allows the perception of all incoming force and torques and minimizes the calibration efforts of many sensor elements to a few sensors. High-frequency sampling of sensing modalities that are sensitive to dynamic impacts support the identification of slipping objects and make it possible to distinguish texture properties of objects. To perceive the geometries of contact, an array sensing solution that acquires static contact rounds off the sensors for contact sensing. Compared to a solution specialized solely in dynamic impacts, static contact forces do not need to be computed from the sensor signal as these parts of the signal cease over time. The same is true for the other way round: relying purely on static contact sensing using a sensor array requires constant computation of moving objects and monitoring of the contact distribution. Integration of measurement modalities separately sensitive to static and dynamic properties of touch is therefore desirable.

The following sections discuss implementation of the determined sensing capabilities in measurement principles that are applicable for usage in deep-sea conditions.

4.3 Sensing absolute overall force and torque

The benefits of choosing a single point sensor for measuring overall force and torque are addressed in the introduction of this chapter. Although usage of the force sensing array reduces the number of sensors to be integrated, this approach requires precise absolute calibration of each sensor element of the respective array. Depending on the number of sensor elements in the array and the chosen measurement principle, this is considered to be time-consuming and unreliable as parasitic influences on the

measurement principle necessitate constant recalibration.

A single sensing element for measuring the overall weight is easier to calibrate and one can expect that a force sensing array can still be used to perceive qualitative force distribution information without precise absolute calibration.

A commonly applied solution for measuring absolute forces and torques is to use strain gauge sensors. The measurement principle is based on piezoresistivity, a change in material length leads to a change in electric resistance. Commonly used materials that exhibit this effect are an alloy of copper and nickel, platinum alloys and silicon. Strain gauges for sensing forces and torques combined into a single device are called a force-torque sensor. The influences of ambient pressure induced by the water column have to be analyzed in a macroscopic view of all sensor elements in a force-torque sensor and for each strain gauge.

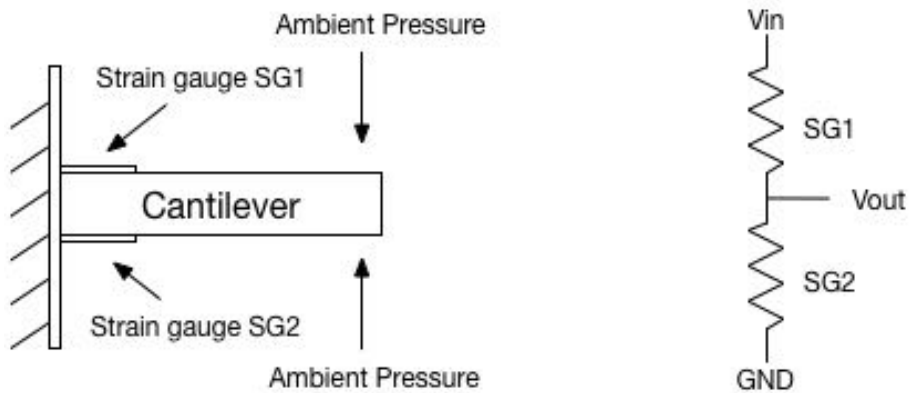


Figure 4.10: Typical measurement setup (left); electric circuit for strain gauges in force-torque sensor (right)

Figure 4.10 shows on the left a typical application of a strain gauge for measuring forces on a cantilever. An incoming and non-uniformly distributed force results in a deflection of the cantilever. Depending on the force direction, an elongation or compression of the strain gauge can be observed. In the event of a uniformly surrounding pressure, as it is the case when applied in the water column, a deflection of the cantilever does not occur.

Examining the influences of ambient pressure for a single strain gauge sensor requires more detail about the specific setup used in the force-torque sensor. In the case described here, the nano25 - a force-torque sensor from ATI - was chosen. This force-torque sensor is equipped with silicon strain gauge sensors. According to the hardware manual of these force-torque sensors [ATI Industrial Automation, 2013] the change in resistance for a single strain-gauge can be computed as:

$$\Delta R = S_a \cdot R_o \cdot \epsilon \quad (4.1)$$

S_a denotes the gauge factor, R_o represents the resistance of the strain gauge without applied strain and the strain applied to the sensor is given by ϵ . The only factor that is varying while a load is applied to the sensor is ϵ , which is defined as the quotient of the relative change in length Δl and the original length l :

$$\epsilon = \frac{\Delta l}{l} \quad (4.2)$$

An examination of this equation with regard to the influence of a uniform load applied by the water column shows that a change in length can only occur in the case where the sensor manufacturing process leads to gas inclusions in the sensor. In the case of silicon strain gauge sensors manufactured using microelectromechanical systems (MEMS) processing technology, this situation can be precluded.



Figure 4.11: Selected force-torque sensing solution: force-torque sensor ATI nano 25 capable of sensing six degrees of freedom

The applicability of strain gauges sensors in underwater applications has already been proven [Inaudi et al., 2007]. The insight that an off-the-shelf solution for underwater force-torque sensors is not available yet [Lemieux et al., 2006] still appears to be valid today. The chosen force-torque therefore requires adjustments to be used under water. The adjustments made to the sensor and the influences on sensor behaviour are discussed in the experiments section in chapter 6. The measurement ranges for forces and torques of the selected sensor are shown in Figure 4.1.

Table 4.1: Sensing range of chosen force torque sensor (ATI nano 25 250-6)

	Sensing range
F_x	250 N
F_y	250 N
F_z	1000 N
T_x	6 Nm
T_y	6 Nm
T_z	3.4 Nm

This modality is to be integrated into an end-effector in the finger base. The mounting is designed to guide all incoming forces and torques from the finger through the sensor. Techniques like intrinsic tactile sensing (compare definition in section 2.3) cannot be realized at this location. This is not a drawback as a combination of the data from static tactile sensing with the data from the force-torque sensor produces the same results.

4.4 Sensing dynamic contact properties

The ability to measure texture by the human skin is achieved by moving the glabrous skin of the hand across a surface. The microvibrations caused by the fingerprint patterns while in contact with a moving surface are sensed by the fast adapting tactile units in the dermal and subcutaneous layer of the skin [Lederman and Browne, 1988].

Sensor materials that react in a similar way to dynamic stimuli as the aforementioned tactile units in the human skin are those with piezoelectric properties [Cingolani, 2014]. In these materials an electric charge is generated by the application of external stress.

A ceramic made of lead-titanate-zirconate (PZT) was chosen for implementation of a piezoelectric sensor in the finger modules. Compared to natural occurrences of the piezoelectric effect as can be found in quartz, the piezoelectric behavior in PZT is achieved by polarizing randomly oriented dipoles in the material. The process is described in [Fraden, 2010]. Initially, the piezoelectric material is heated above the Curie temperature of 300°C. By applying a strong external electric field, the randomly oriented dipoles start to align. After cooling the material, the electric field is removed and the polarization process is finished. After this treatment PZT shows the piezoelectric properties.

The reason for the insensitivity of the measurement principle to changes in am-

bient pressure can be explained by the perovskite crystal structure of the material which is shown in Figure 4.12.

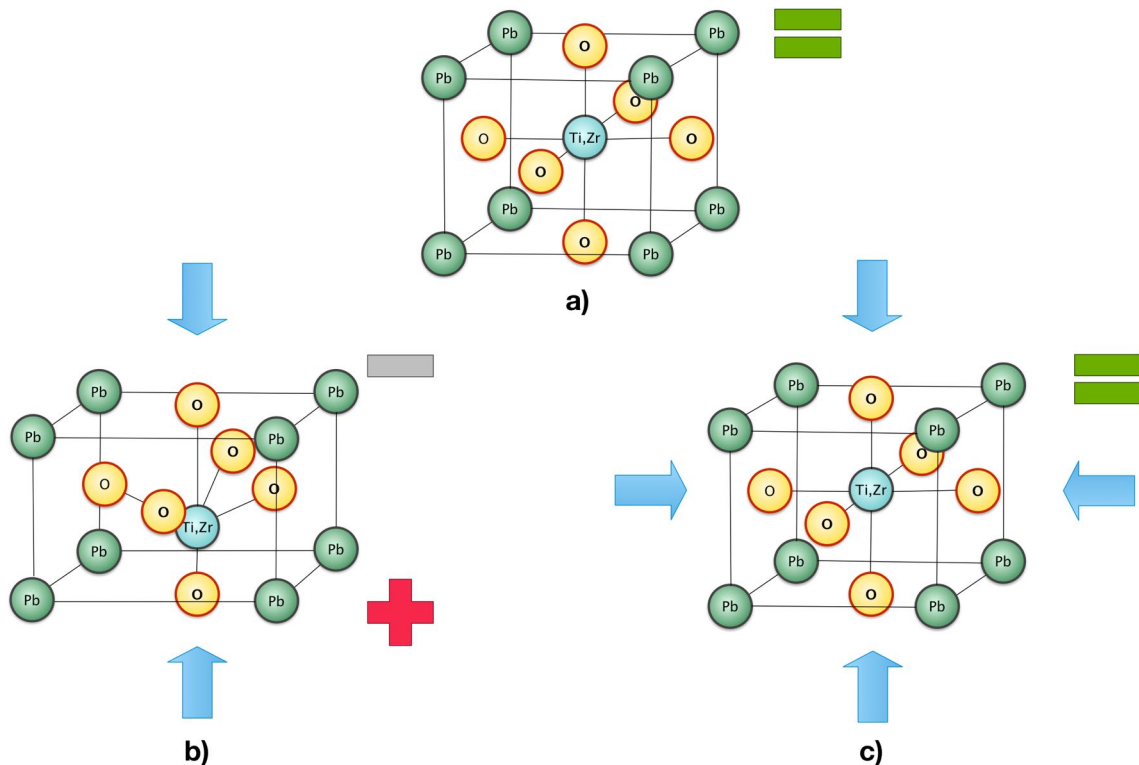


Figure 4.12: Perovskite crystal structure of lead-titanate-zirconate and the polarity of voltages depending on the deflection of the dipole

The state in equilibrium is depicted in subfigure 4.12 a). The dipole is not moved out of its resting position and no voltage generation can be sensed. In the case of unidirectional pressure activation, the dipoles in the material are deflected resulting in a voltage excitation (Figure 4.12 b)). A uniform pressure does not exert any deflection of the crystal structure and thus no measurable voltage signal from the sensor material is perceived (Figure 4.12 c)).

Pressure or high temperature can lead to a loss of the piezoelectric properties of the material. The chosen base material for the developed sensor is piezoceramics manufactured by PI (PIC 255). Having a static compressive strength of 6,000 bar [PI Ceramics GmbH, 2014], the ambient pressure of the water column at a depth of 6,000 m (600 bar) will not depolarize the ceramics. However, the depolarization temperature is reached in the near of black smokers, where temperatures of up to 550°C are measured [Kelley, 2001].

The developed piezosensor is depicted in Figure 4.13. Its dimensions are 60 by 30 mm. The ceramics were lasered to form a piezoelectric sensor array of four by five sensor elements in the contact area (projected in black onto the image). This configu-

ration was chosen because it is expected to perceive more locally precise information about occurring slippage than a single sensor element of the same dimensions. Each sensor element is contacted by its own electrode, a common ground electrode is placed left and right at the outside of the sensor array. The sensor presented is integrated into every limb of the gripper.

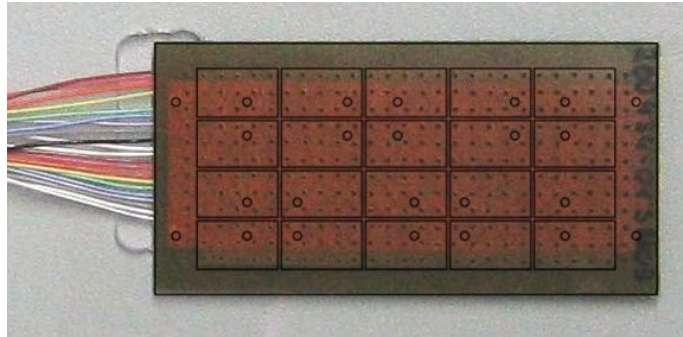


Figure 4.13: Piezoelectric sensor array developed. (Sensor element dimensions are projected onto the image))

Applications of sensors based on the piezoelectric effect for deep-sea applications are manifold. Depth sensors [Boyes, 2009] and sonar [Au and Hastings, 2008] measurements are typical applications.

4.5 Sensing geometry information

Perceiving geometric properties of the object in contact with the gripper requires the use of sensor arrays. A commonly used working principle for tactile array sensors involves pressure sensing resistors. A typical setup of these sensors is described in [Papakostas et al., 2002]. The sensor presented comprises two polyester sheets. Parallel running conductive traces made of a polymer filled with silver particles are placed on each sheet. The two sheets glued together in 90 °rotation so that the traces form a grid structure. Each cross section of the grid represents a sensor element. By applying external forces, the traces are compressed, thus leading to an increase in conductivity at the sensor elements.

When submersing this sensor, the gaps between the two polymer sheets are filled with water. Water, being a considerably better conductor than air, leads to a change in conductance at the sensor elements without contact forces applied. Furthermore, the ambient pressure of the water column acts on the compressible traces as well, which results in activation of the sensor elements. Thus, when using this sensor principle, the measurement range has to include the pressure exerted by the water column in addition to the expected maximum contact forces. As measurement principles

are known to become insensitive at the upper limits of the measurement range, the sensitivity of contact measurement changes with depth.

Another frequently used approach involves sensor arrays based on capacitive sensing. These setups consist of an array of capacitors that use air as a dielectric medium. With increasing ambient pressure the electrodes of the capacitor are compressed until the dielectric medium is fully collapsed. Hence, this approach is not suitable for applications under water without alterations.

Instead of adapting one of the discussed methods, a measurement principle was selected which is based on an optical measurement principle. Figure 4.14 shows the working principle of this sensing technology which was originally developed for space and automotive applications [Reimer and Baldwin, 1999].

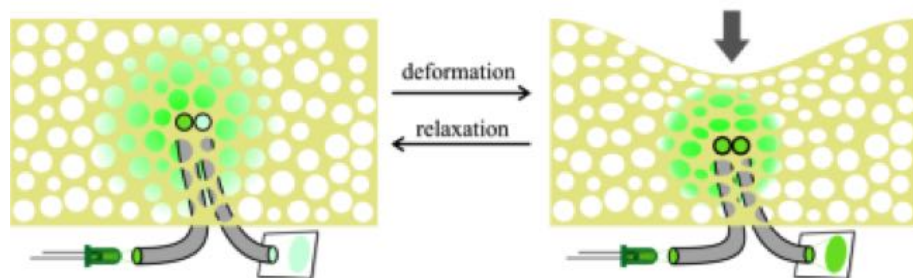


Figure 4.14: Working principle for a fiber-optic tactile sensor

Each sensor element consists of a light source and a light sensing device. These can be LEDs and photo-diodes as shown in configuration c) of the sensor in Figure 4.15. Another option is to use polymer optic fibers that are attached to an LED and a photo-transistor. The emitted light is scattered in the cavities of a foam material where some of the scattered light is collected by the light sensing unit. In case of a deformation of the foam material (Figure 4.14 on the right), the cavities in the foam are compressed. The emitted light is less scattered and light with higher intensity is sampled by the collecting fiber. As a result, the light acquired by the signal conversion results in a proportional change in the electric signal. Three possible configurations of the sensor components are reported in the literature. These are shown in Figure 4.15.

The three configurations differ in terms of placement of the light emission and sensing. In the full-space and the half-space configuration the optical fibers are placed within the compression area of the foam. In the case of full compression the contact forces act directly on the fibers. In the application scenario of manipulation this situation should be avoided as sharp contact can harm the optical fibers. The third solution is based on placing LEDs and a photodiode on a base plate for each sensing element. This configuration leads to high energy consumption as each

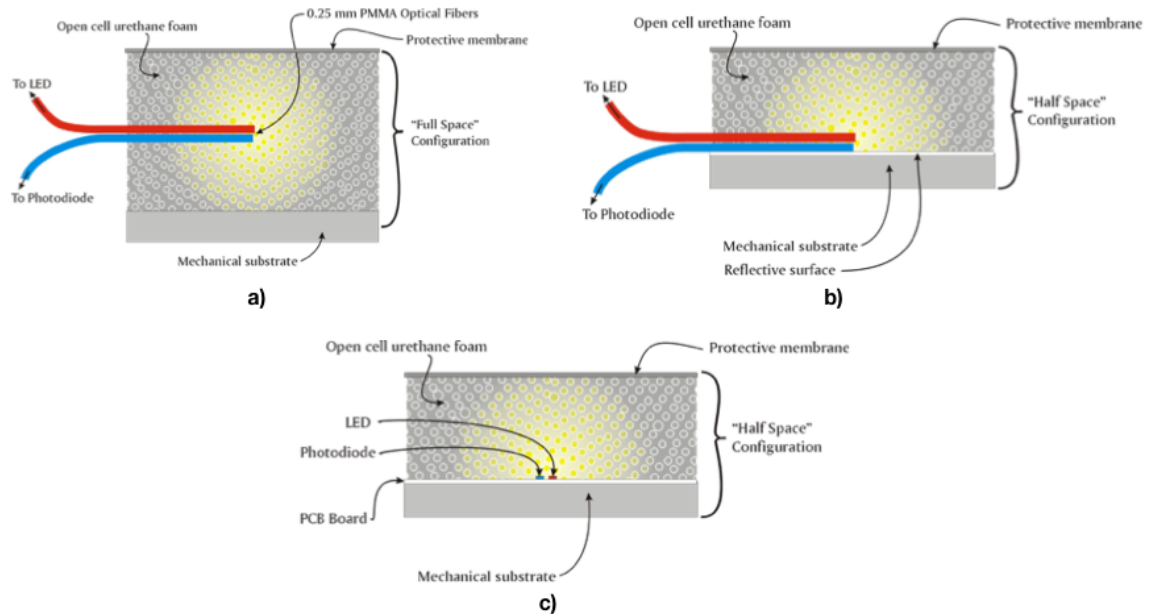


Figure 4.15: Configurations of the components comprising a sensing element of the fiber-optic measurement principle: a) full-space configuration b) half-space configuration c) non-fiber sensor

sensing element requires its own LED. Furthermore, the intended application environment necessitates that the sensing system be able to cope with water in the contact area, which requires sealing of the electrical components in the non-fiber configuration.

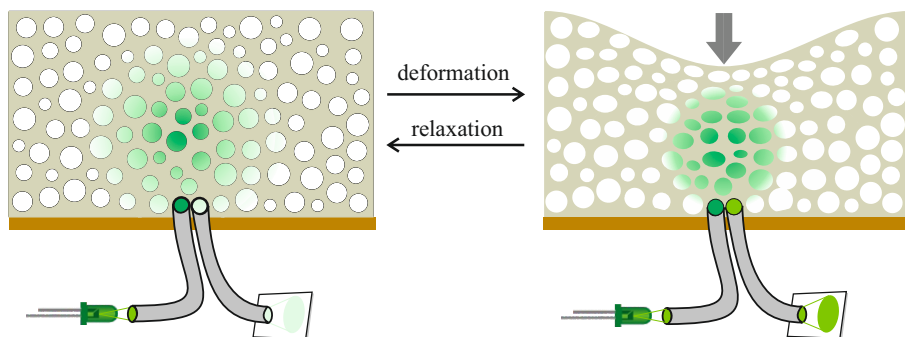


Figure 4.16: Proposed configuration of the sensor for integration into robotic grippers

To overcome the addressed drawbacks of the presented configurations of the sensor, a new configuration was developed. Its setup is shown in Figure 4.16. Optical fibers are used for transmission of light into the cavities of the foam. The sensing fibers transfer the acquired light to photo-transistors. Compared to the proposed configurations in the literature, the configuration developed uses a carrier plate below the foam for attaching the fibers to the foam. During assembly of the sensor the

optical fibers that are fixed in holes of the carrier plate are polished to achieve an even surface. This preparation prevents damage of optical fibers during compression of the foam in manipulation tasks.

The measurement principle presented has several advantageous features which make it an ideal candidate for building an underwater tactile sensor array. No electric components have to be placed directly at the contact area. Applied contact force therefore does not harm any electric acquisition circuit. The usage of optical fibers enables signal transmission over long distances, thus supporting the integration of this sensor in limited integration space in the contact region.

The applicability of this measurement principle in the ambient pressure of the water column depends on the cell structure of the foam that is used. An open cell structure allows fluids to run through the material, a property that enables the foam to keep its shape regardless of the ambient pressure. In the case of contact, the fluid is squeezed out of the cell structure and the foam is deformed accordingly. As this sensor has not been used in underwater applications before, this property was verified by experiments that are described in section 6.

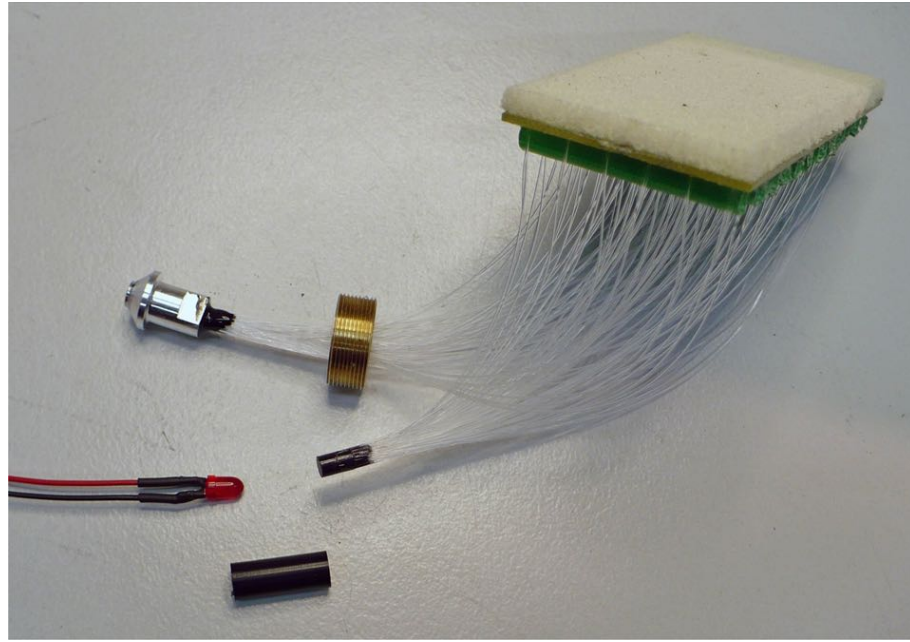


Figure 4.17: Assembled fiber-optic array sensor for perceiving contact geometries

The sensor setup chosen for the underwater gripper developed consists of an open cell foam made of latex having a thickness of 4 mm. An assembled sensor module is depicted in Figure 4.17. The dimensions of the sensing area are 600 by 300 mm. The spatial density and the total number of sensor elements depends on the integration space available for bending the optical fibers below the sensing area. In order to

prevent plastic deformation of the fibers, which leads to a damaged core and loss of light transmission capabilities, the bending of the fibers must not fall below a minimum radius. As a rule of thumb, [The Fibre Optic Association, 2009] specifies a minimum bending radius for polymer optic fibers that does not fall below 20 times the diameter of the fiber. Fibers with a small diameter are thus preferable for minimum integration space. For implementation of the sensors developed in the framework of the thesis polymer-optic fibers having a diameter of $250 \mu\text{m}$ are used, which are the smallest that are commercially available.

With regard to minimal requirements in terms of integration space in the limb structure of the fingers, a maximum height of 10 mm is targeted. The resulting space for placing the polymer fibers allows the integration of 72 sensing elements. The spatial density obtained is 6.25 sensor elements per square centimeter.

Higher spatial densities were evaluated. A sensor array containing 324 sensing elements resulting in a spatial density of 25 sensor elements per square centimeter showed insufficient operation performance. The observed behavior of the sensors can be explained by the small integration space available for bending the required 648 fibers within the limits of the necessary bending radius.

4.6 Proprioceptive Sensing

In addition to the presented measurement modalities for perceiving contact information, proprioceptive information like the gripper pose is required to combine the tactile information with contact position and object dimensions. For applications on land various encoder types, such as reflective encoder wheels or encoders based on the hall effect, are used.

The same drawbacks known for reflective encoders on land are also valid and even more crucial for applications under water. Contamination of the surrounding water might cause undesired reflections perceived by the encoder circuit, resulting in incorrect measurements. As the magnetic field does not experience any damping by water, encoder systems based on the hall effect are ideally suited for measuring the pose of an underwater gripper. This approach was therefore chosen to measure the absolute position of every joint in the gripper system.

4.7 Decentralized hardware architecture for tactile sensing

Local signal conversion has several advantages compared to a solution where all sensor signals are transmitted to a central processing element. With local pre-processing

analog sensor data can be converted to digital signals at the place of acquisition. Precautions can be taken to ensure robust data transmission on a digital channel that is not influenced by crosstalk, loss of signal strength and electromagnetic effects, as those generated by motors. Another advantage is the distribution of processing load within the robotic system. This allows either the usage of smaller central processing modules that require less integration space or the inclusion of more algorithmic processing.

The proposed decentralized processing architecture therefore combines measurement principles directly with a processing electronics enabling local signal conversion, analysis and response to incoming stimuli. The following sections describe the approach for implementing the hardware architecture for the sensors presented as a compound of embedded systems.

4.7.1 Processing force-torque data

The data generated by the force-torque sensor setup described in section 4.3 are analogue signals with small amplitudes (in the case of measurements in the z direction: $5 \frac{mV}{N}$), which have to be amplified. As this modality is intended to be used for absolute force measurements, low noise acquisition is more important than high sampling frequency. These requirements are evaluated in terms of the integration aspect: high precision analog signal pre-processing of the strain gauge data requires analog filters and amplification circuits that are assembled from discrete components.

System-on-chip solutions, that provide configurable analog pre-processing are highly integrated solutions and thus preferable in terms of integration. Although the high degree of integration is accompanied by a reduced quality of the analog pre-processing circuit, this approach is chosen because only a few electrical components need to be prepared for use in high ambient pressure. The quality of the acquired data will be investigated in the experiments section.

Field programmable analog arrays (FPAs) and programmable system-on-chips (PSoCs) are two commercial-off-the-shelf solutions for configurable analogue signal processing known today. While FPAs are developed for purely analogue configurable processing, PSoCs include analogue and digital reprogrammable parts and a microcontroller unit (MCU) for further signal handling. A PSoC5 LP from CyPess is therefore chosen for signal acquisition. This system-on-chip features an ARM Cortex M3 as MCU together with configurable operational amplifiers, analog multiplexers and an ADC with up to 20 bit resolution. To improve the signal quality of the circuit, an additional high precision ADC AD7194 from Analog Devices was added. It comprises a 24 bit delta sigma conversion unit capable of sampling input signals at a sampling frequency of up to 4.8 kHz. Figure 4.18 shows the designed analogue circuit

in the PSoC.

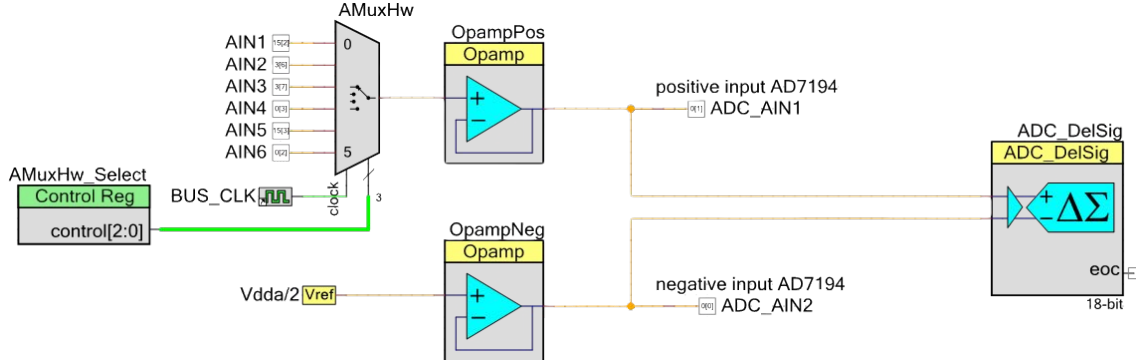


Figure 4.18: PSoC circuit for acquiring force-torque sensor data

The six wires coming from the axial forces and rotary torque sensing strain gauges (AIN1-AIN6) are demultiplexed and run through an operational amplifier configured as a voltage follower. This solution does not amplify the voltage sensor signal but isolates the sensor signal from effects caused by the acquisition electronics. In cases where signal acquisition consists of parts with low impedance, high currents are drawn from these parts. This affects the source signals as they can be pulled down by means of the required currents, resulting in a distorted signal. The voltage follower reduces this effect to a minimum. In theory it is designed to feature an infinitely high impedance, resulting in low currents drawn from the source, which in turn does not affect the original signal.

The signal going through the voltage follower is connected to one of the differential inputs for the internal and the external analog to digital converter. This setup makes it possible to switch the signal acquisition between the internal and external converter during runtime of the electronics. The second differential input is fed by a constant voltage level of half the supply voltage. To lower power consumption, it also runs through a voltage follower. The signal is used to shift the ground voltage level at the ADC. In the case of the circuit configuration shown, voltage levels coming from the sensor below half the supply voltage are sampled as negative values.

Figure 4.19 shows the fully designed and assembled printed circuit board (PCB). Communication with the sensor processing chain is realized via low-voltage differential signalling (LVDS). Baud rates of up to 500,000 baud can be achieved with this electronics setup. The complete specifications are summarized in Table 4.2.

4.7.2 Processing piezoelectric sensor data

Impacts at the contact region, such as slippage events or texture information, are expected to be sensed by the piezoelectric sensor elements. High frequency sampling

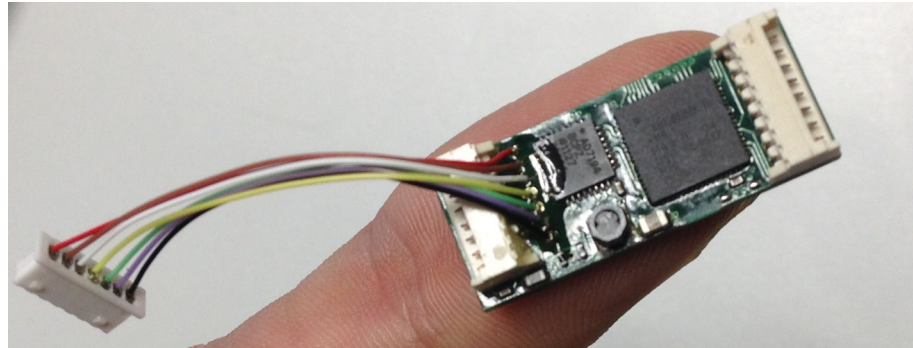


Figure 4.19: Developed electronics for locally processing force torque sensor data

Table 4.2: Properties of the electronics acquiring the force-torque sensor data

Property	Value
Dimensions	30 x 12.4 mm
Weight	3.4 g
Sampling frequency (int.)	100 Hz
Sampling frequency (ext.)	13 Hz
Resolution (int.)	18 bits
Resolution (ext.)	24 bits
Communication datarate	500,000 baud

is thus of greater relevance than absolute measurement precision. In order to achieve a compact electronics setup and simplify the development, the PSoC presented for the acquisition of the force-torque signals is used for this sensor as well. Due to the possible parameterization of the chip, the ADC is configured for higher sampling frequency for the sake of a lower resolution. The internal configuration of the analog and digital components in the PSoC can be seen in Figure 4.20.

The 20 signals coming from the piezoelectric sensor array (Ain_01-Ain_20) are demultiplexed and isolated from electric parts having a low impedance using a voltage follower as described in the previous section. The signal is then transmitted through a programmable gain amplifier that allows adjustment of the amplification during runtime. The input signal on the non-inverting channel of the programmable gain amplifier is connected to a digital to analogue signal converter coming from the micro-controller. This component can be used to set a fixed voltage signal. In the case of the circuit presented, this component is set to ground level voltage. After going through the pre-processing circuit, the sensor signal is connected to the positive differential input of the ADC. The second differential input is connected to ground voltage level, which is used as a reference for the computation of the converter.

Communication is realized using LVDS. The transmission rate is set to 500,000

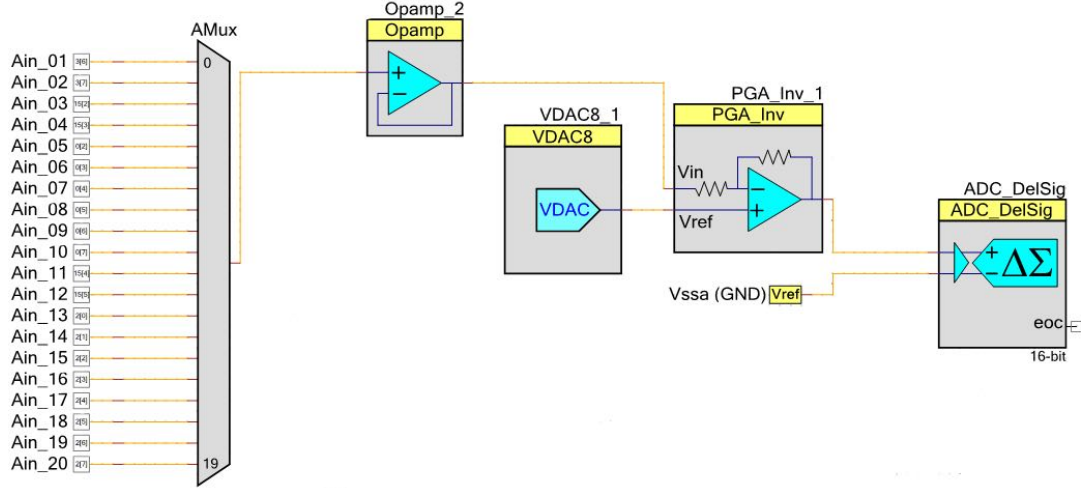


Figure 4.20: PSoC circuit for acquiring piezoelectric sensor data

baud. Table 4.3 summarizes the properties of the designed acquisition electronics.

Table 4.3: Properties of the electronics acquiring the piezoelectric sensor data

Property	Value
Dimensions	600 x 300 mm
Weight	6.2 g
Sampling frequency	580 Hz
Resolution	16 bits
Communication data rate	500,000 baud

4.7.3 Processing fiber-optic sensor data

Sampling of the contact information gathered by the fiber-optic sensors requires conversion from light intensity to a proportional digital signal for further processing. Commonly used electronic devices for this task are photo-transistors. Using a discrete photo-transistor for every sensor element results in a spacious setup which is undesirable in terms of integration.

Using an array of highly integrated photo-transistors is thus favorable as it implements compact acquisition electronics for the task. For this reason, complementary metal on semiconductor (CMOS) camera sensors are chosen for converting the light intensity carried by the optical fibers since these devices can be seen as an array of photo-transistors. Usually, choosing camera systems for acquisition electronics for tactile sensors does not result in compact solutions [Kamiyama et al., 2004],

[Obinata et al., 2007]. The reasons for this are the required distance between the camera and the object to be observed based on the focal point. To overcome this issue, the camera is to be used completely without any lens system. This approach requires less integration space, the air inclusions between the various lenses do not have to be taken into account when preparing the system for deep-sea application. Without any lenses the focal point of the camera is directly in front of camera chip die. To monitor the brightness changes, the optical fibers are fixed directly on the chip.

Besides the higher integration density compared to the discrete setup, this approach is also more robust against defects in signal conversion circuits, as each fiber is sampled by several elements of the photo-transistor array. Furthermore, by fixing the fibers onto the chip die, the fibers cannot become detached from the acquisition electronics by vibrations. As optical fibers have the property of transmitting light over long distances, placing the acquisition electronics outside the contact area is another option. In this case, the fibers have to cross the joints of the gripper, which causes mechanical stress on the fibers during movements of the limbs. Abrasion effects lead to a loss of signal quality in long-term operation which is why this integration solution was not pursued.

Two different approaches were evaluated to arrange camera modules below the sensing area. The two evaluated solutions can be seen in Figure 4.21.

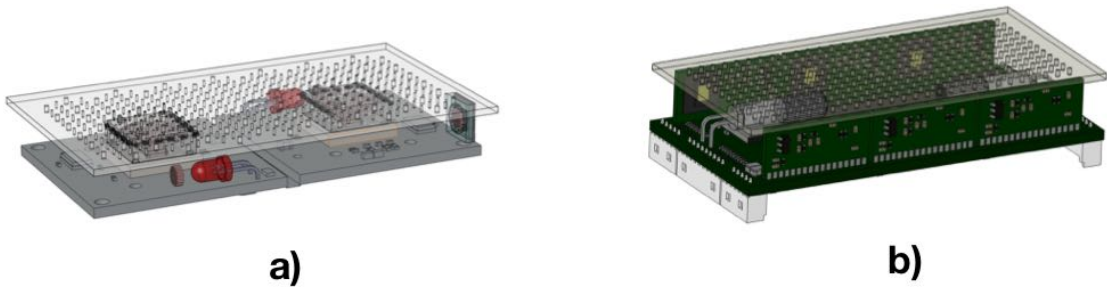


Figure 4.21: Horizontal (a) and vertical (b) placement of camera chips for fiber sensor acquisition

The decision between those two approaches was made based on the required space to safely bend the fibers on the way from the sensing area towards the camera chips. In the case where horizontally aligned camera chips are used, the fibers have to be bent twice in the outer areas of the sensor. While preserving the minimum bending radius of 5 mm per turn, this approach results in a minimum height that of at least 10 mm. In the concept drawing in Figure 4.21 a), two cameras are used for interfacing the optical fibers of the sensor array consisting of 72 sensing elements. This setup means that all light collecting fibers of the sensor array have to be guided to the

center of the sensor area. As a result, this area becomes bulky.

The second approach is designed to improve the integration situation by using six cameras which are placed along the outer edge below the sensor area (compare Figure 5.5 b)). Due to the vertical placement of the cameras, the fibers only have to be bent once, resulting in less integration space. By using several cameras, the integration becomes less bulky as the fibers are distributed among more sensing units.

Based on these considerations, the second solution was chosen for realizing the signal conversion and processing of the fiber-optic sensor array.

The selection of a suitable camera influences various parameters of the sensor system. The frame rate of the camera determines the sampling frequency of the sensor, the color depth is directly proportional to the sensor resolution. The size of the active sensor area of the CMOS chip defines the number of fibers that can be sampled by the camera and finally, the absolute dimensions of the camera system lay the foundation for the required integration space of the acquisition electronics.

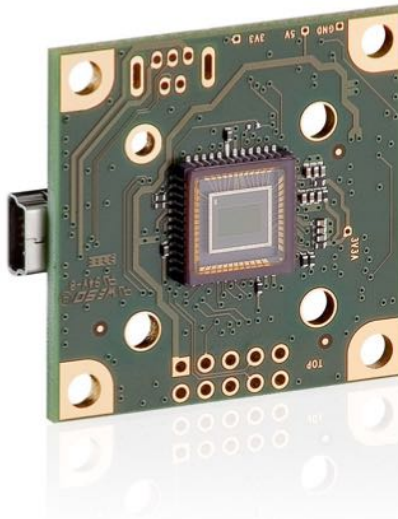


Figure 4.22: Off-the-shelf Universal Serial Bus (USB) camera solution as acquisition electronics for the fiber-optic sensor

To evaluate the effects on the signal quality based on the acquisition electronics, two types of acquisition electronics were used. One solution relies on an off-the-shelf USB camera system developed by IDS (Figure 4.22). It consists of a camera chip with an active sensing size of $\frac{1}{3}$ inches, its dimensions are 36 x 36 mm. With this solution no on-board signal analysis is possible because the electronics transmit the raw image information without the possibility of integrating a custom processing code.

As a second solution, a custom PCB was designed for integration of the fiber-optic

sensing acquisition electronics into the structure of the gripper. It features optimized dimensions for integration and data transmission that is optimized for the interface with embedded electronics.

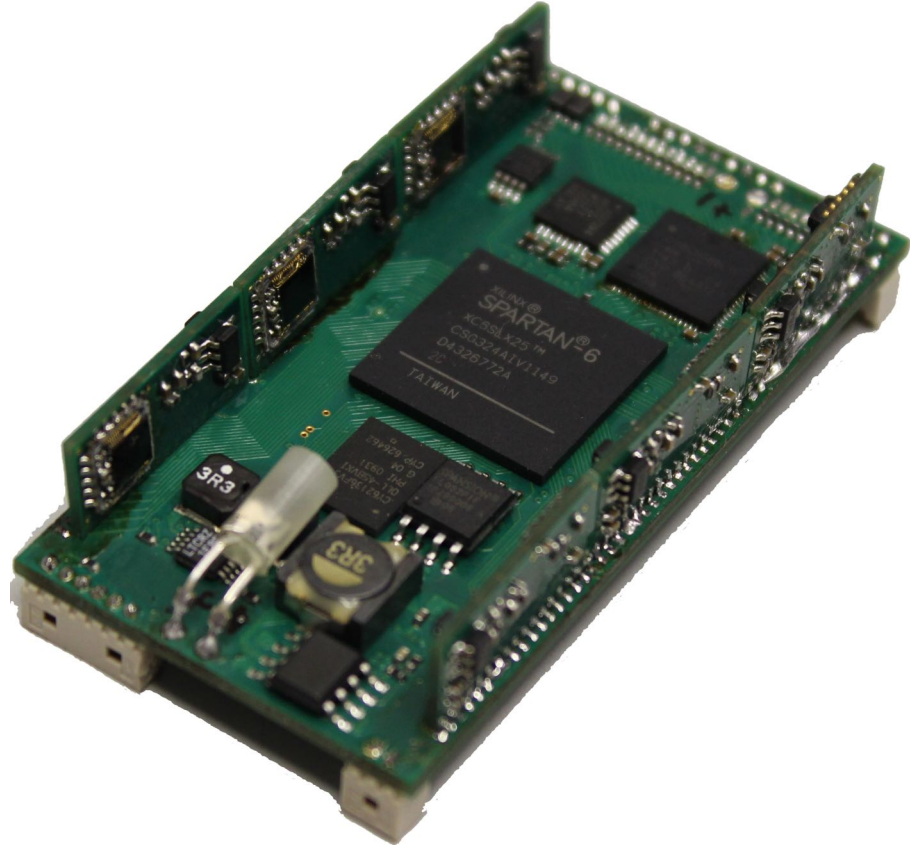


Figure 4.23: Assembled fiber-optic processing electronics

The setup developed consists of cameras commonly used in smartphones that cover a section of the overall sensing area. Sixty sensor elements can be sampled by each camera in this solution. As a result, a maximum of 360 sensors can be acquired by the electronics.

Sampling this number of cameras with embedded electronics is a task which common microcontrollers or digital signal processors cannot handle. A solution based on an FPGA was chosen in which each camera is sampled in parallel by a custom logic.

Figure 4.23 shows the PCB of the designed electronics. The six camera modules mentioned are placed around the base PCB where processing of the fiber optic data is implemented on a Spartan 6 LX25 FPGA from Xilinx. It contains 24,051 logic cells, the chip dimensions are 15 by 15 mm and the system operates with a clock of 20 megahertz. This specific FPGA is chosen because of its balance between the package dimensions of the chip and its number of logic elements. The dimensions of this acquisition electronics is 60x30 mm with a height of 10 mm. Communication to

downstream electronics is carried out via LVDS with a baud rate of 921,600 baud. Table 4.4 summarizes the features of this electronics.

Table 4.4: Properties of the electronics acquiring the fiber-optic sensor data

Property	Value
Dimensions	60 x 30 mm
Weight	13.3 g
Processing unit	Xilinx Spartan 6 LX 25
Operating frequency	20 MHz
Number of cameras	6
Camera type	Toshiba TCM8230MD
Dim. CMOS sensing area	2400 μm x 1800 μm
Sampling frequency	30 Hz
Resolution	8 bits
Communication data rate	921 600 baud

In order to keep the complexity of the mechanical integration of the fiber-optic sensor array to a minimum, the optical fibers are attached to the camera modules without preserving the neighborhood relationship of the sensor elements. This means that fibers that are glued close to each other on the camera sensor are not necessarily neighbors in the sensing area of the tactile sensor. This neighborship, which is important for perceiving geometric properties, will be identified using algorithmic approaches running on the local processing electronics of the sensor. The development of the algorithmic solution is discussed in section 5.1.6.

4.7.4 Embedded sensing module for static and dynamic contact measurement

The aforementioned piezoelectric and fiber-optic sensor arrays are each placed in the finger module. As both measurement principles require direct contact with the object in touch, these sensors have to be integrated in a way that their measurement principles are able to react to stimuli in the same contact area.

The approach developed to accomplish this task is shown in Figure 4.24. The piezoelectric ceramic was applied directly onto the carrier plate of the fiber-optic sensor. The required holes in the carrier plate for the optical fibers are drilled into the ceramics as well. This design allows the measurement of both dynamic and static impacts on the same contact area, thus creating a multi-modal tactile sensing unit. Local pre-processing of the gathered information of both measurement principles is performed by the embedded electronics directly below the sensing surface. A notable

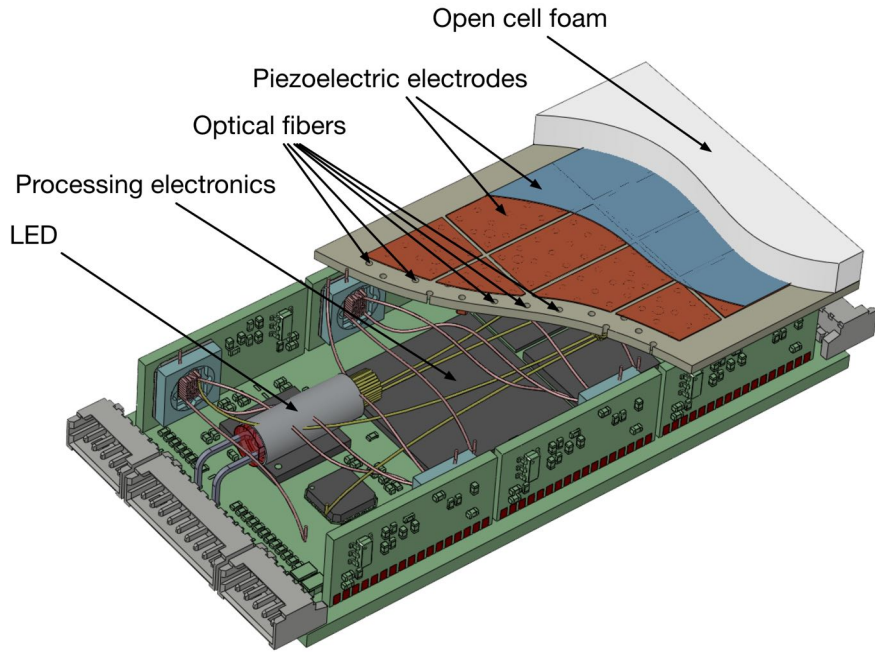


Figure 4.24: Integrated multi-modal sensor system for measuring geometries and dynamic impacts

property of this combination is that the measurement principles do not interfere with each other.

4.7.5 Processing gripper pose information

As discussed in section 4.6 absolute angular encoder measurements based on the hall effect are promising candidates for deep-sea applications. Sensors which operate with this principle rely on integrated circuits that measure the magnetic field of a magnet positioned above the chip and calculate the corresponding absolute position. An absolute angular encoder from IC Haus was selected for development of the gripper (Fig. 4.25). It features a 12 bit data output using a BiSS interface. The maximum output frequency is four megahertz. The designed PCB was integrated into every joint of the gripper allowing the measurement of the gripper pose.

4.7.6 Further processing electronics in the gripper

Apart from the electronics that locally sample the sensor data on acquisition, further electronic circuits are integrated into the gripper structure with different objectives.

Each finger is equipped with a force-torque sensor as well as two fiber-optic and two piezoelectric sensor arrays. The data transmitted by the acquisition electronics is aggregated in each finger using the PCB depicted in Figure 4.26.

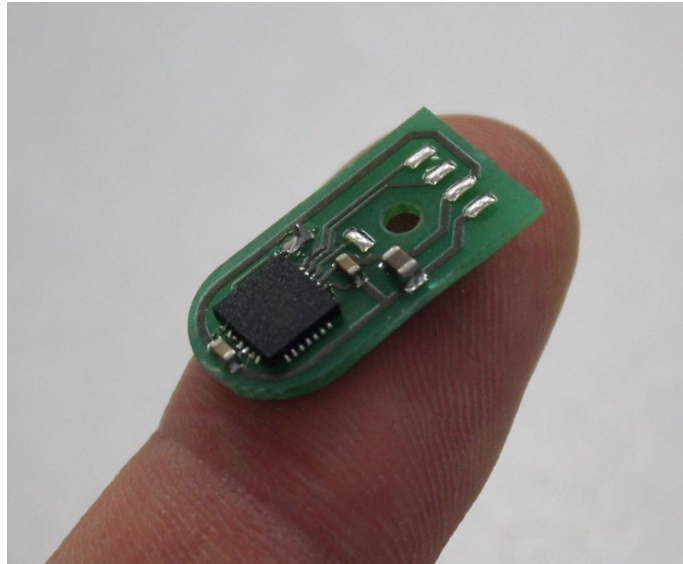


Figure 4.25: PCB developed for measuring the gripper pose



Figure 4.26: Sensorfusion PCB that aggregates the sensor data in every finger

This PCB mainly consists of a Spartan 6 LX25 FPGA that further pre-processes the information coming via LVDS from the sensors and forwards it to a central processing PCB in the wrist of the hand (Figure 4.27). The sensor data transmitted from the fingers is sampled and fused by an FPGA (Xilinx Spartan6 LX 25) and forwarded to a DSP from Analog Devices using a 16bit parallel bus with a transmission rate of up to 190 Mbit/s. The DSP operates at frequency of 600 MHz. The communica-

tion interface to downstream processing units outside of the gripper is performed by means of a 100 MBit/s ethernet connection. In addition to communication with the electronics in the finger end-effectors, this PCB also enables the communication to the PCB controlling the actuators in the gripper using the controller area network (CAN) protocol.

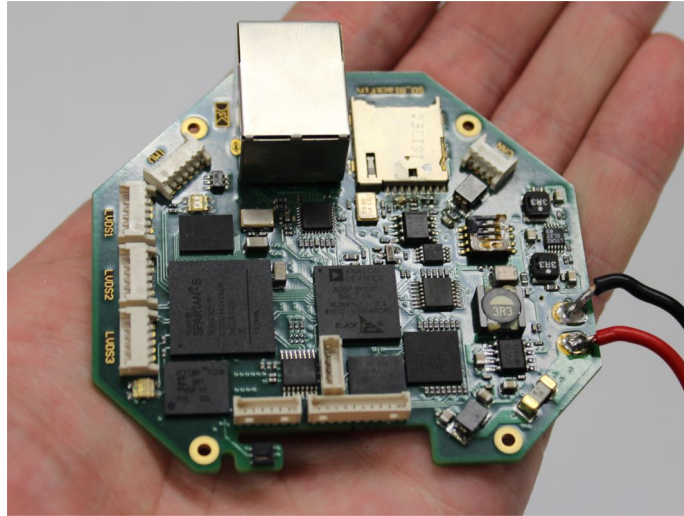


Figure 4.27: *BaseBoard PCB that combines and processes the data coming from all sensors*

The PCB for controlling the actuators is capable of controlling up to 32 hydraulic valves and a brushless DC motor (BLDC). The hydraulic circuit is monitored by this PCB using thirteen pressure sensors measuring the overall supply pressure as well as the pressure in each piston. The control of the BLDC motor is realized using a sensorless BLDC controller from Allegro Microsystems. A Xilinx Spartan 6 LX25 FPGA is used as the central processing unit of the board. It generates the pulse-width modulation (PWM) signal as well as the position controllers for all motors.

4.7.7 Topology of the designed hardware architecture

The combination of the electronic circuits presented constitutes the hardware architecture shown in the diagram in Figure 4.28. Each finger is built up using identical parts, enabling replacement without further adjustments. The tactile sensor information is combined and fused in the *Sensorfusion* electronics and is sent from there to the *BaseBoard* electronics. Local behavior is triggered at in *BaseBoard* electronics. As a result, control commands are sent to the *Actuation Control* board. Sensor information is forwarded to downstream processing units using an Ethernet connection having a throughput of 100 MBit/s.

The topology of the designed architecture can be compared with a tree structure.

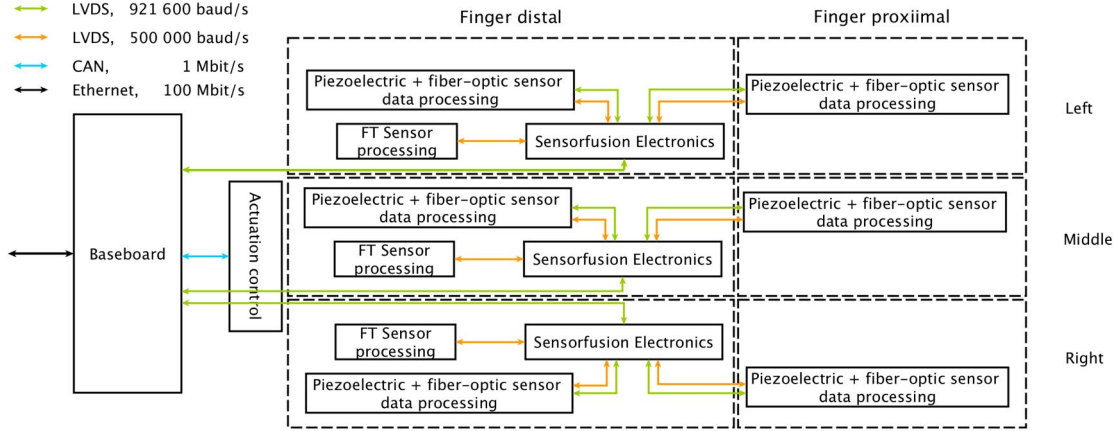


Figure 4.28: Topology of the presented hardware concept for decentralized pre-processing of tactile sensor data

The sensor processing electronics resemble the leaves of the *Sensorfusion* electronics, while these electronics can be regarded as branches coming from the *BaseBoard*. This structure avoids communication conflicts since none of the sensors has to share a communication line to the *Sensorfusion* electronics with another sensor. Furthermore, because an FPGA was selected as the processing unit for sensor fusion, all incoming communication can be processed in parallel.

The chosen approach can be generalized to encompass all kinds of applications where decentralized processing of embedded sensors is required. The tree-like topology shown can be extended by attaching further *Sensorfusion* electronics to the ones already included. As this board allows to connect six LVDS communication lines, further compatible electronics can be attached. The limiting factor is the communication delay caused by the ramification of the topology.

4.8 Integrated gripper system

The discussed morphology decisions together with the actuation, sensor and electronic design are integrated in the gripper system as shown in Figure 4.29. Placement of the presented components is exemplary shown for one finger and the wrist by highlighting the integration regions.

Special attention was paid to the cables going from the *Sensorfusion* electronics to the central electronics in the wrist. To avoid signal disturbances caused by the PWM signals needed for actuating the valves, all cables are placed around the actuation section as far as possible.

In order to achieve minimal spatial requirements for the integration of the selected components, pressure housings for the electronic components and the actua-

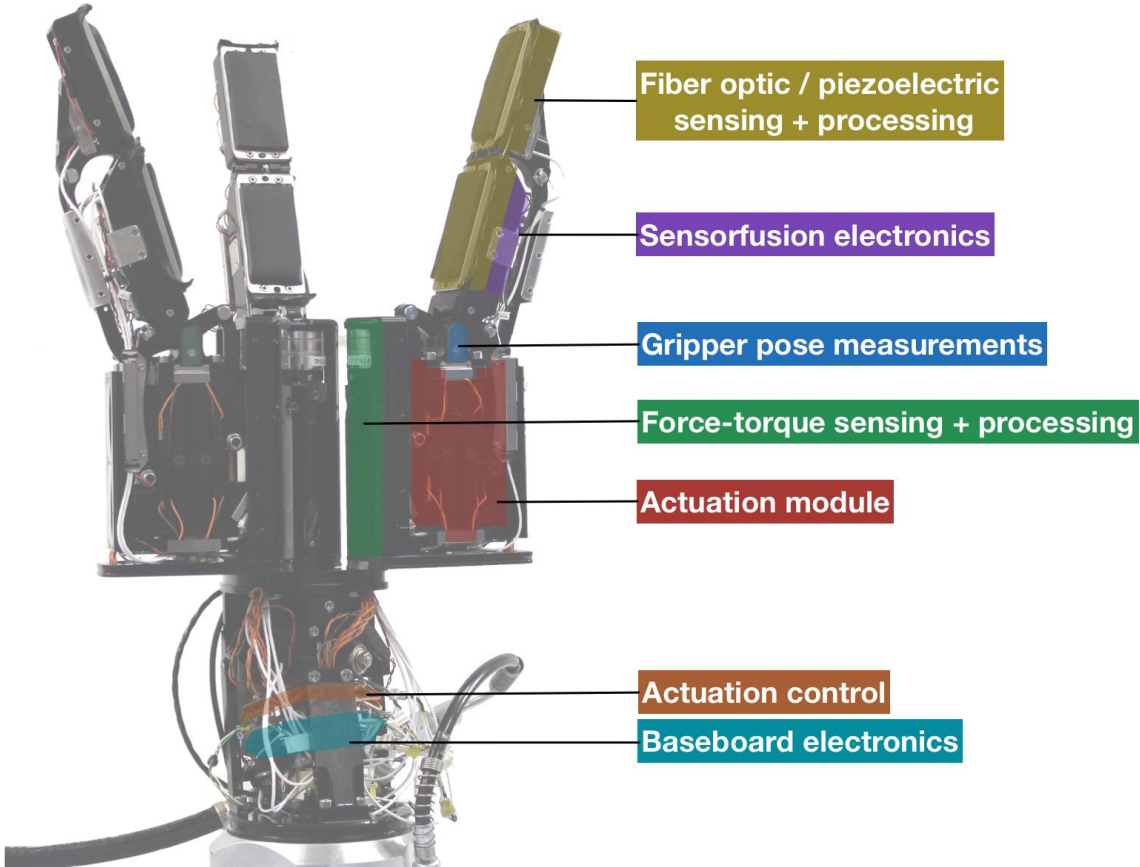


Figure 4.29: Integrated gripper system for deep-sea applications

tors are avoided. All components are therefore designed as pressure-tolerant modules. Implementations of pressure-tolerant setups for deep-sea applications are presented in [Thiede et al., 2009]. The general concept is to choose components that withstand the ambient pressure thanks to their manufacturing process and apply coating material for the prevention of short circuits. The evaluation of the components used in the gripper system developed with respect to their applicability under high pressure is presented in section 6.2.

The overall specification of the gripper is given in table 4.5.

4.9 Discussion

Sensor-oriented end-effector design

The insights gained from the review of the state of the art were crucial for the system design of the tactile sensing system. Most end-effectors have only limited space available for the integration of tactile sensing capabilities in the contact area. As a tactile sensing system is only powerful in combination with a proper end-effector de-

Table 4.5: Properties of gripper system developed for deep-sea applications

Property	Value
Overall Dimensions	450 x 120 x 120 mm
Dimensions finger	165 x 20 x 30 mm
Weight (in air)	9.5 Kg
Degrees of freedom	7
Fingertip force	20 N
Processing units	8 FPGAs, 9 PSoCs, 1 DSP
Num. FT sensors	3
Num. piezosensors	6
Num. fiber-optic sensor arrays	6
Num. Encoders	7

sign, the initial sections of this chapter focus on the mechanical design considerations of an underwater gripper where the requirements for tactile sensing were considered during the entire development process. The driving concept of the design was to avoid placement of actuation modules in the contact area of the fingers to keep the available space for integration of tactile sensors. The result is an actuation concept that uses cantilevers for force transmission.

Sensor requirements for deep-sea application

Based on the requirements laid down by human exploration procedures presented in the state of the art, measurement principles for perceiving contact forces as well as dynamic and static impacts together with the proprioceptive information on the gripper pose are selected. The measurement methods are evaluated considering the suitability for usage under high ambient pressure conditions in the deep-sea.

It is worth noting that suitability in this context does not mean that the measurement range is in principle able to measure the pressure induced by the water column together with the contact stimulus. As most sensors exhibit a sensing sensitivity that changes asymptotically towards its maximum sensing value, the sensitivity near the maximum measurement range is limited. In the case of sensors measuring the pressure of the water column, contact sensing becomes increasingly insensitive at greater depths. Instead, the measurement principles chosen here have been shown in theory to work regardless of the ambient pressure. While the feasibility of strain gauges and piezoelectric sensors in marine applications was already proven by various applications, the applicability of the fiber-optic sensor presented has not been demonstrated yet and will thus be validated in the experiments section.

Challenges of integration

Integrating as many capabilities as possible into a new robotic system is the initial step for a new design. The following phase addresses the question of how to integrate these components and how to balance the requirements. Integration challenges for tactile sensors reported in the literature relate to the efforts needed to addressing each sensor element of a tactile array [Nilsson, 2000] and [Tegin and Wikander, 2005]. Especially integration of tactile sensors that are based on an optical measurement principle into robotic end-effectors is considered to result in a bulky setup [Dahiya et al., 2010]. The reason for this observation is explained by the necessary signal conversion electronics for transferring the optical signal into an electrical one. In cases where cameras are used, the necessary focal depth requires considerable installation height.

The original acquisition electronics for the optical measurement principle presented here supports this observation. The intended signal acquisition comprises discrete photo-transistors. A space-consuming setup is the consequence when realizing sensor arrays. A more compact setup can be achieved by using cameras that can be regarded as arrays of photo-transistors. By omitting a lens system, the installation heights for achieving focal depth are minimized. Though there are reported attempts to implement such a system [Luber et al., 2010], a complex mechanical adapter as well as occurring bending forces prevent integration into robotic end-effectors. By developing a decentralized camera system and attaching the optical fibers directly onto the camera chips, a highly compact setup was achieved. It enables incorporation of the fiber-optic sensing principle together with the processing electronics into the contact area of the gripper.

Conflicting integration requirements at the contact area

Further integration issues arise, when two sensing modalities necessitate placement directly in the contact area. In the system design discussed here, this is the case for the modalities for perceiving contact geometries as well as sensing dynamic impacts. The integration of two tactile sensors in the same contact area in a robotic system has been reported sparsely in the literature [Choi et al., 2005], [Wettels et al., 2014]. By using the piezoelectric sensor array as a carrier for the fiber-optic sensor field, it is possible to combine two tactile array sensors. Due to the different physical properties of the sensing modalities, no interference between the two measurement principles is expected.

Local sensor acquisition and decentralized processing

Local signal acquisition and decentralized pre-processing of the sensor data are the key factors in selecting suitable electronic components. Highly integrated so-

lutions that combine analog and digital components in a compact design are thus preferred over a discrete analog filtering stage. While better signal quality in terms of noise and sensitivity can be expected from the discrete setup, it also entails requirements regarding the integration space. Mixed-signal electronics like the selected programmable system on chip are a compact solution for analog filtering, digital acquisition and processing. The capability of adjusting the parameters of the analog and digital components during runtime supports adaptation to different scenarios. The tree-like communication topology of the sensor network allows extension of the network. It furthermore increases robustness during communication as a faulty sensing element does not affect other sensors. The combination of parallel hardware processors with high speed digital signal processing leads to a hardware architecture that forms the foundation for the design of local pre-processing algorithms. Depending on the nature of the developed algorithms, suitable processing platforms can be selected within the system to execute processing under optimal conditions.

Shifting complexity to software to lower integration efforts

By shifting the complexity in signal acquisition from the mechanical side to the software, the mechanical complexity of integrating the fiber-optic sensor arrays can be reduced. That is why algorithms are developed to identify the neighboring sensor elements in the contact area. Investigating the volume of data perceived every second by the developed sensor system reveals that handling the data solely by transmitting it to a central processing unit is not a suitable solution.

Chapter 5

Handling complexity by local pre-processing

Based on the selected sensing modalities together with the designed data acquisition electronics in the previous chapter, it is possible to conduct a detailed analysis of the sensor resolution and the amount of sampled data. Table 5.1 summarizes the data generated by every sensing modality that was integrated into the presented gripper system.

The sampling frequencies given in the table correspond to the acquisition of all sensing elements of a sensor array. The data volume is given by the number of bits that are stored for each sensor array. The quantity depicts the number of sensors for each modality in the gripper. The fiber-optic sensing modality represents a special case as the amount of data sampled for the fiber optic sensors does not primarily depend on the number of sensor elements in the contact area, but on the image size of the camera images to which the optical fibers are attached. As every fiber-optic tactile sensor module uses six cameras, the quantity is calculated by the number of fiber-optic tactile sensors integrated into the gripper multiplied by the number of cameras necessary to sample them.

Table 5.1: Sampled data per second of the designed tactile sensory system

Sensor	Frequency	Sample size	Quantity	Output
Fiber-optic arrays	30 Hz	640 x 480 x 8 bits	6 x 6	316.400 MB/s
Piezoelectric	80 Hz	20 x 16 bits	6	0.020 MB/s
Force-torque	100 Hz	6 x 16 bits	3	0.343 MB/s
Position encoder	1,000 Hz	12 bits	7	0.009 MB/s
Total				316.772 MB/s

Without further processing, approximately 317 megabytes of data have to be transferred to a processing unit in the robotic system every second. A comparison with conventional transmission standards reveals that even a gigabit Ethernet network connection having a bandwidth of about 120 megabyte per second does not deliver enough bandwidth to transmit all the data fast enough. In fact, to achieve a proper transmission in the case presented, three gigabit Ethernet connections are needed to transport the data under the assumption that the full bandwidth is solely available for the tactile sensors.

The effects of sensor evolution on processing requirements

What this example based on the gripper system developed shows for a specific case is also valid in general. By increasing frequency, resolution in space and sensitivity as well as the amount of sensors in a robotic system, the amount of data generated every second is growing considerably.

Besides tactile sensing, this conclusion also holds for other sensing modalities. It can be expected that cameras, light detection and ranging (LIDAR) systems or multi-modal tactile skins all across the body will be integrated into future robotic systems with continuously increasing resolution, sensitivity and update frequency. As a consequence, the amount of data that is generated by the various sensing modalities will increase accordingly.

Extracting useful information from the stream of multi-modal sensor information to support the tasks of mobile autonomous robotic systems without the requirement of computational power outside a robot is a challenge. This means efforts have to focus on coping with the complexity of this task from the perspective of limited available computing power and limited resources regarding integration space and power.

Local pre-processing as a solution for handling complexity

A way to limit the effects of this development is to distribute the processing as well as the reaction to processed data in the overall system. This starts with sampling and filtering the incoming sensory data and continues with extracting the necessary information for higher-level decision system right from the earliest state possible. By extending this approach, one can conclude that also reactions to certain sensor stimuli can be triggered locally without going through a central processing unit of the robotic system.

This idea is similar to the implementation of reflexes in legged locomotion systems [Spennenberg and Kirchner, 2007], [Bartsch et al., 2012]. Whereas the reflexes override the walking patterns in the central processing board of the robotic system, a gripper system with its sensing and actuation modules can be seen as a robot by itself. Following the approach where distributed decision-making is one of the ways

to tackle complex systems [Alexiou et al., 2010], it is advantageous to implement reactions locally rather than in a central processing unit of the robot.

A key property of the implementation of local behavior is simplicity in the algorithmic concepts. Limited instruction sets, processing power and available memory on the embedded systems in the gripper system require proper design of algorithms that are executed locally in order to achieve acceptable reaction times. Metrics like runtime complexity or memory complexity are thus important measured values to determine suitable implementations for signal processing and local control.

Structure of the chapter

This chapter addresses the second objective formulated in the introduction of this thesis. As stated, local pre-processing of sensory data is seen as an approach to limit the effects that an increasing volume of data from sensing modalities has on the processing capabilities in a robot. Furthermore, it is seen as a way of handling runtime complexity and integration complexity in robots. Approaches for locally pre-processing the data obtained from the various tactile sensing modalities are presented in the following sections. When applicable, analogies to biological concepts like the encoding of spike trains or electric potential are drawn.

The different developments for local pre-processing presented in the next sections are grouped. At first, a general solution to limit the amount of sensor data that needs to be transmitted is presented. As the fiber-optic sensing modality shows the highest potential for further data reduction, a workflow specific to this sensing modality was developed and is discussed herein. The fact that local pre-processing is not limited to data reduction is shown based on the example of making use of redundant information in the sampled camera data of the fiber-optic sensors. The final pre-processing approach presented in this chapter is the development of local behavior that goes beyond the implementation of reflexes.

An additional aspect for local pre-processing is to shift the mechanical integration complexity of the fiber-optic sensing modality to software processing. Up to now industrial mass production of the fiber-optic sensor is not available. All manufacturing steps of the sensors are carried out manually. To pave the way to an industrial manufacturing process, an integration process that does not rely on complex manufacturing steps would be desirable. A pre-processing step for simplifying mechanical integration is thus proposed in section 5.1.6 of this chapter.

Parts of this chapter are based on the following publication from which extended excerpts are used in the following sections:

[Kampmann and Kirchner, 2014]:

Integration of Fiber-Optic Sensor Arrays into a Multi-Modal Tactile Sensor Processing System for Robotic End-Effectors

Peter Kampmann, Frank Kirchner

Sensors - Open Access Journal , MDPI - Open Access Publishing, Special Issue Tactile Sensors and Sensing Systems, number 14(4), pp. 6854-6876, Apr/2014.

5.1 Reduction of data transmission

One way to deal with the amount of data that needs to be transmitted to decision levels of robotic systems is to avoid the transmission of data that does not contain useful information. This leads to the question of what is unnecessary and what is useful, a question that cannot be answered generally for all sensing modalities. The following approaches show the implementation of data reduction for the modality of perceiving the gripper pose and for extracting the relevant contact information from the fiber-optic tactile sensing arrays.

5.1.1 Sensor-value-dependent data transmission

In a system where data transmission of sensor values is based on a policy of using a constant frequency for sending data, situations may arise where the constant stream of incoming data contains no new information because there is only little or no change in the sensor value.

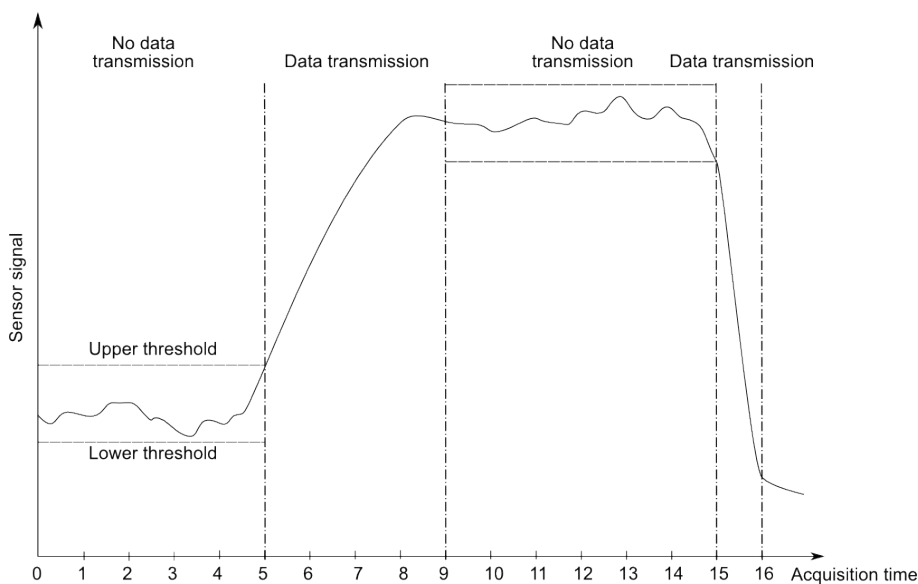


Figure 5.1: Signal sequence of a value-dependent transmission policy

While this data can be processed for monitoring if the sensor processing electronics is still alive, this information is not to be extracted during high-level tasks of a robotic system. It is therefore pre-processed locally. The signal sequence shown in

figure 5.1 shows a solution for transmitting data depending on the extent of changing sensor values.

To determine significant changes in sensor values, a boundary threshold is designed in which no signal transmission occurs. This boundary is chosen, based on the amplitude of the noise component of the sensor signal which can be calculated by the standard deviation. Ideally, this value is constantly adjusted during the robot operation. In the case where the signal change exceeds the signal's standard deviation, the sensor data is transmitted to downstream processing units until the next stable state is reached.

Implementation of this policy can be formalized as follows:

$$t_{trans} = \begin{cases} 0, & |x_{trans-1} - x_{new}| \leq threshold \\ 1, & |x_{trans-1} - x_{new}| > threshold \end{cases} \quad (5.1)$$

The condition for a data transmission t_{trans} is given in cases where the absolute difference between the newly acquired value and the sensor signal from the last executed data transmission exceeds the defined threshold coming from a fixed value or an adapted standard deviation. It is important to make the comparison using the value from the last transmission. Otherwise, a constant signal drift between two consecutive measurements that is smaller than the defined threshold is not recognized by this approach.

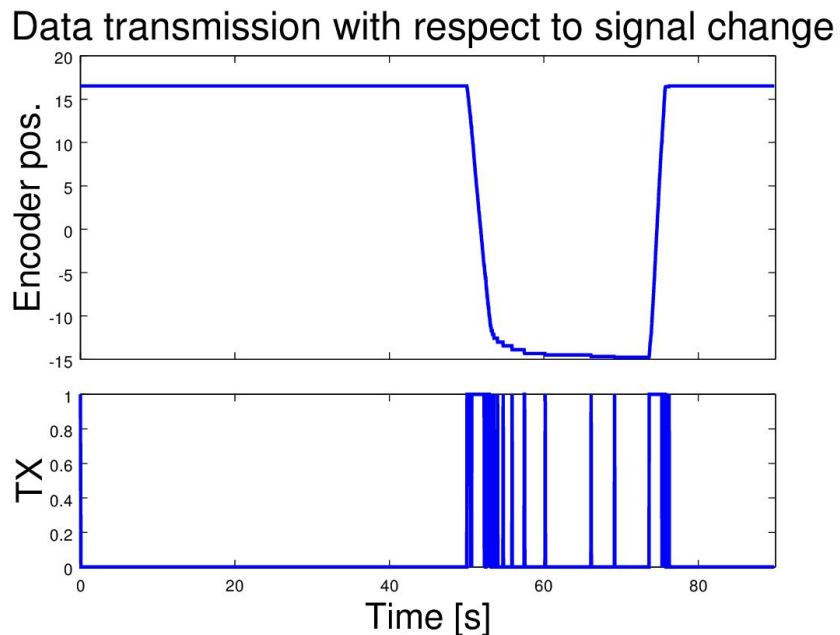


Figure 5.2: Reducing communication intensity through value-dependent transmission

The proposed algorithm is implemented in the gripper for controlling the transmission of the absolute angular encoder data. Figure 5.2 shows the encoder data transmitted during a movement of one joint of the gripper together with the number of packets that are transmitted. The reduction of data transmission is depending on the robot's joint activity. In the case shown here, 97.7% of the transmitted packets could be omitted compared to a transmission using a constant frequency of 100 Hz. Recalling the coding techniques of the mechanoreceptors in the human skin in reaction to an external stimulus briefly shown in Figure 3.1 in section 3.1.1 shows a similarity between the proposed packet transmission policy and the spike trains coming from fast adapting afferent units of type one. Although the sensing modalities are completely different, the transmission of relevant information results in similar ways in terms of encoding the relevant information in both cases .

5.1.2 Handling the fiber-optic sensor array data

A look at Table 5.1 reveals that the major share of the data generated by the sensing system is coming from the fiber-optic sensor arrays. The reasons for this can be found in the way the sensor data is acquired. Due to the use of a camera system for signal conversion where each optical fiber is interfaced by several pixels of the camera, the data obtained from the acquisition electronics contains redundant information.

The fiber-optic sensor information has to be extracted from the camera image to perceive the geometric contact information. The neighborhood relationships of the sensor elements in the contact area have to be reconstructed. To reduce the communication load in the robotic system, the necessary acquisition and calibration steps are implemented in the processing electronics for the fiber-optic sensor arrays presented in section 4.7.3. To enable the implementation in embedded systems, the required algorithms are developed with regard to optimized performance in terms of the required mathematical operations, runtime and memory consumption. Steps to optimize algorithms under these conditions use simple mathematical operations having minimal runtime and memory complexity.

The processing steps from the acquisition of the camera image of the optical fibers to the display of spatially aligned tactile images are shown in Figure 5.3. The processing flow starts with capturing the sensing fibers of the sensor array using the cameras on the electronics (top left). The result is a camera image containing circular objects representing the endings of the fibers. By using image processing, the fibers are identified in the camera image (top right). Knowing the dimensions of the sensor array, the extracted information can be arranged in the geometrical shape of the tactile field.

Further steps are required to identify the spatial alignment of sensor elements

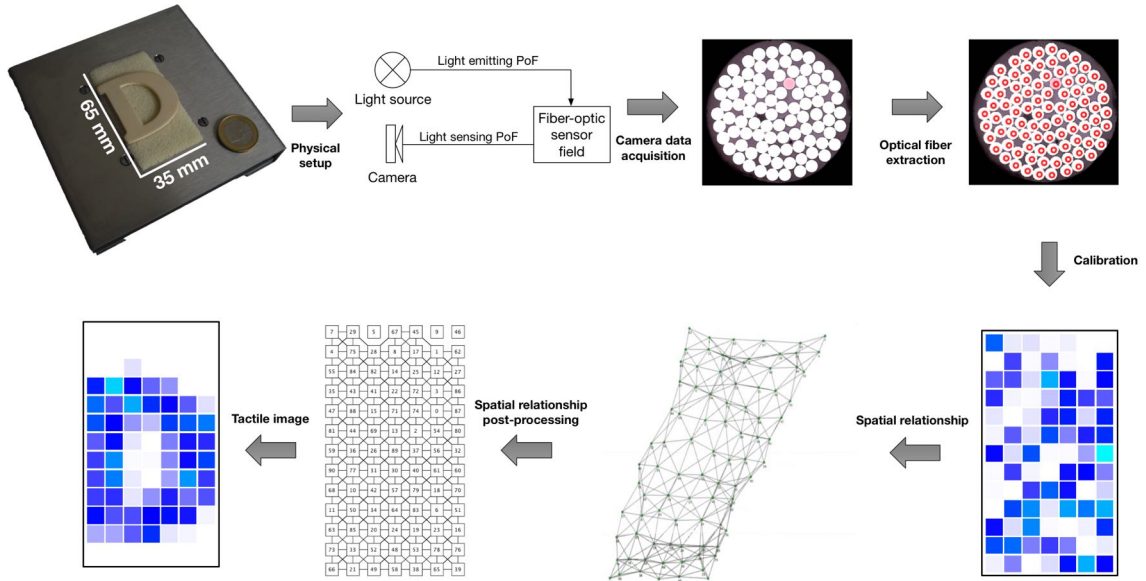


Figure 5.3: Processing flow from raw camera images to tactile sensor array data

in the array to correctly display geometric shapes. At first, sensor elements with limited signal amplitude are identified. Therefore, the sensor elements are activated and the signal response is monitored. Sensing elements with low amplitudes are excluded from the following step, which identifies clusters of sensor elements. To identify these, the sensors are activated by a single point of contact. Those sensors that are activated simultaneously are expected to be placed spatially near to each other on the sensor array. This observation is used to build clusters of sensor elements. The result is a mesh containing sensor elements and their connections to their neighbors. Using graph layout algorithms, this mesh can be used to compute a topology that resembles the final grid structure. Fine tuning is carried out afterwards by using a Self-Organizing Map (SOM). A detailed presentation of the algorithms used in the processing flow is provided in the following sections. To be able to follow each step in the calibration more easily, each chapter that discusses a transition within the workflow is started with a subgraphics from the diagram shown in figure 5.3.

5.1.3 Camera data acquisition

The initial stage in the processing of the fiber-optic sensor arrays involves sampling the camera images. As six camera images on the PCB have to be acquired in parallel, an FPGA is selected for this task. The chosen FPGA is a Xilinx Spartan 6 LX 25. To receive a camera image as shown in Figure 5.4 on the right, acquisition algorithms running in parallel for each camera were implemented.

The required camera interface was implemented in very high speed integrated

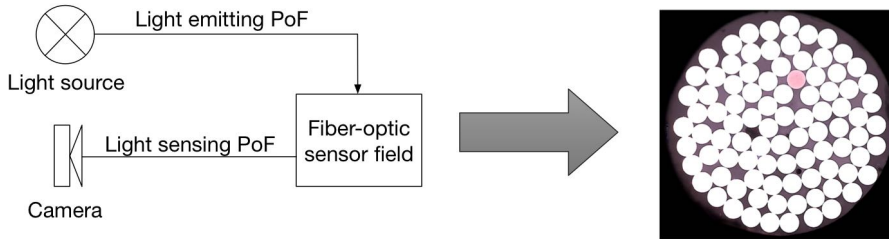


Figure 5.4: Camera image acquisition

circuits hardware description language (VHDL). The configuration of camera parameters is realized using an Inter IC Bus (I^2C) bus. The synchronization with the camera data is achieved via signals from the camera module. Triggered by the synchronization for every pixel, line and frame, the incoming data is sampled from an 8 bit parallel bus.

The following algorithm design was designed taking into account the specification of the PCB for the fiber-optic tactile sensor. Thanks to the capability of extracting the relevant information from the camera images with little memory complexity, a space-consuming memory module to store a complete camera image was not necessary. On the downside, a camera image like the one in Figure 5.4 can only be sampled by streaming the pixel information to a downstream processing unit rather than storing a complete image. Limited by the bandwidth of the low voltage differential signalling communication, the transmission of an unprocessed image results in an update frequency of 0.5 Hz.

5.1.4 Optical fiber extraction

Formulation of the problem and first solution

To effectively reduce the volume of data that needs to be processed from the fiber-optic sensors, the optical fibers are extracted from the camera image. A sample camera image is shown in Figure 5.5. The white circles in the image are the fiber endings of the sensing polymer optical fibers. The varying brightness of these circles corresponds to a different intensity of the received light. By analyzing the raw camera image in Figure 5.5 on the left, the detection of circles in an image seems to be an advantageous way of finding the positions of the optical fibers. Using standard image processing techniques, a Hough Transform [Hough, 1959] adapted to the recognition of circular objects [Kimme et al., 1975] appears to be a straightforward approach to tackle this task. The purpose of this algorithm is to detect of circles in images with varying diameter as well as circles that are partly occluded.

Due to the demanding requirements in terms of computation power and memory consumption, several optimized versions of this algorithm were implemented in

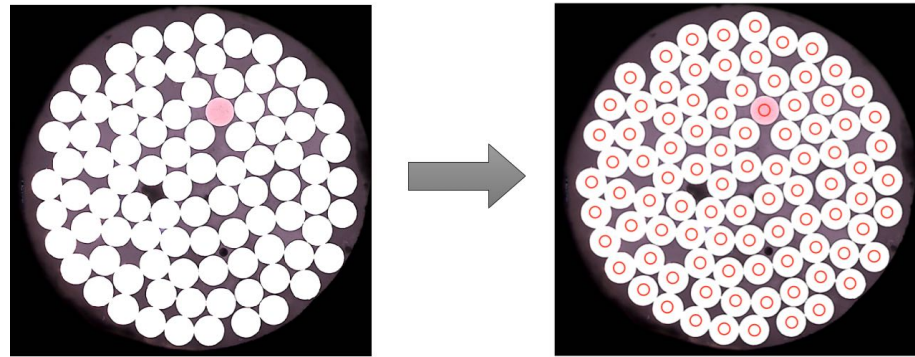


Figure 5.5: Extracting the optical fibers from the camera image

the last years. An optimized version of the circular Hough Transform using gradient information [Bradski and Kaehler, 2008] as implemented in the image processing library OpenCV [Bradski, 2000] is described briefly.

Theory of operation of the Circular Hough Transform

The first step of this algorithm is to detect edges in images using a Canny edge detector [Canny, 1986]. Therefore, the image is transformed into a gray scale representation and filtered using a Gaussian smoothing filter. By applying the Sobel operators [Sobel and Feldman, 1968] as shown in equation 5.2 in the x and y dimension of the image, two images are created where the edges of the image are stressed in the respective dimensions:

$$g_x(x, y) = I(x, y) \cdot \begin{bmatrix} 1 & 0 & -1 \\ 2 & 0 & -2 \\ 1 & 0 & -1 \end{bmatrix}, g_y(x, y) = I(x, y) \cdot \begin{bmatrix} 1 & 2 & 1 \\ 0 & 0 & 0 \\ -1 & -2 & -1 \end{bmatrix} \quad (5.2)$$

The last step of the edge detection algorithm takes the two obtained images $g_x(x, y)$ and $g_y(x, y)$ and combines the data to a single image containing the detected edges. This is achieved by calculating the sum of the absolute values of each pixel from the two resulting images from the Sobel filter:

$$G(x, y) = |g_x(x, y)| + |g_y(x, y)| \quad (5.3)$$

The obtained image containing the edge information is used to calculate the local gradient of every pixel that belongs to an edge, using the Sobel kernels shown in equation 5.2.

A data structure called *accumulator* is used to find potential circle centers within the previously defined upper and lower bounds of the possible radii for the circles. This step is carried out by calculating a possible circle center coordinate based on the

direction of the calculated gradient at the edge position and the defined radius. This process is pictured in Figure 5.6.

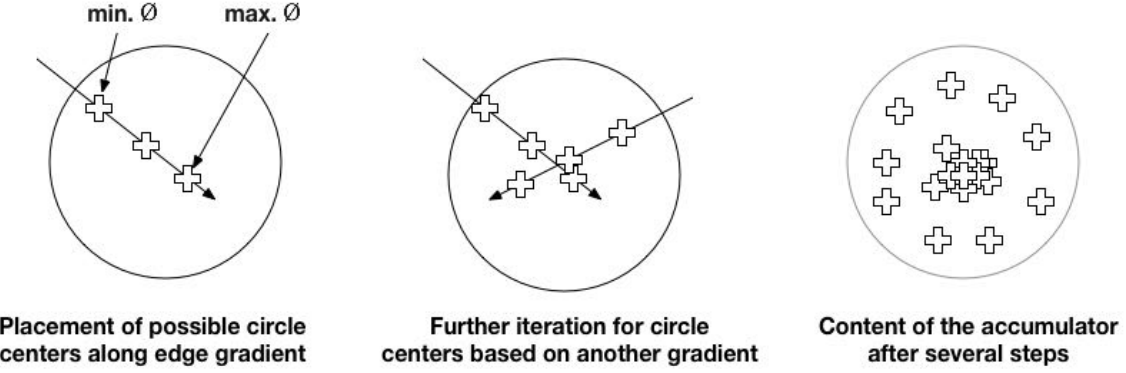


Figure 5.6: Identifying circle centers using circular Hough Transform based on gradients

Possible circle centers are marked with a cross in the graphics. These coordinates are stored in the accumulator. For each placement of a circle center on the same coordinate, this position gains weight. The positions with the highest weights within defined boundaries are processed in a final step in which the number of pixels belonging to an edge are compared with various radii from the circle center. Finally, the radius having the highest number of edge pixels in its range is chosen.

Equation 5.4 shows the computation of the runtime complexity of the presented approach, assuming a gray-scale input image.

$$\begin{aligned}
 O(N)_{max} &= \overbrace{\underbrace{9N}_{\text{Gaussian Filter}} + \underbrace{9N}_{\text{Sobel}_X} + \underbrace{9N}_{\text{Sobel}_Y} + \underbrace{N}_{\text{Absolute sum}}}^{\text{Canny edge detection}} + \overbrace{\underbrace{9N}_{\text{Sobel}_X} + \underbrace{9N}_{\text{Sobel}_Y}}^{\text{Gradient calculation}} + \overbrace{\underbrace{N}_{\text{Fill Accum.}} + \underbrace{N}_{\text{Find centers}} + \underbrace{N}_{\text{Check centers}}}^{\text{Circle detection}} \\
 &\quad (5.4)
 \end{aligned}$$

$$= 49N \quad (5.5)$$

$$\begin{aligned}
 O(N)_{min} &= \overbrace{\underbrace{9N}_{\text{Gaussian Filter}} + \underbrace{9N}_{\text{Sobel}_{X,Y}} + \underbrace{N}_{\text{Absolute sum}}}^{\text{Canny edge detection}} + \overbrace{\underbrace{9N}_{\text{Sobel}_{X,Y}}}^{\text{Gradient calculation}} + \overbrace{\underbrace{N}_{\text{Fill Accum.}} + \underbrace{N}_{\text{Find centers}} + \underbrace{N}_{\text{Check centers}}}^{\text{Circle detection}} \\
 &\quad (5.6) \\
 &= 31N \quad (5.7)
 \end{aligned}$$

Depending on parallel or serial execution of the algorithm, an upper and lower boundary for the runtime can be calculated. The input parameter N refers to the dimensions of the input image. The initial edge detection algorithm examines every pixel of that image resulting in an output image of the same dimensions. When

applying the filter to each pixel, the values of eight neighboring pixels together with the pixel value at the current position are used for the calculation.

The following gradient calculation uses the same Sobel operations as the Canny edge detection calculated previously. In this step the filter is applied to the image containing the detected edges. This image is of the same size as the input image, thus the Sobel operators have to be calculated for all pixel elements of the image. The final circle detection uses the information stored in the accumulator. Its runtime varies depending on the number of potential circles that are identified in the image. The size of the accumulator is initialized to the input image size, which is why the runtime depending on N being the image size is chosen as an upper boundary for this part of the algorithm.

A similar calculation is carried out for the memory complexity of the algorithm:

$$M(N)_{max} = \overbrace{N}^{\text{Input image}} + \overbrace{N}^{\text{Gaussian filter}} + \overbrace{N}^{\text{Sobel}_X} + \overbrace{N}^{\text{Sobel}_Y} + \overbrace{N}^{\text{Absolute sum}} + \overbrace{N}^{\text{Sobel}_X} + \overbrace{N}^{\text{Sobel}_Y} + \overbrace{N}^{\text{Accumulator}} = 8N \quad (5.8)$$

$$M(N)_{min} = \overbrace{N}^{\text{Input image}} + \overbrace{N}^{\text{Sobel}_X} + \overbrace{N}^{\text{Sobel}_Y} + \overbrace{N}^{\text{Accumulator}} = 4N \quad (5.9)$$

An upper and lower boundary is calculated for the required memory depending on the input size. As for the runtime complexity, N represents the image size. In the case of optimized memory usage, the memory required for calculating the Sobel filters is used twice during the Canny edge detection and for the gradient calculation. Furthermore, the optimized memory complexity calculation assumes loss of the original image.

In terms of implementing this approach, the calculations of runtime and memory complexity give an indication of the performance in the specific hardware that was designed for the task. Compared to the runtime- and memory complexity of the original Hough Transform, which is reported to be $O(N) = M(N) = N^3$ [Ioannou et al., 1999], the presented algorithm is a considerable improvement.

Motivation for a situation-aware algorithmic solution

Although the algorithms presented have to run only once during calibration, a low runtime complexity may enable a continuous calibration that allows simplification of the mechanical integration of the sensor. By continuously identifying the position of the optical fibers on the camera image, a displacement of the fibers in the camera image caused by a flexible connection between the camera chip and the optical fibers can be handled. Thus, an algorithm that has a low runtime complexity can contribute

to a reduction in the complexity of robotic integration.

The memory complexity of an algorithm defines the amount of memory required to be available during execution. It therefore defines the requirements for the memory modules, which also influences the dimensions of the electronics since more integration space is required with increasing storage capacity. Regarding the optimized memory complexity of the algorithm that requires storage of four times the size of the input parameter, 1.2 megabytes of data need to be stored during execution of the algorithm. This memory capacity can be calculated by multiplying the resolution of the cameras used on the electronics developed, i.e. 640x480 pixels with a precision of 8 bit for every pixel. A final multiplication with the result of the calculated memory complexity results in the required memory size.

Considering the capabilities of the chosen algorithm with respect to the quality of the images that need to be processed indicates that the algorithm is suited for more challenging conditions than the ones that can be found in the input images as in Figure 5.5. There is a great contrast between the circles and the surrounding environment, all circles are of almost the same size and there is little noise in the image.

Theory of operation: Contrast and geometry based circle detection (CoGe)

An algorithmic approach tailored to the specific conditions may lead to optimized performance in runtime and memory consumption. As the camera image is sampled sequentially line by line, an algorithm that is able to start processing while the image is not fully sampled is desirable to optimize both runtime and required memory.

The following approach is developed to address these issues. The main idea behind its concept is to find the circle centers rather than the whole circle. It exploits the fact that the center of a circle always lies on the plane where a secant line has its maximum length within the circle. As the image is sampled line by line, the requested secant line intersects the circle horizontally:

Given the equation for a circle on a plane:

$$f_c(x, y) = (x - c_x)^2 + (y - c_y)^2 - r^2 = 0 \quad (5.10)$$

There exists a horizontal secant line in the following form:

$$f_s(x) = xb \quad (5.11)$$

This expression can be incorporated into equation 5.10:

$$f_c(x) = (x - c_x)^2 + (xb - c_y)^2 - r^2 = 0 \quad (5.12)$$

The obtained equation has to be transformed into the standard format of a quadratic equation:

$$f_c(x) = x^2 - 2x(c_x + bc_y) + xb^2 - c_x^2 - c_y^2 = 0 \quad (5.13)$$

With the terms:

$$p = -2x(c_x + bc_y) + xb^2 \text{ and } q = -c_x^2 - c_y^2 \quad (5.14)$$

By applying the standard pq formula, we get the x coordinates x_1 and x_2 of a secant crossing the circle. The corresponding y coordinates y_1 and y_2 can be obtained by inserting the values for x_1 and x_2 into equation 5.11. The circle center coordinates are crossed by the secant that has the maximum distance d between the intersections (x_1, y_1) and (x_2, y_2) .

$$d = \sqrt{(x_1 - x_2)^2 + (y_1 - y_2)^2} \quad (5.15)$$

Where d is maximal within the circle. The resulting circle center coordinate c_x, c_y is given by:

$$c_x = x_2, c_y = y_1 + \frac{y_2 - y_1}{2}, \text{ where } (y_2 > y_1) \quad (5.16)$$

Algorithmic implementation of CoGe

The algorithmic implementation of this approach exploits the high contrast between the circles and the background in the image [Kampmann, 2010]. The algorithm is executed on a gray scale image with 8 bit resolution. Pixels with a value in the upper range of the measurement range are considered to belong to a circle. The threshold for distinguishing between pixel values belonging to a circle or to the background can be set empirically or by an initial analysis of the distribution of sensor values. The acquisition of the camera image line by line supports the identification of horizontally aligned secant lines. Each sampled pixel value is evaluated with regard to belonging to a circle or to the background of the image. The number of consecutive pixels assigned to a circle are counted. As soon as a pixel value is sampled that is below the threshold for being part of a circle, the accumulated values are evaluated. The size of the sum represents the distance between the points where the secant line enters and leaves the circle. Based on a pre-defined minimum distance of consecutive white pixels, a decision is made as to whether the coordinates and the length of the secant line are stored for later comparison. After this step the process starts over until the image is fully analyzed. The workflow of the algorithm is visualized in diagram 5.7.

After the image acquisition is finished, the stored coordinates and the lengths of the secant lines are analyzed. Secants whose x and y position is within the range of a defined interval are considered to belong to the same circle. Among these secant lines the one having the largest distance is selected for inclusion in the circle center. In the case that this approach leads to more than one secant line, the selection depends

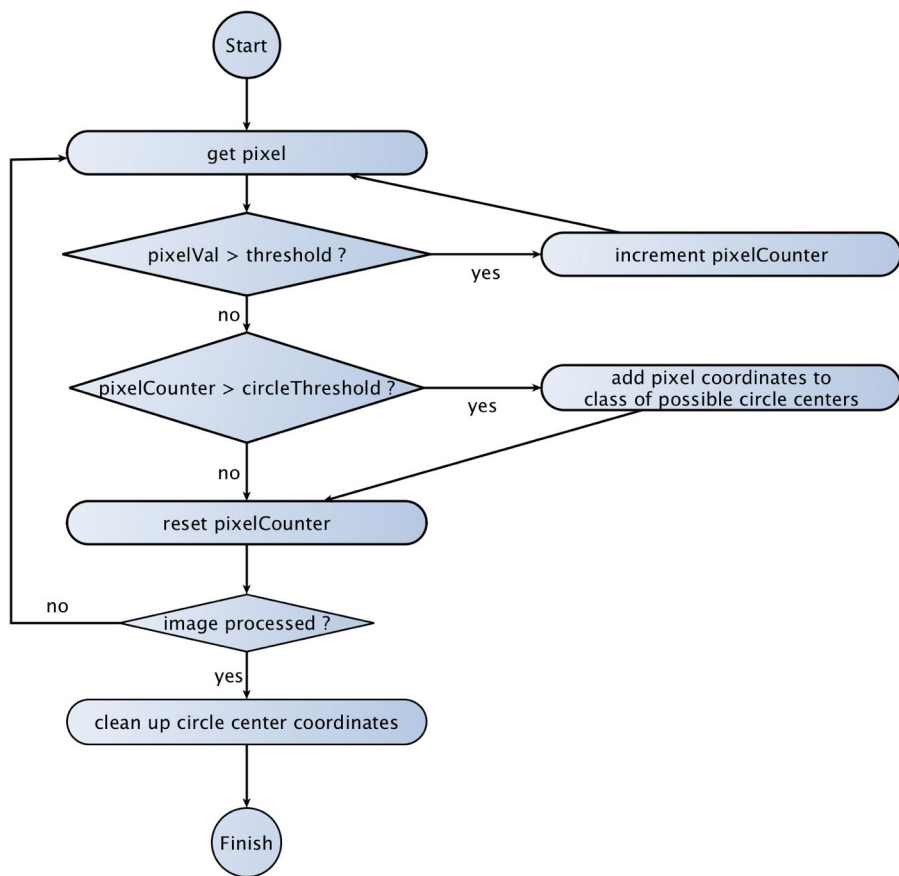


Figure 5.7: Working principle of the algorithm to detect optical fibers

on whether the result is an even or odd number. If an odd number of secant lines is obtained, the one lying in the mid is chosen while in the case of an even number, the one that is closest to the center is selected. The application of the algorithm at the example of a circle is shown in Figure 5.8.

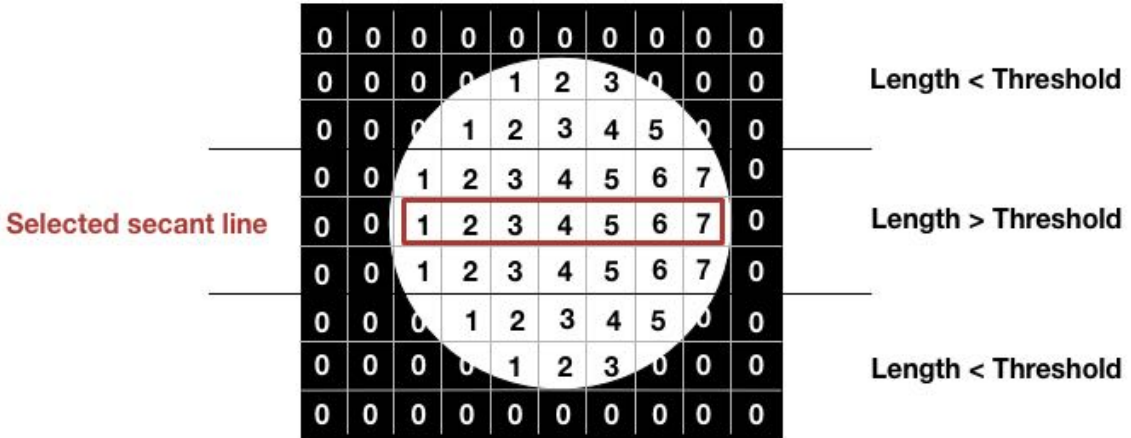


Figure 5.8: Working principle of the algorithm to detect optical fibers

Runtime and memory complexity of CoGe

The proposed algorithm is able to process the image stream during its acquisition as each processing step can be run without including information from surrounding pixels. Partly occluded fibers can be handled as well. The maximum number of consecutive white pixels still indicate the circle center. Mathematical operations, such as roots and trigonometric functions that are complex to implement using logic elements, are avoided. Thanks to the shift operator, which has the property of dividing values by two in binary representations, the required division by two for determining the final x coordinate of a circle center is implemented using resource-saving logical operations. Because the algorithm does not require the full image to operate, the image does not have to be stored. Memory space is required for storing the coordinates and the length of white pixels of the circle center candidates.

The runtime complexity of this approach is calculated by the following equation:

$$O(N) = \overbrace{N}^{\text{Image acquisition}} + \underbrace{height_{image} \cdot \frac{width_{image}}{dim_{min}} \cdot \frac{1}{3}}_{\text{Post processing}} \quad (5.17)$$

With N being the size of the input image, the algorithm has to evaluate the value of each pixel element. Additional processing time is required to analyze the lengths of the identified secant lines. The runtime of the analysis depends on the number of secant lines that were identified to intersect the center of a circle. The obtained

number of secant lines depends on the thresholds that were initially defined for the minimum diameter of a circle. The size of the optical fiber endings in the camera image differs between different camera resolutions and the chosen diameter of the optical fibers. To cope with variations in the contrast and manufacturing variations of the optical fibers, a worst case upper boundary is defined that allows variations of up to a third of the average circle diameter. In the case of an image that is completely covered with circles that have to be analyzed, the runtime of the analysis step is approximated to be $height_{image} \cdot \frac{width_{image}}{dim_{min}} \cdot \frac{1}{3}$, where dim_{min} denotes the minimum length of a secant line to be considered for analysis. The additional runtime required for the analysis is in any case smaller than the time required to capture an image. By implementing the algorithm using a two-stage pipeline, the algorithm is able to run in real time which in this case means that the algorithm finishes between capturing two images.

The memory complexity is computed as:

$$M(N) = height_{image} \cdot \frac{width_{image}}{dim_{min}} \cdot \frac{2}{3} \cdot prec_{coord.} \cdot prec_{secant} \quad (5.18)$$

As can be seen in equation 5.18, the required storage depends on the parameterization of the algorithm. Memory has to be available to store the secant lines that were identified as potentially crossing the center of a circle. The parameter $prec_{coord}$ describes the resolution in bits required for storing the x and y coordinates of circle center candidates in the image. $prec_{secant}$ denotes the precision that is required to store the length of the secant lines.

Applying this observation to the implementation that is used for the embedded modules, the following values can be inserted into the equation:

$$M(N) = 640 \cdot \frac{480}{27} \cdot \frac{2}{3} \cdot 9bit \cdot 5bit = 640 \cdot 17.78 \cdot \frac{2}{3} \cdot 9 \cdot 5 = 41.67kByte \quad (5.19)$$

Performance comparison

Comparing the runtime performance of the CoGe algorithm with the circular Hough implementation a considerable difference between the two approaches can be observed. Thanks to the property of not having to store the full image for processing, the required memory capacity differs from the circular Hough by several orders of magnitude (1.14 Megabyte vs. 41.67 Kilobyte). The memory requirements of the algorithm also affect the design decisions for the hardware as it allows the selection of memory modules having a small footprint. The low runtime complexity of the algorithm enables processing of the images in real time when implementing the approach in a two-stage pipeline.

The proposed algorithmic solution is implemented in the FPGA on the Camera-Control PCB (compare section 4.7.3). The required hardware resources amount to 8% slices used on an FPGA of type Spartan 6 LX25 from manufacturer Xilinx. The absolute runtimes for a test image containing 96 optical fibers are shown in Figure 5.9. For the tests on a personal computer, a 2.4 Ghz Intel Core 2 Duo machine was used having 4 GB RAM.

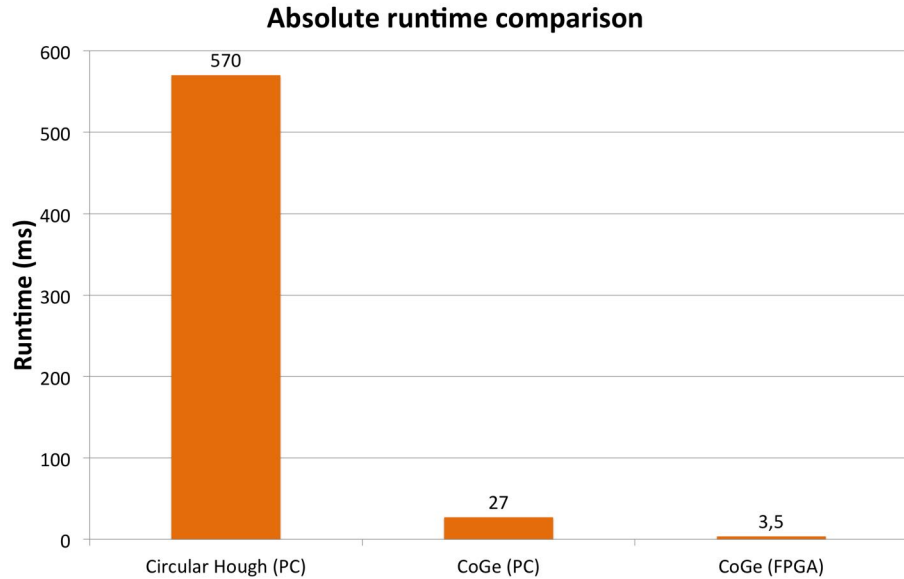


Figure 5.9: Runtime comparison of the different implementations for extracting the optical fiber information

Enhancements to reduce sensor noise and increase dynamic response

The algorithm developed takes the pixel value at the center of each fiber as a sensor value for the fiber-optic sensor array. As each optical fiber is covered by several pixels in the camera images, several camera pixels carry the information for the same tactile sensing element. This property can be exploited in various ways.

The redundant information can be used to increase the robustness of data acquisition. In case of defect pixel elements in the camera image, the information of surrounding pixel elements can still be used to compute reliable sensor feedback.

By averaging the feedback of several pixel elements belonging to the same optical fiber, the noise of the sensing elements can be reduced. This approach does not influence the dynamic response of the tactile sensor data, as the averaging takes place for sensor information acquired in parallel. The impact of this approach was evaluated on a tactile sensor array having 91 sensing elements. The results can be seen in Figure 5.10. The average noise level is reduced up to 50% compared to an approach where the feedback of each tactile sensor element is based on a single pixel value.

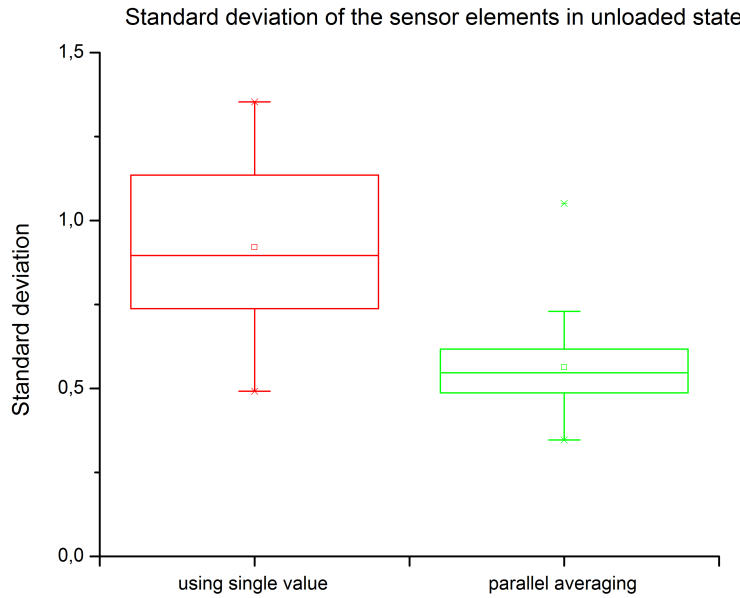


Figure 5.10: Average noise reduction of the sensor element feedback via parallel averaging of the sensor feedback using multiply camera pixel values. (calculations based on feedback from a sensor array with 91 sensor elements)

An analysis of the distribution of the change in light intensity at the optical fibers interfacing the camera reveals a non-uniform brightness distribution in each fiber. Figure 5.11 shows a section of a camera image where differences in brightness can be observed between the circle center and the edge regions of an optical fiber.

To optimize the dynamic range of the tactile sensor, the signal span of each camera pixel belonging to a tactile sensing element is evaluated by recording the differences in brightness while loading and unloading the sensor. The tactile sensor feedback is computed by averaging the pixel values that respond within 10% of the highest dynamic range. The effects of this approach can be seen for a tactile sensor array comprising 91 sensing elements in Figure 5.12. An increase of the dynamic range is achieved for every sensor element. While the sensor feedback was increased by up to 50% for single sensor elements an average improvement of 30% in dynamic range is achieved.

5.1.5 Calibration

Several material properties of the sensor have an influence on the dynamic range and signal offset of a tactile sensor element. One parameter is the alignment of the

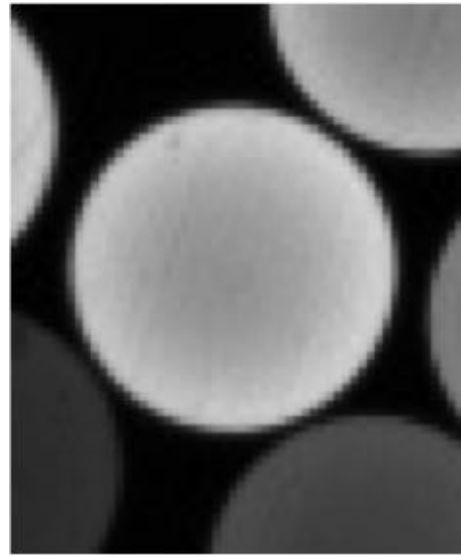


Figure 5.11: Non-uniform light distribution in an optical fiber.

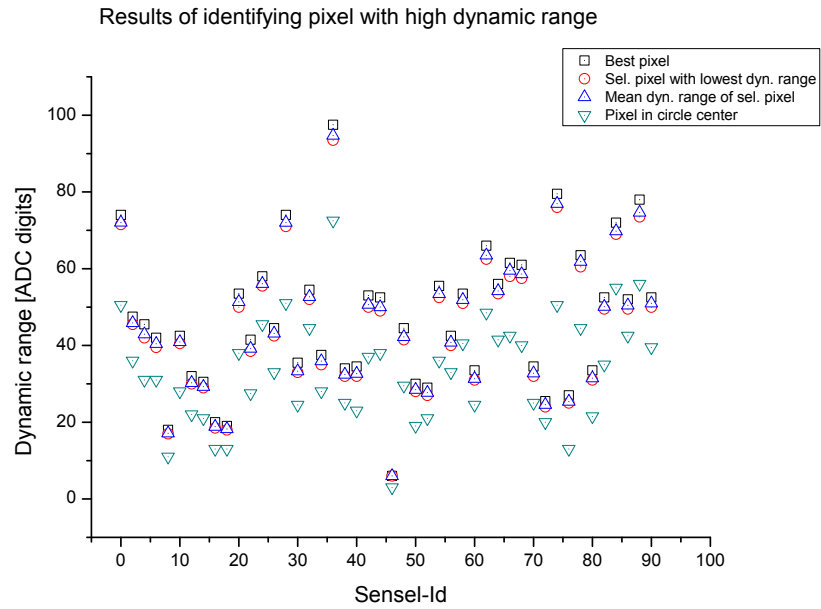


Figure 5.12: Improvements in dynamic range using multiple pixel elements to compute the tactile sensor feedback. (calculations based on feedback from a sensor array with 91 sensor elements)

optical fibers with respect to each other. The fibers are glued together and placed into the holes of the carrier plate. Due to manufacturing tolerances, it cannot be ensured that the sensing and emitting fiber in every pair are aligned in parallel in the sensing area. A variation of the orientation of the two fibers leads to different reaction characteristics of a sensor element.

Another parameter is the structure of the foam itself, see Figure 5.13 for microscope pictures of different foams and their structure. Depending on the manufacturing process, variations in the distribution of cavities in the foam structure may occur which can lead to different scattering behavior of the emitted light depending on the position of an optical fiber pair beneath the foam.

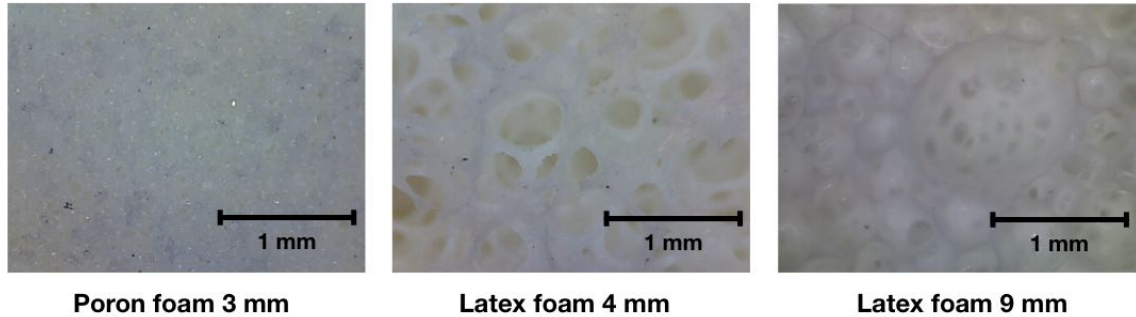


Figure 5.13: Different foam types and their inhomogeneous structure

Based on evaluations on the signal performance in water (discussed in section 6.2.2), a foam made of latex having a thickness of 4 mm was selected. The inhomogeneous structure of this foam material is depicted in Figure 5.13 in the center.

As a result of these effects, the initial sensor offset for each tactile sensing element differs, causing a non-uniform signal response. The data in Figure 5.14 shows the initial idle sensor response (left) and the variations in signal span (right) exemplary for a fiber-optic sensor array having 72 sensing elements using a latex foam having a thickness of 4 mm. Experiments with other fiber-optic sensor arrays with the same working principle confirmed the observations shown.

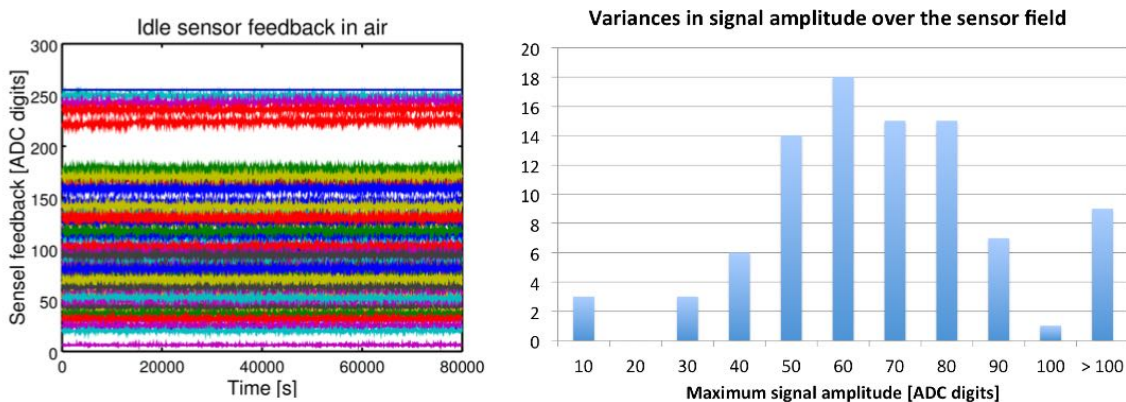


Figure 5.14: Non-uniform sensor response during idle state (left) and variation in the maximum signal amplitude (right). (plots based on feedback from a sensor array with 91 sensor elements)

In order to obtain geometric information from a tactile array sensor, only switch-

ing behavior of the sensor elements is required. Additional information about force distribution can be obtained by means of an equilibration of the sensor elements. The sensor feedback across the sensor array can be adjusted by determining the initial offset and signal span and using this for computing an equilibration factor for the sensor elements.

To enable calibration in the field that does not require specialized calibration tools, a method is developed that can be carried out merely by activating each sensor element by hand. The calibration routine is working as follows: Initially, all sensor idle offsets are recorded and taken as the lower boundary of the sensor dynamic range. By successively activating the sensor elements of the array, the maximum response is recorded. To avoid a calculation of equilibration factors that are based on sensor feedback caused by cross activation, each sensor element has to be activated at least three times with its sensor feedback reaching similar values. To identify suitable intervals in which the sensor feedback is assumed to come from a targeted activation, an experiment was conducted to identify the deviation between several activations of sensor elements on a sensor array. The results are summarized in Figure 5.15. The obtained graph shows the standard deviation for all sensor elements of a sensor array comprising 91 sensor elements after 18 targeted activations of each sensor element.

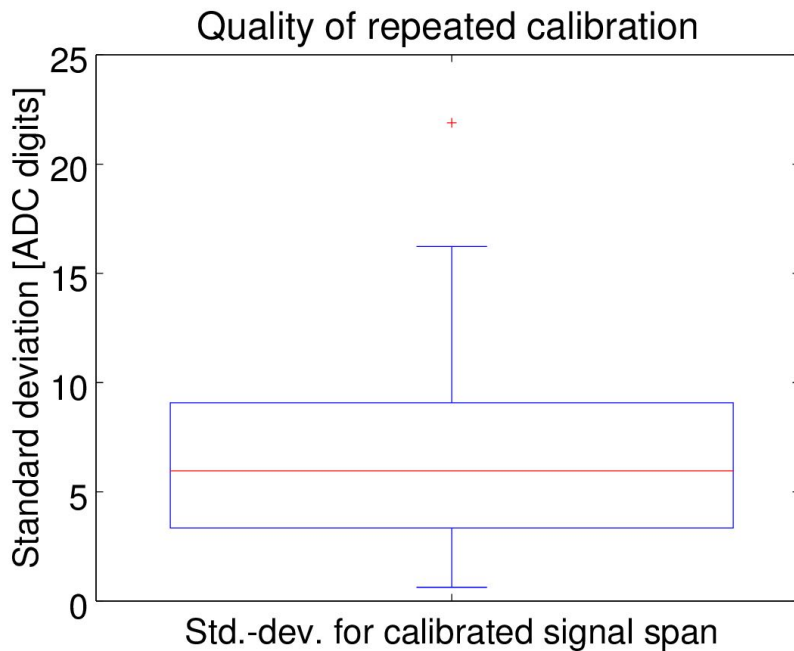


Figure 5.15: Distribution of signal spans after 18 targeted activations of all sensors in a sensor array with 91 elements

The standard deviation of the calibrated signals is 7% at maximum and 2% on

average. As a heuristic, the limits within which the sensor feedback is expected in case of a targeted activation was set to 15% of the maximum signal span.

Identification of the signal range of each sensor element can further be used to identify defect sensor elements. A metric was defined that classifies a sensor element to be non-functional if its maximum dynamic response is below 2% of the possible signal range.

The proposed calibration method to equilibrate the sensor signals works well in cases where the foam material is glued onto the carrier plate and thus has a fixed position. In the case where the tactile sensors were used in the gripper system under water together with silicone oil for electric isolation, the glue to keep the foam at a fixed position loses its adhesiveness. Therefore, the foam is placed loosely onto the carrier plate, in which case the equilibration is not effective. Further techniques for working with sensor data that is not equilibrated are presented in section 5.2 where the sensor data is used for local control.

5.1.6 Spatial relationship

In order to reduce the mechanical integration effort of the tactile sensor array, the optical fibers are mounted onto the camera chip without preserving the spatial relationship of the sensor elements in the sensing area. To perceive the geometric shape of objects in contact, it is necessary to restore the neighborhood relationship of the sensor elements.

A possible solution to reconstruct the spatial relationship in the contact area is to use a calibration tool that is able to activate sensor elements without cross-activating surrounding ones. By activating the sensor elements of the array in a predefined sequence and frequency, sensor elements identified on the camera chip can then be mapped to the sensor elements on the field. The size of the required probe depends on the spatial density of the sensor array. The higher the resolution, the smaller the activation tool needs to be in order to avoid cross-activation. Depending on the contour of the sensor array, the activation needs to adapt to the sensor surface in more than one degree of freedom. This requires a positioning unit that is able to approach positions in the xyz plane. In case of a three-dimensional surface of the sensor array, rotating the probe is necessary as well to activate the sensor elements in the direction of their surface normals. In summary, this approach requires a complex calibration device that necessitates a laboratory environment. Solutions with fewer requirements are favorable.

Another attempt that does not require a complex calibration setup exploits the simultaneous activation of sensor elements in the event of contact by a probe. Assuming single touch activation of the sensor field, all sensors that are activated si-

multaneously are situated in the same area of the array. Using this property along with the knowledge that sensor elements arranged in a grid structure have a maximum of eight neighboring sensor elements enables computation of all neighbors of a sensor element.

The proposed identification of the spatial alignment is implemented by randomly compressing the tactile array with a finger. For each sensor element the activated neighbors and their signal strength are recorded.

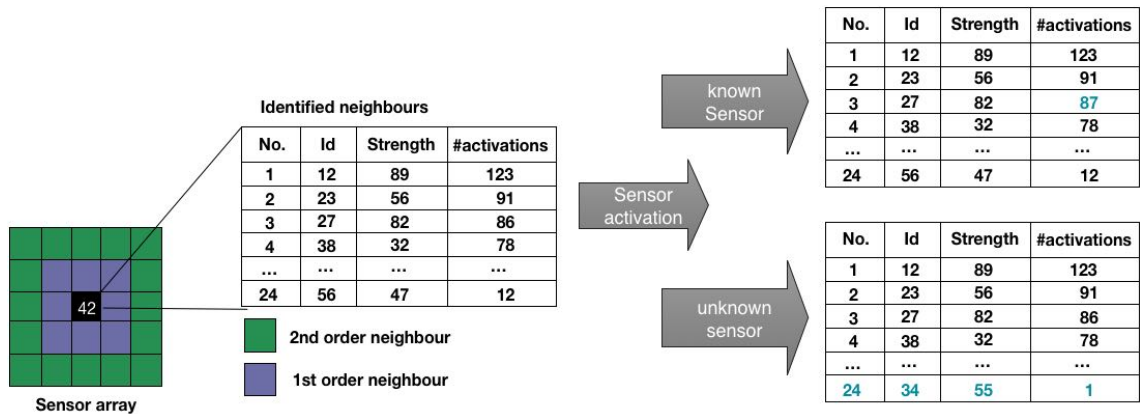


Figure 5.16: Implementation of neighborhood detection

The way neighbors of a sensor element are stored follows the least recently used (LRU) strategy found in cache memory devices as a replacement strategy. The illustration in Figure 5.16 visualizes the approach. A table is assigned to each sensing element where the activated sensor elements are stored together with their signal strength and the number of activations that took place simultaneously. Each table has 24 rows, which allows storage for first order and second order neighbors of the sensor.

The simultaneously activated sensor elements are processed with every sensor activation. In the case of an already known sensor element, its corresponding sensor identifier is already stored in the table. Its activation counter is increased in the respective row. In the case of a previously unknown sensor, either its parameters are stored in an empty row of the table or - if the table is already filled - the sensor element with the lowest occurrence is removed and the new one is inserted in the table. By randomly activating areas of the tactile sensor array, the required neighborships are identified. A good metric for determining the progress of the calibration process is to look at the rate at which sensor elements are newly added to the table of known neighboring sensor elements. The slower it is, the more stable the sensor relationships are.

After the algorithm has reached a stable state and the neighbors of each sensor element are identified, the question remains as to how to arrange the sensor elements

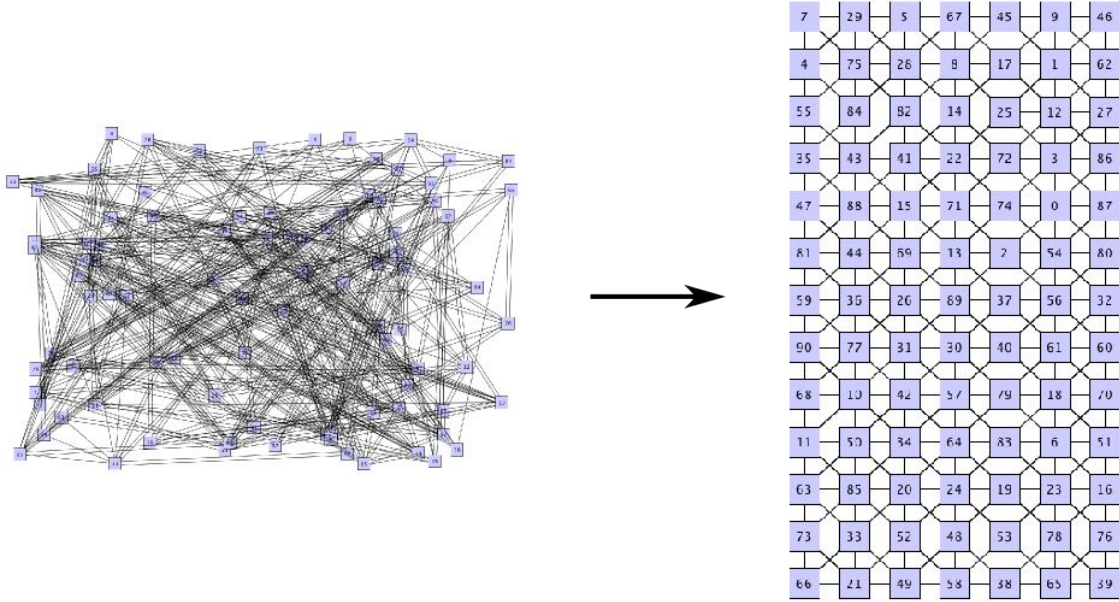


Figure 5.17: Mapping to the grid of the sensor elements after neighborship detection

in relation to each other on the grid. Figure 5.17 visualizes the open computation step. Although the relationships between the sensor elements are known, the exact location in relation to each other is still unknown.

The necessary step is exemplary shown in more detail in Figure 5.18. The sensor element with the id 84 has a known neighbor with id 41. In this state, it is still not known where this sensor element has to be mapped on the grid of the sensor field. One way to obtain the required information is to evaluate the identified neighboring sensor elements for all sensors, resulting in considerable computational effort.

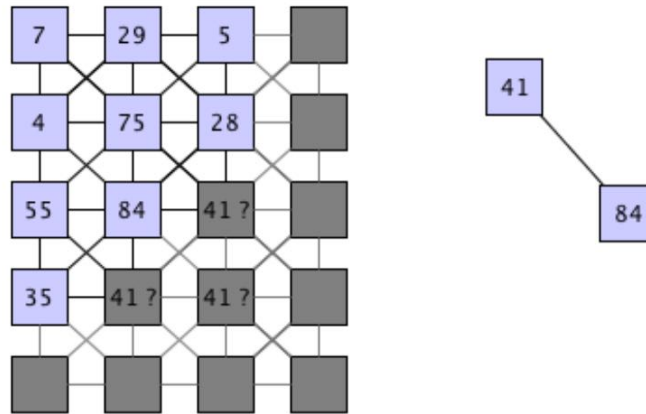


Figure 5.18: Placement of neighboring sensor element

A discipline that deals with similar questions is the domain of hardware synthesis, is used for mapping the logic elements in an FPGA. The challenge here is to map elements that are connected in a logic graph to nearby cells of the reprogrammable logic to ensure low latency in the execution. Placing components together that are connected with each other is therefore a good approach. A technique that is used to solve this problem involves using force-directed layout algorithms [Shahookar and Mazumder, 1991].

A commonly used implementation of these algorithms is the one developed by [Fruchterman and Reingold, 1991]. The working principle of this algorithm is explained using the sensor element placement challenge described above: Initially all sensor nodes are placed randomly on a plane. Each sensor node generates attractive or repulsive forces. Sensor nodes that are linked to each other via an edge exert attractive forces and thus move towards each other. Sensors which are not interconnected exert repulsive forces and move away from each other. By repetitive execution of this algorithm a layout is generated that maps the neighborhood relationships of the sensor elements.

Figure 5.19 shows the result of the implementation of the presented algorithm acting on identified neighborhoods after 450 iterations. The algorithm was applied on a sensor field containing 91 sensor elements after 1440 activations and 605 detected neighborhoods. Three sensor elements were previously detected as defective.

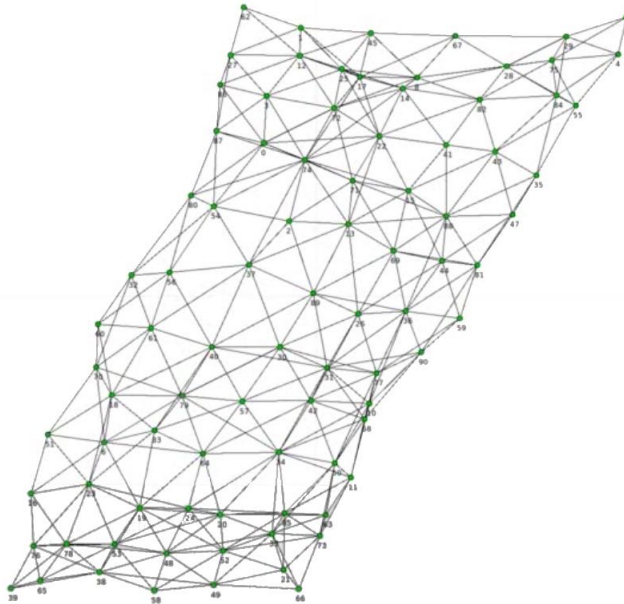


Figure 5.19: Result of the force-based layout algorithm for a sensor field with 91 sensor elements

In the ideal case, the application of the presented layout algorithm results in

equidistant placement of the nodes and a topological arrangement than can be mapped to the sensor structure in the contact area. Although the final grid structure of the sensor can be divined from the obtained graph in Figure 5.19, the nodes and edges are skew. The reason for this are mismatched and missing edges between nodes. A further step is thus required to obtain the correct spatial alignment of the sensor array, in which the result of the force-directed graph layout is mapped to the structure of the sensor array.

Algorithms from the domain of graph matching appear to be suitable for processing the remaining alignment. The mapping challenge can be generalized to find a match between the original graph and the sensed graph that misses some of the original nodes and edges as well as having some additional ones added by noise. This initial situation leads to the conclusion that bijective mapping between the measured graph and the original graph cannot be achieved. It is thus only possible to match subgraphs. The class of algorithms to tackle this issue are approaches that identify subgraph isomorphism using error correction. Graph matching algorithms belonging to this class mostly are regarded to be NP-complete [Olmos et al., 2006]. They have exponential runtime and memory consumption which is why their practical application is limited to a low number of nodes and edges.

While the idea of the graph matching algorithms is to find similarities in both graphs to map them, another approach is to approximate the obtained graph by means of a grid that evolves from the desired structure to the one that was computed.

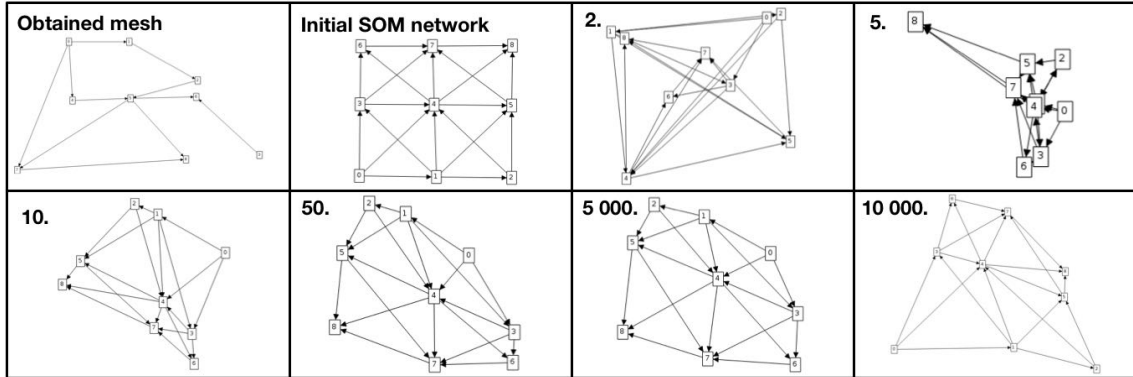


Figure 5.20: Concept of using a SOM to align the obtained mesh to the actual grid pattern. Top left: mesh obtained with noise. Bottom right: mesh obtained after 10 000 training steps starting from the initial grid structure (top row, second to left)

A concept that fits in with this approach makes use of SOM [Kohonen et al., 2001] that are originally used to map an input space by clusters of neurons. The input data that the neural network is trained for is encoded in one- or two dimensional data structures. The input space can thus be represented by a line or a plane. In the initial

step of creating a self-organizing map a defined number of neurons are initialized using random positions on the input plane. During the training phase randomly chosen input stimuli are presented to the map of neurons. Adaptation of the neural network is implemented by selecting the clusters of neurons that best match to the input stimulus by virtue of their position on the input plane. These neurons together with neighboring neurons are repositioned towards the input stimulus to increase the match to the input stimuli. A saturation of the training is achieved by constantly lowering the extent of the repositioning and reducing the radius in which neighboring neurons are repositioned as well.

The SOM approach is applied to find a match between the graphs representing the neighborhood of sensor elements in the following way: Each sensor element is encoded as a neuron. The SOM is therefore initialized with the number of nodes in the original sensor structure. The initial arrangement of the nodes is set to the grid dimensions of the sensor field. During the training phase the coordinates of the nodes obtained from the force-directed layout step are used to feed the map. Consequently, the network of neurons is trained to resemble the positions of the obtained graph. After finishing the training phase, the final mapping between the graph representing the original sensor structure and the graph acquired by contact measurements can be obtained. The result of a trained SOM for the graph shown in Figure 5.19 can be seen in Figure 5.21.

The shown SOM was trained for 10,000 learning steps using a Kohonen network approach that was initialized with 7x13 elements. The algorithmic implementation was based on the implementation presented in [Bendhaiba et al., 2015].

While the lower part of the grid structure is mapped correctly, mismatched mappings can be observed in the upper part of the sensor array. Possible explanations of the mismatching are non-functional sensor nodes in the top row of the sensor array (node ids 5, 9 and 46). These nodes are placed at random positions in the graph layout and cause the SOM to distort.

The proposed approach achieves 83% correct matchings after evaluating five different trained networks. This step finalizes the calibration chain of the fiber-optic sensor arrays.

5.2 Local control for load balancing in robotic systems

The previous sections have addressed the calibration steps for the fiber-optic tactile sensor array to obtain the actual contact information from the sensor. With the calibration done, the data that needs to be transmitted for further processing of the contact information is reduced. While this approach saves bandwidth on the communication channel, further local processing can be used to locally generate reactions to

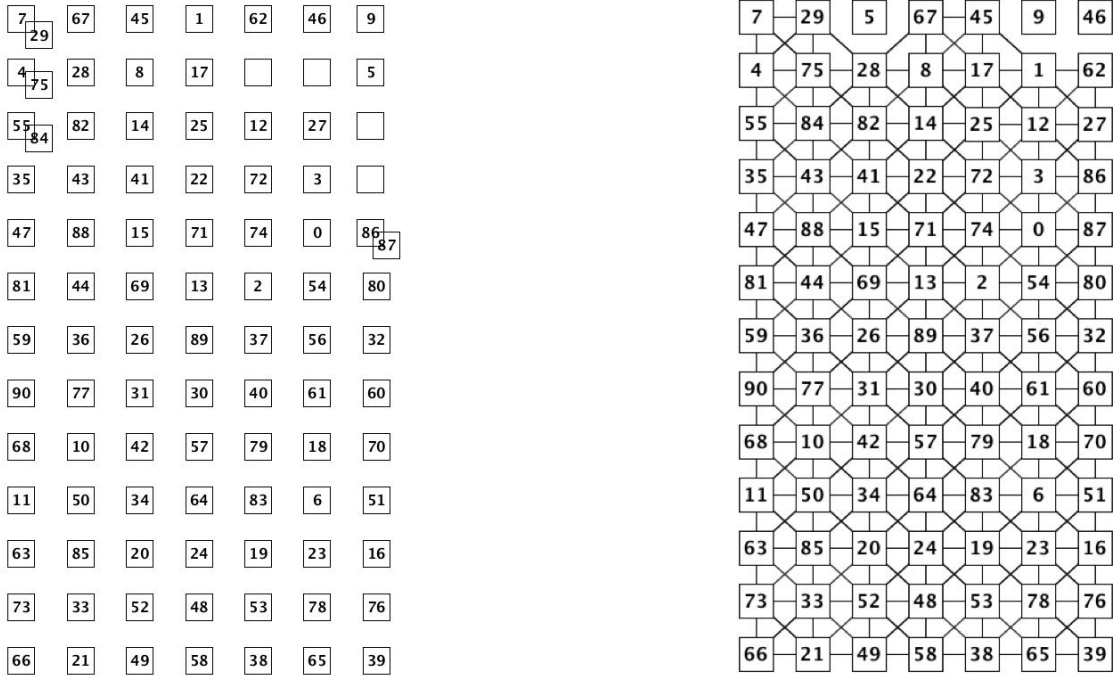


Figure 5.21: Matching result for trained self-organizing map after 10,000 iterations (left); ground-truth grid structure for comparison (right)

sensed events.

The benefits of implementing local control in robotic systems were addressed earlier [Brooks, 1991]. While the motivation has stemmed from increasing the robustness of robots, reducing the communication load and distributing the processing load in robotic systems can be added to the advantages of local control. Because sensing as well as actuation capabilities are available in the end-effector, the available processing power in the gripper can be used to compute a reaction to sensor stimuli without involving a central processing system.

The following sections present the implementation of local controllers for tactile controlled grasping and tactile servoing. Both approaches demonstrate the effectiveness of the developed tactile sensing system with respect to the required algorithmic complexity to obtain the desired behavior.

The approaches presented build on the locally implemented controllers that are implemented in the electronics for powering the joint and wrist actuators.

The proposed solutions are validated in experiments presented in section 6.

5.2.1 Tactile controlled grasping

An approach to exclude a central processing unit from operating the gripper system is to enable the capability of controlling the grasping of objects by the gripper itself.

Therefore, the control loop that triggers actuation commands based on the perceived sensor feedback is implemented in the local processing electronics. By means of this approach, the central processing unit of the robot is able to send a high level command to let the gripper take care of the grasping itself. Communication effort as well as processing power in the central processing unit can be minimized by this approach.

The general idea of tactile controlled grasping is to continuously close the grasp until a contact is sensed by the tactile sensors. In general, all sensing modalities in the gripper respond to contact during grasp. The following approach is implemented using the feedback from the fiber-optic sensor arrays. It can be extended to include the remaining sensing capabilities as well.

Starting from an equilibrated tactile sensor array, if a threshold is set for all sensing elements such that the availability of contact is triggered whenever the threshold is exceeded, this does not lead to satisfying results as such an approach does not take into account the individual sensor offsets and noise characteristics. A more advanced solution was developed that monitors the idle sensor signal and reports the event of contact.

5.2.1.1 Design of a filter to detect sensor element activation

The idea of the filter can be compared to the concept of electric potential, such as membrane, synaptic and action potential found in neurons [Purves, 2012]. As long as the input stimuli of a neuron or a receptor stay below an excitation threshold - which can be adapted - the neuron does not forward a stimulus. When the excitation threshold of a neuron is exceeded, the action potential is fired and transmitted. A technical implementation of this concept monitors the noise level of each sensor element individually in order to detect the activation for a sensor element.

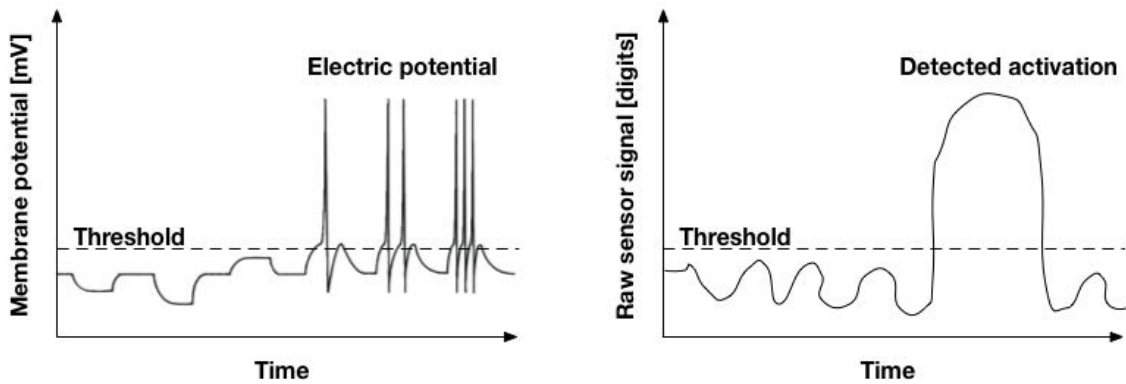


Figure 5.22: Conceptual drawing of similarities between electric potential (left) in neurons (based on [Purves, 2012]) and the filter concept that identifies activated sensor elements (right)

The signal coming from a sensor element is considered to be driven by an external stimulus as soon as its current signal value exceeds the noise level of the sensing element (compare 5.22).

The noise of a sensor signal can be described as a temporal deviation from a base signal. The standard deviation can be used as a measure to define the boundaries of the extent of noise. It is therefore computed for every sensing element:

The initial step is to calculate the variance over a defined time frame of the ten last sensor values. The standard deviation is obtained by taking the square root of the variance:

$$Var(i) = \sum_{n=0}^N (s_n - \tilde{s}_n)^2 \quad (5.20)$$

$$\sigma = \sqrt{Var(i)} \quad (5.21)$$

s_n denotes the sensor value, while \tilde{s}_n represents the averaged sensor value. The formula for calculating the confidence value is given in equation 5.22.

$$c_i = \mu \pm t \frac{\sigma}{\sqrt{n}} \quad (5.22)$$

It is calculated as an upper and lower boundary and is composed of the sensor's signal average value μ , a constant t for the normal distribution depending on the sample size n and the signal's standard deviation σ .

As the ten last sensor signals are taken into account, the window size is set accordingly for the calculations. Since the set of data used for the confidence values is smaller than thirty elements, the t distribution is used for calculating the normal distribution [Altman, 2005]. The corresponding t value for a set of ten values using a confidence interval of 97.5% can be obtained from tables defining the t values depending on a given set. According to [Ott and Longnecker, 2010], it is defined to be 2.281.

Figure 5.23 shows the calculated activation based on the described approach. The signal coloured in green denotes the raw sensor signal from one sensor element of a fiber-optic sensor array. The blue curve shows the low-pass filtered signal of the raw sensor data. The signal curve in pink represents the upper confidence value which is taken as a threshold for identifying the activation of a sensor element. The identified sensor activations are colored in red. As for the low-pass value calculation, the confidence value is calculated only in cases where a sensor element activation was not detected.

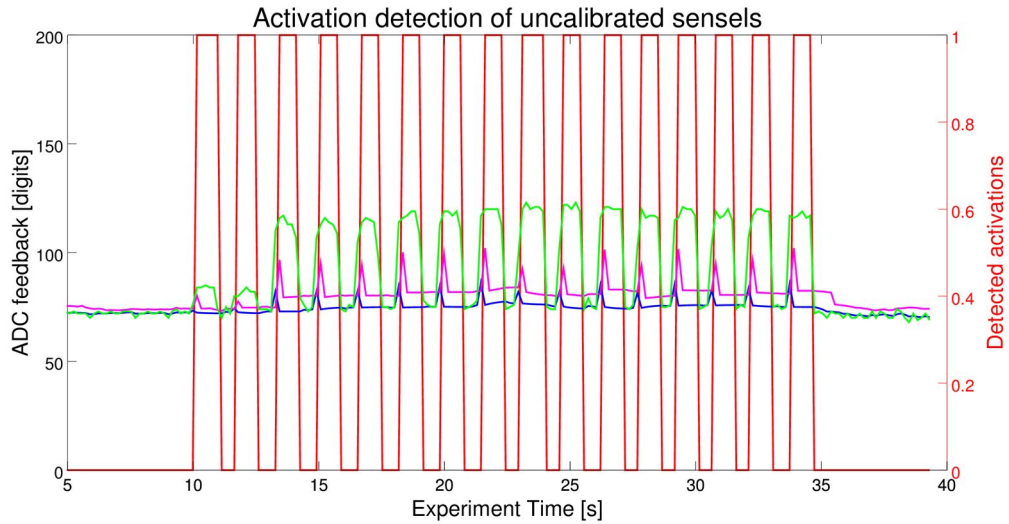


Figure 5.23: Activation detection of a single sensor element through constant monitoring of the idle signal

5.2.1.2 Performance of the developed filter

To evaluate the performance of filters, the frequency and amplitude response are calculated based on the transfer function of the filter. As a transfer function of this filter cannot be easily derived, the filter developed was evaluated by applying test signals with varying amplitude and frequency. The behavior of the algorithm with respect to increasing frequencies can be seen in Figure 5.24. The blue curve denotes the test signal which is a cosine signal with increasing frequency. The red curve shows the output of the activation detection algorithm with respect to the test signal. A transition from zero to one represents a detected activation.

Feeding the approach presented with signals of increasing frequency reveals a detection of sensor activations with frequencies of up to 3 Hz. The detection of higher frequencies is limited by the weights of the low-pass filter that is used and the sensor update frequency which is given by the frame rate of the camera module. A sensor activation frequency of 3 Hz currently appears sufficient for following contours as high dynamic movements are not expected.

The plot in Figure 5.25 shows the feedback of the algorithm with respect to peaks of increasing amplitude. The blue curve denotes the input test signal and the red curve shows the output of the activation detection algorithm with respect to the test signal. It can be seen that the algorithm successfully detects the test signal that represents activation of the sensor with increasing amplitude. Further trials showed that the full possible range of amplitudes up to 255 bits shows no effect on the detection given a constant frequency of 1 Hz.

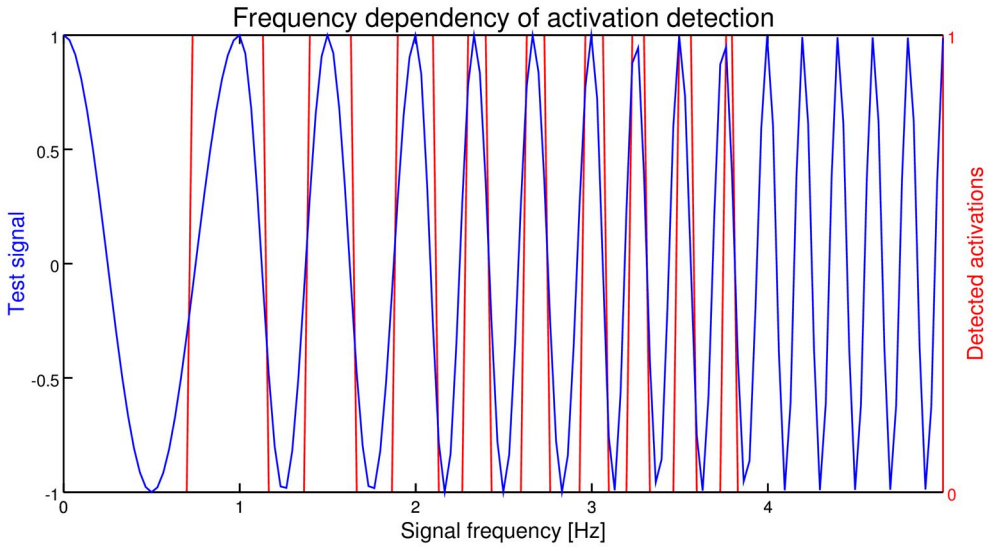


Figure 5.24: Evaluating the activation detection algorithm using increasing frequencies

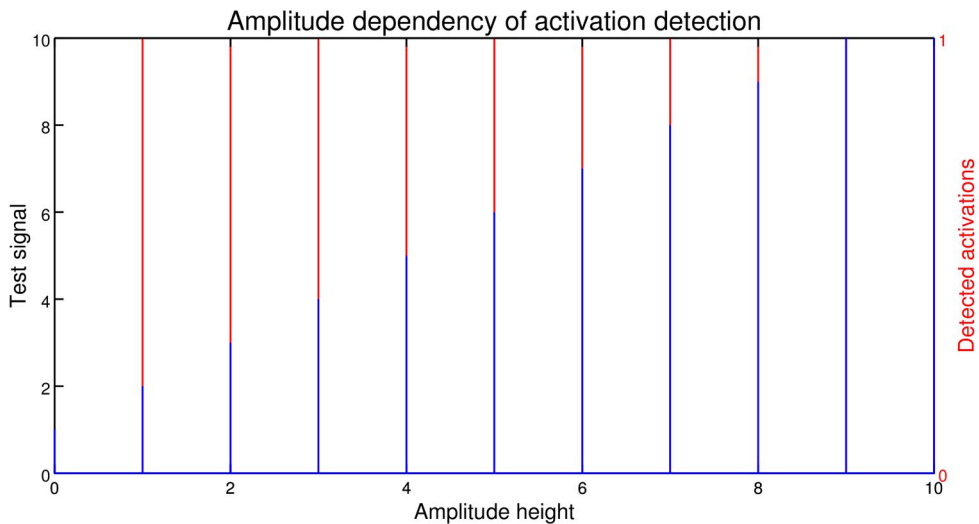


Figure 5.25: Evaluating the activation detection algorithm using increasing amplitudes

Under the discussed constraints, the presented approach is used to identify activated sensors. An initial implementation of grasp controlled contact control is achieved by stopping the grasp closure as soon as there is contact sensed by one of the sensor elements of a tactile sensor array.

5.2.2 Contour following

Recalling the presented tactile exploration strategies in section 3.1.2, the ability to follow a contour using tactile sensing is one way how humans explore objects by touch [Lederman and Klatzky, 1993].

The implementation of contour following for robotic grippers is addressed in relevant literature using the term *tactile servoing*. The proposed solutions from [Chen et al., 1997], [Zhang and Chen, 2000] and [Li et al., 2013] can be divided into two steps. At first, the true dimensions of the contact have to be reconstructed from the perceived tactile image. This step is required as the tactile sensors are covered by a skin that has a low compressibility. In presence of a contact, sensor elements are activated whose corresponding area at the skin is not applied with a contact. This cross-talk results in a *blurred* sensor image. The original contact can be computed by modeling the mechanics of the tactile sensing area [Fearing and Hollerbach, 1984]. The derived information is then used to extract the tactile features to compute required movements of a manipulator arm to follow the identified contour.

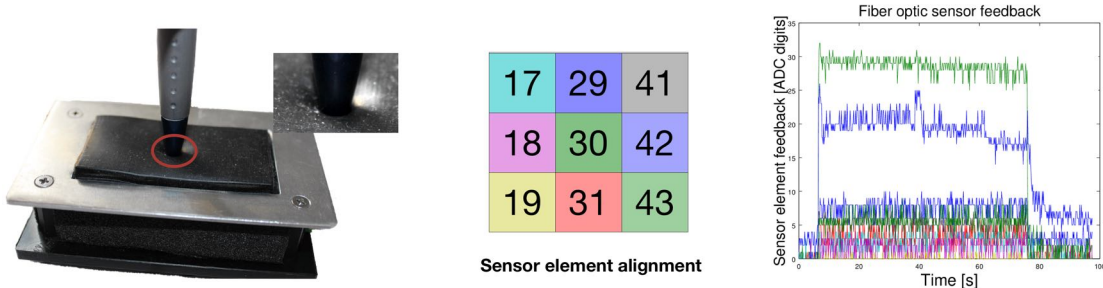


Figure 5.26: Skin deformation and corresponding fiber-optic sensor feedback. The colors of the sensing elements in the graphic on the spatial alignment of the sensor elements correspond to the colors used in the graph showing the sensor feedback during activation.

The reconstruction of the original contact based on modeling the mechanics of the sensor involves trigonometric functions, divisions and square roots. Their implementation in embedded devices like FPGAs is expensive in terms of runtime and consumption of logic elements, which is why this approach is unfavorable.

Unlike in the developments presented, the covering of the tactile array sensor chosen here is exhibiting high flexibility. It is made of silicone resin, having a thickness of 0.2 mm. The deformation of the skin in case of contact and the respective sensor array feedback can be seen in Figure 5.26. Thanks to the high compressibility of the selected foam material for the fiber-optic sensor together with the thin cover, the effects caused by compression are low compared to the actual sensor feedback. The following solution implemented for the developed gripper thus directly derives

the information required for contour following from the tactile image.

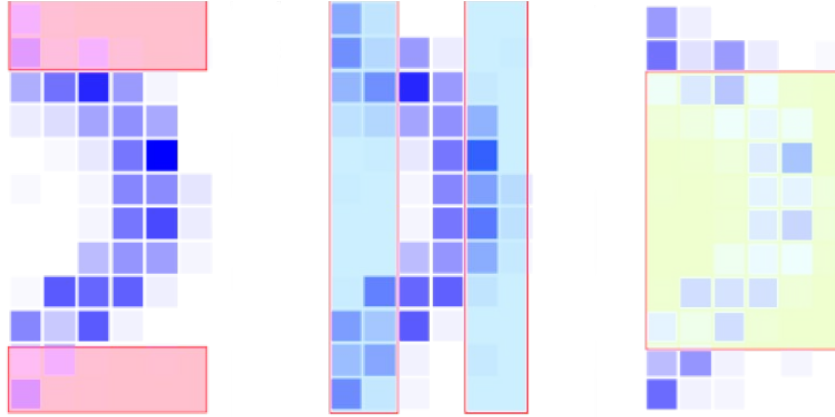


Figure 5.27: Sections of tactile sensor array for calculating a local center of pressure

The approach to identify contours described here can be regarded as a form of active tactile sensing. Contours that exceed the dimensions of the sensing area are explored by guiding the manipulator arm using directional information derived from the contour obtained from the tactile sensor information. The algorithmic idea to acquire the contour from the tactile image is to monitor the sensing area in five different segments as shown in Figure 5.27.

The center of pressure is calculated for these areas and a path between the obtained centers of pressure is derived. If such a path exists, a contour is detected and its orientation of the tactile sensor array can be obtained. The orientation can be used further on, to calculate a movement direction to follow the contour.

At first, the position of each sensor element in the x and y dimension is weighted by its current sensor value p_{sens} .

$$X_s(t) = \sum_{x=0}^w \sum_{y=0}^h x \cdot p_{sens}(t, x, y) \quad (5.23)$$

$$Y_s(t) = \sum_{x=0}^w \sum_{y=0}^h y \cdot p_{sens}(t, x, y) \quad (5.24)$$

In order to scale the obtained sums, the overall sensor feedback is calculated by accumulating all sensor values.

$$C_s(t) = \sum_{x=0}^w \sum_{y=0}^h p_{sens}(t, x, y) \quad (5.25)$$

The scaling for each dimension is achieved by dividing the weighted positioning

in the x and y dimension using the accumulated sensor feedback.

$$COP_x(t) = \frac{X_s(t)}{C_s(t)} \quad (5.26)$$

$$COP_y(t) = \frac{Y_s(t)}{C_s(t)} \quad (5.27)$$

The results of applying the described force center calculations in the regions of the tactile sensor array are shown in Figure 5.28.

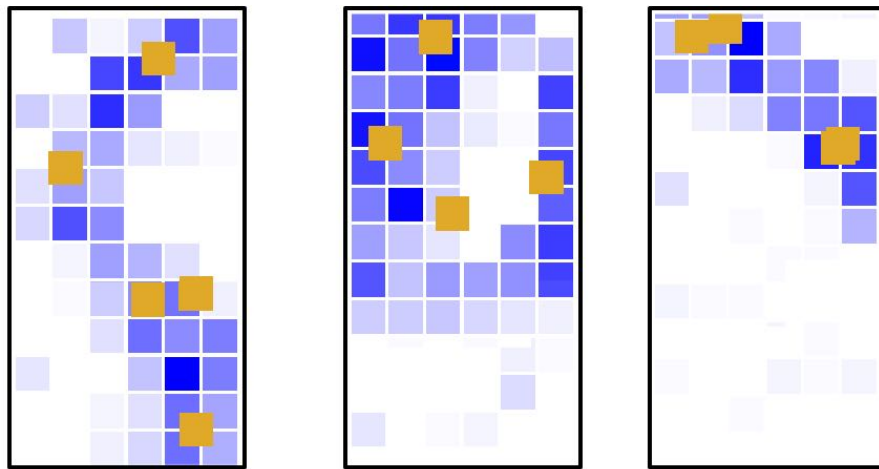


Figure 5.28: Local center or pressure detection for different contact geometries

As the calculations of the center of pressure include the signal strength, varying sensitivity of the sensor elements leads to miscalculations. A sensor element that exerts a strong signal feedback in the presence of a uniform contact pressure leads to undesired shifts of the calculation of the center of pressure. This behavior is visible in the signal feedback from the circular shaped object shown in the center of figure 5.28. The lower center of pressure is assigned to an area where there is no actual sensor feedback. This misplacement can be explained by strong sensor signal feedback in the upper area of the force center calculation.

To overcome this issue, the approach of detecting activated sensor elements on an uncalibrated sensor field presented in section 5.2.1 is used to restrict the sensor elements for the calculation of the center of pressure.

The obtained force center coordinates alone do not ensure the presence of a contour in the contact area as the force centers are also obtained by multi-point contacts. In a subsequent step the existence of a connection between the calculated force centers is checked. This is done by calculating a linear connection between the centers and evaluating the sensor feedback of the sensor elements lying in the calculated path.

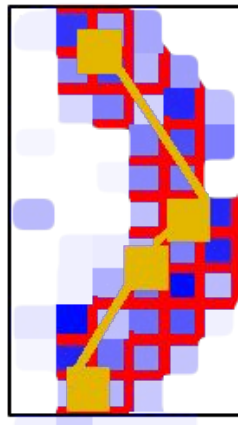


Figure 5.29: Extracted contour (orange) using activated sensor elements (red boxes)

The resulting contour extraction is shown in Figure 5.29. The detected sensor elements that are activated are used to calculate a connection between the local centers of pressure. If a connection exists, the centers of pressure are connected using a straight line. In the case that a contour is detected, directions are calculated to guide the manipulator arm to follow it. The calculation of the directions for the manipulator arm is guided by the center of pressure that is calculated for the sub-area of the sensor field placed in the movement direction. The goal is to always keep the center of pressure in the middle of the respective sub-area. The computed signals from the actual position of the center of pressure are used to control the manipulator either to move left and right or up and down depending on the orientation of the sensed contour in the contact area.

By accumulating the joint positions of the manipulator arm, the overall contour geometry can be computed. Experiments in section 6 demonstrate the capabilities of the presented approach.

5.3 Discussion

Data volume as motivation for local pre-processing

Summing up the amount of data generated every second by the designed tactile sensing system indicates that transferring the raw sensor data to a central processing unit in a robotic system places high demands on the throughput of the communication channel and processing power for information extraction. As a comparison: transferring the raw data of the designed tactile sensor system to upstream processing units requires either 3 gigabit Ethernet connections or a PCI Express connection of the latest generation for operation at frequencies of 4 gigahertz. A closer look at the data volume reveals that a major share is generated by the fiber-optic sensing

modality. On the one hand, this is caused by the number of sensor elements of this modality. On the other hand, this is induced by the selected acquisition method. While handling the communication load can be regarded as a challenge that is specific to the designed solution in this thesis, extending the development to a full robot design including additional sensing modalities justifies the requirement for local data analysis.

Local pre-processing - all data is relevant

A solution for handling the data volume is to locally pre-process the sensor output. The algorithmic solutions presented are aimed at reducing the required bandwidth for further transmission and extracting information that is relevant to tactile exploration in high-level decision-making. The data that is kept back still contains relevant information. In the case of a value-dependent data transmission, the continuous data stream from the sensors can be used to ensure the availability of the sensor. Apart from the compact mechanical setup of using a camera for acquisition of the fiber-optic sensor arrays, the redundant information can be used to increase the robustness, reduce noise and improve the sensitivity of the sensor. The applied mechanisms for data reduction can therefore be regarded as a selective distribution of information to processing units that require it for further processing. In the example of fiber-optic sensors 0.02% of the original data volume is transferred for upstream processing. The remaining 98.8% contains information that can be used locally to perform the presented improvements in signal quality.

Extending local processing to decentralized control

Local integration of the actuator control allows extension of decentralized processing to implementation of in-situ controlled reactions to sensor stimuli. This method enables further load balancing in a robotic system as high-level computing systems can delegate tasks like grasping or following contours of objects to sub-parts of the robot. Such local behavior was proposed earlier [Brooks, 1991] targeting the increasing robustness of the overall system as a motivation. The demand for such an approach can be extended to support load balancing in processing and control as an approach to face the increasing complexity of tasks of robotic systems.

Processing power in robotic structures

To achieve the envisaged decentralization of processing and control, the respective algorithms have to run on processing hardware that can be integrated into the confined structures of robotic systems away from a central processing unit. The available dimensions in these regions require the use of embedded processors that are compared to standard central processing units having an x86 hardware architecture reduced in

its instruction set, memory availability and operating frequency. Technology developments driven by the smartphone industry, internet of things and big data lead to embedded multi-core systems and mixed-signal electronics. The combination of parallel hardware with classical sequential processing is enhancing the capabilities of this class of processing systems while maintaining low power consumption and package dimensions thanks to ongoing miniaturization of the manufacturing processes. Still, compared to classical processor architectures, these modules require adapted algorithms to utilize their power in applications that require high integration, as in complex robotic systems.

Significance of optimized algorithms for local processing

A widespread approach to speed up algorithms is to rely on the effects of Moore's law [Intel Corporation, 2005] - a prediction that by doubling the number of transistors on the same area every 18 months, the processing power doubles as well. On the basis of the roadmaps of chip manufacturers [Fuller and Millett, 2011] and according to several analysts (compare [Huang, 2015], [The Economist, 2015] and [Hruska, 2014]), one can conclude that this trend is going to cease. Other ways to increase the processing speed of algorithms have to be found. One solution is to adapt algorithms to properties of available execution platforms [Adams et al., 2010] like multi-core architectures and specialized processing units, e.g. DSPs, mixed-signal processors or FPGAs. With respect to robotics and the design of long-term autonomous systems that have to perform a variety of tasks requiring a diversity of skills, function integration is a key requirement. To get the best balance between performance and resource requirements, identifying suitable processors for the task and designing the algorithms according to their way of processing data represent a solution for high density function integration in processing units of robots. Metrics for identifying algorithms that have few requirements regarding the instruction sets, memory space and runtime or have potential for parallelization are tools for selecting suitable algorithms for implementation in embedded systems.

Extraction of sensor data with low computation and memory complexity

By making use of the conditions of the camera images, an optimized algorithm was developed that extracts the fiber-optic data without the need to store the full sensor information prior execution. This feature makes it possible to use memory modules with lower capacity, which in turn requires lower package dimensions and wiring effort on the PCB. Furthermore, the algorithm can operate while the image data is acquired from the camera system. This feature opens up new opportunities for mechanical integration since constant identification of the position of the optical fibers on the camera image is possible. Exploiting the capability on the mechanical side en-

ables a less rigid connection between the optical fibers and the acquisition electronics. Detachable connections could be used to simplify the recombination of sensors and the acquisition hardware.

Algorithmic approach to restore spatial alignment of a sensor array

To reduce the mechanical integration efforts, the spatial alignment of the sensor elements in the contact area was neglected while attaching the optical fibers to the acquisition electronics. Restoring the spatial alignment of the tactile sensor arrays is thus required on the software side to use the sensor modality for identifying geometric properties. Shifting this integration step from mechanical integration to an algorithmic solution reduces the efforts of integration as the software implementation has to be done once while the work on the mechanical side has to be done for every sensor. The algorithmic solution presented was developed with future applications of the fiber-optic sensing technology in mind where robotic skins comprise a three-dimensional structure. Identifying the spatial alignment of such tactile arrays requires complex calibration tools to activate each sensor element to identify its position. A solution that requires simple calibration steps is thus preferable. The approach developed requires common activation of sensor elements in a random order. Indentation can thus be achieved by touch, performed either by a human or eventually by the robot itself. Especially the possibility of performing the calibration using the dexterous capabilities of the robot is a helpful tool to recalibrate the sensor and identify defect sensor elements during long-term missions.

Analogies to biological concepts

Some of the algorithms presented showed similarities to the encoding in neurons which indicates that similar concepts can be found in biology. The encoding of spike trains from mechanoreceptors and the electronic potential mechanism are techniques that lower the intensity of transmitted signals either by omitting redundant information or by some sort of pre-processing. While the reduction of data transmission is presumably not the only reason for the biological concepts mentioned, it shows that reducing the amount of data and pre-processing the information is also a concept in nature to handle the variety of sensor stimuli.

Another observation in biology regarding the encoding of signals from sensory inputs relates to receptive fields and signal processing by lateral inhibition [Blakemore et al., 1970]. This concept, where a cell prevents surrounding cells from responding in the same manner, can be found in the eye as well as in processing of skin stimuli. It was observed that this technique results in an increase in contrast. While this is desired for technical implementation of senses as well, the number of available sensor elements that can be combined to a receptive field in which

inhibitory processing is applied limits the effectiveness. The human hand, in which [Vallbo and Johansson, 1984] discovered that even the number of the fast adapting mechanoreceptors in the fingertip amounts to 141 elements per square centimeter, has a much higher spatial density of sensing elements compared to the tactile system developed, in which the sensing modality with the highest spatial density reaches 6.25 sensor elements per square centimeter.

The approach of lateral inhibition applied to the technical implementation presented results in a reduction of the spatial resolution, which limits the geometric sensing capabilities. Thus, implementation of this concept is currently not feasible but might become relevant with the advancement of tactile sensing technology.

Chapter 6

Experiments

This section addresses the third objective of this thesis which is to experimentally verify the theoretical concepts of multi-modal tactile force sensing in the deep-sea and the algorithmic approaches of local pre-processing. The chapter is grouped as follows: first of all, the different experiment environments that were used to evaluate the technology developed are presented. The section is followed by experiments that were conducted to find out how to prepare the electronics and sensors in the gripper system for application in water. The further experiments are grouped by the experiment environments.

Experiment overview

The motivation for selection of the experiment environments was based on the different aspects that were to be evaluated in the respective experiments. The experiments in combination with an underwater manipulator were used to evaluate two aspects: First, they were used to show the interaction between standard tools for underwater manipulation and the underwater gripper system developed. The combination with a manipulator arm was used to validate the benefits of multi-modality in sensing while distinguishing objects of similar shape only by the sense of touch.

The tests in the pressure chamber focus on the performance evaluation of the fiber-optic measurement principle as the measurement principle that has not been used in deep-sea pressure conditions before. Parameters like the variation of the sensor offset and dynamic response in air and under water as well as the pressure dependability of the sensor feedback are evaluated. Further experiments deal with the long-term drift and the applicability of the measurement principle as a tactile array sensor for sensing contact geometries. The effects of the acquisition electronics on the sensor performance are discussed in a section that compares the two approaches that were used throughout the experiments in the pressure chamber: an off-the-shelf USB camera board and a custom designed PCB whose technical details were discussed in

section 4.7.3.

The experiments in combination with an industrial manipulator arm for applications on land were conducted to demonstrate the benefits of local control using pre-processing of tactile data in the gripper system using the example of following a contour by using only touch information. This experiment environment was chosen in preference over an experiment scenario under water for two reasons. First of all, following a contour using tactile feedback makes it necessary to constantly keep track of the contour. The manipulator is therefore required to be able to move its end-effector with a precision accuracy that depends on the size of the contour. Experimental validations of the movement precision of the available industrial underwater manipulator arm that were conducted previously [Hildebrandt et al., 2009] indicate a low precision accuracy resulting in a position error at the fingertip of over a cm. For this reason, an industry manipulator arm for applications on land was chosen that is able to operate with a precision of several millimeters. Another reason for conducting this experiment on land is to demonstrate the generality of the solution developed. The area of operation of the developed tactile system is not limited to application under water.

6.1 Experiment environments

This section describes the technical aspects of the different experiment environments that were used in the following experiments.

6.1.1 Deep-sea manipulator: Schilling Robotics Orion 7P

Experiments in combination with an industrial underwater manipulator are performed using an Orion 7P deep-sea manipulator manufactured by Schilling Robotics. The manipulator is actuated using hydraulics operating at a supply pressure of 200 bar. The end-effector is capable of exerting 4,850 N of gripping force.

The gripper system developed was designed to fit in the place of the original claw of the manipulator. The hydraulic valves of the gripper operate at a maximum pressure of 50 bar and therefore require a pressure reducer to connect them to the hydraulic circuit of the manipulator arm. Using a connector with deep-sea capability, the connection to a computer and a laboratory power supply is established for transmitting power and data.

The experimental setup consisting of the manipulator in combination with the gripper is submersed in a test basin with dimensions of 5x4x2 meters (LxWxH). During the experiments, the basin is filled with fresh water. The experimental setup is shown in Figure 6.1.

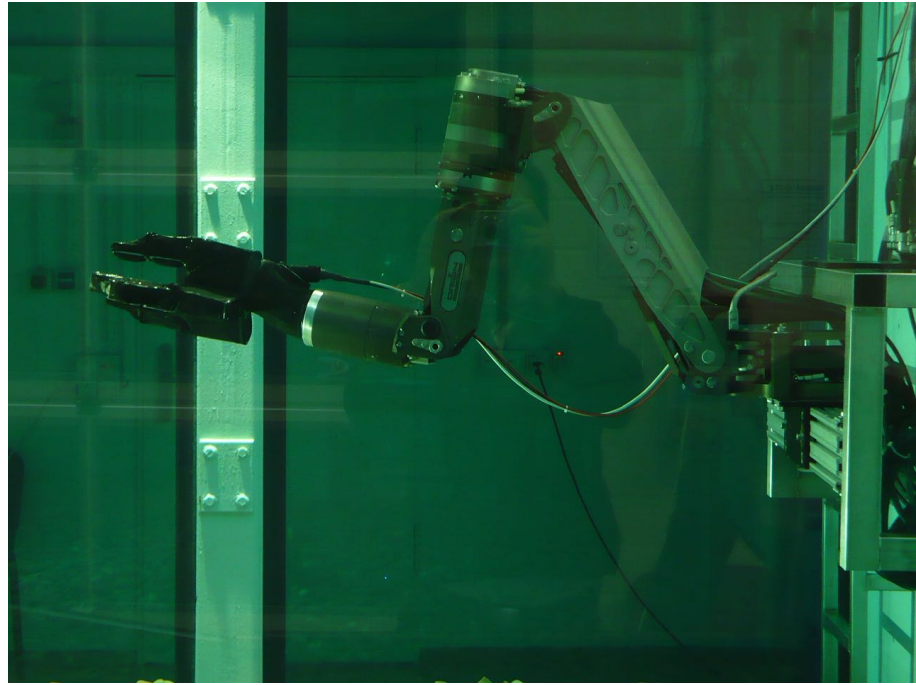


Figure 6.1: Gripper attached to the Orion 7P deep-sea manipulator

6.1.2 Pressure chamber

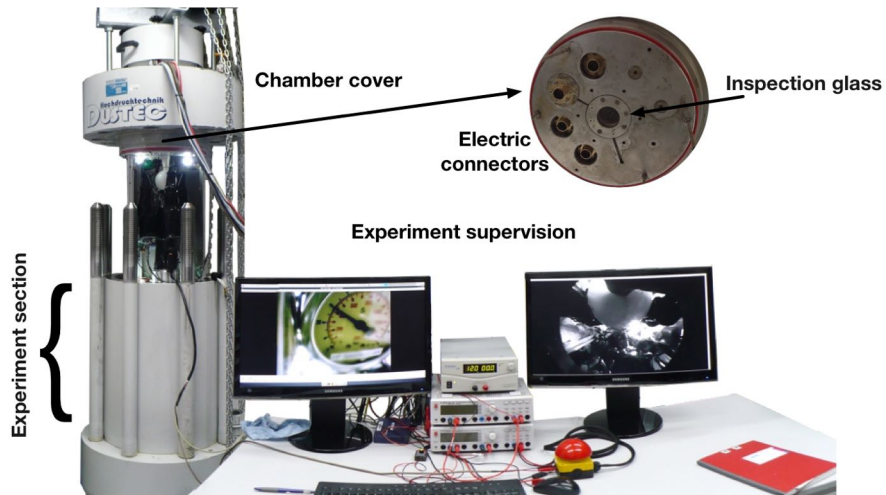


Figure 6.2: Pressure chamber experiment environment for deep-sea experiments

In order to test the system's capabilities under ambient pressure conditions as they exist at depths of up to 6,000 m in the oceans, a pressure chamber is used that is able to exert the corresponding ambient pressure (Figure 6.2). It comprises a cylindrical experiment section and has a diameter of 400 mm and a height of 600 mm. The supply of electric power for in-situ tests is provided by four deep-sea connectors. An

inspection glass in the cover of the chamber allows visual supervision of experiments. The chamber is used for tests under pressure according to the following procedure. At first, the experiment section is filled with water and the chamber is closed. The increase in pressure is achieved using a high-pressure plunger pump that pumps water into the closed pressure chamber. In order to reach an ambient pressure of 600 bar, approximately two liters of water are pumped into the already filled chamber. The ambient pressure applied in the pressure chamber is measured by a pressure sensor with a measurement range of 0 - 1,000 bar, having an accuracy class of 1.0 (according to DIN EN 837) allowing a measurement accuracy of 1% of the measurement range. The depth measurements thus have a measurement uncertainty of 10 bar.

6.1.3 Manipulator for applications on land: Mitsubishi PA-10

An industrial manipulator is used for experiments that require high movement precision. The experimental setup is depicted in Figure 6.3. It comprises a manipulator arm manufactured by Mitsubishi of type PA10. Its precision is within ± 0.1 mm. Without limiting the workspace of the manipulator, the maximum load should not exceed 10 kg. As the developed gripper has a weight of 9.5 kg and additional loads applied by grasped objects have to be considered, a combination with the manipulator is not feasible.

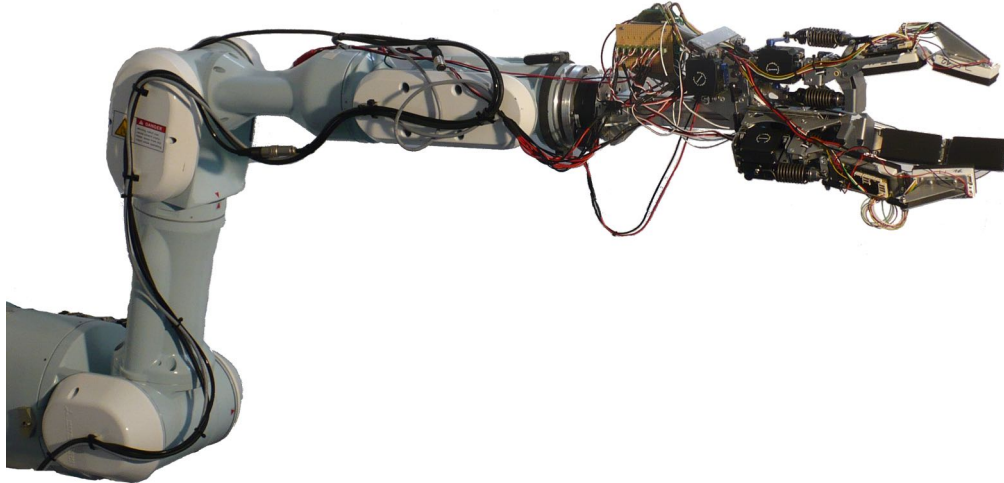


Figure 6.3: Experimental setup using an industrial manipulator arm in combination with a simplified version of the gripper system comprising the same processing electronics and the developed fiber-optic sensor arrays.

To perform experiments with the manipulator, a lightweight model of the gripper was developed. It is made of sheetmetal and is actuated using model servo-motors in series with a spring of fixed elasticity. The kinematics is identical to the underwater gripper. The gripper is equipped with the same electronics as the underwater gripper.

The sensing capabilities of this gripper are limited to the fiber-optic sensing arrays.

6.1.4 Experiment guide

The matrix in Figure 6.4 shows the different possible combinations of the presented experiment environments, the evaluated sensing modalities as introduced in section 4.2 on page 40 and in the case of using the fiber-optic measurement principle: the acquisition electronics used in experiments where fiber-optic sensing was involved. The introduction of the two acquisition electronics can be found in section 4.7.3 on page 54.

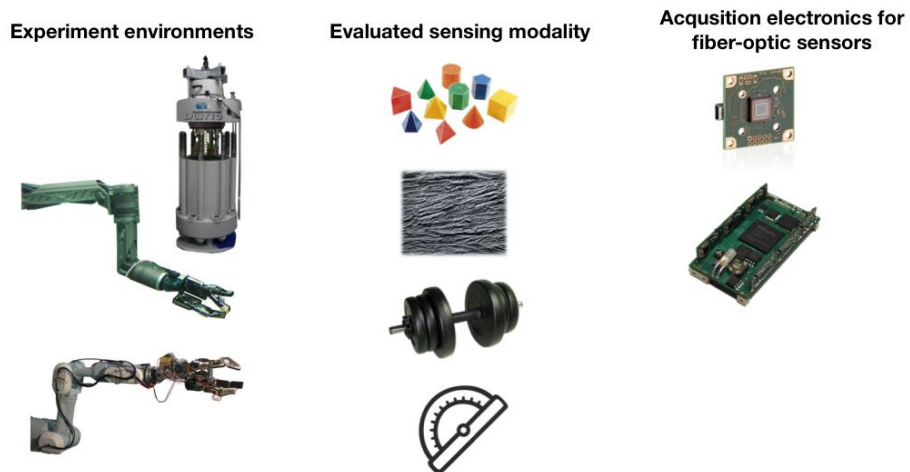


Figure 6.4: Overview of the different experiment environments, evaluated sensing modalities, and selected acquisition electronics

Pictograms from the shown matrix are used in the beginning of each section where the combination of experiment components is changed.

6.2 Preparations for application in deep-sea conditions

The harsh environmental conditions in the deep-sea domain require preparation of the gripper system prior to the actual evaluation of the performance. The high ambient pressure of 600 bar poses heavy stress on the sensor materials, the actuation and the electronics. In comparison, 600 bar ambient pressure correspond to a weight of 600 kg per square centimeter acting on every part of the system.

The following sections deal with the evaluation of electronic components, sensor sealing and sealing processes of the gripper to cope with the described conditions.

6.2.1 Electronics

6.2.1.1 General considerations

Besides the necessary sealing to avoid short circuits from contact with water, the avoidance of pressure housings for electronic components means that each chip on the printed circuits boards has to withstand the ambient pressure.

The first step for identifying components that survive the high forces is to check the electrical components for gas inclusions. For chips manufactured using the surface mount device (SMD) technique, this is already ensured by the manufacturing process [Harper, 2005]. Figure 6.5 shows an example in which electrolytic capacitors are replaced by a stack of capacitors manufactured in SMD process. The electrolytic capacitors are typically chosen for their high capacity. Because of gas inclusions, these devices collapse in high ambient pressure conditions. An equivalent part in a gas-bubble-free manufacturing process is not available. A suitable replacement of these electrical parts is to use a combination of standard capacitors manufactured by means of the SMD technique to attain the original capacity.

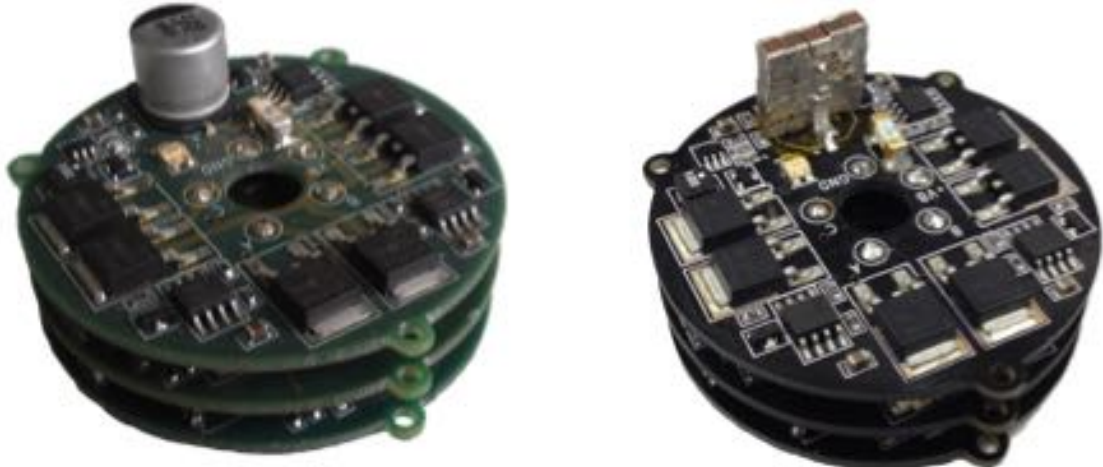


Figure 6.5: PCB with electrolytic capacitor (left) and the pressure-tolerant replacement of the component (right)

6.2.1.2 Oscillators

The clock signal for a microcontroller or FPGAs is generated by oscillator parts. Quartz oscillators are commonly used for this application. They consist of a piezoelectric cantilever that vibrates at the required frequency in a cavity filled with nitrogen [Jauch Quartz GmbH, 2007]. Although manufactured by means of the SMD technique, these electronic parts require more detailed investigation because gas inclusions are required for the working principle. As choosing a component manufactured

using the SMD technique does not eliminate the cavity within the part, experiments for selecting suitable packaging and working principles were conducted.

A combination of oscillators having different working principles and packing material were wired on a PCB (Figure 6.6). To provide better repeatability, three instances of each oscillator under test were wired on the experiment board. To prevent short circuits through contact with water, a thin layer of silicone was applied. The assembled experimental setup was placed in the pressure chamber and the output of the oscillators was monitored using an oscilloscope outside of the pressure chamber. The signal quality was measured while increasing the ambient pressure in steps of 100 bar.

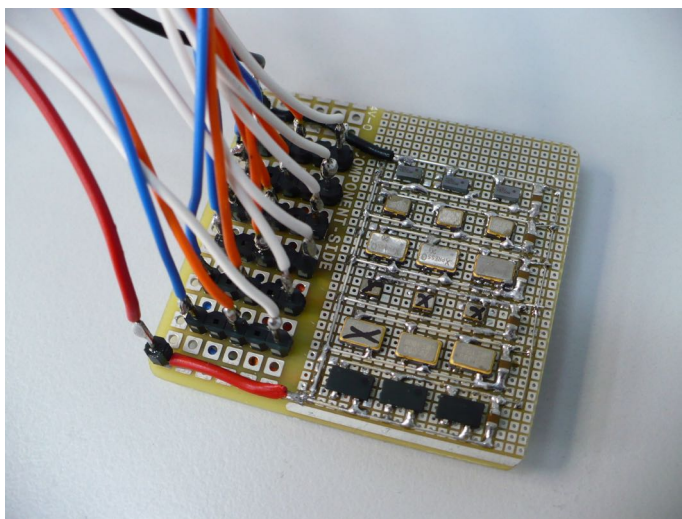


Figure 6.6: Selection of oscillators with different packaging material and working principles

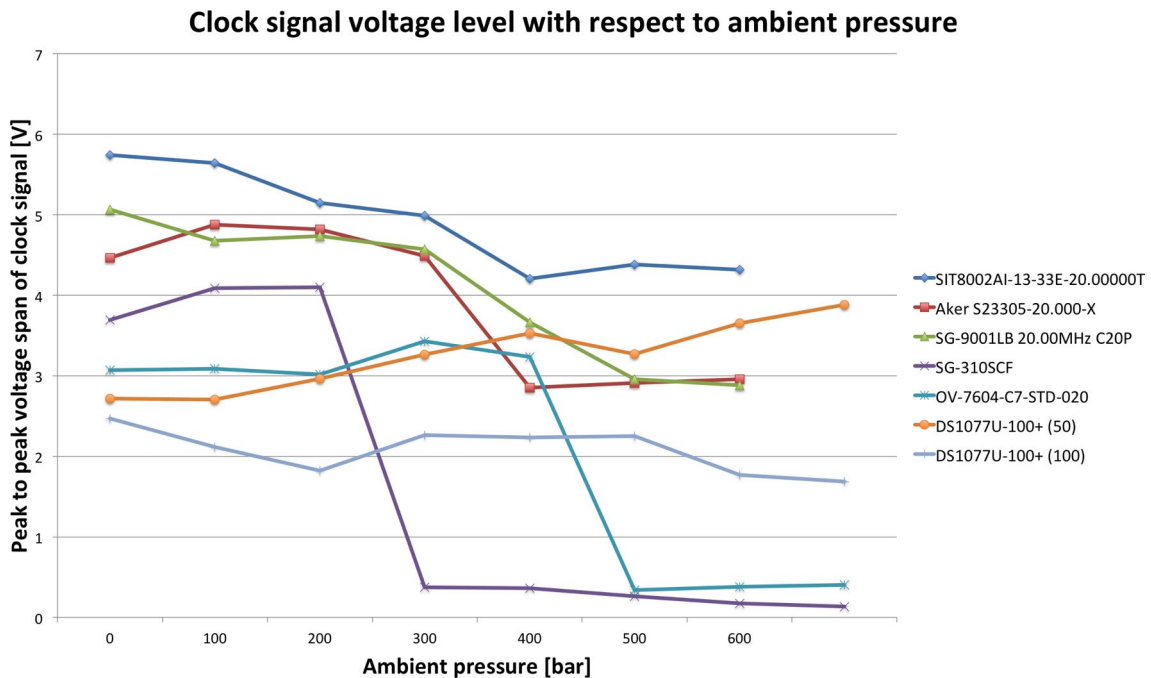
The expected output of this experiment was to gather knowledge about the signal stability of oscillators using different working principles like solid-state oscillators or different packaging using ceramics or plastic material. Table 6.1 summarizes the selected oscillators for testing and points out their working principle and packaging material.

Most electronic modules that require a clock signal input expect a certain voltage level of the input signal to discriminate between a logical '0' and a logical '1'. That is why the signal span or peak-to-peak voltage level of the oscillators is of interest during the conducted experiment. Figure 6.7 shows the peak-to-peak voltage levels of the selected oscillators with increasing ambient pressure. Each graph representing an oscillator type is based on an average signal from three instances of the same oscillator. It can be seen that the signal strength of the evaluated oscillators remains stable at pressure levels of up to 200 bar. If the pressure increases further, the signal quality starts to differentiate. A drop in the voltage span below 1V is observed for

Table 6.1: Selected oscillators for pressure testing

Manufact.	Identifier	Packaging	Type	Frequency
Aker	Aker S23305-20.000-X	Hybrid ¹	Crystal	20 MHz
SiTime	SIT8002AI-13-33E-20.00000T	Plastic	MEMS	20 MHz
Epson	SG-9001LB 20.00MHz C20P	Plastic	Crystal	20 MHz
Epson	SG-310SCF	Metal	Crystal	20 MHz
Micro Cryst.	OV-7604-C7-STD-020	Ceramics	Crystal	0.327 MHz
Maxim	DS1077U-100+ (50)	Plastic	Solid state	50 MHz
Maxim	DS1077U-100+ (100)	Plastic	Solid state	100 MHz

two oscillator types. In this case, a logical '1' cannot be distinguished from a logical '0' following the definition of the standard logic levels [Nolan and Soltero, 2003]. The drop in the signal span can be explained by the working principle of the oscillator and the packaging material, which in this case is a quartz oscillator in a metal package filled with nitrogen.

**Figure 6.7:** Experimental results showing the averaged peak-to-peak voltage of selected quartz oscillators with respect to increasing ambient pressure

The oscillator with the highest peak-to-peak voltage during the whole experiment uses a MEMS resonator working principle and a plastic package. It is therefore

¹Metal/Ceramics

chosen as the oscillator module for all electronic printed circuit boards in the gripper.

6.2.1.3 Ethernet jack

Further electronic modules with known air inclusions are the RJ45 Ethernet jack used on the *BaseBoard* PCB. This module is replaced by an impulse transformer module that incorporates the necessary electronic parts in the Ethernet jack. The image in figure 6.8 shows the impulse transformer after a test under pressure.

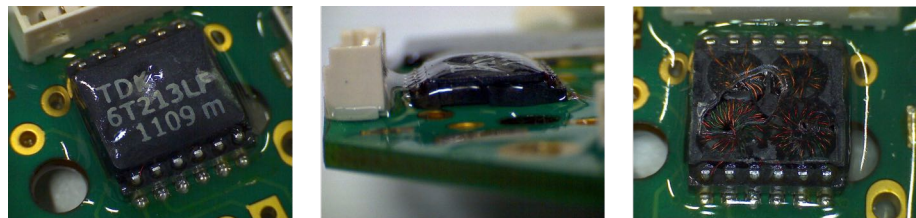


Figure 6.8: Impulse transformer module after exerting 600 bar ambient pressure

As can be seen in the picture on the right side and in the center, the package was damaged during the dive, causing the module to stop working at depths of 500 bar. The reason can be found in air inclusions that reside in the package. For the following attempts the package was opened and filled with epoxy resin for isolation purposes.

6.2.2 Sensors

The applicability of the selected measurement principles was discussed in theory in section 4. Prior to testing the sensors in underwater and deep-sea conditions, the sensor modules were prepared for potential damage through contact with pressure or water.

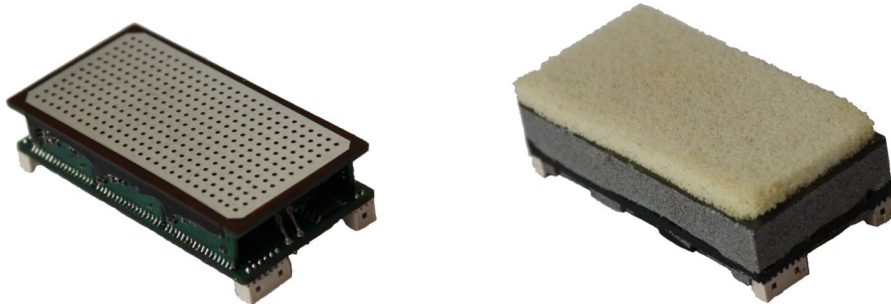


Figure 6.9: Integrated multi-modal sensor (left) and sensor module prepared for underwater usage using epoxy resin with ceramic spheres (right)

Figure 6.9 on the left shows the integrated multi-modal sensor module comprising the fiber-optic and piezoelectric sensors together with the processing electronics.

Before applying this sensor under water, the electronic circuit needs to be isolated. As the sensor module is exposed to high forces during manipulation tasks, a rigid setup is desirable. Experiments showed that high material stress occurs when using pure epoxy resin to fill the cavities between sensor surface and processing electronics. Destroyed soldering contacts on the electronics can be the consequence. The results of an experiment to reduce the volume shrinkage of epoxy resin during curing are shown in Figure 6.10. Both molds were filled with the same volume. While the mold on the left is filled with pure epoxy, ceramic spheres were added to the resin in the mold on the right.



Figure 6.10: Volume shrinkage of epoxy resin during curing without (left) and with (right) filler material

Compared to the mold purely filled with epoxy resin, the volume shrinkage was reduced. The effects of cross-linking which is the reason for the volume shrinkage in epoxy resin is reduced by mixing ceramic spheres (diameter: 0.125-0.250 mm) into the compound. To avoid material stress and lower the risks of broken soldering connections, the cavities between the processing electronics and the carrier plate of the sensor were filled with a mix of ceramic spheres and epoxy resin.

6.2.2.1 Foam parameters for ambient pressure-tolerant fiber-optic sensing

The properties of the foam material define the sensitivity of the fiber-optic sensor arrays. Different types of foam can be distinguished by the type of cell structure, size and distribution of cavities, thickness and material. Preservation of the shape of the foam is essential for operation under pressure. Based on naturally occurring sponges that live at depths of up to 1,300 m [Christiansen, 2010], an open-cell structure is required. This setup allows fluids to float through the cavities, thus preventing compression of the material. In order to identify further crucial foam parameters for

application under water, a test setup was designed where single sensor elements using different types of foam were evaluated. A pre-selection of foam types was carried out to examine only foams that have an open-cell structure. The sensor elements were sampled using photo-transistors for conversion into electric signals, thus the dynamic range is given in volts in the diagram in Figure 6.11.

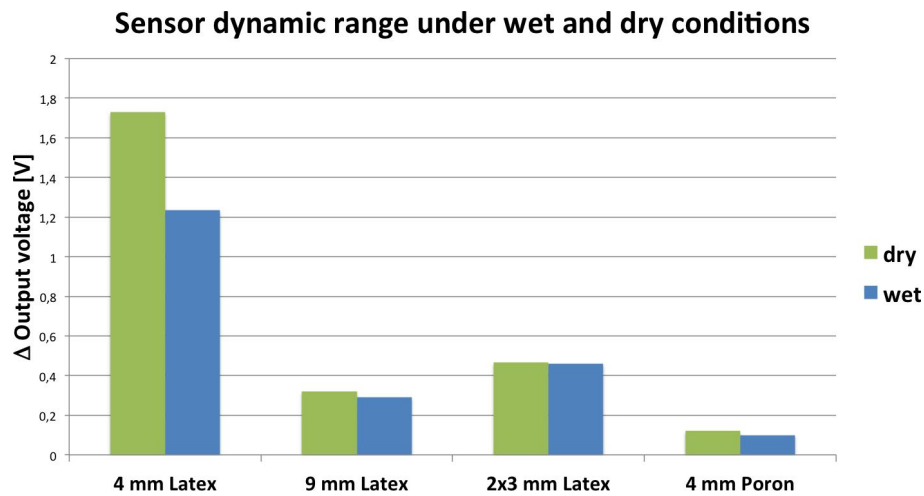


Figure 6.11: Performance of fiber-optic sensor elements using different foam material in air and in water

Variations in the dynamic range were observed among the different types of foam. Based on the high dynamic range under dry as well as wet conditions a foam made of latex was chosen that is manufactured with an open-cell structure and a thickness of 4 mm.

6.2.2.2 Preparation of force-torque sensors for application in water

An inspection of the force-torque sensors used in each finger base of the gripper revealed a small printed circuit board integrated into every sensor. This electronic component needs to be secured from contact with water (Figure 6.12a). The strain gauge sensors itself are already coated during manufacturing and do not require additional preparation.

Obtaining access to the mentioned PCB is a delicate task because of the thin Teflon strands used for cabling. These can easily break. This means the force-torque sensors have to be opened from the top as shown in Figure 6.12b. The cavities in the inner structure were used to fill the sensor with a silicone gel. After curing, this gel remains flexible which helps to avoid additional forces acting on the strain gauge sensors.

The plots in Figure 6.13 show the sensor feedback of a force-torque sensors applied with 1 kg of load prior to the described coating process (a), after coating (b) and while

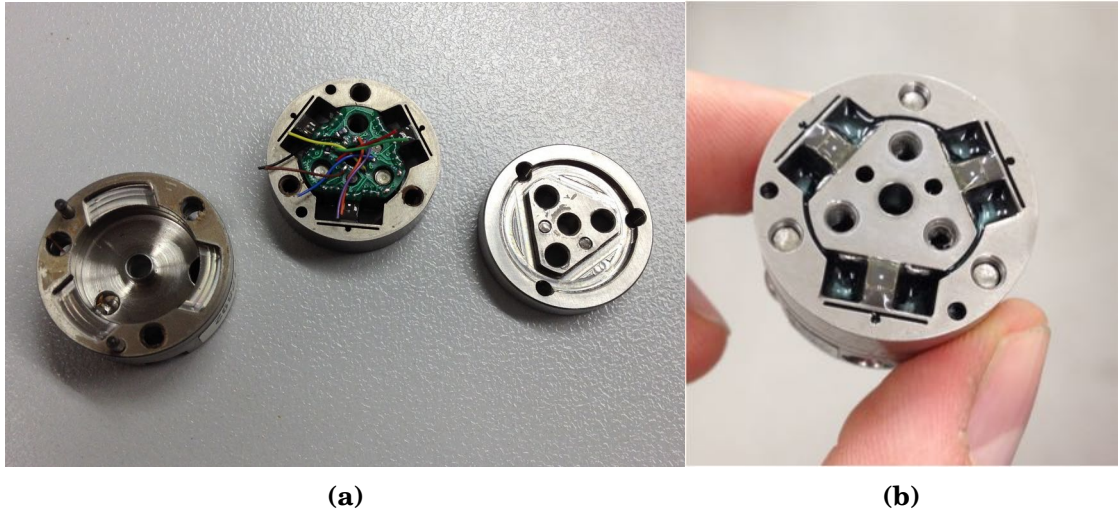


Figure 6.12: (a) Parts of a force-torque sensor (ATI nano 25); (b) sensor coated for underwater use

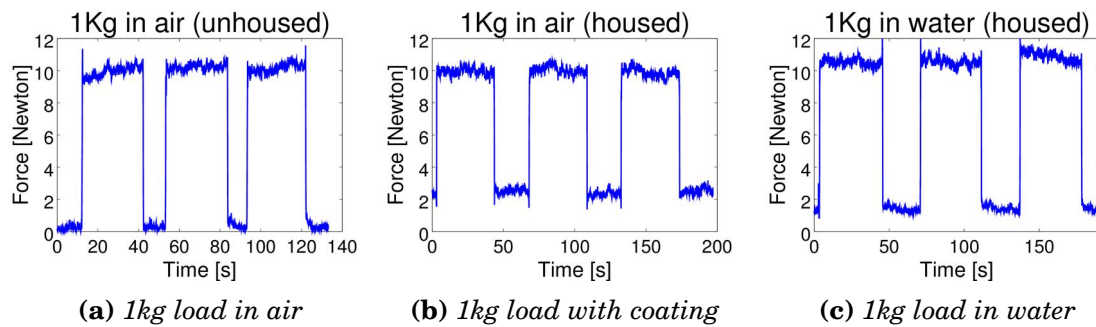


Figure 6.13: Force-torque feedback without coating (a), with coating (b) and submerged in water (c)

submerged in water (c).

It was observed that after coating the sensors, the force-torque feedback requires some settling time in order to work properly. Figure 6.14 shows the long-term feedback of a force-torque sensor that was applied with a weight of 1 kg over two and half hours.

From the beginning of the recording the overall force measured by the force-torque sensors continuously increased until it reached nearly twice the force that was actually applied on the sensor. During the recording the sensor feedback slowly decreased until it reached the initially expected quantity. A possible explanation for this behavior is a temperature dependency of the strain gauge sensors in the sensor. As shown in Figure 6.12b, the cavities of the sensor were filled with coating material. Originally, these cavities allowed temperature transport within the force-torque sensor to adapt to changing ambient temperature quickly and to carry away the dissipated

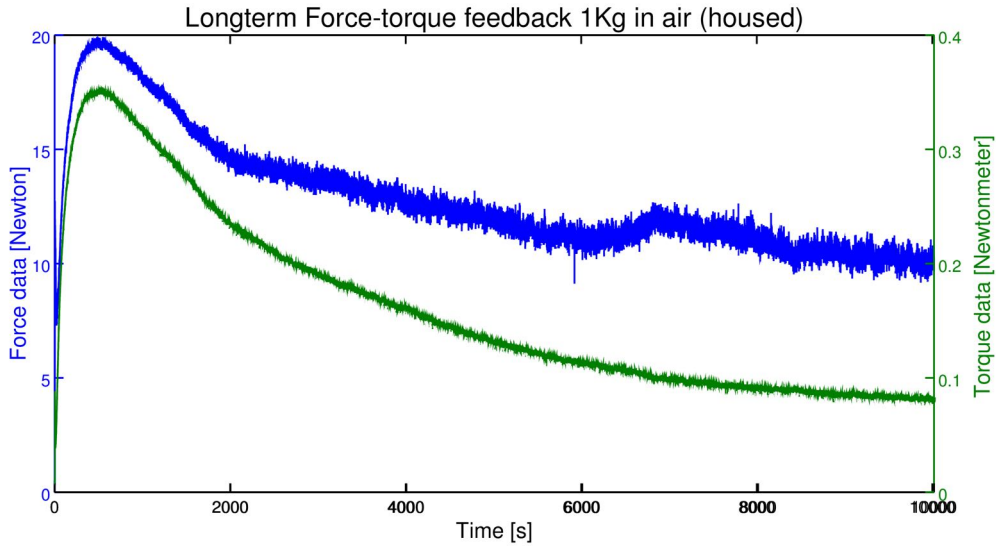


Figure 6.14: Long-term observation of force-torque feedback while applying 1kg weight

Table 6.2: Effects of sensor coating on repeatability and drift ($n = 10$ trials)

FT treatment	sensor state	Mean	Std.-dev.	Mean drift	Noise
Uncoated & in air	under load	10.08 N	0.13 N	0.4 N	0.58 N
Uncoated & in air	no load	0.44 N	0.07 N	0.2 N	0.93 N
Coated & in air	under load	9.93 N	0.09 N	0.1 N	0.48 N
Coated & in air	no load	2.48 N	0.11 N	0.1 N	0.86 N
Coated & in water	under load	10.91 N	0.23 N	0.6 N	0.56 N
Coated & in water	no load	1.35 N	0.12 N	0.3 N	0.50 N

heat from the strain gauge sensors while in operation. As these cavities are now filled with resin, the temperature adaptation did not occur as quickly as before. The two plots showing the sensor feedback after coating in air and underwater (Fig. 6.13) were therefore recorded after three hours after powering up the sensor and its processing electronics.

Table 6.2 summarizes the effects of coating the force-torque sensors on the repeatability, drift and noise of the signal values while a load of 1 kg is applied to the sensor. Each value is calculated from 10 repeated measurements. Significant differences are observed in the constant offset of the force-torque signal at around 2 newton after coating the sensor. A possible reason for this effect are variations in the coating process that lead to different initial load conditions of the strain gauge sensors. While submersed in water, the drift during loading and unloading the sensor increases.

6.2.2.3 Preparation of absolute angular encoders for application in water

Shielding the electronics of the absolute angular encoder is necessary to prevent short circuits. As the magnetic field that is to be sensed is not influenced by resins, these sensors were coated with a thin layer of epoxy resin (Fig. 6.15).



Figure 6.15: Coated absolute angular encoder ready for underwater usage

6.2.3 Sealing connectors

Two approaches to avoid short circuits occurring in the electric connectors within the gripper were evaluated. One attempt is to avoid sealing every single connector, resulting in easier maintenance. Therefore, a complete cover of the end-effector using a skin made of nylon material coated with latex was designed. Use of the skin leads to cavities in the inner structure that need to be evacuated in order to avoid collapsing caused by high ambient pressure. The evacuation is carried out by filling the complete gripper structure with a silicone oil. The assembled gripper using the protected skin is depicted in Figure 6.16.



Figure 6.16: Assembled gripper using a protective skin

Apart from the mentioned benefits of this approach, the necessity to fill the gripper with silicone oil has several drawbacks. For high sensitivity in the contact area the skin needs to be thin and flexible which makes it prone to damage caused by contact with sharp materials. Oil leakage is the consequence. Another issue is the fitting of the skin and the oil evacuating process itself, which is time-consuming. To perform maintenance on the PCBs and sensors in the gripper, the silicone oil has to be washed from the components, which comes with high efforts.

A second approach to protect the gripper electronics from contact with water is to seal each connector and component separately. Using this approach, the skin can be omitted and the usage of silicone oil is avoided. The silicone gel used for the sealing remains in a flexible state after curing. This gel is highly adhesive but can be stripped from electrical components without residues. As the material is able to repolymerize, indentation by test probes does not lead a loss of its sealing capabilities. These properties allow performance of maintenance tasks in the sealed state. Figure 6.17 shows the final setup of the gripper. As the wrist section is filled with PCBs and connectors, it was entirely housed in silicone. The DC motor and its gear, which is responsible for the rotary movements of the outer fingers, were covered in a blob of grease prior to coating the wrist section. The differences in viscosity between the grease and the silicone allow a rotation of the motor without twisting the outer silicone layer.

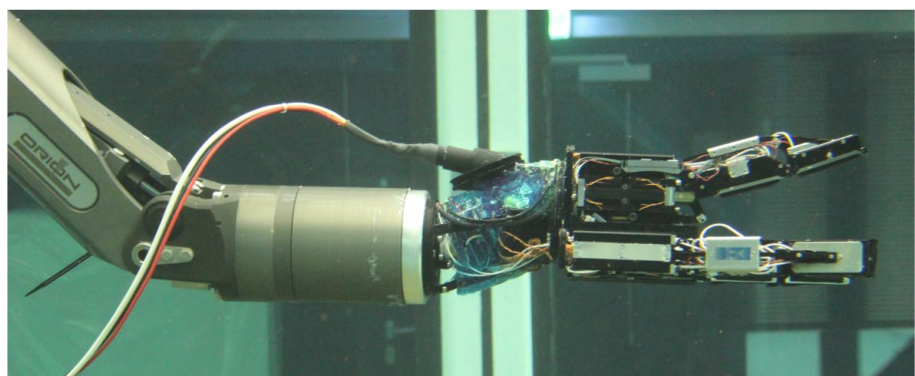


Figure 6.17: Assembled gripper attached to a deep-sea manipulator without protective skin

Both approaches were used in the experiments shown in the next sections. The protective skin was applied in experiments in the pressure chamber and in combination with the manipulator arm. The approach without a protective skin was used during the experiments conducted in combination with the manipulator arm.

6.3 Experiments in combination with an underwater manipulator

To test the capabilities of the gripper, experiments under water in combination with an industrial manipulator arm were conducted. Figure 6.18 shows the experimental setup. The gripper is attached to the manipulator arm and was submerged in a test basin having a depth of 2m. Three test objects - a ball made out of Styrofoam, a rubber ball and a tennis ball - were attached to wires fixed to the floor of the basin.

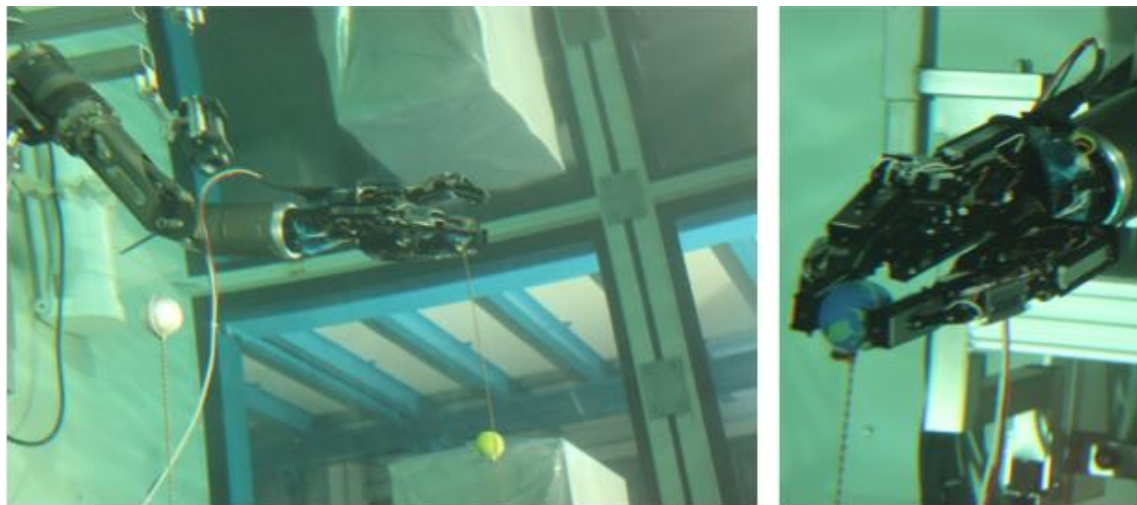


Figure 6.18: Experimental setup for testing the gripper in combination with a manipulator arm underwater

6.3.1 Distinguishing objects of similar shape

The objective of this experiment was to demonstrate the advantages of multi-modal sensor information in the gripper to distinguish three test objects by their compression hardness and geometry without adding visual information. The shape and the diameter of the test objects are depicted in Figure 6.19.

The three spherical objects have similar dimensions and differ in their stiffness. As the geometrical shape is similar among the objects, an identification based on geometrical properties does not lead to successful identification of the grasped object. Instead, the grasp force and the gripper closing angle are used to identify differences between the objects. The corresponding combination of sensing modalities together with the experiment environment are depicted in Figure 6.20.

The objects were grasped using a tweezers grasp posture of the gripper. To eliminate variations in the length of the lever arm from the finger base to the contact location, the object contact at the gripper module was within the same area with

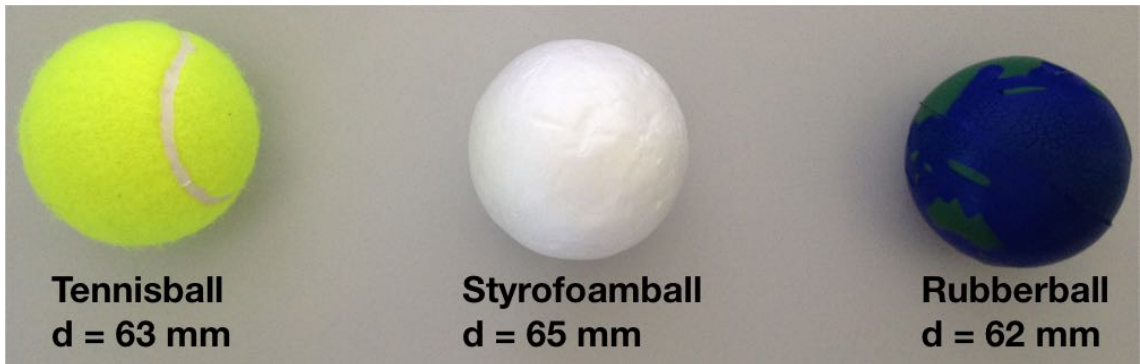


Figure 6.19: Spherical shaped test objects of similar dimensions

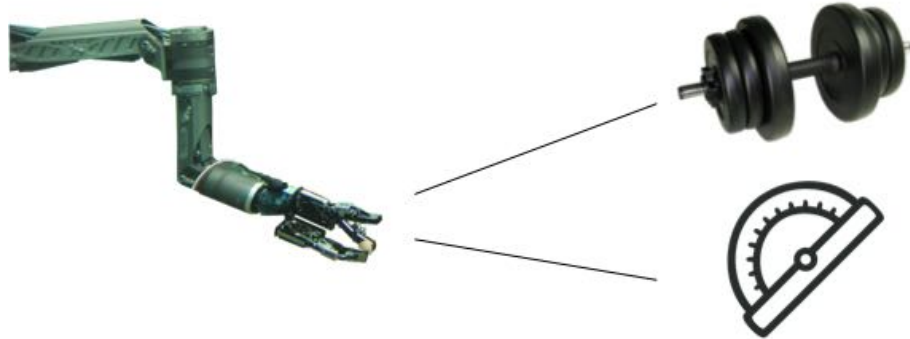


Figure 6.20: Combination of experiment environment and sensing modalities

differences in the millimeter range.

To obtain information about the compression hardness, the objects were grasped with maximum force. The averaged values over 4 trials for each test object together with the standard deviation are depicted in Figure 6.21. The independence of the samples was evaluated using the Kruskal-Wallis test [Kruskal and Wallis, 1952]. Unlike the classic approach of averaging and calculating the standard deviation, the Kruskal-Wallis test does not assume a normal distribution for each population analyzed. The null hypothesis of the test is to assume that all evaluated populations are identical. The obtained p value of the test indicates allows the rejection of the null hypothesis at a pre-defined significance level. It is common practice to define the significance level to 0.05 which means that with 95% probability there is a significant difference between the evaluated groups.

The results show statistically significant differences between the obtained values for the applied grasp force on the tennis ball and the Styrofoam ball as well as between the tennis ball and the rubber ball. Distinguishing the Styrofoam ball from the rubber ball is not possible using the modality grasp force alone based on the sampled measurements.

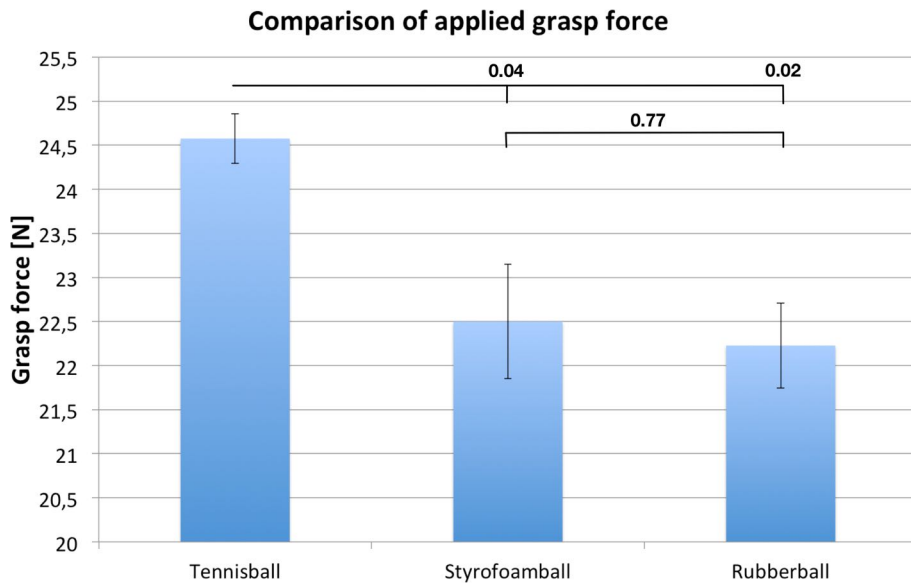


Figure 6.21: Applied forces for grasped test objects ($n = 4$ trials); p values between the populations are calculated using the Kruskal-Wallis test.

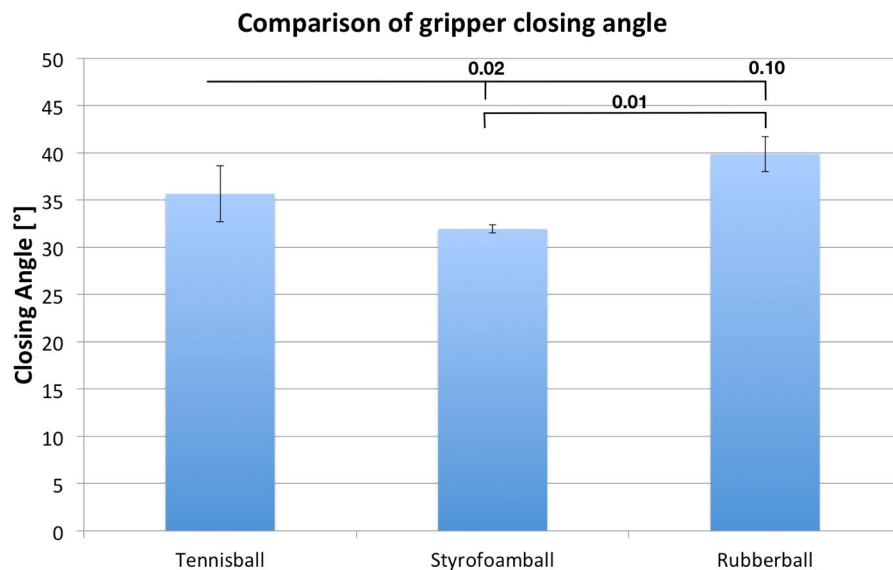


Figure 6.22: Applied closing angles of the gripper for grasped test objects ($n = 4$ trials). p -Values between the populations are calculated using the Kruskal-Wallis-Test.

To improve the ability to distinguish the objects, the sensing modality finger position was evaluated. The plot in Figure 6.22 shows the closing angle of the distal finger modules of the left and right finger during the grasp of the test objects. The independence of the samples was verified using the Kruskal-Wallis test.

It can be observed that the Styrofoam ball can be distinguished from the rubber

ball and the tennis ball whereas a distinction between the tennis ball and the rubber ball is not possible using only the encoder data information.

Distinguishing the three test objects by contact can be done by exploring the shape, hardness or texture of the objects. For two of the three objects the shape and hardness is nearly equal. The tennis ball and the rubber ball differ only by 1 mm in their diameter. The same is valid for the material hardness. With the given measurement precision of the sensing modalities, the objects cannot distinguished. By combining several modalities, distinction is possible.

6.3.2 Evaluation of piezoelectric sensor signal feedback

The piezoelectric sensing modality was originally integrated to sense texture and detect slippage. Gathering information on these two properties requires movement across an object. The experiment described here was used to assess the available additional information and the limitations of the piezoelectric sensing property during a single contact grasp.

Therefore, the output of the piezoelectric sensor arrays was evaluated during grasping of the three test objects from the experiment before. The experiment environment and the sensing modalities involved in this experiment are depicted in Figure 6.23.

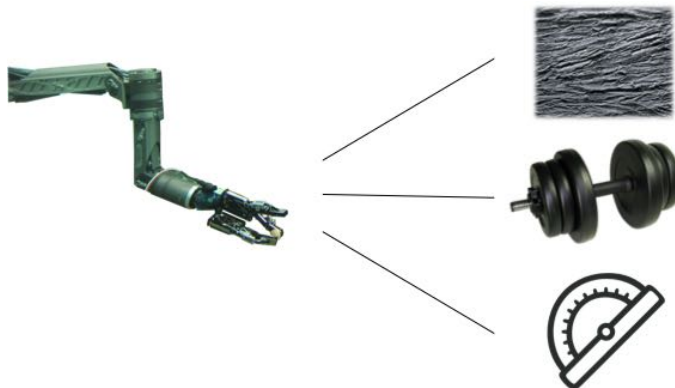


Figure 6.23: Combination of experiment environment and sensing modalities

The plots in Figure 6.24 shows an example of the averaged signal of the piezoelectric sensor array together with the corresponding force-torque sensor data (left) and the combination of the piezoelectric signal together with the encoder data from the distal limb module in the left finger (right). This data is shown for the distal left finger module.

Two observations can be made. The vibrations induced by the hydraulic valves operating in the finger base during movement influence the signal's standard deviation. The data from the right subfigure in Figure 6.24 supports this hypothesis since

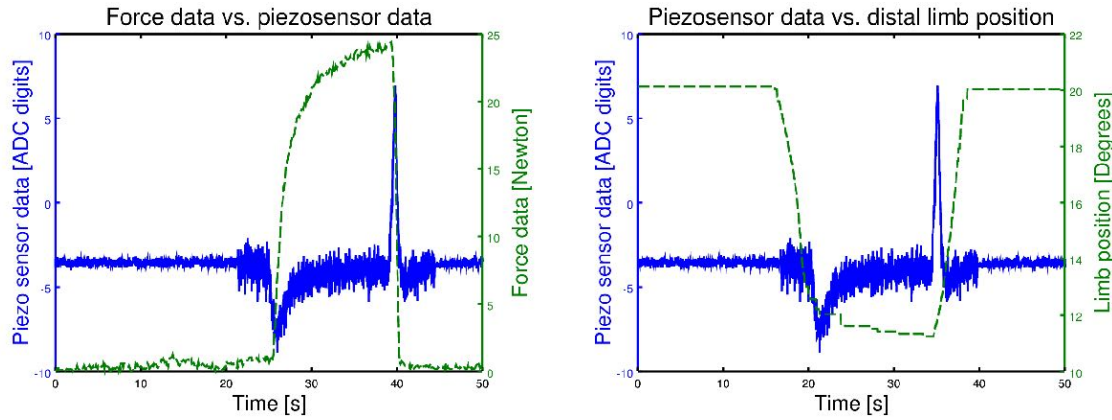


Figure 6.24: *Left: Force-torque sensor signal and piezo sensor signal during grasp operation (dashed line: force data, continuous line: piezo sensor data).*
Right: Encoder signals of distal left limb and corresponding averaged piezoelectric sensor signal (dashed line: encoder signal, continuous line: piezo sensor data)

the sensor signal varies in noise depending on the limb movement. Furthermore, the piezoelectric sensor data shows interesting properties that are suited for calibrating other sensor modalities using general contact information. Peaks during contact establishment and loss of contact have a high signal-to-noise ratio. By processing the polarity of the sensor's signal, it is possible to discriminate between creation or loss of contact.

6.4 Experiments under high pressure

Further experiments were conducted in a pressure chamber under ambient pressure conditions of up to 600 bar. The focus of the experiments was on the feasibility of the presented fiber-optic measurement principle as a tactile sensor array for deep-sea applications.

The results of two experiments are presented. The first experiment evaluates a single finger of the gripper that is equipped with fiber-optic sensor arrays comprising 72 sensor elements. Further experiments focusing on the fiber-optic sensor arrays were conducted in combination with the complete gripper module in the pressure chamber. The experiments were run with two aims. One was to evaluate the performance of the calculation of the center of pressure while rolling on an object surface, which is an important property concerning the sensitivity of the sensor modules. A further aspect was to gather information about the sensor performance depending on the electric acquisition modules. Therefore, experiments with two different camera chips were carried out.

6.4.1 Experimental setup using a single finger

The combination of the chosen experiment environment, evaluated sensing modalities and used acquisition electronics is shown in Figure 6.25.

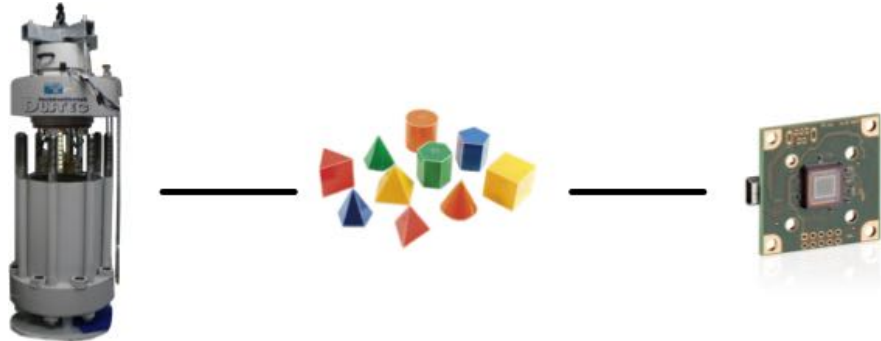


Figure 6.25: Combination of experiment environment, sensing modalities and acquisition electronics chosen

The electrical interface is implemented using a USB camera module that is equipped with an Aptina 1/3" camera chip having a resolution of 752x480 pixel. The setup in the pressure chamber is shown in Figure 6.26.

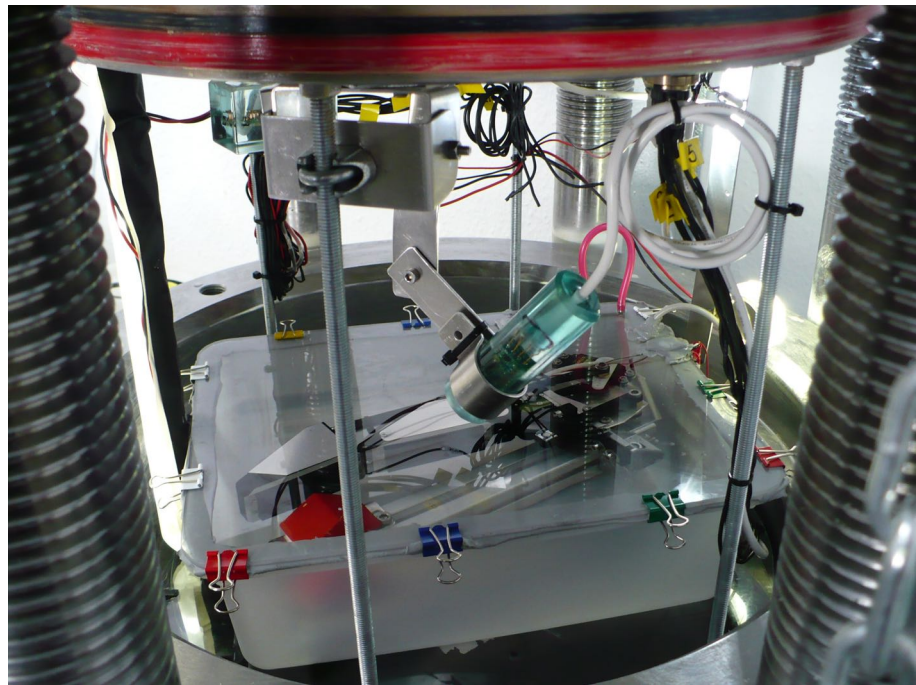


Figure 6.26: Experimental setup for evaluating the fiber-optic sensor array feedback

In order to minimize sealing efforts for this experiment, the experimental setup is integrated into a box filled with silicone oil. The finger itself is actuated using a servo motor. A triangular shaped building brick is fixed in the manipulation area of the

finger in order to evaluate the geometric sensor feedback during contact at different pressure conditions. The camera data is transferred, monitored and recorded by an external PC using the connectors of the pressure chamber.

6.4.2 Sensor signal variations between air and water

The two plots in Figure 6.27 show the variations of the sensor feedback while working in air and submerged in water. A change in the signal's initial sensor offset can be observed.

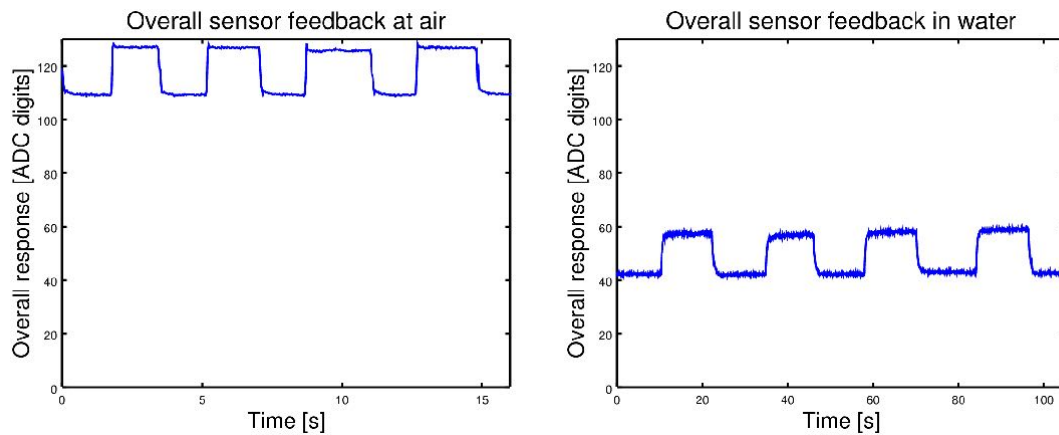


Figure 6.27: Sensor feedback of fiber-optic sensor array while operating in air and submerged in water

The reason for this observation can be found in the different refraction indices of air and water or silicone oil. The change of the exit angle of the emitted light from the optical fibers results in a different exit angle into the foam material. Table 6.3 lists the refraction indices for the media in which the sensor was evaluated.

Table 6.3: Refraction indices and exit angles for different media

Medium	Refraction index	Exit angle for 90°
Air	1.003	85.57/°
Water	1.333	48.61/°
Silicone oil	1.403	45.46/°

As can be seen, the indices and the exit angles of water and silicone oil significantly differ from those for air. In the selected fluids the scattered light that can be collected by the sensing fiber has less intensity which results in feedback of lower brightness during compression of the foam.

6.4.3 Pressure dependency of sensor feedback

While the applicability of piezoelectric sensors and strain gauges in deep-sea environments was proven elsewhere, the pressure independence of the fiber-optic sensor feedback is only discussed in section 4.5 in theory. The following experiment addresses this issue. The sensor array feedback is therefore evaluated under different pressure levels while contacting a test object with maximum force. Table 6.4 summarizes the maximum overall feedback acquired from the fiber-optic sensor. All measurements were carried out three times, the contact during measurement was applied for at least 20 seconds.

Table 6.4: Maximum overall sensor response during contact with test object at different ambient pressure ($n = 3$ trials)

Pressure	Averaged sensor feedback [ADC digits]
0 bar	42.32
100 bar	42.44
200 bar	42.09
300 bar	43.92
400 bar	43.62
500 bar	43.30
600 bar	43.11
Std.-dev.	0.69

The data suggests that the sensor signal span is independent of the ambient pressure conditions. A pressure dependent recalibration of the sensor signals is therefore not required. The acquired data also provides an indication of the repeatability performance of the sensor system. The sensor feedback of an experiment running on constant ambient pressure is depicted in Figure 6.28. The graph shown is obtained by repeating maximum contact pressure on the test object at the same contact location. Each curve represents the sensor feedback for one sensor element of the sensor array. An analysis of the averaged feedback yields a standard deviation of 0.03 ADC digits. Comparing this with the average signal span of the same sensor module under conditions in air of 60 ADC digits leads to a signal variation of 0.04%.

Of particular note is the flat line sensor response of sensor elements, such as the curve with the highest sensor feedback in the plot shown. This sensor behavior can be explained by the dynamic range of the camera module. The chosen camera system features a resolution of 8 bits which results in a maximum value of 255. For some sensor elements, this limit is reached taking into account the offset each sensor element has prior to indentation as can be seen by comparing the idle signal sensor

offset in Figure 6.29.

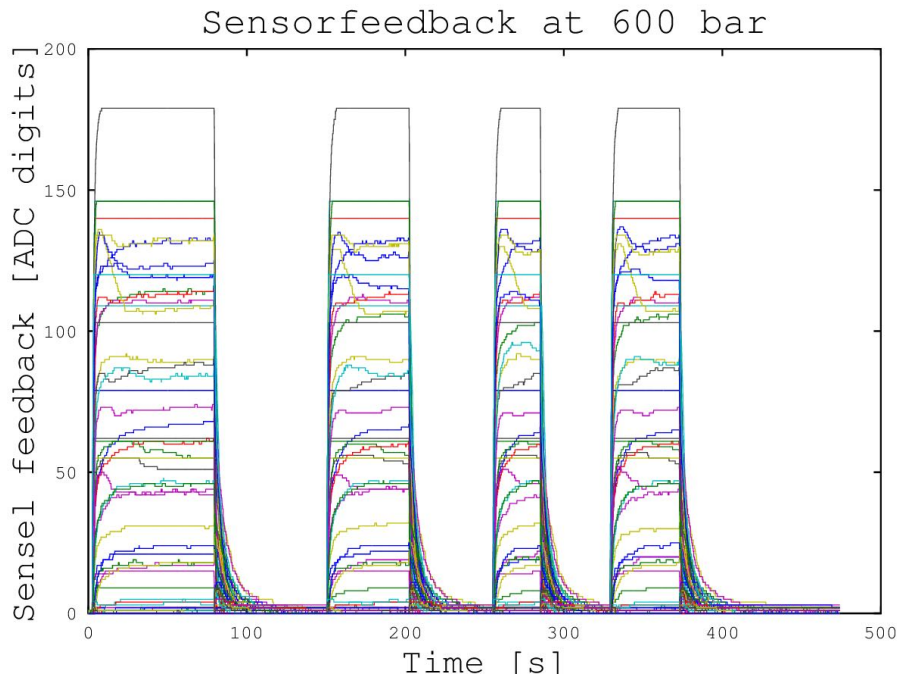


Figure 6.28: Sensor response for each sensor element during experiment repetition.
Plot based on average sensor feedback from four trials with a sensor array with 72 sensor elements

The variations in the sensor offset are due to the inhomogeneous structure of the foam material. While some sensor elements are placed below a cavity of the foam, others face structural material of the latex foam. The variations in the setup lead to different reflection conditions in the idle state as well as in the signal span during activation.

Variations in the sensor relaxation can be observed when comparing the sensor signal feedback at 600 bar (fig. 6.30) with the observed feedback in air (fig. 6.27). The slow convergence to a stable signal level can be explained by the different viscosities of the elements flowing through the foam structure. Caused by the different viscosities of air and water, the cavities collapse and return to their original shape in different periods.

6.4.4 Long-term sensor response under deep-sea conditions

Statements on the pressure dependence and repeatability can be made based on experiments performed. The following test examined the long-term response of the sensor while contacting an object. The sensor was therefore touching the test object under application of a constant force for one hour. Possible parasitic effects like drift

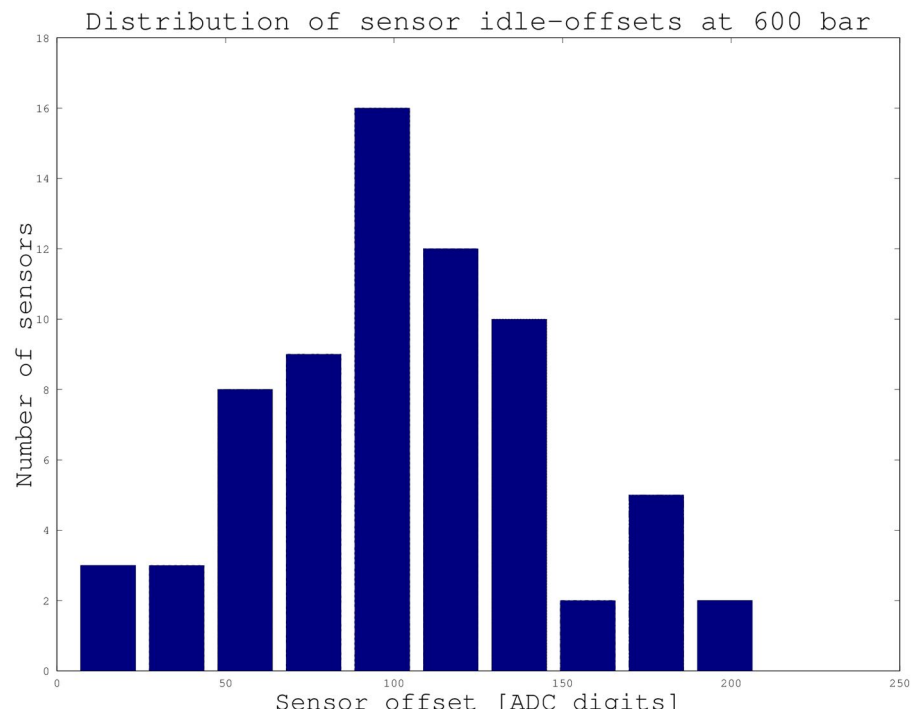


Figure 6.29: Idle sensor signal offset for each sensor element at 600 bar

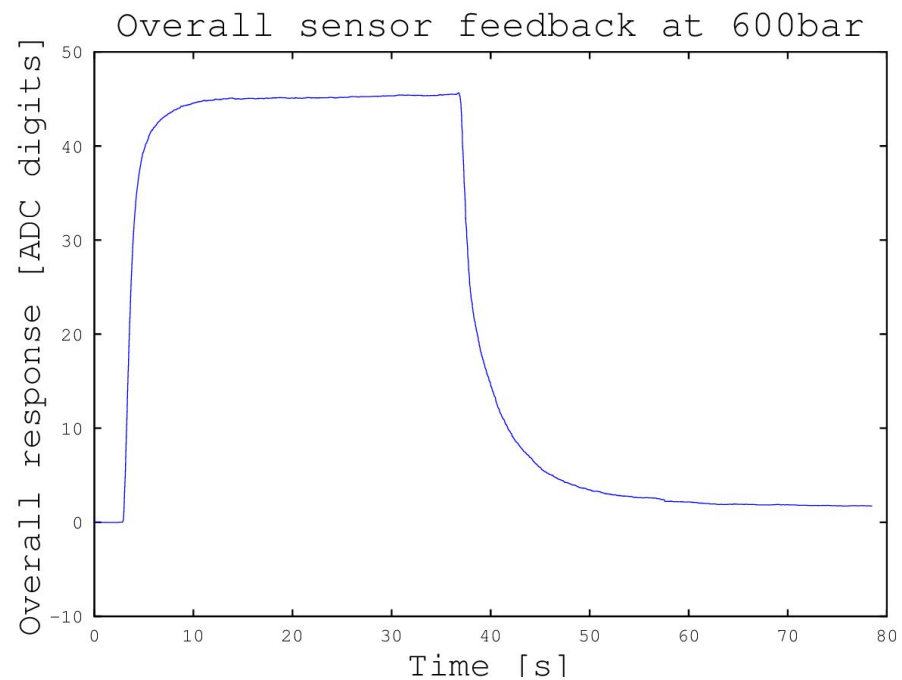


Figure 6.30: Averaged sensor signal response contacting test object at 600 bar

should be visible during that period.

Figure 6.31 shows the sensor feedback for each sensor element of the fiber-optic

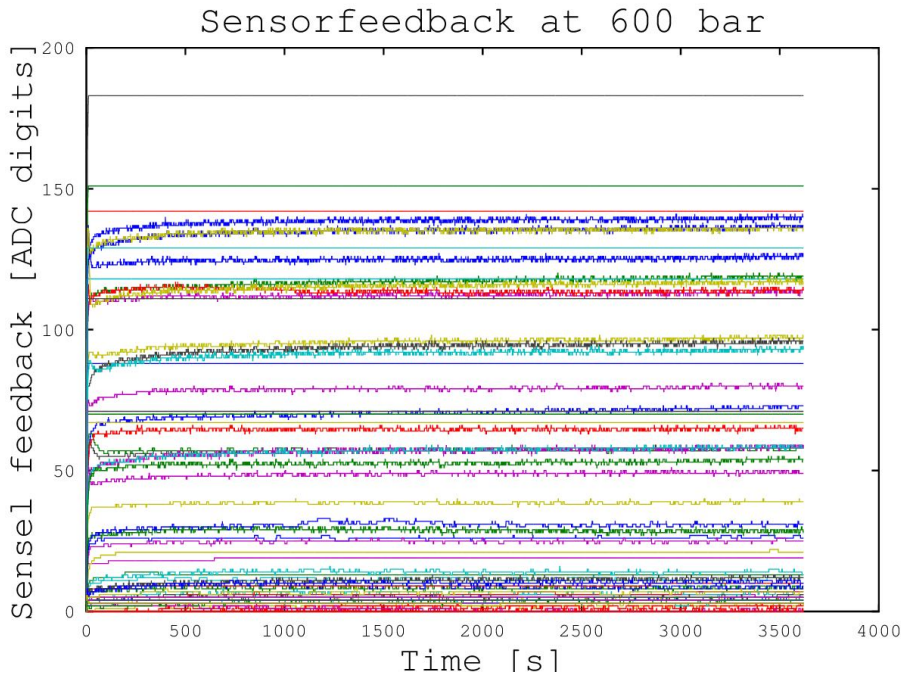


Figure 6.31: Long-term sensor signal response at 600 bar

sensor array while in contact with the test object for 60 minutes at 600 bar. The analysis of the averaged sensor signal beginning at 30 seconds after the experiment start up to the end of the experiment run shows that there is a constant increase in the signal response. A deviation of 2% in average was measured during the experiment run. This effect can be explained by the setting behavior of the foam. In cases where the fluid going through the foam cannot drain easily, the cavities collapse slowly. The ongoing compression of the foam leads to a continuous increase in the sensor feedback which describes the observed effect.

6.4.5 Ability to perceive geometries under deep-sea conditions

Use of the fiber-optic sensor array as a tactile sensing element for identifying object geometries under deep-sea pressure conditions was evaluated. The experimental setup comprises a fiber-optic sensing array integrated into a single finger and a triangular shaped test object. The finger was repeatedly pressed onto the test object which is at a fixed position to ensure reproducibility of the contact location. The way in which the triangular shape of the test object is sampled by the sensor array was investigated.

The processed experiment data is depicted in Figure 6.32. The triangular shaped object was measured prior to the dive in the pressure chamber (a). The acquired tactile image at 600 bar (b) was binarized (c). Based on the known spatial resolution of

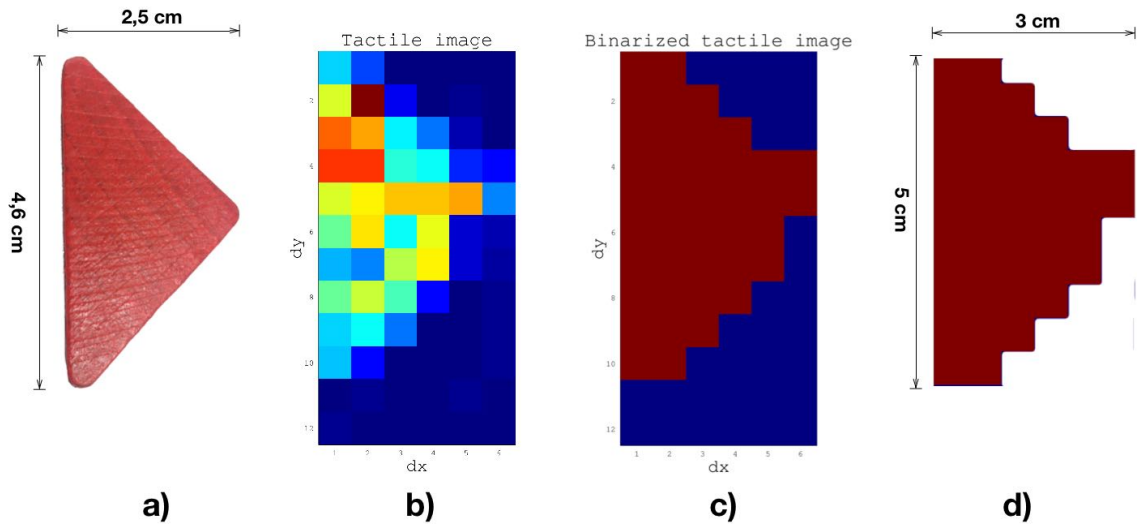


Figure 6.32: Triangular shaped test object (a), perceived tactile image at 600 bar (b), binarized image (c), derived dimensions (d)

the sensor elements, the dimensions in the x and y direction were calculated (d). The recording of the sensor dimensions was discretized to the spatial distance between the sensor elements which is 5 mm in the case presented here. Higher accuracy can be achieved by triangulation between the feedback intensity. This requires prior equilibration of the sensor.

6.4.6 Center of pressure detection in deep-sea conditions

Detecting the center of pressure is one of the key concepts for realizing human tactile exploration strategies like contour following. Following a contour requires the ability to move along the identified structure through the dexterous capabilities of the gripper and the manipulator. For the evaluation under deep-sea pressure conditions, the dexterity of the gripper is used to calculate the shift in the center of pressure of the tactile sensor modules while moving across a surface.

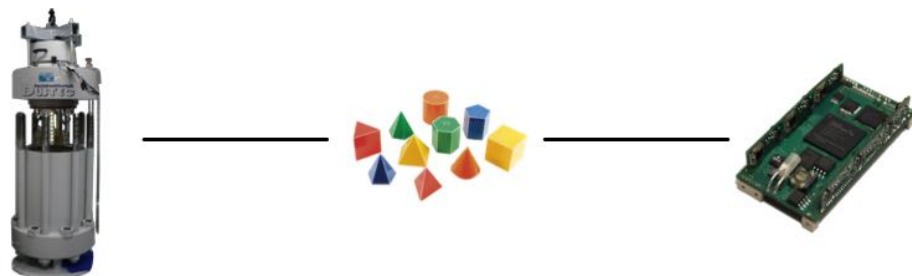


Figure 6.33: Experiment structure for evaluating the center of pressure detection under deep-sea pressure conditions

The experiment was composed of the parts shown in the structure diagram in Figure 6.33. The gripper system was used in the pressure chamber, the sensor feedback of the fiber-optic tactile sensor elements was evaluated using the developed acquisition electronics.



Figure 6.34: Experimental setup for evaluating the center of pressure detection under deep-sea pressure conditions

The experimental setup is depicted in Figure 6.34. The gripper system was mounted in an upright position. A spherical test object was fixed in the center of the finger elements such that it could be explored by the tactile sensors. The application of in-house developed pressure-tolerant cameras and lighting modules [Kampmann et al., 2012] as well as an overview camera mounted in the cover of the chamber enabled monitoring of the experiment. To actuate the gripper in the pressure chamber, the hydraulic supply for the gripper system was integrated within the pressure chamber, as placing the pressure supply outside the chamber would have meant to operate the supply pressure against the high pressure in the chamber.

To measure the center of pressure, a movement of the test object in the sensor contact area is required. Figure 6.35 shows the limb movements that were performed to generate a maximum movement of the center of pressure sensed by the distal sensor elements of the gripper.

The data coming from the fiber-optic sensor was used to calculate the center of

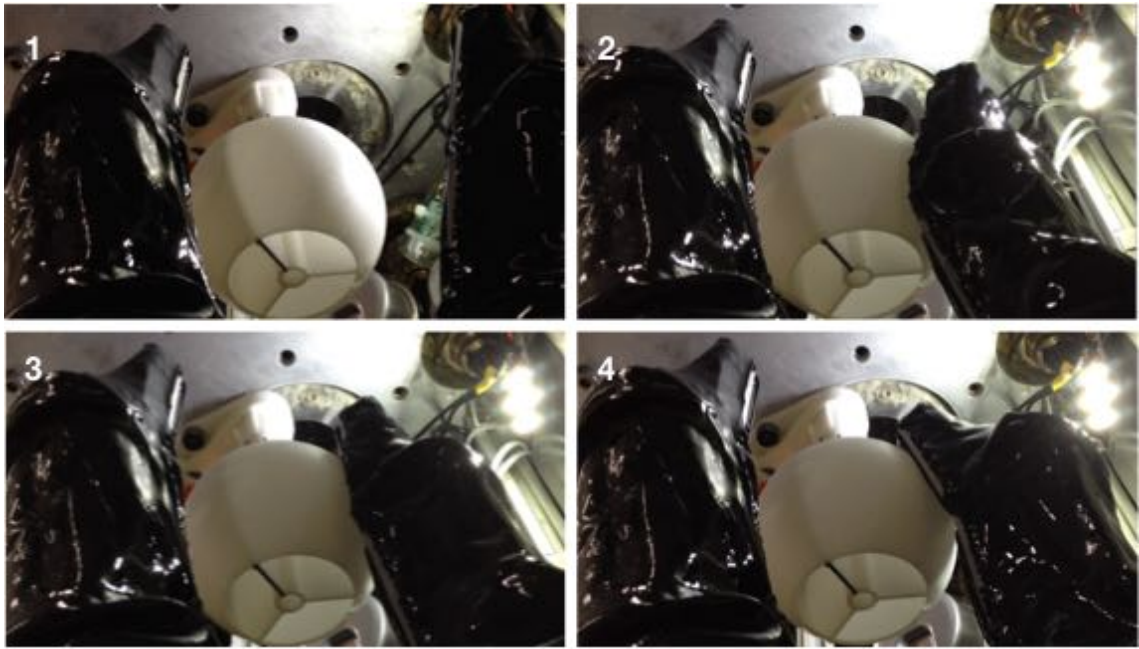


Figure 6.35: Rolling movement of the left finger to generate moving center of pressure on the tactile sensor array

pressure using the equations 5.23 - 5.27 introduced in chapter 5.2.2. The equations were implemented in the processing electronics of the gripper to locally process the data. The results obtained were recorded and transferred to a computer system external to the pressure chamber. The calculated force centers for the movements described in Figure 6.35 for different pressure levels are presented in Figure 6.36.

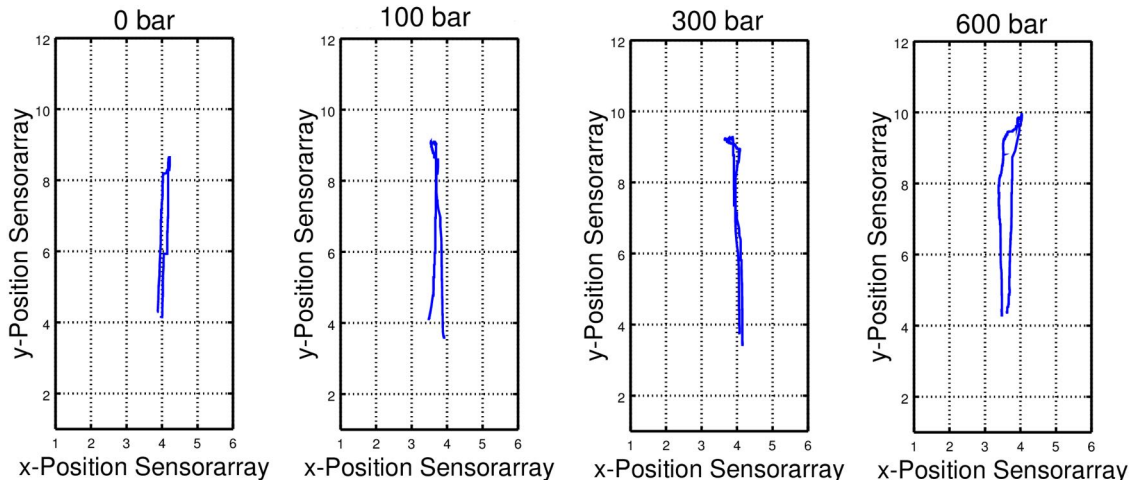


Figure 6.36: Force center calculations during exploration movements at various pressure levels

The graphs presented show a start of contact location around the center of the x

dimension in the lower section of the y dimension. A constant movement along the y-dimension was sensed which matches with the expected behavior. A comparison of the plots leads to the conclusion that only deviations within the range of a single sensor element in the feedback at different pressure levels occur. The requirements for implementing the approaches developed for tactile based contour following on objects are therefore met.

6.4.7 Performance comparison of fiber-optic sensing interfaces

Throughout the previous experiments two different interface electronics were used to acquire the signals from the fiber-optic sensors. Both interfaces rely on camera modules for the conversion of incoming light to an electrically proportional signal. The influence on the sensor signal quality depending on the selected interface was evaluated in the experiments described in this section. Table 6.5 summarizes relevant properties of the two CMOS camera chip modules.

Table 6.5: Comparison of the camera modules

Property	USB camera module	Embedded camera system
Camera chip	Aptina MT9V032STM	Toshiba TCM8230MD
Optical format	1/3 inch	1/6 inch
Sensor area	752x480 pixels	640x480 pixels
Pixel size	$6.0\mu m \times 6.0\mu m$	$3.75\mu m \times 3.75\mu m$
Resolution	8 bit	8 bit
Chip dimensions	11.43x11.43 mm	6x6 mm

Based on the properties presented, it can be concluded that the Aptina camera module has larger dimensions, which is critical for integration, but also has a bigger chip size. For application to fiber-optic sensor arrays, this means more space for fibers that can be attached to the chip. With the optical fibers that were used for the sensor modules having a diameter of $250\mu m$, a maximum of 90 fibers fit on the Aptina chip and 60 fibers on the chip from Toshiba. Further properties like noise or dynamic range could not be obtained from the publicly available information from both cameras. The following plots present the experimental evaluation of these properties.

Noise recordings were made during idle states of the sensor system, in order to investigate whether an increase in ambient pressure has any influence on the noise. The noise value for each run was determined by calculating the standard deviation of each signal for 20 seconds. It was averaged for an overall result.

The diagram in Figure 6.37 summarizes the results. A significant difference between the two sensor modules can be observed.

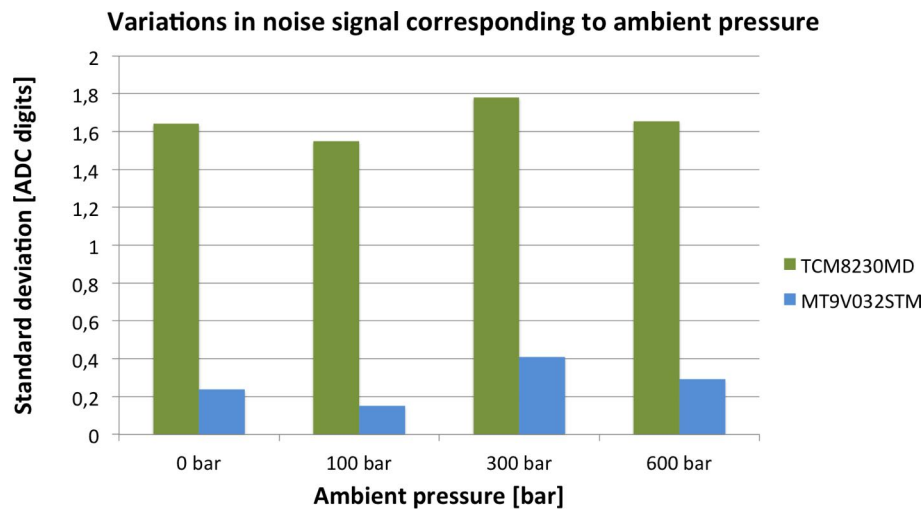


Figure 6.37: Comparison between idle signal sensor noise at different pressure levels ($n = 91$ sensels)

The differences in signal amplitude between activation and idle state of the sensor types were investigated. For this purpose the average signal amplitude between these two sensors was compared. The results are shown in Figure 6.38. A significant difference concerning the dynamic response of the two sensor systems can be observed. While the dynamic response of the USB camera module is reduced by 15% while submerged in water, the embedded camera module loses 40% of its dynamic range under wet conditions.

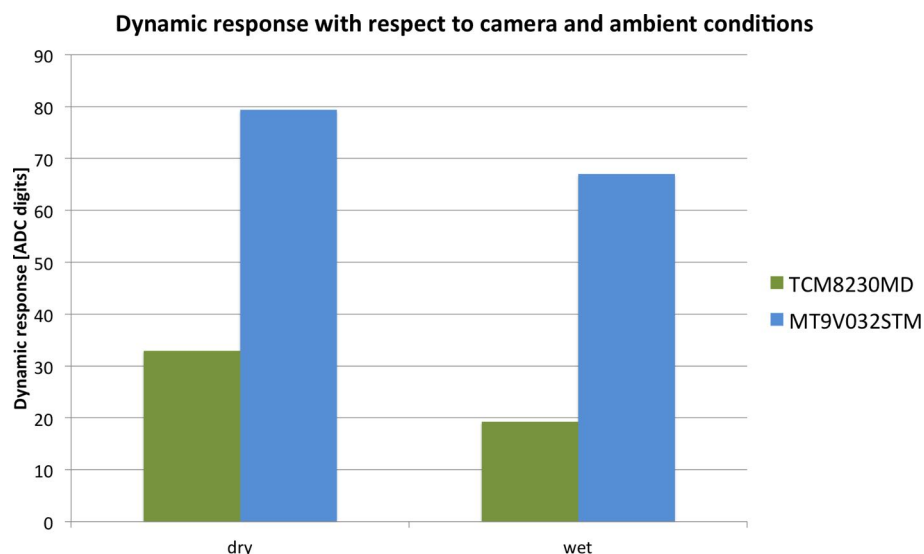


Figure 6.38: Comparison of dynamic response between the two camera systems in dry and wet environment ($n = 91$ sensels)

To summarize the comparison between the two sensor elements, the USB camera

module shows better performance in desired properties like signal noise and dynamic response compared to the embedded camera module. These differences in performance can be explained by the pixel sizes and the dynamic ranges of the camera chip. As the USB camera module features pixel sizes that are nearly double the size compared to the embedded camera module, a better noise performance can be achieved. The changes in dynamic response between the two camera modules is based on the dynamic range the two camera systems are able to perceive.

Besides the discussed advantages of the USB camera module, its dimensions present a challenge regarding integration of the module into limb structures of robotic end-effectors, which is why the embedded camera module was developed for the complete gripper system. It is expected that the development of camera systems for smartphones will increase the availability of high-quality camera systems with small dimensions that feature an increase in the quality of the sensor signals.

6.5 Local behavior evaluation: contour following

To identify objects solely by means of tactile sensing, decomposing an object into its geometrical primitives is one way to obtain information on their shape. Following contours of objects is thus a necessary ability. This task can be achieved best if its geometrical shape can be processed for calculating the next movement of a manipulator. Therefore, tactile sensing arrays are used for this task. The spatial resolution of the tactile sensor array in combination with the precision of the manipulator define how small the contours can be that the system is able to follow. While the tactile sensor must be able to resolve the contour, the precision of the manipulator is required to keep track of changes in directions.

Investigations on the position error of the Orion 7P deep-sea manipulator [Hildebrandt et al., 2009] reveal a deviation between the desired and measured position of up to 4 cm at the end-effector. Depending on the dimensions of the contour that should be followed, the extent of the position error can lead to a loss of contour by the tactile sensors in the finger modules. Hence, the experiment was conducted using an industrial manipulator arm for applications on land. The combination of experiment environment, sensing modality and acquisition electronics is depicted in Figure 6.39.

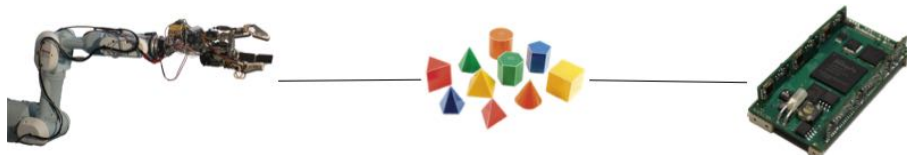


Figure 6.39: Serpentine contour used for conducting the experiment

This experiment demonstrates the capabilities of the algorithmic approach presented in section 5.2.2. The serpentine contour shown in Figure 6.40 was used as a test object. To explore the contour in the center of the disc, the fingers of the gripper were placed parallel to each other and positioned at the end of the contour by the manipulator. Commands for controlling the movements of the manipulator are calculated from the tactile feedback coming from the distal sensor element in the middle finger.

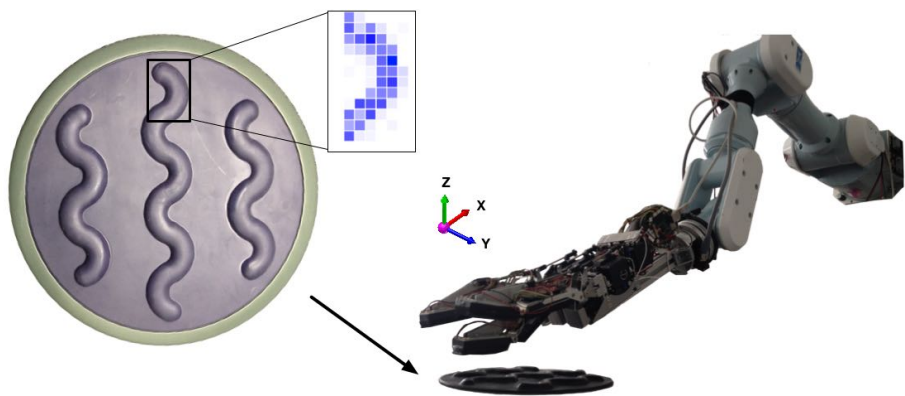


Figure 6.40: Left: Serpentine contour used for conducting the experiment. Right: Posture of the manipulator and the gripper during the experiment run.

To follow the contour, a hierarchical controller concept was implemented in the digital signal processor of the central electronics of the gripper. Its design is depicted in Figure 6.41. To ensure constant contact pressure between the tactile sensor and the contour, the averaged sensor array feedback is fed into a contact controller. When the average pressure leaves pre-defined limits, this controller overrides the commands from the contour follower and the orientation controller. The center of pressure belonging to the sub-area of the tactile sensor that is placed in the movement direction of the orientation controller is evaluated to generate commands to follow the perceived contour. The goal of the contour follower is to keep the center of pressure always in the middle of the tactile area. The direction to move the end-effector towards the center of pressure is computed. When the control goal of the contour follower is reached, the orientation controller is enabled to move the end-effector position along the x axis of the contour.

The diagram in Figure 6.42 shows the end-effector position superimposed onto the followed contour. High-level commands like *move left/right/up/down* are sent via Ethernet to the position controller of the manipulator running on a standard PC.

Transformation of the high-level command to a relative change in position is handled by adding a delta of a fixed step size to the current end-effector position. The calculated position is fed into a solver for the inverse kinematics of the manipulator

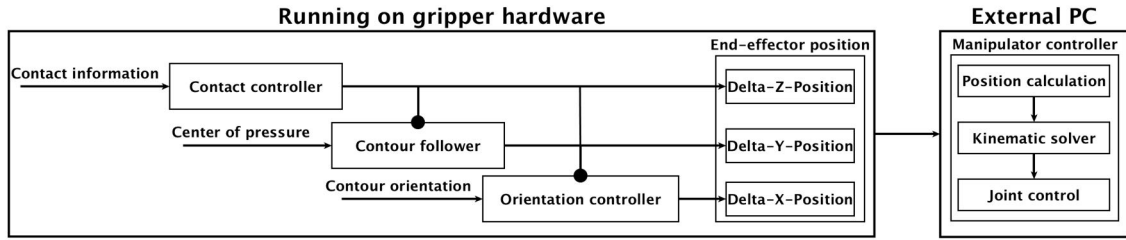


Figure 6.41: Hierarchical controller for contour following behavior. Lines ending with a dot indicate inhibitory effects to the subsequent controller.

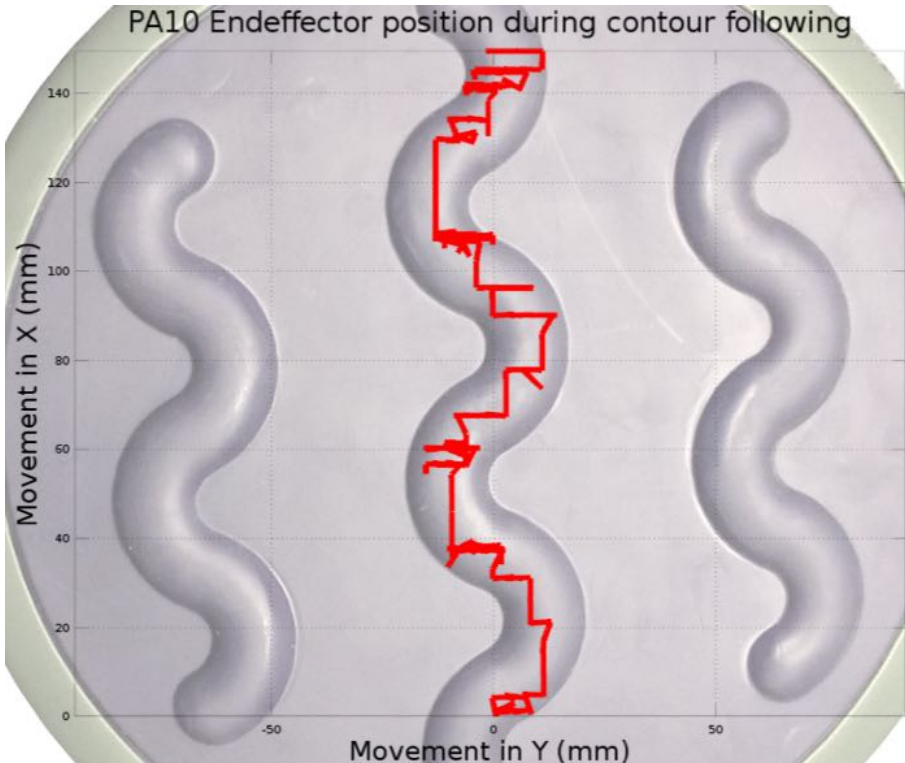


Figure 6.42: Calculated contour followed by the PA10 manipulator using control commands from tactile sensing.

that is implemented as a library for the ROS. The resulting joint angles are then sent to the actuators. The pre-emptive interface of the movement controller makes it possible to stop the current movement of the manipulator. Delays in the communication between the gripper electronics and the controller for the manipulator cause the jitters that can be seen in the diagram. Possible explanations for the communication delays are the computation time for the kinematic solver and delays caused by the operating system of the PC or the routing of Ethernet packages. Using the methods presented, the pre-defined step size determines the increments in which the contour is followed. In the case shown here, the minimum step size is set to 4 mm.

By lowering the step size, a more fine grained following of the contour is expected.

6.6 Discussion

Pressure-tolerant components for optimized integration space

Minimal integration space is achieved by avoiding housings that keep the influences of ambient pressure of the water column away from the components of the gripper system. Instead of using housings, a pressure-tolerant design approach was chosen for the gripper. Although the development of pressure-tolerant devices has been investigated before [Thiede et al., 2009], little information is available on the process of how to achieve pressure-tolerant configurations. After several experiments, avoiding gas inclusions in packages of electric parts was derived as a rule of thumb. In situations where this cannot be avoided, packaging and the working principles of components have to be evaluated to cope with the ambient pressure. Suitable replacements for capacitors with high capacity and oscillators were identified.

An inspection of the force-torque sensors revealed further necessary preparations to seal electronic parts. The developed coating process changes the signal behavior of the sensors. A significant difference is the limited heat transfer caused by the coating. Long initialization phases are the consequence.

Advantages of multi-modal sensing

The advantages of multi-modal sensing were demonstrated using the example of grasping objects with similar shape and dimensions. The combination of the fiber-optic arrays enables acquisition of the contact location while the force-torque sensor data can be used to distinguish objects based on their compression hardness. In cases where similar compression hardness makes a comparison based on this modality unfeasible, further data that exploits the slight variations in dimensions was used to distinguish the grasped objects. In general, the limitations in sensitivity with only one sensing modality were compensated for by adding a second modality to the analysis of the touched objects.

Further distinction can be achieved by adding the piezoelectric sensor data to the computation. This sensing modality is expected to generate varying feedback while moving across the surfaces of the presented test objects. In the experiments within the thesis, the basic working functionality of these sensors was evaluated. A connection between the actuator control and the noise variations of the piezoelectric sensor signal was observed. Further tests, such as evaluating the influence of the foam layer on the sensor feedback, are required.

Dependency on acquisition electronics of fiber-optic array feedback

The sensor quality of a sensor is significantly influenced by the accompanying acquisition electronics. For the electric interface of the fiber-optic sensor arrays, two different camera modules were used during the described experiments. The performance evaluation revealed variations between the two systems in terms of noise and dynamic response. Explanations for these observations can be found in the differences in the size of a pixel element, the optical format and the sensor area. While a better signal performance is preferred in general, integration into the end-effector structures of robots requires minimal integration space. An acquisition solution with lower spatial dimensions is therefore preferred over a solution with higher signal quality.

Fiber-optic sensor arrays under different levels of pressure

Due to their insensitivity to magnetic fields and electrostatic interferences [Fraden, 2010], optical sensors are not affected by parasitic influences often found in robotic systems. Tests in the pressure chamber were conducted in order to see if these properties still persist when using fiber-optic sensors under water and high pressure. Table 6.6 summarizes the evaluated properties.

Table 6.6: *Fiber-optic sensor performance under pressure*

Property	Value
Long-term drift (1h)	2 %
Avg. noise	0.25 digits
Pressure dependability	0.69 digits
Repeatability error	0.03 digits
Spatial accuracy	5 mm

Properties like drift, noise, pressure dependency and repeatability error show variations from the ideal signal feedback in the lower percentage margin. The spatial accuracy of the sensor is mostly defined by the spatial density of the sensing elements. Further improvements can be achieved by using triangulation of signal intensities in the case of an equilibrated sensor array.

Differences between the signal response in air and under water were observed. A changing signal offset of the sensor elements and variations in the signal path during activation and deactivation of a sensor element were observed. While the sensor offset has only minor influence on the sensor feedback, the dynamic response of the sensor is limited under water due to the viscosity of the fluid that flows through the foam.

Decentralized control

The capability of using decentralized control in a complex robotic system was demonstrated at on the basis of the example of following a contour by controlling the movements of the manipulator arm using the tactile feedback. This task resembles one of the exploration procedures humans perform when the sense of touch is used to explore objects. As all information is available locally to trigger control commands to follow the identified contour, this behavior shows how communication between sub-modules of robotic systems can help to shift the load from central processing units to processing units in the extremities.

Limits of current industrial underwater manipulator control

This task requires a degree of precision of the manipulator that makes it possible to keep track of the contour during movement. The position controller of the underwater manipulator that was used in the experiments does not meet the requirements for the test object that is used. Future underwater manipulators that use tactile sensors for more than ensuring the presence of contact require a position accuracy that is within mm range rather than cm. While this requirement increases the complexity of the actuator design, further parameters for manipulators like repeatability are of less importance as fine positioning of the manipulator can be adapted by using the tactile capabilities of the gripper. To demonstrate the applicability of the approach developed, an industrial manipulator for applications on land was used. This also required a more lightweight gripper system as the gripper capable of deep-sea operation is too heavy to be lifted by the chosen robotic arm.

Fixed versus variable compliance

The gripper used is made of sheet metal and features the same dimensions and morphology as the underwater gripper. Major differences are in the actuation, which is based on servo motors, the unavailable force-torque sensors and the compliance, which is fixed. During contour following, the fixed compliance damps the contact forces, leading to lower signal feedback at the tactile sensor arrays. Therefore, a variable compliance is preferred as this can be used to stiffen the limbs during contact where strong feedback is required and lower the stiffness prior to contact to reduce the impact of possible collisions.

Chapter 7

Conclusion and Outlook

This chapter puts the results from the previous chapters into the context with the stated objectives in the introduction of the thesis. Besides these objectives, further insights were gained during this work. These findings and the lessons learned are presented as well. The chapter concludes with an outlook on further steps in the development of robotic manipulation in the deep-sea using tactile sensors.

7.1 Conclusions related to the thesis objectives

Identification of suitable measurement principles for multi-modal tactile force sensing in deep-sea

The surrounding water and the rising ambient pressure with increasing depth are demanding requirements when selecting suitable tactile sensor elements for application in deep-sea environments.

Regarding the state of the art in underwater grippers for the application in the deep-sea, only a few prototypes are documented. The developments in the last decades include few sensing elements for contact measurement. There are no reports of an array solution that allows acquisition of geometrical information. The deepest point in which a system was evaluated is documented to be at a depth of 25 m.

In order to obtain tactile feedback of high quality, the measurement principles should work independently of the water column. Measurement principles not affected by rising ambient pressure do not require recalibration of sensor offsets at different depths. As most sensor feedback curves tend to express an asymptotic response to increasing stimuli, a sensor that measures the ambient pressure in addition to the actual contact stimuli loses its sensitivity at greater depths. Being insensitive to the ambient pressure allows the sensor to have the same sensitivity at all operating depths.

Measurement principles based on effects that use varying conductivity of materials cannot be utilized for application in water. The high conductivity of water leads to saturation of the sensor feedback or even to short circuits. Without special preparation for application in water, classical concepts like capacitive or piezoresistive sensing cannot be applied. Measurement principles that require electronic components in the contact area are susceptible to damage due to high contact forces. The risk of short circuits caused by direct water contact has to be taken into account as well.

These preconditions were taken into account during the selection of suitable measurement principles. A theoretical discussion on the applicability of the selected sensor working principles is provided in section 4.2 of the thesis. The approach of sensing multiple modalities of touch with the designed tactile sensing system was addressed by a biological inspired approach in which measurement principles specialized in sensing a specific modality were integrated into the system.

In the tactile system developed geometric contact stimuli are sensed by an array-based sensor solution. The chosen sensor is based on an optical measurement principle which is known to feature a static response with low signal drift and noise. Additionally, optical measurement principles are known to be unaffected by electromagnetic fields that are exerted by actuation components like motors. To acquire absolute incoming forces, a single point measurement technique was selected using strain gauge sensors. The approach of using a single point sensor to measure the overall force has the advantage of a lower calibration effort compared to adding up the sensor response from an array-based sensor solution. Instead of calibrating all sensor elements of the sensor array, only six sensor elements for axial forces and torques have to be calibrated. The sensor feedback coming from an array sensor can be used to identify the force center which helps to calculate the lever arm. Furthermore, the force distribution can be qualitatively measured. The multi-modality of the tactile sensor system was completed by a piezoelectric sensor array that is sensitive to dynamic contact sensing and proprioceptive sensors that measure the joint angles.

The selection of two array sensing solutions of different modality posed a challenge regarding the mechanical integration. Tactile array sensing solutions require placement directly at the contact area. This situation caused competing requirements with respect to the integration space since the fiber-optic sensor and the piezoelectric sensor array need to be placed at the same location in order to acquire the same tactile stimuli with different modalities. A solution that combines the two approaches was developed in which the piezoelectric sensor array serves as the carrier plate for the optical fibers of the fiber-optic sensor.

The applicability of the selected measurement principles was verified in combination with a robotic gripper in experiments in shallow water, under pressure of up to 600 bar and on land. The experiments and their results are discussed in chapter

6. The focus in the experimental validation was on evaluation of the sensor feedback coming from the force-torque sensors and the fiber-optic sensor arrays as piezoelectric sensors were used in deep-sea environments before. The difference of the sensor response under dry conditions in ambient pressure and under water was evaluated. Although the experiments were repeated at least three times for each analysis and several different sensors were used for each experiment, all sensors were treated manually and thus show effects that can be explained by variations in the sensor quality. The conclusions drawn regarding sensor performance thus give an indication of the expected performance. Twenty fiber optic sensors, eight piezoelectric sensors and three force-torque sensors were used to conduct the experiments.

Preparations of the force-torque sensor for application under water lowered the sensor performance in terms of sensor drift and in the sensor offset. Especially under loading conditions below 5 N, the sensitivity was lower compared to a sensor that was not adapted for application in water.

The piezoelectric sensing modality was evaluated briefly while showing promising overall sensitivity and sensor performance; a sensor feedback coming from vibrations of the actuation was observed. Approaches for avoiding processing of this undesired sensor signal are based on a frequency analysis of the sensor signal and suppression of the frequencies that correlate with the PWM signal for the actuators. The response of the piezoelectric sensor showed the potential of the acquisition of contact stimuli with several contact sensing modalities. The averaged signal feedback during grasping indicated a clear response while loading and unloading the contact area. The signal can be used in combination with the other modalities in many ways, such as increasing the confidence in the acquired sensor data and recalibrating other sensing modalities.

A change in the sensor offset and dynamic response was observed for the fiber-optic sensing setup. Physical effects like the different refraction indices of air and water were identified as a reason for this observation. Further observations showed a difference in the signal rise and descent underwater and in air. Explanations for this behavior can be found in the relaxation of the foam material that depends on the viscosity of the substance flowing through the foam. Experiments that evaluate the pressure dependency of the sensor feedback match the expected results from the theoretical sensor concept. A low standard deviation below one digit from the analog-to-digital conversion and a repeatability error of 0.04% of the signal range show a low pressure dependency of the measurement principle.

Local pre-processing as a solution for handling complex robotic systems

Increasing the autonomy of robotic systems with the goal of coping with unstructured environments is one of the driving motivations in the research of robotics and

artificial intelligence. The discipline of behavior-based robotics combines these two research domains with the modeling of a robot in sets of behavior of different levels. All these types of behavior are triggered by stimuli which are acquired by sensors at the lowest level. As a consequence of this, a modeled robot behavior is only useful if the required stimulus can be generated within the robot in order to be able to react to intended and unintended states during a mission. Aside from the actuation capabilities of a robot that ultimately allow realization of behaviors that are triggered, the sensing capabilities define which mission states can be observed. For the increase of autonomy in robotic systems, sensing the environment with high spatial and time resolution with different modalities and high sensitivity can be considered as a way to accomplish this goal.

The consequences of this development are an increasing volume of data that needs to be handled online in a robot in order to extract useful information as stimuli for behavior. This development requires integration of computational power to process the sensor data which poses challenges regarding integration into the robot, the power consumption and the hardware architecture. Within the scope of the thesis, a robot where these challenges have to be faced, is considered to be a complex robotic system. Instead of transmitting the acquired raw sensor data to a set of central processing units in the body of a robot, a distributed approach is necessary that involves selection of suitable processing electronics, adapted processing algorithms and forwarding of the sensor information to suitable levels in the computation hierarchy is required.

This general observation is dealt with in the practical example of processing the tactile sensor data stream within a robotic gripper. The data obtained from all sensing modalities in the gripper amounts to approximately 300 megabytes per second. An approach which only transmits the data to a processing unit requires three gigabit Ethernet connections under the assumption that the sensor data transmission is the only communication taking place on these channels. A hardware architecture comprising eight FPGAs, nine PSoCs and one DSP were integrated into the gripper to acquire and pre-process the sensor data as well as actuate the joints (compare section 4.7).

Several pre-processing algorithms that were implemented in the hardware architecture in the gripper are presented in section 5. General approaches to reduce the communication load by discarding the transmission of redundant information were developed and similarities between spike trains in response of tactile stimuli on the human skin were shown. Discarding the transmission of redundant information does not result this data remaining unprocessed. Approaches on how to make use of the redundant information were discussed. Examples are to use the data in order to monitor the function of a sensor, to reduce the noise signal or to increase the dynamic range of a sensor.

Further processing algorithms were presented that focus on extraction and calibration of the fiber-optic sensing arrays. Handling the complexity of robotic systems that use these sensors was tackled in two ways. In order to reduce the integration efforts on the mechanical side, algorithms were developed that reconstruct the topology of the sensor elements in the contact area. Additional algorithms extract the relevant sensor information of the sensor array from the acquired camera images that are used to convert the light intensity information of the sensor into an electric signal.

By extracting information at the earliest stage in the processing chain, decision making can also be implemented locally. This concept is demonstrated by implementing a local controller that uses the tactile sensor data rather than a position of the joints to grasp an object. Extending the concept to further extremities of a robot, a control concept was developed which uses local information from the sensors in the gripper to guide a manipulator arm to follow a contour. The general idea of this approach is to avoid the inclusion of a central processing unit in the task and thus reduce its processing load. Rather than receiving the tactile signal and computing the next steps from a central controller, the tactile information is processed in the gripper and the required movement direction is sent to the controller of the manipulator arm. This approach is demonstrated in the experiment chapter in section 6.5. Extending this to a complete robotic system leads to a design where sections of a robot are to some extent self-organized. It supports the reduction of complexity by allowing a central robot controller to send out high-level commands to its sub-components that take care of the task execution themselves.

The combination of the developments to handle the amount of data coming from the sensors enables transmission of the tactile sensor information which adds up to 300 megabytes per second in the unprocessed state via a communication channel that is capable of transmitting 12 megabytes per second.

Validation of the approaches under relevant conditions

The third objective of the thesis deals with the verification of the developed concepts during system development and the algorithmic development level under conditions that are relevant in real world applications. All experiment environments and the conducted experiments are presented in section 6 of this thesis.

An approval verifying the capability of operation under pressure conditions of 600 bar allows application of the system on the sea floor with coverage of 97%. Suitable tests in a pressure chamber focusing on demonstrating the applicability of the pressure-tolerant setup and the working principle of the tactile sensor array were conducted.

During these tests the developed approaches to prepare the electronics for deep-

sea applications proved to be successful. The independence of the fiber-optic measurement principle from the ambient pressure conditions was shown. Additional testing under high pressure involved the repeatability and long-term stability of the sensor signal which demonstrated the qualities of the measurement principle and resulted in data-sheet-like summary of the performance of the sensor. During the experiments that were conducted fiber-optic sensors were operated more than 30 hours under pressure levels of up to 600 bar.

Experiments in combination with a manipulator arm under water showed how a multi-modal sensor system leads to a rise in performance compared to analysing a single modality. At the example of distinguishing objects with similar shape and dimensions, the combination of force-torque sensor data and the gripper posture was demonstrated to be capable of differentiating the test objects. In total, the tactile sensing system was operated for more than 12 hours under water. The system was submersed for more than 60 hours.

Limitations in precision of the standard position controller for an underwater industrial manipulator were identified in terms of contour following using tactile data. The validation of the developed approach was successfully shown on a manipulator arm for applications on land.

The two experiments showed the capabilities of the system to implement some of the exploration procedures that identified as being performed by humans for exploring unknown objects. Further experiments of identifying objects by touch through comparison with a database of known objects were successfully conducted with the system developed in [Aggarwal et al., 2015].

A multi-modal tactile force sensing system for the deep-sea

The three sub-goals of the thesis combine to form the overall objective which was the development of a multi-modal tactile force sensing system able to operate in deep-sea applications. The literature research in this field revealed that the manipulator prototypes that incorporate tactile sensing were not evaluated for depths below 250 m. The sensor configuration of the underwater grippers did not exceed twelve sensor elements per finger module. Sensing modalities that allowed acquisition of contact geometries were not integrated. Furthermore, the pre-processing of the sensor information was reduced to signal data acquisition by electronic modules that were integrated in pressure housings. Commercial off-the-shelf components for sensor elements that are capable of operating under water or pressure-tolerant electronic modules are rare and in most cases do not meet the requirements for high integration density.

Based on the observations in connection with the state of the art on manipulators for applications on land and under water, requirements were derived on the design of

the tactile sensing system and its processing.

Off-the-shelf components for this task are rare and mostly do not meet the requirements for high integration density. Literature research on underwater manipulators with tactile sensing revealed only little research towards working under pressure conditions below a depth of 250 m.

Thus pioneering work was required to develop suitable concepts for compact actuation, pressure-tolerant electronics and proprioceptive as well as exteroceptive sensors.

The multi-modal tactile force sensing system developed is able to operate at depths of up to 6,000 m. It comprises 570 exteroceptive sensing elements and six proprioceptive sensors. Besides measuring the presence of contact, it can be used to measure absolute forces, dynamic impacts and the geometric shape of the contact. To the best of the author's knowledge, especially the availability of a tactile sensing array for sensing geometries in deep-sea conditions was not documented in relevant literature prior to the developments presented in this thesis.

7.2 Further results

Advances in pressure-tolerant electronics

At the time of writing this thesis, the design of pressure tolerant components was presented in the literature on a system level perspective [Thiede et al., 2009]. Off-the-shelf components offered as pressure-tolerant systems were not available. Knowledge about the susceptibility of electrical parts was thus required to achieve the desired integration density that was expected to in combination with a pressure-tolerant approach. Detailed investigations on the identification of electronics parts that are vulnerable to the ambient pressure were conducted. The required experiments to establish rules of thumb for pressure-tolerant designs are presented in this thesis. Suitable ways treating these parts, either by coating or replacement, were identified.

A tactile sensor for perceiving geometric contact properties in the deep-sea

Strain gauges and piezoelectric measurement principles are components needed to create a multi-modal tactile sensing system and were used in deep-sea scenarios before. One of the missing modalities was the ability to sense geometric properties with sensing elements arranged in an array. An existing fiber-optic sensing principle was identified whose applicability under high pressure was discussed in theory and verified in various experiments under relevant ambient conditions. Further development of the sensing principle was carried out within the scope of this thesis on the structure of the sensor focusing on low integration density and the combination with

other sensing modalities to form a multi-modal tactile force sensing system. Highly integrated interface electronics together with calibration algorithms contribute to the improvements of the sensor solution. The new developments have aroused the interest of the manufacturing company of the original sensor. It resulted in a partnership that combines the developed approaches and the sensor system in commercial prototypes for the automotive and healthcare industry.

7.3 Lessons learned

In addition to achieving the objectives of this thesis, general methodologies for the design of technical systems were identified. These are presented here.

Realizing pressure tolerant electronic parts

As literature research did not reveal any best practices for preparing sensors and electronics for a pressure-tolerant setup, these were identified in the thesis.

- **Identify parts that have gas inclusions**

Known components are, for instance quartz oscillators and capacitors. Further components can be identified either by their working principle or by using x-rays to look for cavities within the modules.

- **Replace these parts if possible**

Using packaging material like ceramics or plastic minimizes the risk of collapse for small components. A working principle that does not require any gas inclusions is advantageous. If this is not feasible, a small pressure housing has to be build for the component that cannot be replaced.

- **Unsolder unnecessary parts and connectors**

In the case of use of off-the-shelf PCBs, some components might not be required for the intended use of the electronics. Examples for this are outgoing video data signals in underwater applications because it is unlikely that a monitor to display data in this case. As such parts potentially include cavities filled with gas within their structure, it is safer to remove them.

- **Replace connectors with copper wires**

Modules that should be interfaced can be connected to external cabling by using copper wires soldered to the PCB. Within this thesis, epoxy resin was used as a coating material. Using standard cabling having a jacket made of silicone turned out to have poor adhesive qualities in combination with epoxy resin, leading to water ingress to the soldering point.

- **Coating**

In the case of occurring stress while curing, ceramic spheres were added to the epoxy resin. Short glass fibers added to the epoxy resin prevent the occurrence of cracks within the hardened epoxy resin structure. An alternative coating material is silicone gel, which can be used if access to electrical parts is required after coating.

On complexity in robotic system design

The term complexity applied to technical systems is used to refer to various aspects. In this thesis, it is used to address the increasing functional density required for designing robots that are able to cope with an increasing variety of situations. This involves all disciplines of robotic development. It requires autonomous capabilities that rely on sensory input from as many modalities as possible to assess the current situation and derive further actions. It also requires advanced mobility and manipulation capabilities based on mechanical structures as well as sensing and actuation. All these demands influence the robot design. In most cases, they mean additional effort to keep the overall design within the targets for weight, power consumption and dimensions.

During development of the underwater gripper system, steps were identified where the involved disciplines mechanical development, hardware architecture design and software development are interacting to shift integration challenges to the discipline that is able to cope with those involving the least effort. The derived interaction process is sketched in Figure 7.1. It is based on observations made during development of the gripper system and is assumed to be valid for technical systems in general.

The following examples describe the interaction of the several disciplines. By discarding the spatial relation of the optical fibers on the sensor array during mechanical integration, the amount of manual work was reduced. The task of reconstructing the spatial relation was shifted to the algorithmic side. Suitable algorithms had to be developed to reconstruct the spatial alignment of the sensor elements. As software development takes place only once during design, the algorithmic efforts can be considered to be significantly lower compared to a mechanical solution especially when building many instances of the sensor.

The optimized approach to extract the information of the optical fibers from the camera image can be extended to continuously monitor their positions. It is thus enabling a mechanical solution that does not require fixing the sensor elements on the camera image. A solution using a connector that does not ensure a rigid position of the optical fibers on the camera chip can therefore be used to further reduce the mechanical integration effort.

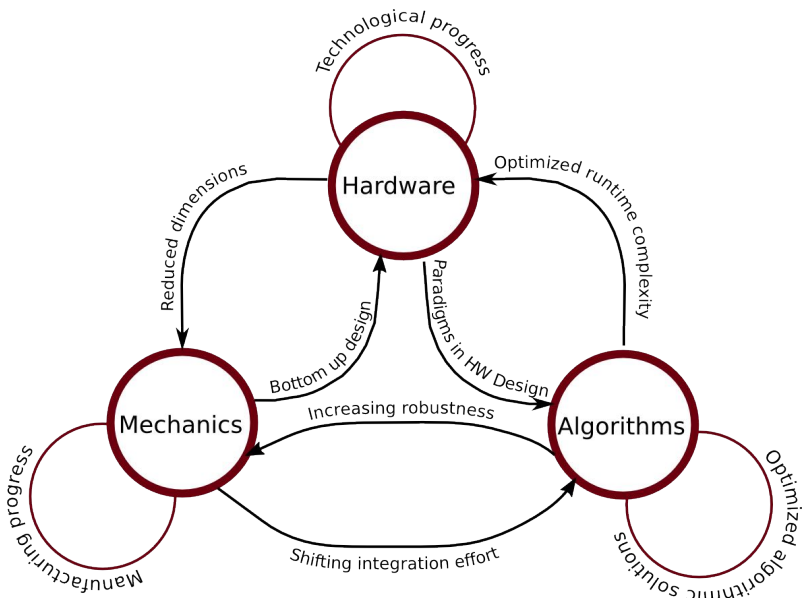


Figure 7.1: Interaction between disciplines in robotic design in handling integration of functionality for complex robotic systems.

The optimized algorithms with low computation and memory complexity lower the requirements regarding computing power of the hardware architecture. Lower processing power requirements mean smaller package dimensions which in turn facilitate integration into the mechanical structure of the robot. Further improvements like manufacturing progress or changing programming paradigms support the compact function integration for complex robotic systems.

7.4 Outlook

A concept for handling complex systems is to identify steps that simplify parts in each involved discipline. Several ways to accomplish this in the developed system are addressed in this section.

Working towards reproducible sensor quality

Work within the scope of the thesis involved integration of 18 fiber-optic sensor modules were integrated. While software approaches were developed to reduce the integration effort, placement of the optical fibers is still a time-consuming task. Furthermore, the quality of the sensor feedback varies between these modules. Further research is therefore required to simplify the manufacturing process and achieve automated mass production. A promising approach is the ability to print polymer fibers by means of a 3D printing technique that is presented in [Pereira et al., 2014]. At the time of their work becoming a mature technology, the most time consuming and

complex step during the integration of the sensor will be automated and can be reproduced with constant quality.

Further work on the piezoelectric sensor signal processing

Integration of the piezoelectric sensor feedback into the design of behaviors that are based on tactile feedback has many possible applications and further improves the ability to explore objects by touch. The multi-modal design approach led to the combination of the piezoelectric sensor array and the fiber-optic sensing solution in the same contact area. In the current configuration, the piezoelectric sensor is covered under the foam material while in contact with objects. Although the system is still sensitive enough to respond to light touches on the foam surface, a signal amplification in the contact surface can improve the ability to sense different surface structures during sliding movements across touched objects. A biologically inspired approach for this is the application of papillary structures on the sensor skin. [Scheibert et al., 2009] found out that the epidermal ridges on the skin of the human hand support tactile perception of fine textures. By applying a papillary structure to the skin surface of the sensor, a technical implementation of this concept can be achieved which amplifies the vibrations in the contact area induced by the object's texture. Promising results with such a concept were already made in combination with robotic tactile sensors [Wettels et al., 2014].

Application of tactile sensing for industrial underwater manipulation

In discussions with ROV operators about the solution developed two things were identified as possible ways to further improve the systems for industrial application in underwater missions. One issue is the usage of the gripper developed as a tool for standard manipulator arms. It should therefore be capable of being grasped by a standard two-jaw gripper and only require little cabling. A design that is powered by a battery pack using electric actuators and thus omitting the cables for hydraulic supply is therefore envisioned.

Furthermore, the working conditions during underwater manipulation are often compared to the situation at a construction site. This means harsh environmental conditions and the necessity of a robust design of the tools used. Among the most delicate parts on the gripper developed are the skins used to cover the fiber-optic sensors from ambient light. A simplified version of the tactile sensing system comprising the fiber-optic sensor array was integrated into a replica of the two-jaw gripper structure of the industrial underwater manipulator Orion 7P [Kampmann et al., 2015]. The contact area of the designed gripper is shown in figure 7.2. Instead of using a delicate skin material, pins indent the foam material below the contact surface. Using this approach prevents damage to the foam material as the pin modules are designed



Figure 7.2: Details of the two-jaw gripper developed with integrated tactile sensing elements for industrial underwater manipulators

such that they never fully compress the foam.

The next steps in this direction include the test in cooperation with ROV operators to increase acceptance of the tactile feedback. Furthermore, incorporation of the sensing modalities presented in this thesis is envisioned. By continuously evaluating design approaches so as to achieve robust dexterous end-effectors, the gap between the industrial end-effector solution and the gripper system developed can be narrowed.

Alternative ways of manipulator control

The use of tactile sensors during manipulation tasks opens new ways of performing manipulation tasks. A common approach for controlling manipulation arms is to use the inverse kinematics of a manipulator arm to compute the required joint angles in order to move the end-effector to a desired position. During development of the contour follower, an alternative way of controlling the manipulator movements was considered. A suitable solution for moving the manipulator arm in small steps along the direction of the contour is to find a way of directly addressing the joints that can move the arm in the desired direction in the current pose. Using this approach requires knowledge about the current orientation in the end-effector and in each joint of the manipulator. This can be achieved by integrating acceleration sensors in the gripper and the manipulator joints.

In the case of a required change of direction computed on the base of the tactile information in the end-effector, joints on the kinematic chain can be identified that allow movement in the requested direction. If no joint is directly able to move the

manipulator in the requested direction, summation of the direction vectors of several joints can lead to the desired movement. Preventing manipulator postures with limited moving capabilities can be achieved by taking the limits of the joints into account in every step.

It is envisioned that this approach will support the idea of distributing the computation in a robotic system as the calculation of the joint movement can be computed using the available computing power in each joint rather than calculating the inverse kinematics on a single processor.

List of Figures

1.1	Structure of the thesis	7
2.1	Schematic drawing of a gripper with force-torque sensors for intrinsic tactile sensing	10
3.1	Spike trains in response to a tactile stimulus from the different types of mechanoreceptors (from [Vallbo and Johansson, 1984])	15
3.2	Procedures performed by humans to explore unknown objects by touch, from: [Lederman, 1991]	16
3.3	Multi-modal tactile sensor module for integration into the fingertips of the SKKU Hand (from [Choi et al., 2005])	17
3.4	Sensor skin consisting of hexagonal shaped contact sensing modules [Mittendorfer and Cheng, 2011]	18
3.5	Multi-modal force sensing module for robot fingertips ([Wettels et al., 2014])	18
3.6	Proposed tactile sensor for sensing sliding objects based on microbending fiber-optic sensing [Tan et al., 2008]	19
3.7	Tactile sensor in combination with a tactile sensing computer (from: [Raibert and Tanner, 1982])	20
3.8	Architectural concept for a tactile retina for the detection of slipping objects (from: [Maldonado-López et al., 2006])	21
3.9	Assembled Gifu Hand 3 (left), structure of the tactile sensor module (right) (from: [Mouri et al., 2002])	23
3.10	Cross-sectional view of the finger structure of the DLR/HIT Hand 2 (from: [Liu et al., 2008])	24
3.11	Schunk Dexterous Hand 2.0 (left), details of the actuation modules in the joints (center), tactile sensing module in the distal finger elements (with material from: [Schunk GmbH & Co. KG, 2008] and [Weiss Robotics GmbH & Co. KG, 2009])	24
3.12	Example of a standard manipulation arm used in the deep-sea	25

3.13 Morphology of the AMADEUS dexterous gripper (left) and finger structure (right) (from: [Lane et al., 1997]	26
3.14 Structure of the Heu Hand II gripper (left), cross-sectional view of a finger (center) and fingertip structure (right) (from: [Meng et al., 2006])	27
3.15 Structure of the gripper (left), details of the tactile sensor (right), from: [Palli et al., 2014]	28
3.16 Measurement principle of the optical force-torque sensor (from: [Palli et al., 2014])	28
4.1 Summary of underwater manipulation tasks performed in the scientific domain using a jaw gripper (images courtesy of: [Ocean Networks Canada, 2014])	34
4.2 Peg-in-a-hole task ROV intervention during the Deepwater Horizon incident (image Source: U.S. Coastguard)	35
4.3 Taxonomy of grasp types of the human hand (from [Kapandji, 2007])	36
4.4 A three-fingered glove for industrial divers working offshore	37
4.5 Morphology of the designed gripper	37
4.6 Comparison of standard hydraulic valves for deep-sea manipulators (front) and the selected micro solenoid valves (back)	39
4.7 Section view of micro solenoid valves.1: Valve seat, valve nozzle; 2: Closing spring; 3: Valve coil; 4: Stationary anchor; 5: Medium; 6: Valve ball; 7: Mobile anchor; 8: Switch (Source: [Fritz Gyger AG,])	39
4.8 Hydraulic circuit in the finger modules of the gripper for one DoF [Lemburg et al., 2011]	40
4.9 Derived sensing capabilities for implementing exploration tasks	41
4.10 Typical measurement setup (left); electric circuit for strain gauges in force-torque sensor (right)	42
4.11 Selected force-torque sensing solution: force-torque sensor ATI nano 25 capable of sensing six degrees of freedom	43
4.12 Perovskite crystal structure of lead-titanate-zirconate and the polarity of voltages depending on the deflection of the dipole	45
4.13 Piezoelectric sensor array developed. (Sensor element dimensions are projected onto the image))	46
4.14 Working principle for a fiber-optic tactile sensor	47
4.15 Configurations of the components comprising a sensing element of the fiber-optic measurement principle: a) full-space configuration b) half-space configuration c) non-fiber sensor	48
4.16 Proposed configuration of the sensor for integration into robotic grippers	48
4.17 Assembled fiber-optic array sensor for perceiving contact geometries . .	49

4.18 PSoC circuit for acquiring force-torque sensor data	52
4.19 Developed electronics for locally processing force torque sensor data	53
4.20 PSoC circuit for acquiring piezoelectric sensor data	54
4.21 Horizontal (a) and vertical (b) placement of camera chips for fiber sensor acquisition	55
4.22 Off-the-shelf USB camera solution as acquisition electronics for the fiber-optic sensor	56
4.23 Assembled fiber-optic processing electronics	57
4.24 Integrated multi-modal sensor system for measuring geometries and dynamic impacts	59
4.25 PCB developed for measuring the gripper pose	60
4.26 Sensorfusion PCB that aggregates the sensor data in every finger	60
4.27 BaseBoard PCB that combines and processes the data coming from all sensors	61
4.28 Topology of the presented hardware concept for decentralized pre-processing of tactile sensor data	62
4.29 Integrated gripper system for deep-sea applications	63
 5.1 Signal sequence of a value-dependent transmission policy	70
5.2 Reducing communication intensity through value-dependent transmission	71
5.3 Processing flow from raw camera images to tactile sensor array data	73
5.4 Camera image acquisition	74
5.5 Extracting the optical fibers from the camera image	75
5.6 Identifying circle centers using circular Hough Transform based on gradients	76
5.7 Working principle of the algorithm to detect optical fibers	80
5.8 Working principle of the algorithm to detect optical fibers	81
5.9 Runtime comparison of the different implementations for extracting the optical fiber information	83
5.10 Average noise reduction of the sensor element feedback via parallel averaging of the sensor feedback using multiply camera pixel values. (calculations based on feedback from a sensor array with 91 sensor elements)	84
5.11 Non-uniform light distribution in an optical fiber.	85
5.12 Improvements in dynamic range using multiple pixel elements to compute the tactile sensor feedback. (calculations based on feedback from a sensor array with 91 sensor elements)	85
5.13 Different foam types and their inhomogeneous structure	86

5.14 Non-uniform sensor response during idle state (left) and variation in the maximum signal amplitude (right). (plots based on feedback from a sensor array with 91 sensor elements)	86
5.15 Distribution of signal spans after 18 targeted activations of all sensors in a sensor array with 91 elements	87
5.16 Implementation of neighborhood detection	89
5.17 Mapping to the grid of the sensor elements after neighborship detection	90
5.18 Placement of neighboring sensor element	90
5.19 Result of the force-based layout algorithm for a sensor field with 91 sensor elements	91
5.20 Concept of using a SOM to align the obtained mesh to the actual grid pattern. Top left: mesh obtained with noise. Bottom right: mesh obtained after 10 000 training steps starting from the initial grid structure (top row, second to left)	92
5.21 Matching result for trained self-organizing map after 10,000 iterations (left); ground-truth grid structure for comparison (right)	94
5.22 Conceptual drawing of similarities between electric potential (left) in neurons (based on [Purves, 2012]) and the filter concept that identifies activated sensor elements (right)	95
5.23 Activation detection of a single sensor element through constant monitoring of the idle signal	97
5.24 Evaluating the activation detection algorithm using increasing frequencies	98
5.25 Evaluating the activation detection algorithm using increasing amplitudes	98
5.26 Skin deformation and corresponding fiber-optic sensor feedback. The colors of the sensing elements in the graphic on the spatial alignment of the sensor elements correspond to the colors used in the graph showing the sensor feedback during activation.	99
5.27 Sections of tactile sensor array for calculating a local center of pressure	100
5.28 Local center or pressure detection for different contact geometries . . .	101
5.29 Extracted contour (orange) using activated sensor elements (red boxes)	102
6.1 Gripper attached to the Orion 7P deep-sea manipulator	109
6.2 Pressure chamber experiment environment for deep-sea experiments .	109
6.3 Experimental setup using an industrial manipulator arm in combination with a simplified version of the gripper system comprising the same processing electronics and the developed fiber-optic sensor arrays.	110

6.4 Overview of the different experiment environments, evaluated sensing modalities, and selected acquisition electronics	111
6.5 PCB with electrolytic capacitor (left) and the pressure-tolerant replacement of the component (right)	112
6.6 Selection of oscillators with different packaging material and working principles	113
6.7 Experimental results showing the averaged peak-to-peak voltage of selected quartz oscillators with respect to increasing ambient pressure . .	114
6.8 Impulse transformer module after exerting 600 bar ambient pressure .	115
6.9 Integrated multi-modal sensor (left) and sensor module prepared for underwater usage using epoxy resin with ceramic spheres (right) . . .	115
6.10 Volume shrinkage of epoxy resin during curing without (left) and with (right) filler material	116
6.11 Performance of fiber-optic sensor elements using different foam material in air and in water	117
6.12 (a) Parts of a force-torque sensor (ATI nano 25); (b) sensor coated for underwater use	118
6.13 Force-torque feedback without coating (a), with coating (b) and submerged in water (c)	118
6.14 Long-term observation of force-torque feedback while applying 1kg weight	119
6.15 Coated absolute angular encoder ready for underwater usage	120
6.16 Assembled gripper using a protective skin	120
6.17 Assembled gripper attached to a deep-sea manipulator without protective skin	121
6.18 Experimental setup for testing the gripper in combination with a manipulator arm underwater	122
6.19 Spherical shaped test objects of similar dimensions	123
6.20 Combination of experiment environment and sensing modalities	123
6.21 Applied forces for grasped test objects (n = 4 trials); p values between the populations are calculated using the Kruskal-Wallis test.	124
6.22 Applied closing angles of the gripper for grasped test objects (n = 4 trials). p-Values between the populations are calculated using the Kruskal-Wallis-Test.	124
6.23 Combination of experiment environment and sensing modalities	125

6.24 Left: Force-torque sensor signal and piezo sensor signal during grasp operation (dashed line: force data, continuous line: piezo sensor data). Right: Encoder signals of distal left limb and corresponding averaged piezoelectric sensor signal (dashed line: encoder signal, continuous line: piezo sensor data)	126
6.25 Combination of experiment environment, sensing modalities and acquisition electronics chosen	127
6.26 Experimental setup for evaluating the fiber-optic sensor array feedback	127
6.27 Sensor feedback of fiber-optic sensor array while operating in air and submerged in water	128
6.28 Sensor response for each sensor element during experiment repetition. Plot based on average sensor feedback from four trials with a sensor array with 72 sensor elements	130
6.29 Idle sensor signal offset for each sensor element at 600 bar	131
6.30 Averaged sensor signal response contacting test object at 600 bar	131
6.31 Long-term sensor signal response at 600 bar	132
6.32 Triangular shaped test object (a), perceived tactile image at 600 bar (b), binarized image (c), derived dimensions (d)	133
6.33 Experiment structure for evaluating the center of pressure detection under deep-sea pressure conditions	133
6.34 Experimental setup for evaluating the center of pressure detection under deep-sea pressure conditions	134
6.35 Rolling movement of the left finger to generate moving center of pressure on the tactile sensor array	135
6.36 Force center calculations during exploration movements at various pressure levels	135
6.37 Comparison between idle signal sensor noise at different pressure levels ($n = 91$ sensels)	137
6.38 Comparison of dynamic response between the two camera systems in dry and wet environment ($n = 91$ sensels)	137
6.39 Serpentine contour used for conducting the experiment	138
6.40 Left: Serpentine contour used for conducting the experiment. Right: Posture of the manipulator and the gripper during the experiment run.	139
6.41 Hierarchical controller for contour following behavior. Lines ending with a dot indicate inhibitory effects to the subsequent controller.	140
6.42 Calculated contour followed by the PA10 manipulator using control commands from tactile sensing.	140

7.1	Interaction between disciplines in robotic design in handling integration of functionality for complex robotic systems.	154
7.2	Details of the two-jaw gripper developed with integrated tactile sensing elements for industrial underwater manipulators	156

List of Tables

3.1 Mechanoreceptors in the glabrous skin (with data from: [Dahiya et al., 2010], [Johansson and Flanagan, 2009] and [Lederman, 1991])	14
4.1 Sensing range of chosen force torque sensor (ATI nano 25 250-6)	44
4.2 Properties of the electronics acquiring the force-torque sensor data	53
4.3 Properties of the electronics acquiring the piezoelectric sensor data	54
4.4 Properties of the electronics acquiring the fiber-optic sensor data	58
4.5 Properties of gripper system developed for deep-sea applications	64
5.1 Sampled data per second of the designed tactile sensory system	67
6.1 Selected oscillators for pressure testing	114
6.2 Effects of sensor coating on repeatability and drift (n = 10 trials)	119
6.3 Refraction indices and exit angles for different media	128
6.4 Maximum overall sensor response during contact with test object at different ambient pressure (n = 3 trials)	129
6.5 Comparison of the camera modules	136
6.6 Fiber-optic sensor performance under pressure	142

Acronyms

AC	alternating current
ADC	analog to digital converter
ASIC	application specific integrated circuit
AUV	autonomous underwater vehicle
BLDC	brushless DC motor
BOP	blowout prevention system
CAN	controller area network
CMOS	complementary metal on semiconductor
CPU	central processing unit
DC	direct current
DoF	degrees of freedom
DSP	digital signal processor
FPA	field programmable analog array
FPGA	field programmable gate array
I ² C	Inter IC Bus
LED	light-emitting diode
LIDAR	light detection and ranging
LRU	least recently used
LVDS	low-voltage differential signalling
MCU	microcontroller unit
MEMS	microelectromechanical systems

OTA operational transconductance amplifier

PCB printed circuit board

PSoC programmable system-on-chip

PVDF polyvinylidene flouride

PWM pulse-width modulation

PZT lead-titanate-zirconate

ROS Robot Operating System

ROV remotely operated vehicle

SMD surface mount device

SOM Self-Organizing Map

USB Universal Serial Bus

VHDL very high speed integrated circuits hardware description language

Bibliography

- [Arg, 2010] (2010). A survey of Tactile HumanRobot Interactions. *Robotics and Autonomous Systems*, 58(10):1159–1176.
- [Adams et al., 2010] Adams, J. C., Ernst, D. J., Murphy, T., and Ortiz, A. (2010). Multicore education: Pieces of the parallel puzzle. In *Proceedings of the 41st ACM Technical Symposium on Computer Science Education*, SIGCSE ’10, pages 194–195, New York, NY, USA. ACM.
- [Aggarwal et al., 2015] Aggarwal, A., Kampmann, P., Lemburg, J., and Kirchner, F. (2015). Haptic Object Recognition in Underwater and Deep-sea Environments. *Journal of Field Robotics*, 32(1):167–185.
- [Alexiou et al., 2010] Alexiou, K., Johnson, J., and Zamenopoulos, T. (2010). Embracing complexity in design: emerging perspectives and opportunities. In Inns, T., editor, *Designing for the 21st century: research methods & findings*, volume 2, pages 87–100. Gower Ashgate, United Kingdom.
- [Allen and Michelman, 1990] Allen, P. and Michelman, P. (1990). Acquisition and interpretation of 3-D sensor data from touch. *Robotics and Automation, IEEE Transactions on*, 6(4):397–404.
- [Altman, 2005] Altman, D. G. (2005). *Statistics with confidence*. BMJ, London, 2nd ed. edition. Previous ed.: as edited by Martin J. Gardner and Douglas G. Altman. 1989.
- [ATI Industrial Automation, 2013] ATI Industrial Automation (2013). *F/T Transducer without Electronics (TWE) Six-Axis Force/Torque Transducer Installation and Operation Manual*. ATI Industrial Automation , Pinnacle Park, 1031 Goodworth Drive, Apex, NC 27539.
- [Au and Hastings, 2008] Au, W. W. and Hastings, M. C. (2008). Measurement and Generation of Underwater Sounds. In *Principles of Marine Bioacoustics, Modern Acoustics and Signal Processing*, pages 27–56. Springer US.

- [Bahleda, 2002] Bahleda, M. (2002). Remotely Operated Vehicle (ROV)Technology: Applications and Advancements at Hydro Facilities. Technical Report TR-113584-V7, Electric Power Research Institute Inc., Palo Alto, California.
- [Bai and Bai, 2012] Bai, Y. and Bai, Q. (2012). *Subsea Engineering Handbook*. Gulf Professional Publishing. Elsevier Science & Technology Books.
- [Barry and Hashimoto, 2009] Barry, J. P. and Hashimoto, J. (2009). Revisiting the Challenger Deep Using the ROV Kaiko. *Marine Technology Society Journal*, 43(5):77–78.
- [Bartsch et al., 2012] Bartsch, S., Birnschein, T., Langosz, M., Hilljegerdes, J., Kuehn, D., and Kirchner, F. (2012). Development of the six-legged walking and climbing robot SpaceClimber. *Journal of Field Robotics*, Volume 29, Issue 3, Special Issue on Space Robotics(Part 1):506–532.
- [Bemfica et al., 2014] Bemfica, J. R., Melchiorri, C., Moriello, L., Palli, G., and Scarcia, U. (2014). A three-fingered cable-driven gripper for underwater applications. *2014 IEEE International Conference on Robotics and Automation (ICRA)*, pages 2469–2474.
- [Bendhaiba et al., 2015] Bendhaiba, L., Boelaert, J., Olteanu, M., and Villa-Vialaneix, N. (2015). *SOMbrero: SOM Bound to Realize Euclidean and Relational Outputs*. R package version 1.0.
- [Bicchi, 1990] Bicchi, A. (1990). Intrinsic contact sensing for soft fingers. *Robotics and Automation, 1990. Proceedings.*, 1990, pages 968–973.
- [Blakemore et al., 1970] Blakemore, C., Carpenter, R. H. S., and Georgeson, M. A. (1970). Lateral inhibition between orientation detectors in the human visual system. *Nature*, 228(5266):37–39.
- [Boyes, 2009] Boyes, W. (2009). *Instrumentation Reference Book*. EngineeringPro collection. Elsevier Science.
- [Bradski, 2000] Bradski, G. (2000). The OpenCV Library. *Dr. Dobb's Journal of Software Tools*.
- [Bradski and Kaehler, 2008] Bradski, G. and Kaehler, A. (2008). *Learning OpenCV: Computer Vision with the OpenCV Library*. O'Reilly Media.
- [Brooks, 1991] Brooks, R. (1991). Intelligence without representation. *Artificial Intelligence*, 47:139–159.

- [Cannata and Maggiali, 2006] Cannata, G. and Maggiali, M. (2006). Processing of Tactile/Force Measurements for a Fully Embedded Sensor. *2006 IEEE International Conference on Multisensor Fusion and Integration for Intelligent Systems*, 1:160–166.
- [Canny, 1986] Canny, J. (1986). A computational approach to edge detection. *IEEE Transactions on Pattern Analysis and Machine Intelligence*.
- [Charette and Walter, 2010] Charette, M. and Walter, S. (2010). The Volume of Earth’s Ocean. *Journal of The Oceanography Society*, 23(2):112–114.
- [Chen et al., 1997] Chen, N., Zhang, H., and Rink, R. (1997). Touch-driven robot control using a tactile Jacobian. *Robotics and Automation, 1997.*, (April):1737–1742.
- [Choi et al., 2005] Choi, B., Choi, H., and Kang, S. (2005). Development of tactile sensor for detecting contact force and slip. *2005.(IROS 2005). 2005 IEEE/RSJ*, pages 2638–2643.
- [Choi et al., 2006] Choi, B., Lee, S., Choi, H. R., and Kang, S. (2006). Development of Anthropomorphic Robot Hand with Tactile Sensor : SKKU Hand II. In *Intelligent Robots and Systems, 2006 IEEE/RSJ International Conference on*, pages 3779–3784.
- [Christiansen, 2010] Christiansen, S. (2010). Background Document for Deep-sea sponge aggregations. Technical report, OSPAR Biodiversity Series.
- [Cingolani, 2014] Cingolani, R. (2014). *Bioinspired Approaches for Human-Centric Technologies*. Springer International Publishing.
- [Ciobanu et al., 2013] Ciobanu, V., Petrescu, A., Hendrich, N., and Zhang, J. (2013). Tactile sensor value preprocessing pipeline. *2013 17th International Conference on System Theory, Control and Computing (ICSTCC)*, pages 674–680.
- [Cordes et al., 1997] Cordes, S., Berns, K., and Leppanen, I. (1997). Sensor components of the six-legged walking machine LAURON II. In *Advanced Robotics, 1997. ICAR ’97. Proceedings., 8th International Conference on*, pages 71–76.
- [Cutkosky et al., 2008] Cutkosky, M. R., Howe, R. D., and Provancher, W. R. (2008). Force and Tactile Sensors. In Siciliano, B. and Khatib, O., editors, *Springer Handbook of Robotics*, pages 455–476. Springer.
- [Dahiya et al., 2010] Dahiya, R. S., Metta, G., Valle, M., and Sandini, G. (2010). Tactile Sensing—From Humans to Humanoids. *IEEE Transactions on Robotics*, 26(1):1–20.

- [Dennerlein et al., 2000] Dennerlein, J., Howe, R., Shahonian, E., and Olroyd, C. (2000). Vibrotactile feedback for an underwater telerobot. In *Robotics and applications; Robotic and manufacturing systems recent results in research, development and applications International symposium; 8th*, pages 244–249.
- [Fearing, 1987] Fearing, R. (1987). Some experiments with tactile sensing during grasping. In *Robotics and Automation. Proceedings. 1987 IEEE International Conference on*, volume 4, pages 1637–1643.
- [Fearing and Hollerbach, 1984] Fearing, R. and Hollerbach, J. (1984). Basic Solid Mechanics for Tactile Sensing. *Robotics and Automation*.
- [Feix et al., 2009] Feix, T., Schmiedmayer, H.-B., Romero, J., and Kragić, D. (2009). A comprehensive grasp taxonomy. In *Robotics, Science and Systems Conference: Workshop on understanding the human hand for advancing robotic manipulation*.
- [Fraden, 2010] Fraden, J. (2010). *Handbook of Modern Sensors: Physics, Designs, and Applications*. Springer.
- [Fresnada, 2012] Fresnada, J. F. (2012). Manipulation in the Seabed: A New Underwater Manipulation System for Shallow Water Intervention. *Embedded Systems*, (April):314–319.
- [Fritz Gyger AG,] Fritz Gyger AG. Micro Valve - Functional Principle. http://www.fluidics.ch/index.php?article_id=58&clang=1. Online; accessed 2 - July - 2015.
- [Fruchterman and Reingold, 1991] Fruchterman, T. M. J. and Reingold, E. M. (1991). Graph Drawing by Force-directed Placement. *Softw. Pract. Exper.*, 21(11):1129–1164.
- [Fuller and Millett, 2011] Fuller, S. H. and Millett, L. I. (2011). *The Future of Computing Performance: Game Over or Next Level?* The National Academies Press, Washington, DC.
- [George A. Gescheider, 2009] George A. Gescheider, John H. Wright, R. T. V. (2009). *Information-Processing Channels in the Tactile Sensory System: a psychophysical and physiological analysis*. Psychology Press Taylor and Francis Group New York London.
- [Grebenstein et al., 2012] Grebenstein, M., Chalon, M., Friedl, W., Haddadin, S., Wimböck, T., Hirzinger, G., and Siegwart, R. (2012). The hand of the DLR Hand Arm System: Designed for interaction. *The International Journal of Robotics Research*, 31(13):1531–1555.

- [Grünwald, 2008] Grünwald, M. (2008). *Human haptic perception: basics and applications.*
- [Harper, 2005] Harper, C. (2005). *Electronic packaging and interconnection handbook.* Electronic packaging and interconnection series. McGraw-Hill.
- [Hildebrandt et al., 2009] Hildebrandt, M., Kerdels, J., and Albiez, J. (2009). A Multi-Layered Controller Approach for High Precision End-Effectuator Control of Hydraulic Underwater Manipulator Systems. In *OCEANS 09 MTS / IEEE Biloxi - Marine Technology for Our Future: Global and Local Challenges. OCEANS MTS/IEEE Conference (OCEANS-09), Marine Technology for our Future: Global and Local Challenges, October 26-29, Biloxi, USA.* o.A.
- [Hough, 1959] Hough, P. V. C. (1959). Machine Analysis of Bubble Chamber Pictures. In *International Conference on High Energy Accelerators and Instrumentation*, CERN.
- [Hruska, 2014] Hruska, J. (2014). This is what the death of Moore's law looks like: EUV rollout slowed, 450mm wafers halted, and an uncertain path beyond 14nm. <http://www.extremetech.com/computing/178529-this-is-what-the-death-of-moores-law-looks-like-euv-paused-indefinitely-450mm-wafers-halted-and-no-path-beyond-14nm>. Online; accessed 19 - September - 2015.
- [Huang, 2015] Huang, A. (2015). The Death of Moore's Law Will Spur Innovation. <http://spectrum.ieee.org/semiconductors/design/the-death-of-moores-law-will-spur-innovation>. Online; accessed 19 - September - 2015.
- [Inaudi et al., 2007] Inaudi, D., Gasparoni, F., Zecchin, M., Glisic, B., and Cenedese, S. (2007). Strain sensors for deepwater applications. *SHMII-3 2007. The 3rd International Conference on Structural Health Monitoring of Intelligent Infrastructure.*
- [Intel Corporation, 2005] Intel Corporation (2005). Excerpts from a conversation with gordon moore: Moore's law. http://ext02.fh-kaernten.at/auer/MET/pdf/A_Conversation_with_Gordon_Moore.pdf. Online; accessed 19 - September - 2015.
- [Ioannou et al., 1999] Ioannou, D., Huda, W., and Laine, A. (1999). Circle recognition through a 2D Hough Transform and radius histogramming. *Image Vision Comput.*, 17(1):15–26.

- [Jauch Quartz GmbH, 2007] Jauch Quartz GmbH (2007). Quartz Crystal Theory. http://www.jauch.de/ablage/med_00000818_1327049076_Quartz%20Crystal%20Theory%202007.pdf. Online; accessed 22 - June - 2015.
- [Jayawant, 1989] Jayawant, B. V. (1989). Tactile sensing in robotics. *Journal of Physics E: Scientific Instruments*, 22(9):684.
- [Johansson and Flanagan, 2009] Johansson, R. and Flanagan, R. (2009). Coding and use of tactile signals from the fingertips in object manipulation tasks. *Nature reviews. Neuroscience*, 10(5):345–59.
- [Jun et al., 2008] Jun, B.-H., Lee, P.-M., and Kim, S. (2008). Manipulability analysis of underwater robotic arms on ROV and application to task-oriented joint configuration. *Journal of Mechanical Science and Technology*, 22(5):887–894.
- [Kamiyama et al., 2004] Kamiyama, K., Kajimoto, H., Kawakami, N., and Tachi, S. (2004). Evaluation of a vision-based tactile sensor. In *Robotics and Automation, 2004. Proceedings. ICRA '04. 2004 IEEE International Conference on*, volume 2, pages 1542–1547 Vol.2.
- [Kampmann, 2010] Kampmann, P. (2010). Electronic and Software Interface for Sensor Arrays Based on Fiber-Optic Sensing Technology. DFKI Research Report, DFKI Robotics Innovation Center Bremen, Robert-Hooke-Straße 1, 28359 Bremen.
- [Kampmann and Kirchner, 2012] Kampmann, P. and Kirchner, F. (2012). A Tactile Sensing System for Underwater Manipulation. In *Proceedings of the workshop on: Advances in Tactile Sensing and Touch based Human-Robot Interaction to be held in conjunction with the 7th ACM/IEEE International Conference on Human-Robot Interaction (HRI 2012)*.
- [Kampmann and Kirchner, 2014] Kampmann, P. and Kirchner, F. (2014). Integration of Fiber-Optic Sensor Arrays into a Multi-Modal Tactile Sensor Processing System for Robotic End-Effectors. *Sensors - Open Access Journal*, Special Issue Tactile Sensors and Sensing Systems(14(4)):6854–6876.
- [Kampmann and Kirchner, 2015] Kampmann, P. and Kirchner, F. (2015). Towards a fine-manipulation system with tactile feedback for deep-sea environments. *Robotics and Autonomous Systems*, 67:115 – 121. Advances in Autonomous Underwater Robotics.
- [Kampmann et al., 2012] Kampmann, P., Lemburg, J., Hanff, H., and Kirchner, F. (2012). Hybrid Pressure-Tolerant Electronics. In *Proceedings of the Oceans 2012 MTS/IEEE Hampton Roads Conference & Exhibition. OCEANS MTS/IEEE Conference (OCEANS-2012), October 14-19, Hampton Roads, Virginia, USA*.

- [Kampmann et al., 2015] Kampmann, P., Stoffregen, T., and Kirchner, F. (2015). Equipping industrial deep-sea manipulators with a sense of touch. In *Proceedings of the Oceans 2015 MTS/IEEE Conference & Exhibition. OCEANS MTS/IEEE Conference (OCEANS-2015), October 19-22, Washington D.C., USA.*
- [Kapandji, 2007] Kapandji, I. (2007). *The Physiology of the Joints: The upper limb*, volume 1 of *The Physiology of the Joints*. Churchill Livingstone.
- [Kelley, 2001] Kelley, D. S. (2001). Black smokers: incubators on the seafloor. *Earth: Inside and Out*, pages 183–189.
- [Kimme et al., 1975] Kimme, C., Ballard, D., and Sklansky, J. (1975). Finding circles by an array of accumulators. *Commun. ACM*, 18(2):120–122.
- [Kleinberg and Tardos, 2006] Kleinberg, J. and Tardos, É. (2006). *Algorithm Design*. Alternative Etext Formats. Pearson/Addison-Wesley.
- [Kohonen et al., 2001] Kohonen, T., Schroeder, M. R., and Huang, T. S., editors (2001). *Self-Organizing Maps*. Springer-Verlag New York, Inc., Secaucus, NJ, USA, 3rd edition.
- [Kruskal and Wallis, 1952] Kruskal, W. H. and Wallis, W. A. (1952). Use of ranks in one-criterion variance analysis. *Journal of the American Statistical Association*, 47(260):pp. 583–621.
- [Kuwada et al., 2006] Kuwada, A., Tsujino, K., Suzumori, K., and Kanda, T. (2006). Intelligent Actuators Realizing Snake-like Small Robot for Pipe Inspection. In *Micro-NanoMechatronics and Human Science, 2006 International Symposium on*, pages 1–6.
- [Lagakos et al., 1987] Lagakos, N., Cole, J. H., and Bucaro, J. A. (1987). Microbend fiber-optic sensor. *Appl. Opt.*, 26(11):2171–2180.
- [Lane et al., 1997] Lane, D., Davies, J., Casalino, G., Bartolini, G., Cannata, G., Veruggio, G., Canals, M., Smith, C., O'Brien, D., Pickett, M., and Others (1997). AMADEUS: advanced manipulation for deep underwater sampling. *Robotics & Automation Magazine, IEEE*, 4(4):34–45.
- [Lederman, 1991] Lederman, S. (1991). Skin and Touch. In *Encyclopedia of Human Biology*, volume 251, pages 51–63. Academic Press, Inc., 7th edition.
- [Lederman and Browse, 1988] Lederman, S. and Browse, R. (1988). The physiology and psychophysics of touch. *NATO ASI Series*, F43(Sensors and Sensory System for Advanced Robots):71–91.

- [Lederman and Klatzky, 1993] Lederman, S. J. and Klatzky, R. L. (1993). Extracting object properties through haptic exploration. *Acta psychologica*, 84(1):29–40.
- [Lemburg et al., 2011] Lemburg, J., Kampmann, P., and Kirchner, F. (2011). A small-scale actuator with passive-compliance for a fine-manipulation deep-sea manipulator. In *Proceedings of the OCEANS 2011 MTS/IEEE KONA Conference & Exhibition*.
- [Lemieux et al., 2006] Lemieux, S., Beaudry, J., and Blain, M. (2006). Force control test bench for underwater vehicle-manipulator system applications. In *IEEE Industrial Electronics, IECON 2006 - 32nd Annual Conference on*, pages 4036–4042.
- [Li et al., 2013] Li, Q., Schürmann, C., Haschke, R., and Ritter, H. (2013). A control framework for tactile servoing.
- [Liu et al., 2008] Liu, H., Wu, K., Meusel, P., Seitz, N., Hirzinger, G., Jin, M. H., Liu, Y., Fan, S., Lan, T., and Chen, Z. P. (2008). Multisensory five-finger dexterous hand: The DLR/HIT Hand II. In *IROS*, pages 3692–3697. IEEE.
- [Luber et al., 2010] Luber, M., Poisel, H., and Ziemann, O. (2010). Taktile Sensormatte mit intelligen-tem Multifaser-Empfänger. Poster presentation at the Sensor & Test in Nürnberg (18.05.-20.05.2010).
- [Lumpkin et al., 2010] Lumpkin, E. a., Marshall, K. L., and Nelson, A. M. (2010). The cell biology of touch. *The Journal of cell biology*, 191(2):237–48.
- [Ly et al., 2004] Ly, D. N., Regenstein, K., Asfour, T., and Dillmann, R. (2004). A modular and distributed embedded control architecture for humanoid robots. In *IROS*, pages 2775–2780.
- [Maldonado-López et al., 2006] Maldonado-López, R., Vidal-Verdú, F., and Liñán, G. (2006). Tactile Retina for Slip Detection. *Human-Computer Interfaces and Measurement Systems, Proceedings of 2006 IEEE International Conference on Virtual Environments*, (July):10–12.
- [Meng et al., 2006] Meng, Q., Wang, H., Li, P., Wang, L., and He, Z. (2006). Dexterous Underwater Robot Hand: HEU Hand II. In *2006 International Conference on Mechatronics and Automation*, pages 1477–1482. Ieee.
- [Michel et al., 2003] Michel, J. L., Klages, M., Barriga, F. J. A. S., Fouquet, Y., Sibuet, M., Sarradin, P. M., Siméoni, P., and Drogou, J. F. (2003). Victor 6000: design, utilization and first improvements. In *ISOPE 2003 : [proceedings of the Thirteenth (2003) International Offshore and Polar Engineering Conference, Honolulu,*

- Hawaii, USA, May 25 - 30, 2003] ; conference proceedings, [Cupertino, Calif.] : International Society of Offshore and Polar Engineers, Pa.
- [Mittendorfer and Cheng, 2011] Mittendorfer, P. and Cheng, G. (2011). Humanoid multimodal tactile-sensing modules. *Robotics, IEEE Transactions on*, pages 1–10.
- [Mouri et al., 2002] Mouri, T., Kawasaki, H., Yoshikawa, K., Takai, J., and Ito, S. (2002). Anthropomorphic Robot Hand : Gifu Hand III. *Iccas2002*, pages 1288–1293.
- [Nicholls and Lee, 1989] Nicholls, H. and Lee, M. (1989). A Survey of Robot Tactile Sensing Technology. *International Journal of Robotics Research*, 8(3):3–30.
- [Nilsson, 2000] Nilsson, M. (2000). Tactile sensors and other distributed sensors with minimal wiring complexity. *IEEE/ASME transactions on mechatronics*, 5(3):253–257.
- [Nilsson, 1984] Nilsson, N. J. (1984). Shakey The Robot. Technical Report 323, AI Center, SRI International, 333 Ravenswood Ave., Menlo Park, CA 94025.
- [Nolan and Soltero, 2003] Nolan, S. M. and Soltero, J. M. (2003). Understanding and Interpreting Standard-Logic Data Sheets. Technical report, Texas Instruments.
- [Obinata et al., 2007] Obinata, G., Dutta, A., Moriyama, N., and Watanabe, N. (2007). *Vision Based Tactile Sensor Using Transparent Elastic Fingertip for Dexterous Handling*. INTECH Open Access Publisher.
- [Ocean Networks Canada, 2014] Ocean Networks Canada (2014). Seatube from ocean networks canada. "<https://cas.neptunecanada.ca/cas-server-webapp-3.3.5/login>". Online; accessed 12 - December - 2014.
- [Odeberg, 1995] Odeberg, H. (1995). A tactile sensor data-processing system. *Sensors and Actuators A: Physical*, 49:173–180.
- [Olmos et al., 2006] Olmos, I., Gonzalez, J. A., and Osorio, M. (2006). Inexact Graph Matching: A Case of Study. In Sutcliffe, G. and Goebel, R., editors, *FLAIRS Conference*, pages 586–591. AAAI Press.
- [Ott and Longnecker, 2010] Ott, R. L. and Longnecker, M. (2010). *An Introduction to Statistical Methods and Data Analysis*.
- [Palli et al., 2014] Palli, G., Moriello, L., Scarcia, U., and Melchiorri, C. (2014). An Intrinsic Tactile Sensor for Underwater Robotics. In *Preprints of the 19th World Congress The International Federation of Automatic Control Cape Town, South Africa. August 24-29*, pages 3364–3369.

- [Papakostas et al., 2002] Papakostas, T. V., Lima, J., and Lowe, M. (2002). A Large Area Force Sensor for Smart Skin Applications. In *Sensors, 2002. Proceedings of IEEE*, volume 2, pages 1620–1624.
- [Pereira et al., 2014] Pereira, T., Rusinkiewicz, S., and Matusik, W. (2014). Computational light routing: 3D printed fiber optics for sensing and display. *ACM Transactions on Graphics*, 33(3).
- [PI Ceramics GmbH, 2014] PI Ceramics GmbH (2014). Material Data - PIC 255. http://picericam.de/download/PI_Ceramic_Werkstoffdaten.pdf. Online; accessed 2 - July - 2015.
- [Purves, 2012] Purves, D. (2012). *Neuroscience*. Sinauer Associates.
- [Raibert and Tanner, 1982] Raibert, M. and Tanner, J. (1982). Design and Implementation of a VLSI Tactile Sensing Computer. *The International Journal of Robotics Research*, 1(3):3.
- [Reimer and Baldwin, 1999] Reimer, E. M. and Baldwin, L. H. (1999). Cavity Sensor Technology for Low Cost Automotive Safety and Control Devices. In *Air Bag Technology '99, Cobo Convention Center, Detroit*.
- [Scheibert et al., 2009] Scheibert, J., Leurent, S., Prevost, A., and Debrégeas, G. (2009). The role of fingerprints in the coding of tactile information probed with a biomimetic sensor. *Science*, 323(5920):1503–1506.
- [Schunk GmbH & Co. KG, 2008] Schunk GmbH & Co. KG (2008). *SCHUNK Dexterous Hand 2.0 (SDH 2.0) Datasheet v1.1*. SCHUNK GmbH & Co. KG, Spann- und Greiftechnik, Bahnhofstr. 106-134, D-7438 Lauffen/Neckar.
- [Shahookar and Mazumder, 1991] Shahookar, K. and Mazumder, P. (1991). VLSI cell placement techniques. *ACM Computing Surveys (CSUR)*, 23(2):143–220.
- [Smith et al., 2008] Smith, C., Levin, L., Koslow, A., Tyler, P., and Glover, A. (2008). The near future of the deep seafloor ecosystems. *Aquatic Ecosystems: Trends and Global Prospects*.
- [Sobel and Feldman, 1968] Sobel, I. and Feldman, G. (1968). A 3x3 Isotropic Gradient Operator for Image Processing. Never published but presented at a talk at the Stanford Artificial Project.
- [Spennenberg and Kirchner, 2007] Spennenberg, D. and Kirchner, F. (2007). *The Bio-Inspired SCORPION Robot: Design, Control & Lessons Learned*, volume Climbing & Walking Robots, Towards New Applications, pages 197–218. I-Tech Education and Publishing, Wien, Austria. ISBN: 978-3-902613-16-5.

- [Tan et al., 2008] Tan, D.-z., Wang, Q.-m., Song, R.-h., Yao, X., and Gu, Y.-h. (2008). Optical fiber based slide tactile sensor for underwater robots. *Journal of Marine Science and Application*, 7(2):122–126.
- [Technip USA, Inc., 2011] Technip USA, Inc. (2011). Shell / Perdido - The world's deepest Spar production and drilling facility Alaminos Canyon, U.S. Gulf of Mexico. https://www.technip.com/sites/default/files/technip/fields/shell-perdido_sept_2011_web.pdf. Online; accessed 30 - October - 2015.
- [Tegin and Wikander, 2005] Tegin, J. and Wikander, J. (2005). Tactile sensing in intelligent robotic manipulation – a review. *Industrial Robot: An International Journal*, 32(1):64–70.
- [The Economist, 2015] The Economist (2015). The end of Moore's law. <http://www.economist.com/blogs/economist-explains/2015/04/economist-explains-17>. Online; accessed 19 - September - 2015.
- [The Fibre Optic Association, 2009] The Fibre Optic Association (2009). User's Guide To Fiber Optic System Design and Installation. Online. Accessed: 13.05.2015.
- [Thiede et al., 2009] Thiede, C., Buscher, M., Lück, M., Lehr, H., Korner, G., Martin, J., Schlichting, M., Krueger, S., and Huth, H. (2009). An overall pressure tolerant underwater vehicle: Dns pegel. In *OCEANS 2009 - EUROPE*, pages 1–6.
- [Tyler, 2003] Tyler, P. (2003). *Ecosystems of the Deep Oceans*. Ecosystems of the World. Elsevier Science.
- [Vallbo and Johansson, 1984] Vallbo, A. and Johansson, R. (1984). Properties of cutaneous mechanoreceptors in the human hand related to touch sensation. *Human neurobiology*, 3(1):3–14.
- [Wegener, 2007] Wegener, K. (2007). *Ein flexibles Greifsystem für Roboterassistenten im Haushalt*. PhD thesis, Universität Stuttgart, Holzgartenstr. 16, 70174 Stuttgart.
- [Weiss and Wörn, 2005] Weiss, K. and Wörn, H. (2005). The working principle of resistive tactile sensor cells. *IEEE International Conference Mechatronics and Automation, 2005*, pages 471–476.
- [Weiss Robotics GmbH & Co. KG, 2009] Weiss Robotics GmbH & Co. KG (2009). *DSA 9210 Tactile Sensor with curved sensing surface*. Weiss Robotics GmbH & Co. KG, In der Gerste 2, D-71636 Ludwigsburg.

[Wettels et al., 2014] Wettels, N., Fishel, J., and Loeb, G. (2014). Multimodal Tactile Sensor. *The Human Hand as an Inspiration for Robot Hand Development, Springer Tracts in Advanced Robotics (STAR) series*, (0912260):1–20.

[Zhang and Chen, 2000] Zhang, H. and Chen, N. (2000). Control of contact via tactile sensing. *IEEE Transactions on Robotics and Automation*, 16(5):482–495.